Annals of the ICRP

ICRP PUBLICATION 116

Conversion Coefficients for Radiological Protection Quantities for External Radiation Exposures

Editor
C.H. CLEMENT

Authors on behalf of ICRP
N. Petoussi-Henss, W.E. Bolch, K.F. Eckerman, A. Endo, N. Hertel, J. Hunt, M. Pelliccioni, H. Schlattl, M. Zankl

PUBLISHED FOR

The International Commission on Radiological Protection and
The International Commission on Radiation Units and Measurements

by

ELSEVIER

Please cite this issue as 'ICRP, 2010. Conversion Coefficients for Radiological Protection Quantities for External Radiation Exposures. ICRP Publication 116, Ann. ICRP 40(2–5).'

CONTENTS

TITLE PAGE 1

GUEST EDITORIAL 5

ABSTRACT 9

PREFACE 11

MAIN POINTS 13

EXECUTIVE SUMMARY 15

GLOSSARY 19

1. INTRODUCTION 27

1.1. References 29

2. QUANTITIES USED IN RADIATION PROTECTION FOR EXTERNAL EXPOSURE 31

2.1. Fluence and kerma 31
2.2. Dose quantities used for radiological protection 32
2.3. Operational quantities 39
2.4. References 42

3. DETERMINATION OF ORGAN ABSORBED DOSES OF THE ICRP/ICRU REFERENCE PHANTOMS 45

3.1. The ICRP/ICRU reference computational phantoms 45
3.2. Irradiation geometries considered 47
3.3. General descriptions of the Monte Carlo codes used to simulate radiation transport 48
3.4. Special considerations for assessing dose to skeletal tissues 53
3.5. Skin dosimetry 55
3.6. References 57

4. CONVERSION COEFFICIENTS FOR EXTERNAL EXPOSURE 61

4.1. Photons 67
4.2. Electrons and positrons 75
4.3. Neutrons 83
4.4. Protons 91

4.5. Positive and negative muons 97
4.6. Positive and negative pions 102
4.7. Helium ions 107
4.8. References 111

5. RELATIONSHIPS BETWEEN DOSE CONVERSION COEFFICIENTS FOR OPERATIONAL AND PROTECTION QUANTITIES 115

5.1. Changes in protection quantities 116
5.2. Photons 117
5.3. Electrons 118
5.4. Neutrons 119
5.5. Comparison of dose to the lens of the eye with the operational quantities 121
5.6. Conclusions 123
5.7. References 124

ANNEX A. EFFECTIVE DOSE CONVERSION COEFFICIENTS 125

ANNEX B. ORGAN ABSORBED DOSE CONVERSION COEFFICIENTS FOR PHOTONS 139

ANNEX C. ORGAN ABSORBED DOSE CONVERSION COEFFICIENTS FOR NEUTRONS 171

ANNEX D. SKELETAL FLUENCE-TO-DOSE RESPONSE FUNCTIONS: PHOTONS 203

ANNEX E. SKELETAL FLUENCE-TO-DOSE RESPONSE FUNCTIONS: NEUTRONS 221

ANNEX F. SPECIAL CONSIDERATIONS FOR ASSESSING ABSORBED DOSE IN THE LENS OF THE EYE 235

ANNEX G. SPECIAL CONSIDERATIONS FOR ASSESSING THE LOCAL SKIN-EQUIVALENT DOSE 247

ANNEX H. EFFECTIVE DOSE FOR SUPERIOR HEMISPHERE SEMI-ISOTROPIC IRRADIATION FOR AIRCRAFT CREW DOSIMETRY 251

ANNEX I. METHODS USED FOR EVALUATION OF REFERENCE DATA 253

ANNEX J. CD USER GUIDE 255

ELSEVIER

ICRP Publication 116

Annals of the ICRP

Guest Editorial

REFERENCE PERSON, REFERENCE PHANTOMS, REFERENCE DOSE COEFFICIENTS: IT ALL COMES TOGETHER!

Since its creation in 1928 at the 2nd International Congress on Radiology, ICRP has had the mandate to develop the concepts, methods, and guidance to limit the harmful effects, initially in medical applications of radiation, and its first recommendation introduced the concept of exposure limitation on the number of working hours of medical staff. In the 1950s, the radiation exposure of workers and members of the public became a concern to ICRP, and exposure limits were expressed in terms of dose: maximum permissible dose for external exposure, and maximum permissible body burden for internal emitters. Exposure limitation and thereby risk limitation in modern radiological protection is based on use of the quantity 'effective dose', the concept of which was introduced by ICRP in 1978 as the quantity 'effective dose equivalent' (ICRP, 1978).

Effective dose is the primary radiation protection quantity used in the 2007 Recommendations (ICRP, 2007). Following the principle of justification, this quantity enables the necessary summation of doses from internal emitters and external radiation fields to provide a single numerical value for use in exposure limitation, and optimisation of radiological protection for both workers and members of the public. The basis of the summation is the health detriment within the exposed population. The health detriment associated with effective dose can be assigned a nominal value; for example, 0.05/Sv in ICRP *Publications 60* (ICRP, 1991) and *103* (ICRP, 2007). The radiation and tissue weighting factors used to weight the tissue-specific absorbed doses are invariant with respect to age and sex, and hence the weighted sum, the effective dose, is not applicable to a specific individual. The effective dose serves as the basis for the contractual relationship in the regulatory framework, and it also has utility in comparative evaluation of alternative work practices. It must be noted, however, that the quantity is not capable of representing the stochastic health risk (hereditary and carcinogenic) of exposures to a specific worker or member of the public. Dose limits, dose constraints, and reference levels specified in terms of effective dose serve a role in the contractual relationship between workers and the regulated licensee, as well as between licensees and the public within a regulatory framework. In this role, the coefficients are used in the process of assigning values

of effective dose to individuals for a given exposure, and they have no uncertainties for this process.

This publication is more than an update of ICRP *Publication 74* (ICRP, 1996), which was also published as ICRU Report 57 (ICRU, 1998). Additional radiation types are considered in the present publication, and coefficients for all radiations are tabulated over a greatly expanded energy range. The publication addresses photons (10 keV–10 GeV), electrons (negatrons and positrons 50 keV–10 GeV), neutrons (0.001 eV–10 GeV), protons (1 MeV–10 GeV), pions (negative and positive 1 MeV–200 GeV), muons (negative and positive 1 MeV–10 GeV), and helium ions (1 MeV/u–100 GeV/u). Calculation of the coefficients was enabled by today's advanced computing environment, and the availability of a suite of Monte Carlo radiation transport codes with supporting data and physics models. The annexes of this publication and accompanying CD detail the tissue-specific absorbed dose coefficients derived for Reference Male and Reference Female as a function of incident energy for the various idealised exposure geometries. The effective dose coefficients of Reference Person, as a function of incident energy, are tabulated in the main body of the publication.

To what extent are the current operational quantities of external exposure still a valid reflection of the protection quantities? Reference conversion coefficients for operational quantities were only published for photons, neutrons, and electrons in ICRP *Publication 74* (ICRP, 1996). Differences in the photon and electron dose coefficients between ICRP *Publication 74* and this publication are generally small, not exceeding 20–30%, and are largely attributable to specific aspects of the computational phantoms. Somewhat greater differences seen for low- and high-energy neutrons are attributable to the changes in their energy-dependent radiation weighting factors, and are not a consequence of the changes in computational phantoms. The authors of this publication conclude that '...the operational quantities for photons, neutrons, and electrons continue to provide a good approximation for broad particle energy and direction distributions and to be of practical application for most radiation protection practices...'. The numerical consistency of the dose coefficients in ICRP *Publication 74* (ICRP, 1996) and this publication is a consequence of the robust nature of the quantity 'effective dose'. Thus, the current operational coefficients still serve the needs of radiation protection very well at 'conventional' energies. The consideration of additional radiation types and the extension to higher energy is important with respect to space applications and ratiation exposures at high-energy accelerators. The relationship between the operational and radiation protection quantities at higher energies warrants further investigation.

For more than three decades, ICRP and ICRU have used computational models (phantoms) of the human anatomy without formal adoption of the phantoms. The ad-hoc phantoms used were, to some degree, based on the Reference Man concept of ICRP *Publication 23* (ICRP, 1975), which provided some of the necessary anatomical data. ICRP initiated use of such reference data with Standard Man in ICRP *Publication 2* (ICRP, 1959), expanded the data coverage in ICRP *Publication 23* (ICRP, 1975), and further strengthened its age and gender aspects in ICRP *Publication 89* (ICRP, 2002). At last, computational phantoms representing adult

Reference Male and Reference Female were formally adopted in the joint ICRP/ICRU *Publication 110* (ICRP, 2009). Adoption of these phantoms, so necessary in the calculation of tissue dose, provides a critical degree of completeness to ICRP's dosimetry framework. This publication is the first application of the adopted phantoms, and the resultant protection coefficients are based on the 2007 Recommendations of ICRP (ICRP, 2007).

The values of the coefficients tabulated in this publication were developed for the ICRP system of dose limitation, a well-defined framework, following documented procedures using reference computational phantoms that were critically evaluated, verified for accuracy, and judged by ICRP and ICRU to serve their intended purpose. Within the scope of their intended use, the coefficients as issued by an international authority have no uncertainties and, as such, are considered by ICRP and ICRU to be reference data, in accordance with the guidance of the Joint Committee for Guides in Metrology (JCGM, 2008).

Hans-Georg Menzel, ICRU and ICRP
Keith F. Eckerman, ICRP Committee 2

References

ICRP, 1959. Report of Committee II on Permissible Dose for Internal Radiation. ICRP Publication 2. Pergamon Press, Oxford.

ICRP, 1975. Report on the Task Group on Reference Man. ICRP Publication 23. Pergamon Press, Oxford.

ICRP, 1978. Statement from the 1978 Stockholm Meeting of the ICRP. Ann. ICRP 2 (1).

ICRP, 1991. 1990 Recommendations of the International Commission on Radiological Protection. ICRP Publication 60. Ann. ICRP 21 (1–3).

ICRP, 1996. Conversion coefficients for use in radiological protection against external radiation. ICRP Publication 74. Ann. ICRP 26 (3/4).

ICRP, 2002. Basic anatomical and physiological data for use in radiological protection: reference values. ICRP Publication 89. Ann. ICRP 32 (3/4).

ICRP, 2007. The 2007 Recommendations of the International Commission on Radiological Protection. ICRP Publication 103. Ann. ICRP 37 (2–4).

ICRP, 2009. Adult reference computational phantoms. ICRP Publication 110. Ann. ICRP 39 (2).

ICRU, 1998. Conversion Coefficients for use in Radiological Protection Against External Radiation. ICRU Report 57. International Commission on Radiation Units and Measurements, Bethesda, MD.

JCGM, 2008. Joint Committee for Guides in Metrology, International vocabulary of metrology – Basic and general concepts and associated terms (VIM). Sèvres.

ELSEVIER

ICRP Publication 116

Annals of the ICRP

Conversion Coefficients for Radiological Protection Quantities for External Radiation Exposures

ICRP PUBLICATION 116

Approved by ICRP in October 2010 and

adopted by ICRU in November 2010

Abstract–This report gives fluence to dose conversion coefficients for both effective dose and organ absorbed doses for various types of external exposures, consistent with the 2007 Recommendations of the ICRP (ICRP, 2007). These coefficients were calculated using the official ICRP/ICRU computational phantoms (ICRP, 2009) representing the Reference Adult Male and Reference Adult Female (ICRP, 2002), in conjunction with Monte Carlo codes simulating the transport of radiation within the human body such as EGSnrc, FLUKA, GEANT4, MCNPX, and PHITS.

The incident radiations and energy ranges considered were external beams of mono-energetic photons of 10 keV–10 GeV, electrons and positrons of 50 keV–10 GeV, neutrons of 0.001 eV–10 GeV, protons of 1 MeV–10 GeV, pions (negative/positive) of 1 MeV–200 GeV, muons (negative/positive) of 1 MeV–10 GeV, and helium ions of 1 MeV/u–100 GeV/u.

For the simulations, idealised whole-body irradiation geometries were considered. These included unidirectional broad parallel beams along the antero-posterior, postero-anterior, left lateral and right lateral axes, and 360° rotational directions around the phantoms' longitudinal axis. Fully isotropic irradiation of the phantoms was also considered.

Simulations were performed specifically for this report by members of the Task Group. For quality assurance purposes, data sets for given radiations and irradiation geometries were generated by different groups using the same reference computational phantoms but different Monte Carlo codes.

From the simulations, the absorbed dose to each organ within the reference phantoms was determined. The fluence to effective dose conversion coefficients were derived from the obtained organ dose conversion coefficients, the radiation weighting factor w_R and the tissue weighting factor w_T, following the procedure described in ICRP *Publication 103* (ICRP, 2007).

The operational quantities for photons, neutrons, and electrons continue to provide a good approximation for the conversion coefficients for effective dose for the energy ranges considered in ICRP *Publication 74* (ICRP, 1996) and ICRU Report 57 (ICRU, 1998), but not at the higher energies considered in the present report.

The conversion coefficients obtained for this report represent the ICRP/ICRU reference values. They were established using various original data sets with the application of averaging, smoothing, and fitting techniques. They are partly tabulated in annexes, and fully tabulated in an accompanying CD in ASCII format and Microsoft Excel software.

Separate Monte Carlo simulations were made to determine the absorbed dose to the lens of the eye for incident photons, electrons, and neutrons using a stylised model of the eye. Similarly, localised skin-equivalent dose conversion coefficients for electrons and alpha particles are given as derived by Monte Carlo calculations simulating the transport of a normally incident, parallel beam on a tissue-equivalent slab.

Additionally, photon and neutron dose–response functions are given in this report, defined as the absorbed dose per particle fluence. Their use would compensate for the limited spatial resolution of the voxel geometry, as well as for dose enhancement or dose depression at the microscopic level of the marrow cavities.
© 2011 Published by Elsevier Ltd.

Keywords: External radiation; Conversion coefficients; Effective dose; Skeletal dosimetry

Authors on Behalf of ICRP

N. Petoussi-Henss, W.E. Bolch, K.F. Eckerman, A. Endo,
N. Hertel, J. Hunt, M. Pelliccioni, H. Schlattl, M. Zankl

References

ICRP, 1996. Conversion coefficients for use in radiological protection against external radiation. ICRP Publication 74. Ann. ICRP 26(3/4).

ICRP, 2002. Basic anatomical and physiological data for use in radiological protection: reference values. ICRP Publication 89. Ann. ICRP 32(3/4).

ICRP, 2007. The 2007 Recommendations of the International Commission on Radiological Protection. ICRP Publication 103. Ann. ICRP 37(2–4).

ICRP, 2009. Adult reference computational phantoms. ICRP Publication 110. Ann. ICRP 39(2).

ICRU, 1998. Conversion Coefficients for use in Radiological Protection Against External Radiation. ICRU Report 57. International Commission on Radiation Units and Measurements, Bethesda, MD.

PREFACE

The present report is a joint publication of the International Commission on Radiological Protection (ICRP) and the International Commission on Radiation Units and Measurements (ICRU).

This report was compiled by a Subgroup of the Task Group on Dose Calculations (DOCAL) of ICRP Committee 2. The membership of this Subgroup was:

N. Petoussi-Henss (Chairperson)	A. Endo	M. Pelliccioni
W.E. Bolch	N. Hertel	H. Schlattl
K.F. Eckerman	J. Hunt	M. Zankl

Additional contributors to this publication were:

A.A. Bahadori	M. Sutton Ferenci	H.G. Menzel
D.T. Bartlett	M.C. Hough	T. Sato
R. Behrens	P.B. Johnson	G. Simmer
M.B. Bellamy	D.W. Jokisch	K. Veinot
B. Han	R.P. Manger	X.G. Xu
E. Burgett	M. Kraxenberger	

The membership of the DOCAL Task Group of ICRP Committee 2 during the preparation of this report was:

2005–2009 (full members)

W.E. Bolch (Chairman 2007–2008)	N. Petoussi-Henss (Vice-Chair, External Dosimetry)	J. Hunt
K.F. Eckerman (Chairman 2005–2007)	V. Berkovski	H.G. Menzel (2005–2007)
D. Nosske (Vice-Chair, Internal Dosimetry)	E. Blanchardon	M. Pelliccioni
	A. Endo	A. Phipps (2005–2007)
	N. Hertel	M. Zankl

2005–2009 (corresponding members)

L. Bertelli	R. Richardson	A. Ulanovsky
T. Fell	M.G. Stabin	X.G. Xu

2009–2011 (full members)

W.E. Bolch (Chairman)	V. Berkovski	N. Hertel
D. Nosske (Vice-Chair, Internal Dosimetry)	L. Bertelli	J. Hunt
N. Petoussi-Henss	K.F. Eckerman	N. Ishigure

(Vice-Chair, External Dosimetry)	A. Endo	M. Pelliccioni
	T. Fell	M. Zankl

2009–2011 (corresponding members)

A. Birchall	C. Lee	M.G. Stabin
G. Gualdrini	R. Leggett	R. Tanner
D. Jokisch	H. Schlattl	X.G. Xu

The membership of ICRP Committee 2 during the preparation of this report was:

2005–2009

H.G. Menzel (Chairman 2007–2009)	G. Dietze	F. Paquet
C. Streffer (Chairman 2005–2007)	K.F. Eckerman	H.G. Paretzke (2005–2007)
M. Balonov	J.D. Harrison (Secretary)	A.S. Pradhan
V. Berkovski	N. Ishigure	J.W. Stather (2005–2007)
W.E. Bolch	P. Jacob (2007–2009)	Y.Z. Zhou
A. Bouville	J.L. Lipsztein	

2009–2013

H.G. Menzel (Chairman)	G. Dietze	J.L. Lipsztein
M. Balonov	K.F. Eckerman	J. Ma
D.T. Bartlett	A. Endo	F. Paquet
V. Berkovski	J.D. Harrison (Secretary)	N. Petoussi-Henss
W.E. Bolch	J.N. Ishigure	A.S. Pradhan
R. Cox	R. Leggett	

The ICRU sponsors of the report were:

H.G. Menzel	H.G. Paretzke

Members of ICRU during the preparation of this report were:

H.G. Menzel (Chairman)	R.A. Gahbauer	H. Tatsuzaki
P. Dawson	D.T.L. Jones	A. Wambersie
P.M. DeLuca	B.D. Michael	G.F. Whitmore
K. Doi	H.G. Paretzke	
E. Fantuzzi	S.M. Seltzer	

MAIN POINTS

- **This report presents reference conversion coefficients for effective dose and organ absorbed doses for various types of external exposures, calculated following the 2007 Recommendations of the International Commission on Radiological Protection (ICRP, 2007).**
- **The phantoms used for the calculations were the official computational models of ICRP (2009) representing Reference Male and Reference Female (ICRP, 2002, 2007). These reference computational models are based on computed tomographic data of real people, and hence are digital three-dimensional representations of human anatomy.**
- **The radiations considered were external beams of mono-energetic photons of 10 keV–10 GeV, electrons and positrons of 50 keV–10 GeV, neutrons of 0.001 eV–10 GeV, protons of 1 MeV–10 GeV, pions (negative/positive) of 1 MeV–200 GeV, muons (negative/positive) of 1 MeV–10 GeV, and helium ions of 1 MeV/u –100 GeV/u. These energies are kinetic energies.**
- **Unlike the work reported previously in ICRP *Publication 74* (ICRP, 1996) and ICRU Report 57 (ICRU, 1998), in which published values of conversion coefficients were used to establish reference values, the organ dose conversion coefficients given here were calculated specifically for this report by members of the Task Group. For quality assurance purposes, data sets for given radiations and irradiation geometries were generated by different groups using the same reference computational phantoms but different Monte Carlo radiation transport codes, such as EGSnrc, FLUKA, GEANT4, MCNPX, and PHITS.**
- **The conversion coefficients tabulated in this report represent the ICRP/ICRU reference values. They were established using various original data sets with the application of averaging, smoothing, and fitting techniques.**
- **The operational quantities for photons, neutrons, and electrons continue to provide a good approximation for the conversion coefficients for effective dose for the energy ranges considered in ICRP** *Publication 74* (ICRP, 1996) **and ICRU Report 57** (ICRU, 1998)**, but they do not extend to the higher energies considered in the present report.**

References

ICRP, 1996. Conversion coefficients for use in radiological protection against external radiation. ICRP Publication 74. Ann. ICRP 26(3/4).

ICRP, 2002. Basic anatomical and physiological data for use in radiological protection: reference values. ICRP Publication 89. Ann. ICRP 32(3/4).

ICRP, 2007. The 2007 Recommendations of the International Commission on Radiological Protection. ICRP Publication 103. Ann. ICRP 37(2–4).

ICRP, 2009. Adult reference computational phantoms. ICRP Publication 110. Ann. ICRP 39(2).

ICRU, 1998. Conversion Coefficients for use in Radiological Protection Against External Radiation. ICRU Report 57. International Commission on Radiation Units and Measurements, Bethesda, MD.

EXECUTIVE SUMMARY

(a) The purpose of this report is to present fluence to dose conversion coefficients for effective dose and organ absorbed doses for various types of external exposures, consistent with the 2007 Recommendations of the ICRP (ICRP, 2007). For this purpose, the official ICRP/ICRU computational models (ICRP, 2009) representing Reference Male and Reference Female (ICRP, 2002) were used, in conjunction with Monte Carlo codes simulating the transport of radiation within the human body. The ICRP/ICRU reference computational phantoms are hereafter referred to as the 'reference phantoms'.

(b) The externally incident radiations and kinetic energy ranges considered were external beams of mono-energetic photons of 10 keV–10 GeV, electrons and positrons of 50 keV–10 GeV, neutrons of 0.001 eV–10 GeV, protons of 1 MeV–10 GeV, pions (negative/positive) of 1 MeV–200 GeV, muons (negative/positive) of 1 MeV–10 GeV, and helium ions of 1 MeV/u–100 GeV/u.

(c) In order to calculate the dose conversion coefficients, simulations were performed to evaluate the absorbed dose to each organ within the reference phantoms using the following well-established Monte Carlo codes: EGSnrc (Kawrakow et al., 2009), MCNPX (Waters, 2002; Pelowitz, 2008), PHITS (Iwase et al., 2002; Niita et al., 2006, 2010), FLUKA (Fassò et al., 2005; Battistoni et al., 2006), and GEANT4 (GEANT4, 2006a,b). The fluence to effective dose conversion coefficients were then derived from the organ dose conversion coefficients, the radiation weighting factor w_R and the tissue weighting factor w_T following the procedure described in ICRP *Publication 103* (ICRP, 2007).

(d) For the simulations, idealised whole-body irradiation geometries were considered. These included unidirectional broad parallel beams along the antero-posterior, postero-anterior, left lateral and right lateral axes, and 360° rotational directions around the phantoms' longitudinal axis. Fully isotropic irradiation of the phantoms was also considered.

(e) The organ absorbed dose conversion coefficients were calculated specifically for this report by members of the Task Group. For quality assurance purposes, selected data sets for given radiations and irradiation geometries were generated by different members of the DOCAL Task Group using the same reference computational phantoms but different Monte Carlo codes. Reference values were then determined from the individual data through a procedure that included averaging, smoothing, and data fitting where necessary. The resultant data sets are the ICRP/ICRU reference values intended for use in radiological protection control, and thus they are fixed by convention and are not subject to uncertainties. They are hereafter referred to as 'reference values'.

(f) Separate Monte Carlo simulations were made to determine the absorbed dose to the lens of the eye for incident photons, electrons, and neutrons using a stylised model of the eye, allowing for a more detailed representation of the eye than afforded

by the ICRP/ICRU voxel phantoms due to the limitations on eye structure voxel resolution (ICRP, 2009).

(g) Part of the work of the Task Group involved skeletal dosimetry and the determination of dose–response functions (DRFs) for photons and neutrons. The use of DRFs would compensate for the limited spatial resolution of the voxel geometry of the phantoms, which does not allow the exact fine structure of trabecular spongiosa to be resolved, as well as for the dose enhancement of photo-electrons and the dose depression of recoil protons as they are produced in the bone trabeculae and marrow cavities, respectively, by incident photons and neutrons. However, for the estimation of absorbed doses in the skeletal tissues employed in this report, a simplified method of skeletal dosimetry was applied: absorbed dose to active marrow and endosteum were taken conservatively as the absorbed dose to spongiosa in each individual bone site, and skeletal-averaged absorbed doses to these tissues were taken as the mass-weighted average of the regional spongiosa absorbed dose. For the sake of consistency, this method was applied for all particles. It is noted that for incident charged particles, there are no significant mechanisms for dose enhancement or dose depression, and thus skeletal response functions for externally incident particles other than photons and neutrons are not provided in this report.

(h) The conversion coefficients for the adult male and female reference computational phantoms are compared with their corresponding values given in reports of a Joint ICRP/ICRU Task Group, published as ICRP *Publication 74* (ICRP, 1996) and ICRU Report 57 (ICRU, 1998). Contributing factors for any differences between these sets of conversion coefficients are discussed in terms of both the changes in phantoms employed for the simulations, and changes in both radiation and tissue weighting factors seen between the recommendations given in ICRP *Publication 60* (ICRP, 1991) and those given in ICRP *Publication 103* (ICRP, 2007). One of the issues addressed by the Task Group was the extent to which the operational quantities, as currently defined, adequately represent the protection quantities and provide a satisfactory basis for most measurements for radiological protection against external radiation.

(i) For that purpose, ratios of the effective dose to the operational quantities given in ICRP *Publication 74* (ICRP, 1996) are plotted for photons (10 keV–10 MeV), electrons (2–10 MeV), and neutrons (0.001 eV–200 MeV). It is concluded in this report that, ambient dose equivalent, $H^*(10)$, continues to provide a reasonable assessment of the effective dose under charged-particle equilibrium for photons. For electrons, $H^*(10)$ gives a reasonable estimate of the effective dose up to 10 MeV. For neutrons, $H^*(10)$ overestimates the effective dose or gives a reasonable approximation of this quantity up to ~40 MeV.

(j) Chapter 1 provides an introduction, and Chapter 2 gives a brief description of the quantities used in radiation protection for external dosimetry, as currently defined.

(k) Chapter 3 describes the main aspects of the simulations. It includes a brief summary of the ICRP voxel computational phantoms employed in the calculations and graphical displays of the irradiation geometries considered. The features of the

various Monte Carlo codes are also briefly described. The method of skeletal and skin dosimetry employed for this report is highlighted.

(l) Chapter 4 briefly presents the calculation parameters employed and a short analysis of the obtained organ and effective dose conversion coefficients. Existing differences between the male and female sets of coefficients are highlighted, and some comparisons with the data of ICRP *Publication 74* (ICRP, 1996) are presented and discussed.

(m) Chapter 5 compares effective dose with $H^*(10)$ and $H_p(10)$. Furthermore, dose to the lens of the eye vs personal dose equivalent $H_p(3)$ and directional dose equivalent $H'(3)$ is also presented. As recommended data are not available for all of these operational quantities, additional comparisons are made using data reported in the literature following the release of ICRP *Publication 74* (ICRP, 1996).

(n) Annex A gives the reference conversion coefficients for the effective dose for all particles and irradiation geometries.

(o) Annexes B and C present reference fluence to absorbed dose conversion coefficients for photons and neutrons, respectively, for those organs for which tissue weighting factors are assigned in ICRP *Publication 103* (ICRP, 2007) (red bone marrow, colon, lungs, stomach, breast, stomach wall, gonads, bladder wall, liver, oesophagus, thyroid, endosteum, brain, salivary glands, and skin), as well as for the remainder tissues. The organ absorbed dose conversion coefficients are given separately for the adult male and female models.

(p) Full tables for all particles and organs mentioned above, and for the 14 tissues comprising the remainder tissues (adrenals, extrathoracic region, gall bladder, heart, kidneys, lymphatic nodes, muscle, oral mucosa, pancreas, prostate, small intestine, spleen, thymus, and uterus), are provided in the CD ROM accompanying this report.

(q) Annexes D and E present photon and neutron DRFs, respectively. These functions, when convolved with the scoring of energy-dependent photon or neutron fluence within the spongiosa and medullary cavities of the reference voxel phantoms, permit more refined estimates of active marrow and endosteum dose on a bone-specific basis, and within energy ranges in which secondary charged-particle equilibrium is not fully established at the microscopic level of the marrow cavities. Annex D also provides values of μ_{en}/ρ ratios and dose enhancement factors for red bone marrow and endosteum as needed when applying the three-factor method of skeletal dosimetry (see Section D.2 of Annex D).

(r) Annex F describes the simulations for assessing the absorbed dose to the lens of the eye for photons, electrons, and neutrons, as calculated using a stylised model of the head and eye, for some irradiation geometries.

(s) Annex G discusses the special considerations for skin dosimetry as relevant to stochastic effects and tissue reactions, and gives localised skin-equivalent dose conversion coefficients for electrons and alpha particles.

(t) Annex H gives fluence to effective dose conversion coefficients for an additional geometry (superior hemisphere semi-isotropic irradiation) approximating the conditions typically seen in aircraft crew dosimetry.

(u) Annex I briefly describes the methods used to define the reference data of dose conversion coefficients from the original calculated data sets determined by different Monte Carlo codes.

(v) Finally, Annex J provides a user guide for the CD ROM accompanying this report.

References

Battistoni, G., Muraro, S., Sala, P.R., et al., 2006. The FLUKA code: description and benchmarking. In: Albrow, M., Raja, R. (Eds.), Hadronic Shower Simulation Workshop, 6–8 September 2006, Fermi National Accelerator Laboratory (Fermilab), Batavia, IL, AIP Conference Proceeding 896, pp. 31–49.

Fassò, A., Ferrari, A., Ranft, J., et al., 2005. FLUKA: a multi-particle transport code. CERN-2005-10 (2005), INFN/TC_05/11, SLAC-R-773. CERN, Geneva.

GEANT4, 2006a. GEANT4: Physics Reference Manual. Available at: http://geant4.web.cern.ch/geant4/UserDocumentation/UsersGuides/PhysicsReferenceManual/fo/PhysicsReferenceManual.pdf (last accessed December 2011).

GEANT4, 2006b. GEANT4 User's Guide for Application Developers. Available at: http://geant4.web.-cern.ch/geant4/support/userdocuments.shtml (last accessed December 2011).

ICRP, 1991. 1990 Recommendations of the International Commission on Radiological Protection. ICRP Publication 60. Ann. ICRP 21(1–3).

ICRP, 1996. Conversion coefficients for use in radiological protection against external radiation. ICRP Publication 74. Ann. ICRP 26(3/4).

ICRP, 2002. Basic anatomical and physiological data for use in radiological protection: reference values. ICRP Publication 89. Ann. ICRP 32(3/4).

ICRP, 2007. The 2007 Recommendations of the International Commission on Radiological Protection. ICRP Publication 103. Ann. ICRP 37(2–4).

ICRP, 2009. Adult reference computational phantoms. ICRP Publication 110. Ann. ICRP 39(2).

ICRU, 1998. Conversion Coefficients for use in Radiological Protection Against External Radiation. ICRU Report 57. International Commission on Radiation Units and Measurements, Bethesda, MD.

Iwase, H., Niita, K., Nakamura, T., 2002. Development of a general-purpose particle and heavy ion transport Monte Carlo code. J. Nucl. Sci. Technol. 39, 1142–1151.

Kawrakow, I., Mainegra-Hing, E., Rogers, D.W.O., et al., 2009. The EGSnrc Code System: Monte Carlo Simulation of Electron and Photon Transport. PIRS Report 701. National Research Council of Canada, Ottawa.

Niita, K., Sato, T., Iwase, H., et al., 2006. PHITS – a particle and heavy ion transport code system. Radiat. Meas. 41, 1080–1090.

Niita, K., Matsuda, N., Iwamoto, Y., et al., 2010. PHITS – Particle and Heavy Ion Transport Code System, Version 2.23. JAEA-Data/Code 2010-022. Japan Atomic Energy Agency, Tokai-mura.

Pelowitz, D.B., 2008. MCNPX User's Manual, Version 2.6.0. LA-CP-07-1473. Los Alamos National Laboratory, Los Alamos, NM.

Waters, L.S., 2002. MCNPX User's Manual, Version 2.3.0. Report LA-UR-02-2607. Los Alamos National Laboratory, Los Alamos, NM.

GLOSSARY

Absorbed dose, D

The absorbed dose is given by:

$$D = \frac{\mathrm{d}\bar{\varepsilon}}{\mathrm{d}m}$$

where $\mathrm{d}\bar{\varepsilon}$ is the mean energy imparted by ionising radiation to matter of mass $\mathrm{d}m$. The unit of absorbed dose is joule per kilogram (J/kg), and its special name is gray (Gy).

Active (bone) marrow

Active marrow is haematopoietically active and gets its red colour from the large numbers of erythrocytes (red blood cells) being produced. Active bone marrow serves as a target tissue for radiogenic risk of leukaemia.

Ambient dose equivalent, $H^*(10)$

The dose equivalent at a point in a radiation field that would be produced by the corresponding expanded and aligned field in the ICRU sphere at depth of 10 mm on the radius opposing the direction of the aligned field. The unit of ambient dose equivalent is joule per kilogram (J/kg), and its special name is sievert (Sv).

Bone marrow

Bone marrow is a soft, highly cellular tissue that occupies the cylindrical cavities of long bones and the cavities defined by the bone trabeculae of the axial and appendicular skeleton. Total bone marrow consists of a sponge-like, reticular, connective tissue framework called stroma, myeloid (blood-cell-forming) tissue, fat cells (adipocytes), small accumulations of lymphatic tissue, and numerous blood vessels and sinusoids. There are two types of bone marrow: red (active) and yellow (inactive). See 'Active (bone) marrow'; 'Inactive (bone) marrow'.

Bone surfaces

See 'Endosteum'.

Charged-particle equilibrium

Charged-particle equilibrium in a volume of interest means that the energies, numbers, and directions of the charged particles are constant throughout this volume. This is equivalent to saying that the distribution of charged-particle energy radiance does not vary within the volume. In particular, it follows that the sums of the energies (excluding rest energies) of the charged particles entering and leaving the volume are equal.

Cross section, σ

The cross section of a target entity, for a particular interaction produced by incident charged or uncharged particles of a given type and energy, is given by:

$$\sigma = \frac{N}{\Phi}$$

where N is the mean number of such interactions per target entity subjected to the particle fluence, Φ. The unit of cross section is m^2. A special unit often used for the cross section is the barn, where 1 barn (b) = 10^{-28} m^2. A full description of an interaction process requires, *inter alia*, knowledge of the distributions of cross sections in terms of energy and direction of all emergent particles from the interaction. Such distributions, sometimes called 'differential cross sections', are obtained by differentiations of σ with respect to energy and solid angle.

Deterministic effect

See 'Tissue reaction'.

Directional dose equivalent, $H'(d,\Omega)$

The dose equivalent at a point in a radiation field that would be produced by the corresponding expanded field in the ICRU sphere at a depth, d, on a radius in a specified direction, Ω. The unit of directional dose equivalent is joule per kilogram (J/kg), and its special name is sievert (Sv).

Dose conversion coefficient

A coefficient relating a dose quantity to a physical quantity, both for internal and external radiation exposure. For external exposure, the physical quantity 'fluence' or 'air kerma' is chosen. In internal dosimetry, this term is also called a 'dose coefficient'.

Dose equivalent, H

The dose equivalent at a point in tissue is given by:

$$H = DQ$$

where D is the absorbed dose and Q is the quality factor at that point. The unit of dose equivalent is joule per kilogram (J/kg), and its special name is sievert (Sv).

Dose limit

Recommended value of the effective dose or the organ- or tissue-equivalent dose to an individual that shall not be exceeded in planned exposure situations.

Dose–response function (DRF)

A particular function used in this publication to represent the absorbed dose in a target region per particle fluence in that region, derived using models of the microscopic structure of the target region geometry and the transport of the secondary ionising radiations in those regions.

Effective dose, E

The tissue weighted sum of equivalent doses in all specified organs and tissues of the body, given by the expression:

$$E = \sum_{\mathrm{T}} w_{\mathrm{T}} \sum_{\mathrm{R}} w_{\mathrm{R}} D_{\mathrm{T,R}} = \sum_{\mathrm{T}} w_{\mathrm{T}} H_{\mathrm{T}}$$

where H_{T} is the equivalent dose in an organ or tissue T, $D_{\mathrm{T,R}}$ is the mean absorbed dose in an organ or tissue T from radiation of type R, and w_{T} is the tissue weighting factor. The sum is performed over organs and tissues considered to be sensitive to the induction of stochastic effects. The unit of effective dose is joule per kilogram (J/kg), and its special name is sievert (Sv).

Endosteum (or endosteal layer)

A 50-μm-thick layer covering the surfaces of the bone trabeculae in regions of trabecular spongiosa and those of the cortical surfaces of the medullary cavities within the shafts of all long bones. It is assumed to be the target tissue for radiogenic bone cancer. This target region replaces that previously introduced in ICRP *Publications 26* and *30* (ICRP, 1977, 1979) – the bone surfaces – which had been defined as a single-cell layer, 10 μm in thickness, covering the surfaces of both the bone trabeculae and the Haversian canals of cortical bone.

Equivalent dose, H_{T}

The equivalent dose in an organ or tissue T is given by:

$$H_{\mathrm{T}} = \sum_{\mathrm{R}} w_{\mathrm{R}} D_{\mathrm{T,R}}$$

where $D_{\mathrm{T,R}}$ is the mean absorbed dose from radiation of type R in the specified organ or tissue T, and w_{R} is the radiation weighting factor. The unit of equivalent dose is joule per kilogram (J/kg), and its special name is sievert (Sv).

Fluence, Φ

The quotient of dN by da, where dN is the number of particles incident on a sphere of cross-sectional area da, thus:

$$\Phi = \frac{\mathrm{d}N}{\mathrm{d}a}$$

The unit of fluence is m^{-2}.

ICRU 4-element tissue

ICRU 4-element tissue has a density of 1 g/cm^3 and a mass composition of 76.2% oxygen, 11.1% carbon, 10.1% hydrogen, and 2.6% nitrogen. The ICRU sphere has this assumed composition.

Inactive (bone) marrow

In contrast to the active marrow, the inactive marrow is haematopoietically inactive (i.e. does not directly support haematopoiesis). It gets its yellow colour from fat cells (adipocytes) which occupy most of the space of the yellow bone marrow framework.

Kerma, K

Quantity for ionising uncharged particles, defined by the quotient of dE_{tr} by dm, where dE_{tr} is the mean sum of the initial kinetic energies of all the charged particles liberated in a mass dm of a material by the uncharged particles incident on dm, thus:

$$K = \frac{dE_{\mathrm{tr}}}{dm}$$

The unit of kerma is joule per kilogram (J/kg), and its special name is gray (Gy).

Kerma approximation

Kerma is sometimes used as an approximation to the absorbed dose. The numerical value of kerma approaches that of the absorbed dose to the degree that charged-particle equilibrium exists, that radiative losses are negligible, and that the kinetic energy of the uncharged particles is large compared with the binding energy of the liberated charged particles.

Linear energy transfer/unrestricted linear energy transfer, L or LET

The quotient of dE by dl, where dE is the mean energy lost by the charged particle due to electronic interactions in traversing a distance dl, thus:

$$L = \frac{dE}{dl}$$

The unit of linear energy transfer is joule per metre (J/m), often given in keV/μm.

Marrow cellularity

The fraction of bone marrow volume in a given bone that is haematopoietically active. Age- and bone-site-dependent reference values for marrow cellularity are given in Table 41 of ICRP *Publication 70* (ICRP, 1995). As a first approximation, marrow cellularity may be thought of as 1 minus the fat fraction of bone marrow.

Mean absorbed dose in an organ or tissue, D_{T}

The mean absorbed dose in a specified organ or tissue T, is given by:

$$D_{\mathrm{T}} = \frac{1}{m_{\mathrm{T}}} \int_{m_{\mathrm{T}}} D \, dm$$

where m_{T} is the mass of the organ or tissue, and D is the absorbed dose in the mass element dm. The unit of mean absorbed dose is joule per kilogram (J/kg), and its special name is gray (Gy). The mean absorbed dose in an organ is sometimes termed *organ dose*.

Occupational exposure

The radiation exposure of workers incurred as a result of their work. ICRP limits its use of 'occupational exposures' to radiation exposures incurred at work as a result of situations that can reasonably be regarded as being the responsibility of the operating management.

Operational quantities

Quantities used in practical applications for monitoring and investigating situations involving external exposure and intakes of radionuclides. They are defined for measurements and assessment of doses in the body.

Organ absorbed dose or organ dose

Short phrase for 'mean absorbed dose in an organ or tissue'.

Organ-equivalent dose

Short phrase for 'equivalent dose in an organ or tissue'.

Personal dose equivalent, $H_p(d)$

The dose equivalent in soft tissue at an appropriate depth, d, below a specified point on the human body. The soft tissue is ICRU 4-element tissue. The unit of personal dose equivalent is joule per kilogram (J/kg), and its special name is sievert (Sv). The specified point is usually given by the position where the individual dosemeter is worn. For the assessment of effective dose, a depth of 10 mm is recommended, and for the assessment of equivalent dose to the skin and the lens of the eye, depths of 0.07 mm and 3 mm, respectively, are recommended.

Protection quantities

Dose quantities related to the human body that ICRP has developed for radiological protection to allow quantification of the detriment to people from exposure to ionising radiation from both whole- and partial-body external irradiation and from intakes of radionuclides.

Quality factor, Q

The quality factor at a point in tissue, is given by:

$$Q = \frac{1}{D} \int_{L=0}^{\infty} Q(L) D_L \mathrm{d}L$$

where D is the absorbed dose at that point, D_L is the distribution of D in unrestricted linear energy transfer L at the point of interest, and $Q(L)$ is the quality factor as a function of L. The integration is to be performed over D_L, due to all charged particles, excluding their secondary electrons.

Red (bone) marrow

See 'Active (bone) marrow'.

Radiation weighting factor, w_R

A dimensionless factor by which the organ or tissue absorbed dose is multiplied to reflect the relative biological effectiveness of high-LET radiations compared with photon radiations. It is used to derive the equivalent dose from the mean absorbed dose in an organ or tissue.

Reference Male and Reference Female (Reference Individual)

An idealised male or female with characteristics defined by ICRP for the purpose of radiological protection, and with the anatomical and physiological characteristics defined in ICRP *Publication 89* (ICRP, 2002).

Reference Person

An idealised person for whom the equivalent doses in organs and tissues are calculated by averaging the corresponding doses of Reference Male and Reference Female. The equivalent doses of Reference Person are used for calculation of the effective dose.

Reference phantom

The computational phantom of the human body (male or female voxel phantom based on medical imaging data) defined in ICRP *Publication 110* (ICRP, 2009) with the anatomical and physiological characteristics defined in ICRP *Publication 89* (ICRP, 2002).

Reference value

Value of a quantity recommended by ICRP for use in dosimetric applications or biokinetic models. Reference values are fixed and specified with no uncertainty, independent of the fact that the basis of these values includes many uncertainties.

Response function

See 'Dose–response function'.

Spongiosa

Term referring to the combined tissues of the bone trabeculae and marrow tissues (both active and inactive) located within cortical bone cortices across regions of the axial and appendicular skeleton. Spongiosa is one of three bone regions defined in the ICRP *Publication 110* (ICRP, 2009) reference phantoms, the other two being cortical bone and medullary marrow of the long bone shafts. As the relative proportions of trabecular bone, active marrow, and inactive marrow vary with skeletal site, the homogeneous elemental composition and mass density of spongiosa is not constant but varies with skeletal site [see Annex B of ICRP *Publication 110* (ICRP, 2009)].

Tissue reaction

Injury in populations of cells, characterised by a threshold dose and an increase in the severity of the reaction as the dose is increased further. Also termed 'deterministic effect'. In some cases, these effects are modifiable by postirradiation procedures including biological response modifiers.

Tissue weighting factor, w_T

The factor by which the equivalent dose in an organ or tissue T is weighted to represent the relative contribution of that organ or tissue to overall radiation detriment from stochastic effects (ICRP, 1991). It is defined such that:

$$\sum_{T} w_T = 1$$

Voxel phantom

Computational anthropomorphic phantom based on medical tomographic images in which the anatomy is described by small three-dimensional volume elements (voxels). Collections of these voxels are used to specify the organs and tissues of the human body.

Yellow (bone) marrow

See 'Inactive (bone) marrow'.

References

ICRP, 1977. Recommendations of the International Commission on Radiological Protection. ICRP Publication 26. Ann. ICRP 1(3).

ICRP, 1979. Limits for intakes of radionuclides by workers. Part 1. ICRP Publication 30. Ann. ICRP 2(3/4).

ICRP, 1991. 1990 Recommendations of the International Commission on Radiological Protection. ICRP Publication 60. Ann. ICRP 21(1–3).

ICRP, 1995. Basic anatomical and physiological data for use in radiological protection: the skeleton. ICRP Publication 70. Ann. ICRP 25(2).

ICRP, 2002. Basic anatomical and physiological data for use in radiological protection: reference values. ICRP Publication 89. Ann. ICRP 32(3/4).

ICRP, 2009. Adult reference computational phantoms. ICRP Publication 110. Ann. ICRP 39(2).

1. INTRODUCTION

(1) Practical radiological protection for workers and the general public uses dosimetric quantities that quantify the exposure of humans to ionising radiation appropriately for implementation of the fundamental principles of limitation and optimisation. For the implementation of regulations and guidelines, and demonstration of regulatory compliance, ICRP and ICRU developed a system of protection and operational dosimetric quantities based on reference data, models, and phantoms.

(2) In 2007, the ICRP revised its basic recommendations for a system of radiological protection given previously in ICRP *Publication 60* (ICRP, 1991). The 2007 Recommendations, issued in ICRP *Publication 103* (ICRP, 2007), update, consolidate, and develop additional guidance on the control of exposure from radiation sources published since 1990. They maintain the ICRP Commission's three fundamental principles of radiological protection, namely justification, optimisation, and the application of dose limits, but clarify how they apply to radiation sources delivering exposure and to individuals receiving exposure. Among other revisions, the 2007 Recommendations update the values of radiation and tissue weighting factors in the quantities 'equivalent dose' and 'effective dose', and update the underlying calculation of radiation detriment based on the latest available scientific information regarding the radiobiological consequences of radiation exposure.

(3) The concept and use of equivalent and effective dose remain unchanged, but a number of revisions have been made to the methods used in their calculation. Reviews of the range of available data on the relative biological effectiveness of different radiations at low doses, together with biophysical considerations, have led to changes in the values of radiation weighting factors, w_R, used for neutrons and protons, with values for neutrons presently given as a continuous function of the incident or emitted neutron energy. A value of w_R for charged pions has also been included. Radiation weighting factors for photons, electrons, muons, and alpha particles are unchanged from those given in ICRP *Publication 60* (ICRP, 1991). Furthermore, revisions were made to the tissue weighting factors, w_T, that account for differences in the radiosensitivities of different organs and tissues to stochastic health effects. On the basis of epidemiological studies of cancer induction in exposed populations, and risk estimates for heritable effects, a set of new w_T values was chosen based on the respective values of relative radiation detriment. They represent mean values for humans chosen to apply to both sexes and all ages, and thus do not relate to any given individual.

(4) A further important change is that doses from external and internal sources are now calculated using the ICRP/ICRU reference computational phantoms of the human body (ICRP, 2007). In the past, the Commission did not specify a particular phantom, and various mathematical phantoms such as hermaphrodite medical internal radiation dose (MIRD)-type phantoms (Snyder et al., 1969), the sex-specific models of Kramer et al. (1982), and the age-specific phantoms of Cristy and Eckerman (1987) have been used. Voxel models, constructed from medical image

data of real people, give a more realistic description of the human body than afforded in mathematical (or stylised) phantoms. Thus, ICRP and ICRU decided to use voxel models to define their reference phantoms for use in the calculation of dose distribution in the body for both external and internal exposures. The models (or computational phantoms), described in ICRP *Publication 110* (ICRP, 2009), represent the adult Reference Male and Reference Female, and have organ masses in compliance with the reference anatomical values compiled in ICRP *Publication 89* (ICRP, 2002). These phantoms are designed specifically for calculation of the radiological protection quantities corresponding to the effective dose concept of the 2007 Recommendations (ICRP, 2007). The DOCAL ICRP Task Group is presently developing a series of 10 additional reference phantoms of pediatric ages – newborn, 1-year-old, 5-year-old, 10-year-old, and 15-year-old male and female.

(5) The voxel reference models are thus computational representations of Reference Male and Reference Female and can be used, together with codes that simulate the radiation transport and energy deposition, for assessment of the mean absorbed dose, D_T, in an organ or tissue T, from which equivalent dose and effective dose can be calculated successively.

(6) Equivalent dose in an organ or tissue is calculated by summing the product of absorbed dose in that organ or tissue and the radiation weighting factor over all types of radiations involved. Effective dose is calculated by summing the product of the sex-averaged equivalent dose and tissue weighting factor over all organs and tissues of the human body considered in its definition. The tissue weighting factors are based on updated risk data and are intended to apply as rounded values to a population of both sexes and all ages. Hence, conversion coefficients for the effective dose are calculated for Reference Person and not for any specific individual.

(7) Two sets of quantities are of importance in radiological protection: protection quantities (e.g. equivalent dose and effective dose) and operational quantities (e.g. ambient dose equivalent and personal dose equivalent, defined for use as measurable surrogates of the protection quantities). Compliance with dose limits is expressed in terms of protection quantities and, for external radiations, is demonstrated by determination of the appropriate operational quantity.

(8) The three principal protection quantities remain the mean absorbed dose in an organ or tissue, D_T; the equivalent dose in an organ or tissue, H_T; and the effective dose, E. The protection quantities can be related by calculation to the radiation field in which the exposure occurs. To form a bridge between the protection quantities and the radiation field, ICRU has developed operational quantities for measurement of exposures to external radiations (ICRU, 1985).

(9) The operational quantities are the ambient dose equivalent, $H^*(d)$; the directional dose equivalent, $H'(d,\Omega)$; and the personal dose equivalent, $H_p(d)$. These operational quantities and other related quantities used in radiation protection dosimetry are described in ICRU Report 51 (ICRU, 1993) and ICRU Report 66 (ICRU, 2001).

(10) The 2007 Recommendations (ICRP, 2007) require a review of many of the basic data used in the protection against exposure to sources of ionising radiations, both internal and external to the human body. This report is solely concerned with the implications for external exposure.

(11) The purpose of this report is to present conversion coefficients for the protection quantities for exposure to external radiation, and to investigate their relationships with the operational quantities that are currently in use (ICRU, 1993).

(12) Recent radiation epidemiology studies have indicated that the threshold of cataract induction might be much lower than previously assumed; for absorbed dose, the threshold for the lens of the eye is now considered to be 0.5 Gy (ICRP, 2012). The dose to the lens of the eye represents the mean dose to the entire lens and, under conditions of a high dose gradient within the lens, may not represent the dose to radiosensitive cell layers responsible for cataract formation. The present report addresses this issue, and gives absorbed dose conversion coefficients for the lens of the eye as obtained by Monte Carlo methods using a stylised model of the eye at a resolution finer than afforded within the fixed voxel structure of the ICRP reference phantoms.

(13) Dose conversion coefficients relating to physical quantities (e.g. particle fluence or air kerma) have been produced for idealised irradiation geometries, monoenergetic radiations for the adult reference computational phantoms, and a stylised head phantom for assessment of dose to the lens of the eye. The data given here are intended to provide the basis for comparison between the protection and operational quantities, and to examine the impact of the 2007 Recommendations (ICRP, 2007) on these quantities. The review of data by the Joint Task Group provides an authoritative and stable data set for application to dosimetry in radiological protection.

1.1. References

Cristy, M., Eckerman, K.F., 1987. Specific Absorbed Fractions of Energy at Various Ages from Internal Photon Sources. Vol. 1–7. ORNL Report TM-8381/Vol. 1–7. Oak Ridge National Laboratory, Oak Ridge, TN.

ICRP, 1991. 1990 Recommendations of the International Commission on Radiological Protection. ICRP Publication 60. Ann. ICRP 21(1–3).

ICRP, 2002. Basic anatomical and physiological data for use in radiological protection: reference values. ICRP Publication 89. Ann. ICRP 32(3/4).

ICRP, 2007. The 2007 Recommendations of the International Commission on Radiological Protection. ICRP Publication 103. Ann. ICRP 37(2–4).

ICRP, 2009. Adult reference computational phantoms. ICRP Publication 110. Ann. ICRP 39(2).

ICRP, 2012. ICRP statement on tissue reactions and early and late effects of radiation in normal tissues and organs: threshold doses for tissue reactions in a radiation protection context. ICRP Publication 118. Ann. ICRP 41(1–3).

ICRU, 1985. Determination of Dose Equivalents Resulting from External Radiation Sources. ICRU Report 39. International Commission on Radiation Units and Measurements, Bethesda, MD.

ICRU, 1993. Quantities and Units in Radiation Protection Dosimetry. ICRU Report 51. International Commission on Radiation Units and Measurements, Bethesda, MD.

ICRU, 2001. Determination of Operational Dose Equivalent Quantities for Neutrons. ICRU Report 66. International Commission on Radiation Units and Measurements, Bethesda, MD.

Kramer, R., Zankl, M., Williams, G., et al., 1982. The Calculation of Dose from External Photon Exposures Using Reference Human Phantoms and Monte Carlo Methods. Part I: the Male (Adam) and Female (Eva) Adult Mathematical Phantoms. GSF Report S-885. GSF – National Research Centre for Environment and Health, Neuherberg.

Snyder, W.S., Ford, M.R., Warner, G.G., et al., 1969. Estimates of absorbed fractions for monoenergetic photon sources uniformly distributed in various organs of a heterogeneous phantom. Medical Internal Radiation Dose Committee Pamphlet No. 5. J. Nucl. Med. 10 (Suppl. 3).

2. QUANTITIES USED IN RADIATION PROTECTION FOR EXTERNAL EXPOSURE

(14) The description and quantification of ionising radiation exposures to humans requires the definition of specific quantities and units. The definitions recommended by ICRU and ICRP are given in their various reports and publications (ICRU, 1985, 1993, 2001, 2011; ICRP, 2007). This report presents the definitions of quantities that are relevant for use in radiological protection for external exposure.

2.1. Fluence and kerma

(15) A radiation field of a specific type is fully described by the number of particles N, their distributions in energy and direction, and their temporal distribution. This specification requires the definition of both scalar and vector quantities. Definitions of radiation field quantities are given in detail in ICRU Report 85a (ICRU, 2011), which is a revision of ICRU Report 60 (ICRU, 1998a). While vector quantities providing information on direction distributions are mainly applied in both radiation transport theory and calculations, scalar quantities such as particle fluence or kerma are often used in dosimetry applications.

(16) Radiation field quantities can be defined at any point in a radiation field. Radiation fields can consist of various types of particles, and field quantities that are based on particle numbers are always related to a specific particle type. This is often expressed by adding the particle name to the quantity (e.g. neutron fluence). The quantity 'fluence' is based on the concept of counting the number of particles incident or passing through a small sphere of the irradiated medium.

(17) Fluence, Φ, is the quotient of $\mathrm{d}N$ by $\mathrm{d}a$, where $\mathrm{d}N$ is the number of particles incident on a sphere of cross-sectional area $\mathrm{d}a$, thus:

$$\Phi = \frac{\mathrm{d}N}{\mathrm{d}a} \tag{2.1}$$

The unit of fluence is m^{-2}.

(18) Fluence is independent of the direction distribution of the particles entering the sphere. In radiation transport calculations, fluence is frequently expressed in terms of the length of particle trajectories. Fluence, Φ, is then given by:

$$\Phi = \frac{\mathrm{d}l}{\mathrm{d}V} \tag{2.2}$$

where $\mathrm{d}l$ is the sum of the particle trajectories in the volume $\mathrm{d}V$.

(19) The transfer of energy from uncharged particles (indirectly ionising particles such as photons and neutrons) to matter is through the liberation and slowing down of secondary charged particles in this matter. This phenomenon leads to the definition of the quantity 'kerma'. Kerma, K, for ionising uncharged particles is the quotient of $\mathrm{d}E_{\mathrm{tr}}$ by $\mathrm{d}m$, where $\mathrm{d}E_{\mathrm{tr}}$ is the mean sum of the initial kinetic energies of all the charged particles liberated in a mass $\mathrm{d}m$ of material by the uncharged particles incident on $\mathrm{d}m$. It is given by:

$$K = \frac{\mathrm{d}E_{\mathrm{tr}}}{\mathrm{d}m} \tag{2.3}$$

The unit of kerma is J/kg, and its special name is gray (Gy).

2.2. Dose quantities used for radiological protection

(20) For more than 50 years, ICRP has supported a system for radiological protection based on concepts, quantities, and basic recommendations. The most recent set of protection quantities recommended in ICRP *Publication 103* (ICRP, 2007) includes the mean absorbed dose in an organ or tissue (also called 'organ absorbed dose' or 'organ dose'), D_{T}; the equivalent dose in an organ or tissue (also called 'organ equivalent dose'), H_{T}; and the effective dose, E. The equivalent and effective dose are not measurable but can be calculated if the exposure conditions are known. They are used for specifying limits in radiation protection of occupationally exposed persons and members of the public (see Section 2.2.4).

2.2.1. Absorbed dose

(21) In radiological protection, radiation biology, and clinical radiology, the absorbed dose, D, is the basic physical dose quantity. It is used for all types of ionising radiation and for any irradiation geometry.

(22) Absorbed dose, D, is defined as the quotient of $\mathrm{d}\bar{\varepsilon}$ by $\mathrm{d}m$, where $\mathrm{d}\bar{\varepsilon}$ is the mean energy imparted by ionising radiation to matter of mass $\mathrm{d}m$, that is:

$$D = \frac{\mathrm{d}\bar{\varepsilon}}{\mathrm{d}m} \tag{2.4}$$

The unit of absorbed dose is J/kg, and its special name is gray (Gy).

(23) While the value of kerma depends solely on interactions in the material of mass element $\mathrm{d}m$, the value of absorbed dose for uncharged particles also depends on the secondary charged particles that are released in the surroundings of the mass element $\mathrm{d}m$ and which enter this element. Absorbed dose is derived from the mean value of the stochastic quantity of energy imparted, ε, and does not reflect the random fluctuations of the interaction events in tissue. While it is defined at any point in matter, its value is obtained as an average over $\mathrm{d}m$ and hence over many atoms or molecules of matter. Generally, absorbed dose is a measurable quantity, and primary standards exist to allow its determination by measurement.

(24) In the definition of radiological protection quantities, no attempts are made to specify the stochastic distribution of physical processes at a microscopic level. Instead of considering such distribution functions explicitly, a pragmatic and empirical approach has been adopted to take account of differences in radiation quality. Radiation weighting factors are dimensionless factors by which the organ or tissue absorbed doses are multiplied to reflect the higher biological effectiveness of high-linear energy transfer (LET) radiations compared with low-LET radiations. The values are chosen to take into account the differences in distribution of energy deposited in

microscopic regions, through judgements based on the results of radiobiological experiments and epidemiological studies. The weighting factor values are related to the particle types of the incident radiation or, for internal sources, to the particles emitted from the source.

2.2.2. Mean absorbed dose

(25) The quantity 'absorbed dose' is defined to give a specific value at any point in matter. However, in practical applications, absorbed doses are often averaged over larger tissue volumes. It is assumed that, for low doses, the mean value of absorbed dose in a specific organ or tissue can be correlated with radiation detriment from stochastic effects in all parts of that organ or tissue with sufficient accuracy for the purposes of radiological protection.

(26) The mean absorbed dose in a region of an organ or tissue T is defined by:

$$D_{\mathrm{T}} = \frac{1}{m_{\mathrm{T}}} \int_{m_{\mathrm{T}}} D \, \mathrm{d}m \tag{2.5}$$

where m_{T} is the mass of the organ or tissue, and D is the absorbed dose in the mass element dm. The mean absorbed dose, D_{T}, equals the ratio of the mean energy imparted to the organ or tissue, $\bar{\varepsilon}_{\mathrm{T}}$, and m_{T}, the mass of the organ or tissue, thus:

$$D_{\mathrm{T}} = \frac{\bar{\varepsilon}_{\mathrm{T}}}{m_{\mathrm{T}}} \tag{2.6}$$

The unit of mean absorbed dose is J/kg, and its special name is gray (Gy). The mean absorbed dose in an organ is sometimes termed *organ dose*.

2.2.3. Equivalent dose and radiation weighting factors

(27) The definition of protection quantities is based on the mean absorbed dose, $D_{\mathrm{T,R}}$, in the volume of a specified organ or tissue T due to radiation of type R. The radiation R is given by the type and energy of radiation either incident on the body or emitted by radionuclides residing within the body. The protection quantity 'equivalent dose' in an organ or tissue, H_{T}, is then defined by:

$$H_{\mathrm{T}} = \sum_{\mathrm{R}} w_{\mathrm{R}} D_{\mathrm{T,R}} \tag{2.7}$$

where w_{R} is the radiation weighting factor for radiation R (incident to the body in the case of external exposure). The sum is performed over all types of radiations involved. The unit of equivalent dose is J/kg, and its special name is sievert (Sv).

(28) The values of w_{R} for neutrons and protons given in ICRP *Publication 103* (ICRP, 2007) and shown in Table 2.1 differ from those given in *Publication 60* (ICRP, 1991), and a value for charged pions has been included.

Photons, electrons, and muons

(29) Electrons, muons, and secondary particles generated by photons are radiations with LET values generally less than 10 keV/μm. These radiations have always

Table 2.1 Radiation weighting factors, w_R.

Radiation type*	Radiation weighting factor, w_R
Photons	1
Electrons and muons	1
Protons and charged pions	2
Alpha particles, fission fragments, heavy ions	20
Neutrons	A continuous curve as a function of neutron energy [see Fig. 2.1 and Eq. (2.8)]

Source: ICRP (2007). The 2007 Recommendations of the International Commission on Radiological Protection. ICRP Publication 103. Ann. ICRP 37(2–4).

*All values relate to the radiation incident on the body or, for internal sources, emitted from the source.

been given a radiation weighting of 1. This simplification is only sufficient for the intended application of equivalent dose and effective dose (e.g. for dose limitation and assessment, and control of doses in the low-dose range). In cases for which individual retrospective risk assessments have to be made, more detailed information on the radiation field and appropriate relative biological effectiveness values need to be considered if relevant data are available. Heterogeneity of the radiation dose within cells, as can occur with tritium or Auger emitters incorporated into DNA, also require specific analysis. Equivalent dose and effective dose are not appropriate quantities for use in such assessments [see ICRP *Publication 103* (ICRP, 2007)].

Neutrons

(30) The biological effectiveness of neutrons incident on the human body is strongly dependent on neutron energy. Hence, the radiation weighting factor for

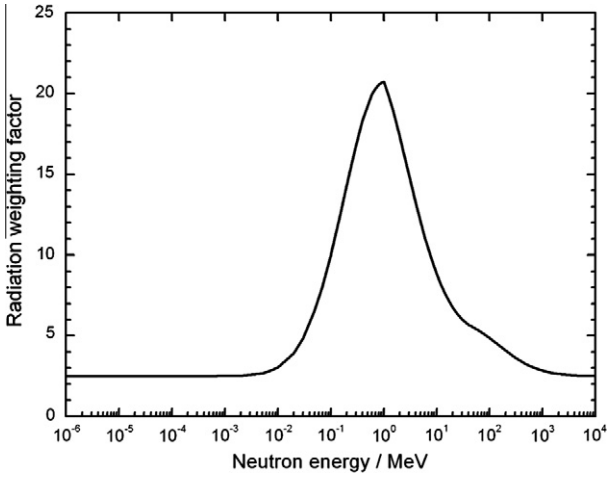

Fig. 2.1. Radiation weighting factor, w_R, for neutrons vs neutron kinetic energy.

neutrons is defined as a function of energy (Fig. 2.1; ICRP, 2007). The most significant changes compared with the data in ICRP *Publication 60* (ICRP, 1991) are the decrease of w_R in both the low-energy range and at neutron kinetic energies above 100 MeV (see Annex B of ICRP *Publication 103* for further explanation). The following continuous function in neutron energy, E_n (in MeV), is defined for the calculation of radiation weighting factors for neutrons:

$$w_R = \begin{cases} 2.5 + 18.2\,e^{-[\ln(E_n)]^2/6}, & E_n < 1 \text{ MeV} \\ 5.0 + 17.0\,e^{-[\ln(2E_n)]^2/6}, & 1 \text{ MeV} \leqslant E_n \leqslant 50 \text{ MeV} \\ 2.5 + 3.25\,e^{-[\ln(0.04E_n)]^2/6}, & E_n > 50 \text{ MeV} \end{cases} \tag{2.8}$$

Protons and pions

(31) For radiological protection purposes, a single w_R value of 2 has been adopted for protons of all energies, mainly based on radiobiological data for high-energy protons above 10 MeV. This has replaced the value of 5 recommended in ICRP *Publication 60* (ICRP, 1991).

(32) Pions are negatively or positively charged or neutral particles encountered in radiation fields resulting from interactions of primary cosmic rays with nuclei at high altitudes in the atmosphere. These particles contribute to exposures in aircraft and space, and are part of the complex radiation fields behind shielding of high-energy particle accelerators. A single w_R value of 2 is recommended for charged pions of all energies.

Alpha particles

(33) A single radiation weighting factor of 20 was recommended in the 1990 Recommendations (ICRP, 1991) and was not changed in the 2007 Recommendations (ICRP, 2007). Humans can be exposed to alpha particles from internal emitters (e.g. from inhaled radon progeny, or ingested alpha-emitting radionuclides such as radioisotopes of plutonium, polonium, radium, thorium, and uranium). For external exposure, alpha particles are of lesser importance because of their short range in tissue.

Fission fragments and heavy ions

(34) Doses from fission fragments are of importance in radiological protection, mainly in dosimetry of internal emitters. For external exposure, the situation regarding radiation weighting factors is similar to that for alpha particles, and a radiation weighting factor of 20 has been recommended by ICRP since the 1990 Recommendations (ICRP, 1991). For applications in space, where heavy charged particles contribute significantly to the total dose in the human body, a different approach to assessing the radiobiological effectiveness of heavy ions should be used.

2.2.4. Effective dose and tissue weighting factors

(35) The effective dose, E, introduced in ICRP *Publication 60* (ICRP, 1991), is defined as a weighted sum of tissue-equivalent doses:

$$E = \sum_{T} w_T \sum_{R} w_R D_{T,R} = \sum_{T} w_T H_T \tag{2.9}$$

where w_T is the tissue weighting factor for tissue T and $\sum w_T = 1$. The sum is performed over all organs and tissues of the human body considered to be sensitive to the induction of stochastic effects. These w_T values are chosen to represent the contributions of individual organs and tissues to the overall radiation detriment from stochastic effects. The unit of effective dose is J/kg, and its special name is sievert (Sv). The unit is the same for equivalent dose and effective dose, as well as for some operational dose quantities (see Section 2.3).

(36) The organs and tissues for which w_T values are specified, according to the 2007 Recommendations (ICRP, 2007), are given in Table 2.2.

(37) The w_T values represent mean values for humans averaged over both sexes and all ages, and thus do not relate to the characteristics of any particular individual (ICRP, 2007). The value of w_T for the remainder tissues (0.12) applies to the arithmetic mean dose of the 13 organs and tissues for each sex listed in the footnote of Table 2.2.

Determination of effective dose

(38) The procedure for determining the effective dose is shown schematically in Fig. 2.2. As shown, absorbed and equivalent doses are assessed separately for Reference Male and Reference Female. The sex-specific equivalent doses are then averaged resulting in equivalent doses for Reference Person. The sex-averaged equivalent doses of Reference Person are then weighted by the tissue weighting factors and summed over all organs and tissues given in Table 2.2. This entire procedure can also be applied to paediatric reference individuals.

(39) The quantities 'equivalent dose' and 'effective dose' are not measurable. For exposures to radiation from external sources, their values are determined by radiation monitoring using operational quantities, or by applying conversion coefficients that relate radiation field quantities to organ equivalent or effective dose. For the calculation of conversion coefficients for external exposure, computational phantoms are used for dose assessment in various radiation fields (see Chapter 3).

Table 2.2. Tissue weighting factors, w_T.

Tissue	w_T	$\sum w_T$
Red bone marrow, colon, lung, stomach, breast, remainder tissues*	0.12	0.72
Gonads	0.08	0.08
Bladder, oesophagus, liver, thyroid	0.04	0.16
Endosteum (bone surface), brain, salivary glands, skin	0.01	0.04
Total		1.00

Source: ICRP (2007). The 2007 Recommendations of the International Commission on Radiological Protection. ICRP Publication 103. Ann. ICRP 37(2–4).

*Remainder tissues: adrenals, extrathoracic region, gall bladder, heart, kidneys, lymphatic nodes, muscle, oral mucosa, pancreas, prostate (male), small intestine, spleen, thymus, and uterus/cervix (female).

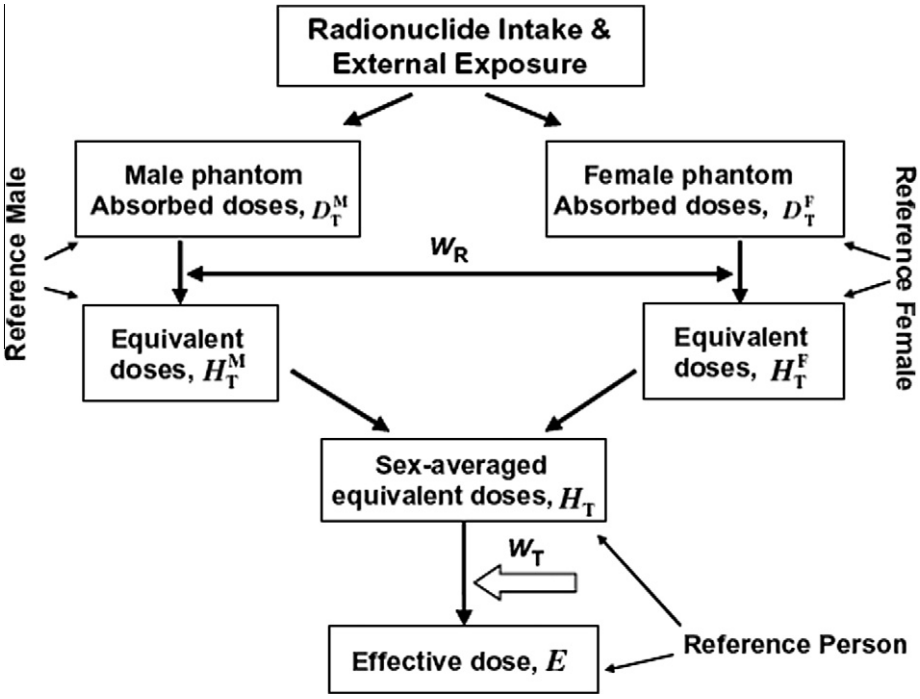

Fig. 2.2. Schematic for calculation of effective dose using sex-specific reference phantoms.

Reference phantoms

(40) The evaluation of equivalent doses for Reference Male and Reference Female, and of the effective dose to Reference Person, is based on the use of computational models or phantoms. In the past, ICRP did not specify a particular phantom, and various mathematical phantoms such as hermaphrodite medical internal radiation dose (MIRD)-type phantoms (Snyder et al., 1969), the sex-specific phantoms of Kramer et al. (1982), and the age-specific phantoms of Cristy and Eckerman (1987) have been used. ICRP now uses adult male and female reference computational phantoms for the calculation of equivalent doses for organs and tissues. The phantoms are based on medical tomographic images (ICRP, 2009). They are composed of small three-dimensional volume elements (voxels). The organ volumes have been adjusted and tissue densities have been given in order to approximate the reference organ masses assigned to Reference Male and Reference Female in ICRP *Publication 89* (ICRP, 2002).

(41) These models are computational representations of Reference Male and Reference Female, and are used to compute the mean absorbed dose, D_T, in an organ or tissue T from radiation fields external to the body, and from decay of radionuclides following their internal incorporation.

Sex averaging for effective dose

(42) For the purposes of radiological protection, a single value of effective dose is applied for both sexes. The tissue weighting factors of Table 2.2 are sex- and age-averaged values for all organs and tissues, including the male and female breast, and the gonads of both sexes. This averaging implies that the application of this approach is restricted to the determination of effective dose in radiological protection and, in particular, cannot be used for the assessment of individual risk. The effective dose is then computed from the equivalent doses assessed for organ or tissue T of Reference Male and Reference Female, according to the following equation:

$$E = \sum w_{\mathrm{T}} \left[\frac{H_{\mathrm{T}}^{\mathrm{M}} + H_{\mathrm{T}}^{\mathrm{F}}}{2} \right] \tag{2.10}$$

(43) Analogous to the approach for other organs and tissues, the equivalent dose to the remainder tissues is defined separately for the Reference Male and Reference Female, and these values are included in Eq. (2.10) (see Fig. 2.2). The equivalent dose to the remainder tissues is computed as the arithmetic mean of the equivalent doses to the 13 tissues for each sex as listed in the footnote to Table 2.2. The equivalent dose to the remainder tissues of Reference Male, $H_{\mathrm{rem}}^{\mathrm{M}}$, and Reference Female, $H_{\mathrm{rem}}^{\mathrm{F}}$, is determined as their sum:

$$H_{\mathrm{rem}}^{\mathrm{M}} = \frac{1}{13} \sum_{\mathrm{T}}^{13} H_{\mathrm{T}}^{\mathrm{M}} \text{ and } H_{\mathrm{rem}}^{\mathrm{F}} = \frac{1}{13} \sum_{\mathrm{T}}^{13} H_{\mathrm{T}}^{\mathrm{F}} \tag{2.11}$$

where T is a remainder tissue given in footnote of Table 2.2.

Table 2.3. Recommended dose limits in planned exposure situations.*

Type of limit	Annual dose limits	
	Occupational	Public
Effective dose	20 mSv, averaged over defined periods of 5 years¶	1 mSv**
Annual equivalent dose in:		
Lens of the eye	20 mSv, averaged over defined periods of 5 years†	15 mSv
Skin‡,§	500 mSv	50 mSv
Hands and feet	500 mSv	–

Source: ICRP (2007). The 2007 Recommendations of the International Commission on Radiological Protection. ICRP Publication 103. Ann. ICRP 37(2–4).

*Limits on effective dose are for the sum of the relevant effective doses from external exposure in the specified time period, and the committed effective dose from intakes of radionuclides in the same period.

†This annual limit was lowered from 150 mSv by ICRP in April 2011, with the further provision that the dose should not exceed 50 mSv in any single year.

‡The limitation on effective dose provides sufficient protection for the skin against stochastic effects.

§Averaged over 1 cm^2 area of skin regardless of the area exposed.

¶With the further provision that the effective dose should not exceed 50 mSv in any single year. Additional restrictions apply to the occupational exposure of pregnant women.

**In special circumstances, a higher value of effective dose could be allowed in a single year, provided that the average over 5 years does not exceed 1 mSv/year.

where T is a remainder tissue given in footnote of Table 2.2.

(44) The effective dose for protection purposes is based on the mean absorbed doses in organs or tissues of the human body. It is defined and estimated in Reference Person (see Fig. 2.2). This quantity provides a value that takes account of the specific exposure conditions of an individual but not of its individual properties. In particular, the tissue weighting factors are mean values representing an average over many individuals of both sexes.

2.2.5. Dose limits

(45) Dose limits only apply in planned exposure situations, but not to medical exposures of patients. In ICRP *Publication 103* (ICRP, 2007), the Commission concluded that the dose limits recommended in ICRP *Publication 60* (ICRP, 1991) continue to provide an appropriate level of protection. The nominal detriment coefficients established in ICRP *Publication 103* for both a workforce and the general public are consistent with, although numerically somewhat lower than, those given in ICRP *Publication 60*. These slight differences are of no practical significance (see Annex A of ICRP *Publication 103*). Within a category of exposure, occupational or public, dose limits apply to the sum of exposures from sources related to practices that are already justified. The recommended dose limits are summarised in Table 2.3.

2.3. Operational quantities

(46) The protection quantities 'equivalent dose' and 'effective dose' are not measurable, and therefore cannot be used directly as quantities in radiation monitoring. Operational quantities are, therefore, used for the assessment of effective dose or equivalent dose in tissues or organs for demonstration of compliance with regulations on occupational exposures and the application of the principle of as low as reasonably achievable, economic and societal factors being taken into account. The operational dose quantities, based on dose equivalent (see Section 2.3.1) and defined by ICRU for measurements in external radiation fields, are the ambient dose equivalent, the directional dose equivalent (see Section 2.3.2), and the personal dose equivalent (see Section 2.3.3). The first two quantities are used for area monitoring, while the last quantity is for individual monitoring.

(47) Operational quantities aim to provide a reasonable estimate, generally conservative, for the value of the protection quantities related to an exposure or potential exposure of persons under most irradiation conditions. They are often used in practical regulations or guidance. For monitoring of external radiation exposures, operational dose quantities as defined by ICRU (1985, 1998b) were introduced into radiological protection practice in many countries.

(48) It is important to determine if the operational quantities provide reasonable estimates of the newly specified effective dose and other protection quantities. Chapter 5 discusses this issue.

2.3.1. Dose equivalent

(49) The dose equivalent, H, is the product of Q and D at a point in tissue, where D is the absorbed dose and Q is the quality factor at that point, thus:

$$H = Q\,D \tag{2.12}$$

(50) The biological effectiveness of ionising radiation is seen to be strongly correlated with its energy deposition properties along the tracks of charged particles in tissue, especially with the ionisation density. For applications in radiological protection, the complex structure of such tracks is characterised by a single parameter, the unrestricted LET, L_∞. The quality factor, Q, is then defined as a function $Q(L)$ with the unrestricted LET of charged particles in water.

(51) The quality factor function $Q(L)$ is defined in ICRP *Publication 60* (ICRP, 1991) by the following:

$$Q(L) = \begin{cases} 1 & L < 10\ \text{keV}/\mu\text{m} \\ 0.32\,L - 2.2 & 10 \leqslant L\ 100\ \text{keV}/\mu\text{m} \\ 300/\sqrt{L} & L > 100\ \text{keV}/\mu\text{m} \end{cases} \tag{2.13}$$

(52) The function is the outcome of judgements taking account of results of radiobiological investigations on cellular and molecular systems, as well as the results from animal experimentation. The radiobiological database for the assessment of this function is largely unchanged since 1990 (see ICRP, 2003).

(53) The quality factor, Q, at a point in tissue is given by:

$$Q = \frac{1}{D}\int_{L=0}^{\infty} Q(L) D_L\,\mathrm{d}L \tag{2.14}$$

where D is the absorbed dose at that point, D_L is the distribution of D in linear energy transfer L, and $Q(L)$ is the corresponding quality factor at the point of interest. The integration is to be performed over L due to all charged particles, excluding their secondary electrons. This function is particularly important for neutrons because various types of secondary charged particles are produced in tissue by neutron interactions.

Table 2.4. Operational quantities for monitoring external exposures.

Task	Operational dose quantities	
	Area monitoring	Individual monitoring
Control of effective dose	Ambient dose equivalent $H^*(10)$	Personal dose equivalent $H_\mathrm{p}(10,\Omega)$
Control of doses to the skin, hands, wrist, and feet	Directional dose equivalent $H'(0.07,\Omega)$	Personal dose equivalent $H_\mathrm{p}(0.07,\Omega)$
Control of dose to the lens of the eye*	Directional dose equivalent $H'(3,\Omega)$	Personal dose equivalent $H_\mathrm{p}(3,\Omega)$

*If the monitoring devices are not designed to measure $H'(3,\Omega)$ or $H_\mathrm{p}(3)$, $H'(0.07,\Omega)$ and $H_\mathrm{p}(0.07)$ may be applied.

(54) For the different monitoring tasks of external exposures, area monitoring and individual monitoring, the scheme shown in Table 2.4 can be used to describe the application of the different operational dose quantities.

(55) There are situations in which personal dosimetry is not used but where area monitoring is applied to assess individual exposures. These situations include the assessment of doses to aircraft crew, prospective dose assessments, and assessment of doses in workplaces and in the natural environment.

2.3.2. Operational quantities for area monitoring

(56) For all types of external radiation, the operational quantities for area monitoring are defined on the basis of a dose-equivalent quantity that would exist in the ICRU sphere as a theoretical construct of tissue-equivalent material (30 cm in diameter, ICRU 4-element tissue with a density of 1 g/cm^3, and a mass composition of 76.2% oxygen, 11.1% carbon, 10.1% hydrogen, and 2.6% nitrogen). In most cases, this phantom adequately approximates the human body with regards to scattering and attenuation of radiation fields under consideration.

(57) The operational quantities for area monitoring defined in the ICRU sphere retain their character of a point quantity and the property of additivity. This is achieved by using a fixed depth in the definition of each quantity.

(58) An expanded radiation field is defined as a hypothetical field in which the fluence and its direction and energy distributions have the same value throughout the volume of interest as in the actual field at the point of reference. The expansion of the radiation field ensures that the whole ICRU sphere is exposed to a homogeneous radiation field with the same fluence, energy distribution, and direction distribution as in the point of interest of the real radiation field.

(59) If all radiation is aligned in the expanded radiation field so that it is opposed to a radius vector Ω specified for the ICRU sphere, the aligned and expanded radiation field is obtained. In this hypothetical radiation field, the ICRU sphere is homogeneously irradiated from one direction, and the fluence of the field is the integral of the direction distribution of fluence at the point of interest in the real radiation field. In the expanded and aligned radiation field, the value of the dose equivalent at any point in the ICRU sphere is independent of the direction distribution of the radiation that might exist in the real radiation field. Conversion coefficients relating radiation field quantities to the operational quantities for area monitoring are calculated for the particles at the point of interest in the real radiation field using the model of the expanded and aligned field and the ICRU sphere phantom, assuming a vacuum outside of the phantom.

Ambient dose equivalent, $H^*(10)$

(60) For area monitoring, the operational quantity for assessing effective dose is the ambient dose equivalent, $H^*(10)$, defined by ICRU (2001).

(61) The ambient dose equivalent, $H^*(10)$, at a point in a radiation field, is the dose equivalent that would be produced by the corresponding expanded and aligned field

in the ICRU sphere at a depth of 10 mm on the radius opposing the direction of the aligned field.

Directional dose equivalent, $H'(d, \Omega)$

(62) For area monitoring, the quantity for assessing the dose to the skin and the extremities (hands, wrists, and feet), as well as the dose to the lens of the eye, is the directional dose equivalent, $H'(d, \Omega)$, defined as follows: the directional dose equivalent, $H'(d, \Omega)$, at a point in a radiation field, is the dose equivalent that would be produced by the corresponding expanded field in the ICRU sphere at a depth, d, on a radius in a specified direction Ω.

(63) For assessing the dose to the skin and the extremities, $d = 0.07$ mm is used and $H'(d, \Omega)$ is then written as $H'(0.07, \Omega)$.

(64) In the case of monitoring the dose to the lens of the eye, the operational quantity $H'(d, \Omega)$ with $d = 3$ mm was recommended for use by ICRU. However, if the monitoring device is not designed to measure $H'(3, \Omega)$, $H'(0.07, \Omega)$ may be used as a surrogate.

2.3.3. Operational quantities for individual monitoring

(65) Individual monitoring of external exposure is usually performed with personal dosemeters worn on the body, and the operational quantity defined for this application takes this situation into account. For individual monitoring, the operational quantity is the personal dose equivalent, $H_p(d)$.

(66) The personal dose equivalent, $H_p(d)$, is the dose equivalent in ICRU soft tissue at an appropriate depth, d, below a specified point on the human body. Soft tissue for this purpose is defined as the ICRU 4-element tissue (ICRU, 1985) (see Glossary). The specified point on the human body for assessing the personal dose equivalent is governed by the task for which the individual dosemeter is worn.

(67) For assessment of the radiation protection quantity 'effective dose', a depth $d = 10$ mm is selected, and for assessing the equivalent dose to the skin, hands, wrists, and feet, a depth $d = 0.07$ mm is recommended. In special cases of monitoring the dose to the lens of the eye, a depth $d = 3$ mm has been proposed to be most appropriate.

2.4. References

Cristy, M., Eckerman, K.F., 1987. Specific Absorbed Fractions of Energy at Various Ages from Internal Photon Sources. Vol. 1–7. ORNL Report TM-8381/Vol. 1–7. Oak Ridge National Laboratory, Oak Ridge, TN.

ICRP, 1991. 1990 Recommendations of the International Commission on Radiological Protection. ICRP Publication 60. Ann. ICRP 21(1–3).

ICRP, 2002. Basic anatomical and physiological data for use in radiological protection: reference values. ICRP Publication 89. Ann. ICRP 32(3/4).

ICRP, 2003. Relative biological effectiveness (RBE), quality factor (Q), and radiation weighting factor (w_R). ICRP Publication 92. Ann. ICRP 33(4).

ICRP, 2007. The 2007 Recommendations of the International Commission on Radiological Protection. ICRP Publication 103. Ann. ICRP 37(2–4).

ICRP, 2009. Adult reference computational phantoms. ICRP Publication 110. Ann. ICRP 39(2).

ICRU, 1985. Determination of Dose Equivalents Resulting from External Radiation Sources. ICRU Report 39. International Commission on Radiation Units and Measurements, Bethesda, MD.

ICRU, 1993. Quantities and Units in Radiation Protection Dosimetry. ICRU Report 51. International Commission on Radiation Units and Measurements, Bethesda, MD.

ICRU, 1998a. Fundamental Quantities and Units for Ionizing Radiation. ICRU Report 60. International Commission on Radiation Units and Measurements, Bethesda, MD.

ICRU, 1998b. Tissue Substitutes, Phantoms and Computational Modelling in Medical Ultrasound. ICRU Report 61. International Commission on Radiation Units and Measurements, Bethesda, MD.

ICRU, 2001. Determination of Operational Dose Equivalent Quantities for Neutrons. ICRU Report 66. International Commission on Radiation Units and Measurements, Bethesda, MD.

ICRU, 2011. Fundamental Quantities and Units for Ionizing Radiation (Revised). ICRU Report 85a. International Commission on Radiation Units and Measurements, Bethesda, MD.

Kramer, R., Zankl, M., Williams, G., et al., 1982. The Calculation of Dose from External Photon Exposures Using Reference Human Phantoms and Monte Carlo Methods. Part I: the Male (Adam) and Female (Eva) Adult Mathematical Phantoms. GSF Report S-885. GSF – National Research Centre for Environment and Health, Neuherberg.

Snyder, W.S., Ford, M.R., Warner, G.G., et al., 1969. Estimates of absorbed fractions for monoenergetic photon sources uniformly distributed in various organs of a heterogeneous phantom. Medical Internal Radiation Dose Committee Pamphlet No. 5. J. Nucl. Med. 10 (Suppl. 3).

3. DETERMINATION OF ORGAN ABSORBED DOSES OF THE ICRP/ICRU REFERENCE PHANTOMS

3.1. The ICRP/ICRU reference computational phantoms

(68) For the computation of organ absorbed doses, the adult male and female reference computational phantoms, representing Reference Male and Reference Female (ICRP, 2007), were used in this report. These phantoms were adopted by ICRP and ICRU as the phantoms for computation of the ICRP/ICRU reference conversion coefficients and are described extensively in ICRP *Publication 110* (ICRP, 2009). The reference computational models are digital three-dimensional representations of human anatomy and are based on computed tomographic data of real people. They are consistent with the information given in ICRP *Publication 89* (ICRP, 2002) on the reference anatomical parameters for both male and female adults. The reference computational phantoms (or models) were constructed by modifying the voxel models (Golem and Laura) (Zankl and Wittmann, 2001; Zankl et al., 2005) of two individuals whose body height and mass closely resembled the reference data. The organ masses of both phantoms were adjusted to the ICRP data on Reference Male and Reference Female with high precision, without altering their realistic anatomy significantly. The phantoms contain all target regions relevant to the assessment of human exposure to ionising radiation for radiological protection purposes (i.e. all organs and tissues that contribute to the quantity 'effective dose') (ICRP, 2007).

(69) Each phantom is represented as a three-dimensional array of cuboid voxels, arranged in columns, rows, and slices. Each entry in the array identifies the organ or tissue to which the corresponding voxel belongs. The male reference computational phantom consists of ~1.95 million tissue voxels (excluding voxels representing the surrounding vacuum), each with a slice thickness (corresponding to the voxel height) of 8.0 mm and an in-plane resolution (i.e. voxel width and depth) of 2.137 mm, corresponding to a voxel volume of 36.54 mm^3. The number of slices is 220, resulting in a body height of 1.76 m. The body mass is 73 kg. The female reference computational phantom consists of ~3.89 million tissue voxels, each with a slice thickness of 4.84 mm and an in-plane resolution of 1.775 mm, corresponding to a voxel volume of 15.25 mm^3. The number of slices is 346, the body height is 1.63 m, and the body mass is 60 kg. The number of individually segmented structures is 136 in each phantom, and 53 different tissue compositions have been assigned to them. The various tissue compositions account for both the elemental composition of the tissue parenchyma (ICRU, 1992) and each organ's blood content (ICRP, 2002). Fig. 3.1 shows frontal (coronal) views of the male (left) and female (right) computational phantoms.

(70) Due to the limited resolution of the tomographic data on which these phantoms are based, and the very small dimensions of some of the source and target regions, not all tissues could be represented explicitly. In the skeleton, for example, the target tissues of interest are the red bone marrow in the marrow cavities of spongiosa

Fig. 3.1. Images of the male (left) and female (right) computational phantoms. The following organs can be identified by different surface colours: breast, bones, colon, eyes, lungs, liver, pancreas, small intestine, stomach, teeth, thyroid, and urinary bladder. Muscle and adipose tissue are displayed as transparent. For illustration purposes, the voxelised surfaces have been smoothed.

and the endosteal layer lining these cavities (presently assumed to be 50 μm in thickness). Due to their small dimensions, these two target tissues had to be incorporated as homogeneous constituents of spongiosa within the reference phantoms. At lower energies of photons and neutrons, secondary charged-particle equilibrium is not fully established in these tissue regions over certain energy ranges. More refined techniques for accounting for these effects in skeletal dosimetry are discussed in Section 3.4 and in Annexes D and E.

(71) Similarly, the fine structure of the lens of the eye could not be described by the voxel geometry of the reference phantoms. Therefore, a stylised model of the eye was

employed for a limited number of particles and irradiation geometries of interest to radiation protection of the lens of the eye (see Annex F). Moreover, the basal cells of the epidermis, the skin tissue at radiogenic risk, cannot be represented in the voxel geometry of the reference phantoms. Thus, localised skin dose per fluence values for electrons and alpha particles have been derived on a tissue-equivalent slab. The dose has been averaged over 50–100 μm, the depth of the sensitive layer of most parts of the skin (see Section 3.5 and Annex G).

3.2. Irradiation geometries considered

(73) To obtain the conversion coefficients for this report, calculations were carried out assuming whole-body irradiation of the phantoms, placed in a vacuum, by broad unidirectional beams assumed to represent occupational exposures. Some typical irradiation geometries are described in the following paragraphs. The geometries are shown schematically in Fig. 3.2.

3.2.1. Antero-posterior and postero-anterior geometries

(73) In antero-posterior (AP) geometry, the ionising radiation is incident on the front of the body in a direction orthogonal to its long axis. In postero-anterior (PA) geometry, the ionising radiation is incident on the back of the body in a direction orthogonal to its long axis.

3.2.2. Lateral geometry

(74) In lateral (LAT) geometry, the ionising radiation is incident from either side of the body in a direction orthogonal to the long axis of the body. LLAT and RLAT indicate left and right lateral geometries, respectively.

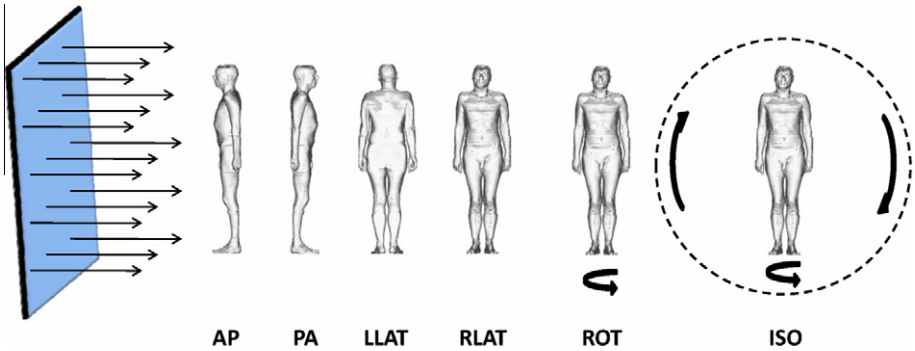

Fig. 3.2. Schematic representation of the idealised geometries considered. AP, antero-posterior; PA, postero-anterior; LLAT, left lateral; RLAT, right lateral; ROT, rotational; ISO, isotropic.

3.2.3. Rotational geometry

(75) In rotational (ROT) geometry, the body is irradiated by a parallel beam of ionising radiation, which rotates at a uniform rate around the long axis from a direction orthogonal to the long axis of the body. Alternatively, ROT geometry may be defined as a rotation of the body at a uniform rate about its long axis, while irradiating the body by a parallel beam of ionising radiation from a stationary source incident at right angles to the long axis of the body.

3.2.4. Isotropic geometry

(76) Isotropic (ISO) geometry is defined by a radiation field in which the particle fluence per solid angle is independent of direction and location in space.

(77) Although the geometries defined above are idealised, they may be taken as approximations to actual conditions of exposure. Thus, for example, AP, PA, and LAT geometries are considered to approximate radiation fields produced by single sources at large distances and particular body orientations, and thus they approximate real occupational exposure geometries. ROT geometry is seen as an approximation to an irradiation from a widely dispersed planar source (e.g. as would be likely from environmental contamination). This approximation results in radiation incident at right angles to the long axis of a person standing or walking about in the field. ROT geometry also approximates that of a person who moves randomly in the radiation field of sources irradiating at right angles to the long axis of the body. The ISO geometry approximates the radiation field to which a body is subjected, if suspended in a large cloud of radioactive gas or placed in a highly scattered radiation field. This geometry is often assumed for exposures in aircraft or in space, for irradiation by naturally occurring radionuclides in homes or the environment, or by atmospheric releases of radionuc1ides into the environment (i.e. a semi-spherical cloud).

(78) For the exposure situations described above, designed to simulate occupational radiation exposures, the body is assumed to be placed in a vacuum. Therefore, no scattering and absorption due to the air surrounding the body is considered.

3.3. General descriptions of the Monte Carlo codes used to simulate radiation transport

(79) The organ dose conversion coefficients were calculated specifically for this report by members of the DOCAL Task Group. For quality assurance purposes, several data sets were generated by different members of the Task Group using the same reference computational phantoms but different radiation transport codes.

(80) A detailed description of the methods used to calculate the absorbed dose distribution and dose-related quantities in the anthropomorphic phantoms is beyond the scope of this report. Only a brief review will be given here of the main characteristics of the radiation transport codes used to generate the organ absorbed doses presented.

(81) The Monte Carlo method of radiation transport calculations, as applied for these recommendations, first simulates the random emission of particles constrained by the specified energy and direction established by the irradiation geometry. The

interactions and subsequent path of the radiation in the phantom are simulated by randomly choosing, from appropriate probability distributions, the values of the energy, direction, and path length of the particles or photons. The probability distributions are determined by the physics of the interactions that the particle or photon can undergo during its passage through matter. The particle or photon history continues as it passes through the media undergoing various interactions, including the production of secondary particles and photons, and ends when a particle or photon becomes absorbed, leaves the region of interest, or no longer has sufficient kinetic energy to be of interest.

(82) The accuracy of the dose conversion coefficients is limited by uncertainties for the physical input parameters, such as interaction cross sections, and deviations of the particle transport simulation from the real exposure situation. The relative statistical uncertainties of conversion coefficients for organ absorbed dose depend on several parameters such as organ size, location in the human body, particle energy, and irradiation geometry.

3.3.1. EGSnrc code

(83) For the calculations presented in this report, the electron-gamma-shower code system EGSnrc Version v4-2-3-0 (Kawrakow et al., 2009) has been used. This code is an extended and improved version of EGS4 (Nelson et al., 1985), maintained by the National Research Council of Canada (NRC). The transport of photons, electrons, and positrons can be simulated for particle kinetic energies from a few keV up to several hundred GeV. Some enhancements to the physics, however, can only be enabled below 1 GeV.

(84) For photon transport, bound Compton scattering and photo-electrons from K, L, and M shells are considered for all energies. In both cases, resulting fluorescence or Auger and Coster-Kronig electrons are followed. The input data for photon cross sections have been updated by Seuntjens et al. (2002), who used the XCOM database (Berger and Hubbell, 1987) to improve the cross sections for the photoelectric effect, Rayleigh scattering, and pair production. Below 1 GeV, radiative Compton corrections in the one-loop approximation based on the Brown and Feynman equation (1952) are applied. However, the effect of reducing the cross section for large scattering angles is partially cancelled by the inclusion of double-Compton events. For the pair-production cross section, the extreme relativistic Born approximation is used, except at photon energies below 85 MeV, where more sophisticated cross sections calculated by NRC are employed following the techniques of Øverbø et al. (1973). Photon–nuclear reactions are not taken into consideration as their contribution to organ dose is considered to be less than 0.1%. In this report, photon transport is terminated when the photon energy falls below 2 keV.

(85) Electron and positron transport calculations are performed by a Class II condensed history technique (Berger, 1963), which transports secondary particles produced above a certain chosen energy. Bremsstrahlung cross sections for kinetic energies below 1 GeV agree with those of the National Institute of Standards and Technology (NIST) database (Seltzer and Berger, 1985, 1986), which in turn form

the basis for the radiative stopping powers recommended by ICRU (1984). Above 1 GeV, Coulomb-corrected relativistic cross sections following Koch and Motz (1959) are used. Below 1 GeV, electron impact ionisation is modelled using default cross sections (Kawrakow, 2002). For higher energies or when the sampling does not lead to ionisation, the classical Møller or Bhabha cross sections are applied. For elastic scattering, spin effects are taken into account. Pair production is simulated as in EGS4 (Nelson et al., 1985). Triplet-production processes are neglected for all particles. In this report, the transport history of electrons is generally terminated when their kinetic energy falls below 20 keV. Exceptions are noted for electrons with an initial kinetic energy below 50 keV, whose histories are followed down to 2 keV. For external irradiation, electrons with kinetic energies below 500 keV rarely reach internal organs. The dose to those organs is low and mainly caused by bremsstrahlung production within the skin voxels of the reference phantoms. A variance reduction technique called 'bremsstrahlung splitting' was employed to decrease the relative statistical uncertainty in the dose conversion coefficients of internal organs (Kawrakow et al., 2009).

3.3.2. FLUKA code

(86) The FLUKA code is a general-purpose Monte Carlo program for the calculation of particle and photon transport in matter (Fassò et al., 2005; Battistoni et al., 2006). The program can simulate radiation transport for ~60 different particles including photons and electrons (1 keV–1 PeV), neutrinos, muons (1 keV–1 PeV), hadrons of energies up to 20 TeV [with extension up to 10 PeV by linking the FLUKA code with the Dual Parton model and JET (DPMJET) code], all corresponding antiparticles, neutrons down to thermal energies, and heavy ions up to 10 PeV/u. Time evolution of the radioactive nuclei inventory and tracking of emitted radiation from unstable residual nuclei can be performed directly. FLUKA 2008 was used in this report.

(87) Depending on the energies of the primary particles, different physical models are used to simulate hadronic interactions. The FLUKA hadron–nucleon interaction models are based on production and decay of resonances for projectile energies below a few GeV. For higher energies, the Dual Parton model is used. Two further models are used in hadron–nucleus interactions. The PEANUT package is employed below 3–5 GeV/u, which includes a very detailed generalised intranuclear cascade (GINC) and a pre-equilibrium stage. At higher energies, the Gribov–Glauber multiple collision mechanism is included in a less-refined version of GINC. The PEANUT model is set to be the default at all energies. Both hadron–nucleus interaction models are followed by an equilibrium stage, in which the residual excitation is dissipated through evaporation, fission, Fermi break-up, and gamma de-excitation. The FLUKA code can also simulate photonuclear interactions (described by Vector Meson Dominance, Delta Resonance, Quasi-Deuteron and Giant Dipole Resonance models). Nuclear interactions generated by ions are treated through interfaces to external event generators, except in the low-energy range (less than 150 MeV/u) for which a model based on the Boltzmann Master Equation model has been implemented recently. The Relativistic Quantum Molecular Dynamics (RQMD) generator is invoked from 100 MeV/u to 5 GeV/u, and the DPMJET code is used for energies over 5 GeV/u.

(88) The transport of charged particles is described by applying a multiple-scattering algorithm based on Moliere's theory of Coulomb scattering. The energy loss is determined according to the Bethe–Bloch theory and from bremsstrahlung and pair production.

(89) For neutrons with kinetic energies below 20 MeV, the FLUKA code employs a multi-group transport algorithm, which uses a subdivision of the neutron energy range in 260 groups and is based on neutron cross section libraries prepared for the FLUKA code. These libraries contain more than 200 different materials, and are derived from the most recently evaluated data. For nuclei other than hydrogen, kerma coefficients are used to calculate energy deposition.

(90) The FLUKA code can handle very complex geometries using an improved version of the well-known Combinatorial Geometry package. Repetitive structures (lattices) and voxel geometries can also be handled.

3.3.3. PHITS code

(91) The PHITS (Particle and Heavy Ion Transport Code System) code is a multipurpose Monte Carlo code that simulates the transport and interaction of hadrons, leptons, and heavy ions in arbitrary three-dimensional geometries (Iwase et al., 2002; Niita et al., 2006, 2010). PHITS 2.14 was used in this report.

(92) In the PHITS code, neutron transport below 20 MeV down to 10^{-5} eV is simulated in a manner similar to that employed in the MCNP4C code (Briesmeister, 2000), and is based on evaluated nuclear data libraries. For neutrons above 20 MeV and for protons, mesons, and other hadrons up to 200 GeV, the PHITS code employs the Jet AA Microscopic Transport (JAM) model (Nara et al., 1999). JAM is a hadronic cascade model, which treats all established hadronic states including resonances with explicit spin and isospin, as well as their antiparticles. The nucleus–nucleus collisions are described by the JAERI Quantum Molecular Dynamics (JQMD) simulation model (Niita et al., 1995) for energies from 10 MeV/u up to 100 GeV/u. The Generalised Evaporation Model (GEM) (Furihata, 2000) is employed for the evaporation and fission processes of the excited residual nuclei, which are created in the JAM and JQMD calculations. For the present calculations, the JQMD model was adopted for nucleon-induced reactions. Energy loss of charged particles and nuclei is calculated by the charge density of the material and the momentum of the particle, taking into account the fluctuations of the energy loss and the angular deviations. Transport of photons and electrons from 1 keV to 1 GeV are simulated in a similar way as in the MCNP4C code, using the evaluated nuclear data libraries.

(93) The PHITS code is capable of: (1) providing good estimations of secondary particle spectra produced from nucleon–nucleus and nucleus–nucleus collisions using the JAM and JQMD models; (2) determining the energy of charged particles emitted from low-energy neutron-induced nuclear reactions using the event generator mode (Iwamoto et al., 2008; Niita et al., 2008), instead of the kerma approximation; and (3) estimating the probability density of absorbed dose in terms of LET or lineal energy (Sato et al., 2009).

(94) The PHITS code defines the geometry of the calculation model in terms of combinatorial geometry and general geometry. In addition, a capability for describing repeated structure and lattice geometry is available to define three-dimensional voxel phantoms. The PHITS code has a function to draw two- and three-dimensional figures of calculation geometries as well as calculated results using a graphic package ANGEL (Niita et al., 2010).

3.3.4. MCNPX code

(95) The Los Alamos Monte Carlo radiation transport code MCNPX (Monte Carlo N-Particle eXtended) (Waters, 2002; Pelowitz, 2008) is capable of tracking 34 particle types (nucleons and light ions) and more than 2000 heavy ions ($Z > 2$) at nearly all energies. It uses standard evaluated data libraries for neutrons, photons, electrons, protons, and photonuclear interactions, and uses physics models for other particle types and at energies for which tabular data are not available. Tabulated cross section data are available for all nuclides of 10^{-11}–20 MeV for neutrons, 1 keV–1 GeV for electrons, and 1 keV–100 GeV for photons. The LA150 cross section library (Chadwick et al., 1999) provides neutron, proton, and photonuclear cross sections up to 150 MeV (250 MeV for protons) for 42 isotopes (including H, C, N, and O) based on experimental data and nuclear model calculations using the GNASH model code (Young et al., 1996). MCNPX Version 2.6.0 was used in this report.

(96) The transport of photons, electrons, and positrons is the same as in the MCNP4C3 code. The electron physics in the MCNPX code is based on the Integrated Tiger Series of codes (ITS3.0) (Halbleib et al., 1992) from Sandia National Laboratories. Electron physics is also used for positron transport.

(97) Current physics modules include the Bertini and Isabel models taken from the LAHET Code system, CEM03, and INCL4 (Kirk, 2010). Recent versions of the code incorporate the necessary physics models (albeit with some limitations) to transport all secondary charged particles produced in neutron elastic and inelastic interactions. The incorporation of a heavy ion physics model has enabled the transport of recoil nuclei. Hence, heavy recoil nuclei (C, N, and O) in tissue can now be transported, in addition to the lighter ions such as protons, deuterons, tritons, helium ions, and alpha particles. The heavy ion model automatically transports all residuals that are produced from any physics model, even if the source particle is not a heavy ion. Current stopping powers for heavy ions have been adjusted in an ad-hoc fashion (Pelowitz, 2008) so that they better match the Stopping and Range of Ions in Matter (SRIM) results (Ziegler et al., 2003). Charged particles are slowed down to a lower kinetic energy limit of 5 MeV, at which point their remaining energy is deposited locally.

3.3.5. GEANT4 code

(98) The GEANT4 code is a general-purpose Monte Carlo code and, like its predecessors, was developed for the needs of high-energy physics and applications at the CERN (European Organization for Nuclear Research) accelerator. It has been

improved and maintained by an international GEANT4 collaboration (http://geant4.web.cern.ch/geant4) (Agostinelli et al., 2003). The GEANT4 code can simulate the transport of neutrons, protons, muons, and pions from energies from 250 eV to 1 TeV, with an extension for low-energy neutrons down to the meV range.

(99) GEANT4 Version 8.2 was used for the calculations in this report. A function called 'G4 phantom parameterisation' was used to implement the voxelised geometry (GEANT4, 2006b).

(100) The GEANT4 code simulates the physics of the transportation processes and decay processes (G4Decay) for unstable particles. Details regarding all GEANT4 physics processes and models can be found in its program physics guide (GEANT4, 2006a). The standard electromagnetic physics list provided by the GEANT4 code was taken for electromagnetic physics, which includes interaction processes for photons, electrons, positrons, and both muons and anti-muons. The default cut-off value for the production of electrons and positrons was set to a range in the medium of 1 mm. In every material, this range corresponds to an energy below which the continuous slowing-down approximation is used.

(101) For hadronic physics, cross section data are taken from three possible sources. Firstly, the data are calculated from parameterised models (Fesefeldt, 1985) using the GEANT3-GHEISHA package for low and high particle energies. The models include physical processes such as induced fission, capture, and elastic scattering as well as inelastic final-state production. Secondly, data-driven models based on experimental or evaluated data (ENDF/B-VI and others) are employed. Thirdly, theoretical models are employed that use different approaches depending on the energy range. For neutrons and protons up to 3 GeV, a theoretical model incorporated in the function G4CascadeInterface was employed. This includes the Bertini Intra-Nuclear Cascade model with excitons, a pre-equilibrium model, a nucleus explosion model, a fission model, and an evaporation model (GEANT4, 2006a).

3.4. Special considerations for assessing dose to skeletal tissues

(102) For purposes of radiological protection, the Commission defines two skeletal cell populations of dosimetric interest relevant to stochastic biological effects: (1) haematopoietic stem cells associated with the risk of radiogenic leukaemia, and (2) osteoprogenitor cells associated with the risk of radiogenic bone cancer. While there is new evidence that haematopoietic stem cells are found preferentially near the surfaces of the bone trabeculae within skeletal spongiosa (Watchman et al., 2007; Bourke et al., 2009), current modelling for radiological protection assumes these cells to be uniformly distributed within the marrow cavities of haematopoietically active marrow. For the osteoprogenitor cells, the Commission had previously defined their location as a single cell layer within trabecular and cortical endosteum, each 10 μm in thickness, and located along the surfaces of the bone trabeculae and Haversian canals, respectively (ICRP, 1977). In ICRP *Publication 110* (ICRP, 2009), the surrogate target tissue for the osteoprogenitor cells was redefined as being 50 μm in thickness along the surfaces of the bone trabeculae in skeletal spongiosa, and along the inner surfaces of the medullary cavities in the shafts of all long bones. As a result, cortical bone and

its cells within the Haversian canals are no longer considered to be a target tissue for dose assessment. In this report, the revised 50 μm surrogate target tissue for the osteoprogenitor cells is termed the 'endosteum' and is given the symbol TM_{50} (total marrow within a 50-μm thickness of the bone surfaces). The term 'bone surfaces' is no longer used to describe the target cell layer of relevance to radiogenic bone cancer.

(103) Neither of these skeletal target tissues at radiological risk can be geometrically represented within the voxel structure of the ICRP reference phantoms. As presented above, the skeleton in the male and female reference computational phantoms is described by voxels defining either cortical bone, medullary marrow, or trabecular spongiosa. The latter is a homogeneous mixture of its microscopic tissue constituents – bone trabeculae, active marrow, and inactive marrow – and thus varies in both elemental composition and mass density across different bones of the skeleton in each reference phantom. Computational algorithms must therefore be applied to relate the absorbed dose to spongiosa and medullary marrow to the absorbed dose to either active marrow or endosteum. The elemental compositions of the constituent tissues of trabecular spongiosa are given in Table 3.1. It is further noted that the elemental composition of endosteum, TM_{50}, is equal to that of the active marrow/inactive marrow mixture in a particular skeletal site as determined by its ICRP *Publication 70* (ICRP, 1995) reference marrow cellularity.

(104) Considering the broad scope of particle types and energies considered in this report, the Task Group has opted to uniformly apply the following approximate estimates of the absorbed dose to active marrow and TM_{50}:

$$D_{skel}(AM) = \sum_x \frac{m(AM,x)}{m(AM)} D(SP,\, x) \tag{3.1}$$

and:

$$D_{skel}(TM_{50}) = \sum_x \frac{m(TM_{50},x)}{m(TM_{50})} D(SP,\, x) + \sum_x \frac{m(TM_{50},x)}{m(TM_{50})} D(MM,\, x) \tag{3.2}$$

Table 3.1. Elemental compositions of active marrow, inactive marrow, and bone trabeculae for the ICRP reference adult male and female, inclusive of their blood content.

Tissue/phantom	Element composition (% by mass)											
	H	C	N	O	Na	Mg	P	S	Cl	K	Ca	Fe
Active bone marrow												
Male	10.44	35.58	3.38	49.76	0.02		0.10	0.20	0.22	0.20		0.10
Female	10.45	35.86	3.38	49.47	0.02		0.10	0.20	0.22	0.20		0.10
Inactive bone marrow												
Male	11.48	63.63	0.74	23.85	0.10		0.00	0.10	0.10	0.00		0.00
Female	11.48	63.65	0.74	23.83	0.10		0.00	0.10	0.10	0.00		0.00
Bone trabeculae												
Male	3.91	15.69	4.14	46.33	0.29	0.19	8.92	0.29	0.02	0.01	20.18	0.01
Female	3.91	15.69	4.14	46.35	0.29	0.19	8.92	0.29	0.02	0.01	20.18	0.01

Source: ICRP, 2009. Adult reference computational phantoms. ICRP Publication 110. Ann. ICRP 39(2). Section 5.3.

where D_{skel} (AM) and D_{skel} (TM_{50}) are the skeletal-averaged absorbed dose to active marrow and endosteum, respectively; $m(AM,x)$ and $m(TM_{50},x)$ are the masses of both these tissues in bone site x; $m(AM)$ and $m(TM_{50})$ are the masses of both target tissues summed across the entire skeleton; and $D(SP, x)$ and $D(MM, x)$ are the absorbed doses to spongiosa and medullary marrow, respectively, in bone site x of the computational phantoms. The mass values of active marrow and endosteum are given in Table 3.2 for the male and female reference computational phantoms.

(105) For higher-energy directly ionising radiations, Eqs. (3.1) and (3.2) are reasonable approximations applied for radiological protection. For indirectly ionising radiations such as photons and neutrons, energy regions exist in which a lack of secondary charged-particle equilibrium can exist across the marrow cavities. This lack of charged-particle equilibrium can occur in spongiosa for both photon and neutron irradiation for different yet complementary reasons. During photon irradiation of spongiosa at energies below ~200 keV, a greater number of photo-electric events will occur in bone trabeculae than in the marrow tissues. As a result, an enhancement of the absorbed dose to both active marrow and endosteum will result as photo-electrons emerge from bone trabeculae and deposit energy in adjacent marrow tissues (Johnson et al., 2011). The dose enhancement to endosteum will be much more significant than that to active marrow because of its smaller 50 μm thickness and closer proximity to the bone trabeculae surfaces in many bone sites. In contrast, elastic and inelastic collisions of neutrons at energies below ~150 MeV in spongiosa will result in a greater number of recoil protons born within the marrow tissues than in the bone trabeculae, due to the higher hydrogen content in the former, and these recoil particles will, in many cases, traverse the marrow spaces with their residual energy being lost to surrounding trabeculae. The net result for neutron irradiation over many energy regions is then a suppression of the absorbed dose to marrow tissues in comparison with that predicted in a kerma approximation (Kerr and Eckerman, 1985; Bahadori et al., 2011).

(106) Additional computational tools for assessing the absorbed dose to the skeletal tissues under photon irradiation (10 keV–10 MeV) and neutron irradiation (10^{-3} eV–150 MeV) are provided in Annexes D and E of this report, respectively. In each annex, tabular data are given for skeletal dose–response functions, defined as the absorbed dose per particle fluence. Additionally, both annexes discuss relative differences introduced through the use of Eqs. (3.1) and (3.2) compared with skeletal tissue doses derived using the dose–response methodology.

3.5. Skin dosimetry

(107) For the skin, both stochastic effects and tissue reactions (i.e. deterministic effects) are relevant for external exposures. Stochastic effects include the induction of skin cancer from ionising radiation exposures. Tissue reactions include acute damage to skin, including skin erythema, blistering, and moist desquamation.

Table 3.2. Skeletal tissue masses in the ICRP reference adult male and adult female computational phantoms.

Organ	Bone site	Reference adult male				Reference adult female			
		Active marrow		Endosteum		Active marrow		Endosteum	
		Mass (g)	Mass (%)	Mass (g)	Mass (%)	Mass (g)	Mass (%)	Mass (g)	Mass (%)
14	Humeri, upper half – spongiosa	26.9	2.3	9.41	1.7	20.7	2.3	7.16	1.8
15	Humeri, upper half – medullary cavities			0.19	0.0			0.14	0.0
17	Humeri, lower half – spongiosa			11.25	2.1			8.32	2.0
18	Humeri, lower half – medullary cavities			0.25	0.0			0.19	0.0
20	Lower arm bones – spongiosa			16.31	3.0			12.03	3.0
21	Lower arm bones – medullary cavities			0.09	0.0			0.07	0.0
23	Wrists and hands – spongiosa			12.50	2.3			7.10	1.7
25	Clavicles – spongiosa	9.3	0.8	2.50	0.5	7.2	0.8	1.90	0.5
27	Cranium – spongiosa	88.9	7.6	83.40	15.3	68.4	7.6	64.20	15.8
29	Femora, upper half – spongiosa	78.4	6.7	43.34	8.0	60.3	6.7	33.53	8.2
30	Femora, upper half – medullary cavities			0.86	0.2			0.67	0.2
32	Femora, lower half – spongiosa			47.83	8.8			23.67	5.8
33	Femora, lower half – medullary cavities			0.67	0.1			0.33	0.1
35	Lower leg bones – spongiosa			87.38	16.1			79.91	19.6
36	Lower leg bones – medullary cavities			5.02	0.9			4.59	1.1
38	Ankles and feet – spongiosa			42.20	7.8			24.40	6.0
40	Mandible – spongiosa	9.4	0.8	2.00	0.4	7.2	0.8	1.60	0.4
42	Pelvis – spongiosa	205.2	17.5	51.70	9.5	157.5	17.5	39.70	9.7
44	Ribs – spongiosa	188.8	16.1	29.80	5.5	144.9	16.1	22.90	5.6
46	Scapulae – spongiosa	32.8	2.8	9.80	1.8	25.2	2.8	7.60	1.9
48	Cervical spine – spongiosa	45.6	3.9	11.50	2.1	35.1	3.9	8.80	2.2
50	Thoracic spine – spongiosa	188.8	16.1	26.90	4.9	144.9	16.1	20.60	5.1
52	Lumbar spine – spongiosa	143.9	12.3	23.40	4.3	110.7	12.3	18.00	4.4
54	Sacrum – spongiosa	115.9	9.9	20.60	3.8	89.1	9.9	15.80	3.9
56	Sternum – spongiosa	36.3	3.1	5.50	1.0	27.9	3.1	4.30	1.1
	Totals	1170.2	100	544.4	100	899.1	100	407.50	100

Source: ICRP, 2009. Adult reference computational phantoms. ICRP Publication 110. Ann. ICRP 39(2).

3.5.1. Stochastic effects

(108) To account for the stochastic risk, the skin has been included among the tissues contributing to the effective dose, and has been assigned a tissue weighting factor $w_T = 0.01$ as shown in Table 2.2. The skin dose contributing to the effective dose is the equivalent dose to the skin, H_{skin}, which is averaged over the entire tissue. The skin dose conversion coefficients given in this report are, therefore, also related to H_{skin}. The coefficients have been evaluated based on the average absorbed dose for all skin voxels of the male and female reference computational phantoms (ICRP, 2009).

(109) For weakly penetrating particles that deposit all of their energy in the skin, the skin thickness is a crucial parameter dictating the magnitude of the absorbed dose. As noted in ICRP *Publication 110* (ICRP, 2009), the voxel thicknesses in both the male and female phantoms (2.137 mm and 1.775 mm, respectively) are larger than the reference skin thicknesses (1.6 mm and 1.3 mm for the reference male and female, respectively). Thus, for particles with continuous-slowing-down approximation (CSDA) ranges shorter than the abovementioned voxel thicknesses, but with CSDA ranges longer than the reference skin thicknesses, the skin dose conversion coefficients given in this report can underestimate actual values by up to 35%.

3.5.2. Deterministic effects

(110) ICRP *Publication 103* (ICRP, 2007) states that 'Effective dose is used to limit the occurrence of stochastic effects (cancer and heritable effects) and is not applicable to the assessment of the possibility of tissue reactions. In the dose range below the annual effective dose limit, tissue reactions should not occur. Only in a few cases (e.g. an acute localised exposure of a single organ with a low tissue weighting factor such as the skin) could the use of the annual limit on effective dose be insufficient to avoid tissue reactions. In such cases, local tissue doses will also need to be assessed.' It is further stated that the specific annual dose limits recommended for the skin – 500 mSv for occupational exposures and 50 mSv for public exposures – apply to the dose averaged over 1 cm^2 of the most highly irradiated area of the skin. Conversion coefficients for local skin-equivalent dose for electrons from 10 keV to 10 MeV and alpha particles from 6.5 MeV to 10 MeV can be found in Annex G.

3.6. References

Agostinelli, S., Allison, J., Amako, K., et al., 2003. GEANT4 – a simulation toolkit. Nucl. Instrum. Methods Phys. Res. A 506, 250–303.

Bahadori, A.A., Johnson, P.B., Jokisch, D.W., et al., 2011. Response functions for computing absorbed dose to skeletal tissues from neutron irradiation. Phys. Med. Biol. 56, 6873–6897.

Battistoni, G., Muraro, S., Sala, P.R., et al., 2006. The FLUKA code: description and benchmarking. In: Albrow, M., Raja, R. (Eds.), Hadronic Shower Simulation Workshop, 6–8 September 2006,

Fermi National Accelerator Laboratory (Fermilab), Batavia, IL, AIP Conference Proceeding 896, pp. 31–49.

Berger, M.J., 1963. Monte Carlo calculation of the penetration and diffusion of fast charged particles. In: Alder, B., Fernbach, S., Rotenberg, M. (Eds.), Methods in Computational Physics. Academic Press, New York, pp. 135–215.

Berger, M.J., Hubbell, J.H., 1987. XCOM: photon cross sections on a personal computer. NBSIR 87-3597. National Bureau of Standards (former name of NIST), Gaithersburg, MD.

Bourke, V.A., Watchman, C.J., Reith, J.D., et al., 2009. Spatial gradients of blood vessels and hematopoietic stem and progenitor cells within the marrow cavities of the human skeleton. Blood 114, 4077–4080.

Briesmeister, J.F., 2000. MCNP – A General Monte Carlo N-Particle Transport Code, Version 4C. Report LA-13709-M. Los Alamos National Laboratory, Los Alamos, NM.

Brown, L., Feynman, R., 1952. Radiative corrections to Compton scattering. Phys. Rev. 85, 231–244.

Chadwick, M.B., Young, P.G., Chiba, S., et al., 1999. Cross section evaluations to 150 MeV for accelerator-driven systems and implementation in MCNPX. Nucl. Sci. Eng. 131, 293–328.

Fassò, A., Ferrari, A., Ranft, J., et al., 2005. FLUKA: a Multi-particle Transport Code. CERN-2005-10 (2005), INFN/TC_05/11, SLAC-R-773. CERN, Geneva.

Fesefeldt, H.C., 1985. Simulation of Hadronic Showers, Physics and Application. Technical Report PITHA 85-02, Physikalisches Institut, Technische Hochschule Aachen, Aachen.

Furihata, S., 2000. Statistical analysis of light fragment production from medium energy proton-induced reactions. Nucl. Instrum. Methods B171, 251–258.

GEANT4, 2006a. GEANT4: Physics Reference Manual. Available at: http://geant4.web.cern.ch/geant4/UserDocumentation/UsersGuides/PhysicsReferenceManual/fo/PhysicsReferenceManual.pdf (last accessed December 2011).

GEANT4, 2006b. GEANT4 User's Guide for Application Developers. Available at: http://geant4.web.cern.ch/geant4/support/userdocuments.shtml.

Halbleib, J.A., Kensek, R.P., Valdez, G.D., et al., 1992. TS Version 3.0: the Integrated TIGER Series of Coupled Electron/Photon Monte Carlo Transport Codes SAND91-1634. Sandia National Laboratories, Albuquerque, New Mexico 87185 and Livermore, California 94550, US.

ICRP, 1977. Recommendations of the International Commission on Radiological Protection. ICRP Publication 26. Ann. ICRP 1(3).

ICRP, 1995. Basic anatomical and physiological data for use in radiological protection: the skeleton. ICRP Publication 70. Ann. ICRP 25(2).

ICRP, 2002. Basic anatomical and physiological data for use in radiological protection: reference values. ICRP Publication 89. Ann. ICRP 32(3/4).

ICRP, 2007. The 2007 Recommendations of the International Commission on Radiological Protection. ICRP Publication 103. Ann. ICRP 37(2–4).

ICRP, 2009. Adult reference computational phantoms. ICRP Publication 110. Ann. ICRP 39(2).

ICRU, 1984. Stopping Powers for Electrons and Positrons. ICRU Report 37. International Commission on Radiation Units and Measurements, Bethesda, MD.

ICRU, 1992. Photon, Electron, Proton and Neutron Interaction Data for Body Tissues. ICRU Report 46. International Commission on Radiation Units and Measurements, Bethesda, MD.

Iwamoto, Y., Niita, K., Sakamoto, Y., 2008. Validation of the event generator mode in the PHITS code and its application. In: Bersillon, O., Gunsing, F., Bauge, E., Jacqmin, R., Leray, S. (Eds.), Proceedings of the International Conference on Nuclear Data for Science and Technology, April 2007, Nice, EDP Sciences, pp. 945–948.

Iwase, H., Niita, K., Nakamura, T., 2002. Development of a general-purpose particle and heavy ion transport Monte Carlo code. J. Nucl. Sci. Technol. 39, 1142–1151.

Johnson, J.B., Bahadori, A.A., Eckerman, K.F., et al., 2011. Response functions for computing absorbed dose to skeletal tissues from photon irradiation – an update. Phys. Med. Biol. 56, 2347–2365.

Kawrakow, I., 2002. Electron impact ionization cross sections for EGSnrc. Med. Phys. 29, 1230.

Kawrakow, I., Mainegra-Hing, E., Rogers, D.W.O., et al., 2009. The EGSnrc Code System: Monte Carlo Simulation of Electron and Photon Transport. PIRS Report 701. National Research Council of Canada, Ottawa.

Kerr, G.D., Eckerman, K.F., 1985. Neutron and photon fluence-to-dose conversion factors for active marrow of the skeleton. In: Schraube, H., Burger, G., Booz, J. (Eds.), Fifth Symposium on Neutron Dosimetry, 17–21 September 1984, Munich, Germany, pp. 133–145..

Kirk, B.L., 2010. Overview of Monte Carlo radiation transport codes. Radiat. Meas. 45, 1318–1322.

Koch, H.W., Motz, J.W., 1959. Bremsstahlung cross-section formulas and related data. Rev. Mod. Phys.31, 920–955.

Nara, Y., Otuka, N., Ohnishi, A., et al., 1999. Relativistic nuclear collisions at 10 A GeV energies from p+Be to Au+Au with the hadronic cascade model. Phys. Rev. C 61, 024901.

Nelson, W.R., Hirayama, H., Rogers, D.W.O., 1985. The EGS4 Code System. SLAC Report 265. Stanford Linear Accelerator Center, Stanford, CA.

Niita, K., Chiba, S., Maruyama, T., et al., 1995. Analysis of the (N, xN') reactions by quantum molecular dynamics plus statistical decay model. Phys. Rev. C52, 2620–2635.

Niita, K., Sato, T., Iwase, H., et al., 2006. PHITS – a particle and heavy ion transport code system. Radiat. Meas. 41, 1080–1090.

Niita, K., Iwamoto, Y., Sato, T., 2008. A new treatment of radiation behaviour beyond one-body observables. In: Bersillon, O., Gunsing, F., Bauge, E., Jacqmin, R., Leray, S. (Eds.), Proceedings of the International Conference on Nuclear Data for Science and Technology, April 2007, Nice, EDP Sciences, pp. 1167–1169.

Niita, K., Matsuda, N., Iwamoto, Y., et al., 2010. PHITS – Particle and Heavy Ion Transport Code System, Version 2.23. JAEA-Data/Code 2010-022. Japan Atomic Energy Agency, Tokai-mura.

Øverbø, I., Mork, K.J., Olsen, A., 1973. Pair production by photons: exact calculations for unscreened atomic fields. Phys. Rev. A8, 668–684.

Pelowitz, D.B., 2008. MCNPX User's Manual, Version 2.6.0. LA-CP-07-1473. Los Alamos National Laboratory, Los Alamos, NM.

Sato, T., Kase, Y., Watanabe, R., et al., 2009. Biological dose estimation for charged-particle therapy using an improved PHITS code coupled with a microdosimetric kinetic model. Radiat. Res. 171, 107–117.

Seltzer, S.M., Berger, M.J., 1985. Bremsstrahlung spectra from electron interactions with screened atomic nuclei and orbital electrons. Nucl. Instrum. Methods Phys. Res. Sect. B 12, 95–134.

Seltzer, S.M., Berger, M.J., 1986. Bremsstrahlung energy spectra from electrons with kinetic energy from 1 keV to 10 GeV incident on screened nuclei and orbital electrons of neutral atoms with Z = 1-100. Atom. Data Nucl. Data Tables 35, 345–418.

Seuntjens, J.P., Kawrakow, I., Borg, J., et al., 2002. Calculated and measured air-kerma response of ionization chambers in low and medium energy photon beams. In: Seuntjens, J.P., Mobit, P. (Eds.), Recent Developments in Accurate Radiation Dosimetry,Proceedings of an International Workshop, Montreal, July 14–18, 2002. Symposium Proceedings 13, Medical Physics Publishing, Madison, USA. pp. 69–84.

Watchman, C.J., Bourke, V.A., Lyon, J.R., et al., 2007. Spatial distribution of blood vessels and CD34+ hematopoietic stem and progenitor cells within the marrow cavities of human cancellous bone. J. Nucl. Med. 48, 645–654.

Waters, L.S., 2002. MCNPX User's Manual, Version 2.3.0. Report LA-UR-02-2607. Los Alamos National Laboratory, Los Alamos, NM.

Young, P.G., Arthur, E.D., Chadwick, M.B., 1996. Comprehensive nuclear model calculations: theory and use of the GNASH code. In: Reffo, G.A. (Ed.), IAEA Workshop on Nuclear Reaction Data and Nuclear Reactors—Physics Design, and Safety, Trieste, 15 April–17 May, pp. 227–404.

Zankl, M., Wittmann, A., 2001. The adult male voxel model 'Golem' segmented from whole body CT patient data. Radiat. Environ. Biophys. 40, 153–162.

Zankl, M., Becker, J., Fill, U., et al., 2005. GSF male and female adult voxel models representing ICRP Reference Man – the present status. In: The Monte Carlo Method: Versatility Unbounded in a Dynamic Computing World. Chattanooga, TN.

Ziegler, J.F., Biersack, J.P., Ziegler, M., et al., 2003. SRIM – the Stopping and Range of Ions in Matter. American Nuclear Society, La Grange Park, USA. Available at: www.srim.org (last accessed December 2011).

4. CONVERSION COEFFICIENTS FOR EXTERNAL EXPOSURE

(111) The protection quantities 'equivalent dose' and 'effective dose' are not measurable and thus their values are determined using their relationship to physical radiation field quantities such as particle fluence, Φ, or air kerma, K_a. Conversion coefficients defined for Reference Person provide numerical links between radiation protection and physical field quantities. Consequently, it is important that ICRP/ICRU reference conversion coefficients are available for general use in radiological protection practice for occupational exposures.

(112) Based on the work of a joint ICRP/ICRU Task Group, the Commissions published reports (ICRP, 1996; ICRU, 1998) on 'Conversion Coefficients for Use in Radiological Protection against External Radiation'. The reports recommended data sets of conversion coefficients for protection and operational quantities for external exposure to mono-energetic photon, neutron, and electron radiations under specific whole-body irradiation conditions. Furthermore, ICRP *Publication 74* (ICRP, 1996) explored the relationship between the protection quantity 'effective dose' and the operational dose quantities for specific idealised irradiation exposure geometries. Most of the data for protection quantities used for the evaluation were calculated on the basis of stylised models of human anatomy.

(113) The ICRP voxel-based reference phantoms representing Reference Male and Reference Female (ICRP, 2002) require new calculations of conversion coefficients for all radiations and irradiation geometries of interest to replace the existing ICRP/ICRU data sets (ICRP, 1996). The conversion coefficients for effective dose are dependent on w_R and w_T values, and the influence of the changes in these weighting factors, as well as the influence of the use of voxel-based reference phantoms, on the value of the conversion coefficients are investigated in this publication, particularly for photons and neutrons.

(114) All data sets presented in this publication are based on calculations made by the DOCAL Task Group using the male and female reference computational phantoms (ICRP, 2009). A number of Monte Carlo codes were used for the simulation of radiation transport, as indicated in Section 3.3. For quality assurance purposes, the data sets were calculated by a primary group of Monte Carlo calculators and a confirmatory group (secondary calculators). In most cases, additional validation calculations were also made by a third or fourth group. The primary calculators covered all energies and geometries, the secondary calculators covered most of these parameters, and the third or fourth calculators performed calculations for selected geometries and particle energies. In general, very good agreement was found for results from different codes; in most cases, the deviations were smaller than the relative statistical uncertainties. However, for certain particles and energy ranges, transport model differences were noted and these were examined more extensively. Reference values were arrived at through a combination of methods including data averaging, data smoothing, and data fitting (see Annex I). Effective dose conversion coefficients were evaluated as described in Section 2.2.4.

Table 4.1. Summary of calculations used to determine organ and effective dose conversion coefficients.

Particles	Energies	Geometries	Primary calculations	Secondary calculations	Validation calculations
Photons	10 keV–10 GeV including energies: 0.511, 0.662, 1.170, 1.330, 6.129 MeV	AP, PA, LLAT, RLAT, ISO, ROT	EGSnrc HMGU (Schlattl)	MCNPX 2.6-CEM GaTech (Hertel)*	GEANT4 HMGU (Simmer)
Neutrons	0.001 eV–10 GeV	AP, PA, LLAT, RLAT, ISO, ROT	PHITS JAEA (Sato)	FLUKA INFN (Pelliccioni)	MCNPX 2.5 RPI (Xu) GEANT4 HMGU (Simmer)
Electrons	50 keV–10 GeV	AP, PA, ISO	MCNPX 2.6-CEM MCNPX 2.6 Bertini (below 1 MeV) GaTech (Hertel)*	EGSnrc HMGU (Schlattl)	GEANT4 HMGU (Simmer)
Positrons	50 keV–10 GeV	AP, PA, ISO	MCNPX 2.6-CEM GaTech (Hertel)*	EGSnrc HMGU (Schlattl)	GEANT4 HMGU (Simmer)
Protons	1 MeV–10 GeV	AP, PA, LLAT, RLAT, ISO, ROT	PHITS JAEA (Sato)	FLUKA INFN (Pelliccioni)	MCNPX 2.6 JAEA (Endo) GEANT4 HMGU (Simmer)
Negative pions	1 MeV–200 GeV	AP, PA, ISO	FLUKA JAEA (Endo) PHITS JAEA (Sato)		
Positive pions	1 MeV–200 GeV	AP, PA, ISO	FLUKA JAEA (Endo) PHITS JAEA (Sato)		

Table 4.1. (*continued*)

Particles	Energies	Geometries	Primary calculations	Secondary calculations	Validation calculations
Negative muons	1 MeV–10 GeV	AP, PA ISO	FLUKA JAEA (Endo)	MCNPX 2.6-CEM GaTech (Hertel)*	GEANT4 HMGU (Simmer) FLUKA INFN (Pelliccioni) MCNPX 2.6-Bertini JAEA (Endo)
Positive muons	1 MeV–10 GeV	AP, PA, ISO	FLUKA JAEA (Endo)	MCNPX 2.6-CEM GaTech (Hertel)*	GEANT4 HMGU (Simmer) FLUKA INFN (Pelliccioni)
Helium ions	1 MeV/u–100 GeV/u	AP, PA, ISO	PHITS JAEA (Sato)	FLUKA JAEA (Endo)	

AP, antero-posterior; PA, postero-anterior; LLAT, left lateral; RLAT, right lateral; ROT, rotational; ISO, isotropic; HMGU, Helmholtz Zentrum München, German Research Centre for Environment and Health; JAEA, Japan Atomic Energy Agency; GaTech, Georgia Institute of Technology; INFN, Instituto Nazionale di Fisica Nucleare; RPI, Rensselaer Polytechnic Institute.

* Nolan Hertel with Eric Burgett, Idaho State University; Michele Sutton Ferenci, Penn State University Medical Center; Ken Veinot, Y-12 National Security Complex, Oak Ridge, TN.

(115) This report considers a wider range of particles and energies than was given in ICRP *Publication 74* (ICRP, 1996). Table 4.1 shows the particles, energy ranges, and irradiation geometries considered in this report. Also listed in Table 4.1 are the Monte Carlo codes used for these calculations. For simplicity in radiation transport literature, the term 'energy' is used to denote 'kinetic energy' and will be used hereafter in the figures and tables of this report and accompanying CD.

(116) As described in Section 3.4, the active marrow and endosteum doses were estimated as the absorbed dose to spongiosa in each individual bone site. Skeletal-averaged absorbed doses to these tissues were then taken as the mass-weighted average of the regional spongiosa dose. For the sake of consistency, this method was applied for all particles and calculations. The Task Group decided that this approach is adequate for the purposes of this report. Test calculations performed with the EGSnrc code for photons have shown that the inclusion of dose-response functions (DRF) does not influence effective dose values significantly. This is demonstrated in Fig. 4.1.

(117) Annex A lists reference conversion coefficients for the effective dose for all particles, energies, and irradiation geometries. Annexes B and C list the organ absorbed dose conversion coefficients for photons and neutrons, respectively, for those organs that contribute to the effective dose as defined in ICRP *Publication 103* (ICRP, 2007) (i.e. red (active) bone marrow, colon, lung, stomach, breast, ovaries, testes, urinary bladder wall, oesophagus, liver, thyroid, endosteum, brain, salivary glands, and skin), as well as the remainder tissues. Data are given separately for the male and female phantoms, and for each specific irradiation geometry considered. In Annex F, eye lens dose conversion coefficients for photons, electrons and neutrons are shown. In the CD accompanying this report, a full complement of organ dose conversion coefficients are given, including those for individual organs of the remainder tissues. These additional organs include the adrenals, extrathoracic region, gall bladder, heart, kidneys, lymphatic nodes, muscle, oral mucosa, pancreas, prostate, small intestine, spleen, thymus, and uterus/cervix. Dose conversion coefficients for the lens of the eye and all particles can be also found in the CD. Table 4.2 includes a list of acronyms for all target tissues, and is taken from Annex D of ICRP *Publication 110* (ICRP, 2009). For the composition of target tissues regarding organ identification numbers, the reader is referred to Table A.1 of the same document. The organ absorbed doses are given as a ratio to the incident particle fluence, Φ, in units of pGy cm^2. Additionally, for photons with energies up to 10 MeV, the conversion coefficients are also tabulated as organ-equivalent doses per air kerma, K_a, in Sv/Gy. In all cases, the phantoms were assumed to be irradiated in a vacuum.

(118) When a precise interpolation among the values of the conversion coefficients presented in this publication is required, it is recommended that a procedure similar to that used in ICRP *Publication 74* (ICRP, 1996) should be followed. For interpolations of absorbed dose and effective dose per fluence, a four-point (cubic) Lagrangian interpolation formula is recommended, and a log–log graph scale is more appropriate. Interpolations of absorbed dose and effective dose per air kerma of photons should be carried out using a four-point (cubic) Lagrangian interpolation formula, and a linear–log graph scale is more appropriate.

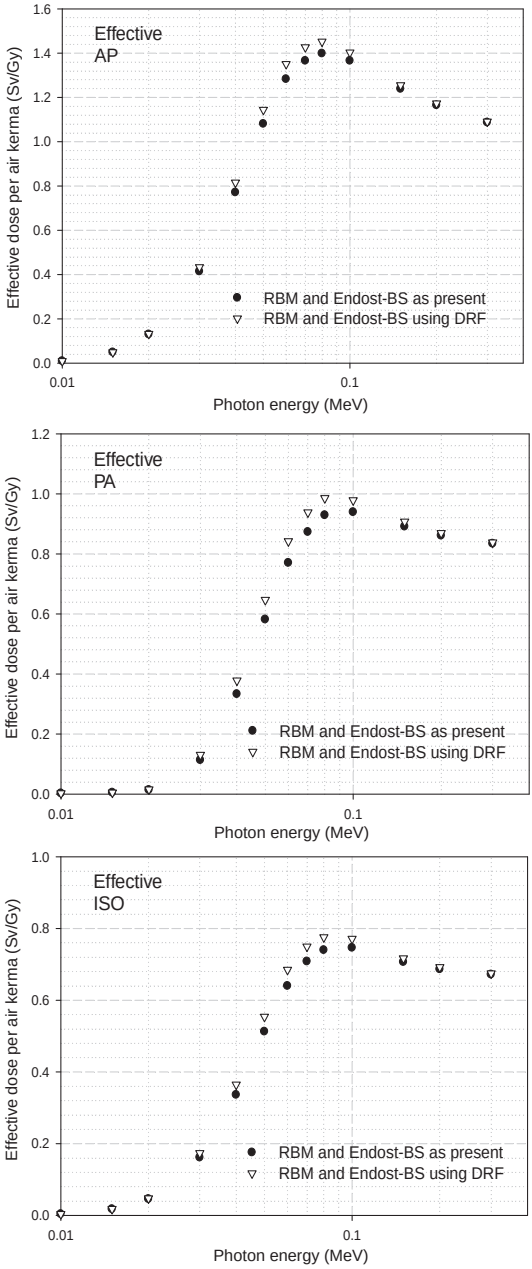

Fig. 4.1. Comparison of effective dose per air kerma evaluated using active bone marrow (RBM) and endosteum (Endost-BS) doses, calculated with the methodology used in the present report and the methodology using dose–response functions (DRF) for antero-posterior (AP), postero-anterior (PA), and isotropic (ISO) irradiation geometries.

Table 4.2. List of target regions and their acronyms in the ICRP *Publication 110* phantoms.

Target region	Acronym
Active (red) marrow	R-marrow
Colon	Colon
RLung + LLung	Lungs
Stomach wall	St-wall
Breast-a + Breast-g	Breast
ROvary + LOvary	Ovaries
Testes	Testes
Urinary bladder wall	UB-wall
Oesophagus (wall)	Oesophagus
Liver	Liver
Thyroid	Thyroid
50-μm endosteal region	Endost-BS
Brain	Brain
Salivary gland	S-glands
Skin	Skin
RAdrenal + LAdrenal	Adrenals
Extrathoracic region	ET
Gall bladder wall	GB-wall
Heart wall	Ht-wall
RKidney + LKidney	Kidneys
Lymph nodes, except LN-ET and LN-Th	Lymph
Muscle	Muscle
Oral mucosa	O-mucosa
Pancreas	Pancreas
Prostate	Prostate
Small intestine wall	SI-wall
Spleen	Spleen
Thymus	Thymus
Uterus/cervix	Uterus
Tongue	Tongue
Tonsils	Tonsils
Right colon wall (ascending + right transverse)	RC
Left colon wall (left transverse + descending)	LC
Sigmoid colon wall + rectum wall	RSig
Basal cells of anterior nasal passages	ET1-bas
Basal cells of posterior nasal passages + pharynx	ET2-bas
Lymph nodes of extrathoracic (ET) region	LN-ET
Basal cells of bronchi	Bronchi-bas
Secretory cells of bronchi	Bronchi-sec
Secretory cells of bronchioles	Brchiol-sec
Alveolar-interstitium	AI
Lymph nodes in thoracic region	LN-Th
Right lung lobe	RLung
Left lung lobe	LLung
Right adrenal gland	RAdrenal
Left adrenal gland	LAdrenal
Inactive (yellow) marrow	Y-marrow
Right breast adipose	RBreast-a
Right breast glandular	RBreast-g
Left breast adipose	LBreast-a
Left breast glandular	LBreast-g

Table 4.2. (*continued*)

Target region	Acronym
RBreast-a + RBreast-g	RBreast
LBreast-a + LBresat-g	LBreast
RBreast-a + LBreast-a	Breast-a
RBreast-g + LBreast-g	Breast-g
Lens of eye	Eye-lens
Right kidney cortex	RKidney-C
Right kidney medulla	RKidney-M
Right kidney pelvis	RKidney-P
Right kidney C + M + P	RKidney
Left kidney cortex	LKidney-C
Left kidney medulla	LKidney-M
Left kidney pelvis	LKidney-P
Left kidney C + M + P	LKidney
Right ovary	ROvary
Left ovary	LOvary
Pituitary gland	P-gland
Spinal cord	Sp-cord
Ureters	Ureters
Adipose/residual tissue	Adipose

Source: ICRP, 2009. Adult reference computational phantoms. ICRP Publication 110. Ann. ICRP 39(2).

4.1. Photons

4.1.1. Characteristics of energy deposition by photons in the human body

(119) Photons undergo three main interactions in which they transfer their energy to electrons or positrons: the photo-electric effect, Compton scattering, and pair (and triplet) production. Energy deposition in the human body is due to the energy transferred to and then lost by electrons and positrons along their paths. Electrons and positrons can produce secondary photons as bremsstrahlung and characteristic x rays emitted after ionisation, and positrons by particle annihilation.

(120) In soft tissue, the photon energy deposition at energies below 30 keV is dominated by the photo-electric effect, while for energies between 30 keV and 25 MeV, the photon energy is transferred to electrons through Compton scattering. Pair production is the dominant interaction for energies above 25 MeV.

4.1.2. Calculation conditions for photons

(121) The primary calculations for external photons were performed with EGSnrc Version v4-2-3-0 (Kawrakow et al., 2009). The reader is referred to Section 3.3.1 and Schlattl et al. (2007) for more details on the code used. The dose conversion coefficients for large organs (e.g. lungs or liver) could be determined in all geometries with relative statistical uncertainties up to 0.5%. Importance sampling was used to reach

relative statistical uncertainties of less than 2%, even in the smallest organs. The number of particles reaching the gall bladder, prostate, testes, ovaries, thymus, and thyroid was artificially enhanced by a factor of five, while the number of photons in the region of the glandular breast tissue and adrenals was 10 times higher than in tissue regions outside these organs. Generally, statistical uncertainties were smaller at lower photon energies. Nevertheless, at the lowest energies considered (from 10 to 20 keV), relative statistical uncertainties for small organs, such as gall bladder, up to 10% were found, as only a few photons are able to reach these organs.

(122) Secondary calculations for external photons were performed with MCNPX Version 2.6. In order to include possible photonuclear interactions, the CEM03 physics model was selected for photon transport calculations. The resulting absorbed doses were compared with a sampling of doses computed at the same energies, with the Bertini model selected to model photonuclear interactions. The differences observed were negligible as the photonuclear interactions are a small contribution to the absorbed dose over this energy range. The dose conversion coefficients for large organs (e.g. lungs and liver) were determined in all geometries and energies with relative statistical uncertainties of less than 0.5%. Smaller organs were limited to relative statistical uncertainties of less than 2% even in the smallest organs, except for very high energies at which they approached 5%. Generally, the uncertainties were smaller at lower photon energies. Nevertheless, at the lowest energies considered (10–20 keV), relative statistical uncertainties for small organs, such as gall bladder, up to 10% were found, as relatively few photons are able to reach these organs.

(123) Validation calculations were performed with the GEANT4 code for AP irradiation. Relative statistical uncertainties for photons with energies above 30 keV were, at most, 3% for larger organs and 10% for smaller organs. Below 30 keV, when relatively few energy deposition events take place in deeper regions of the phantom, the relative statistical uncertainties for smaller organs (e.g. adrenals) exceeded 10%.

(124) Dose conversion coefficients for idealised external exposures were evaluated as absorbed dose per particle fluence and given in units of pGy cm^2. Additionally, for energies up to 10 MeV, the conversion coefficients have been tabulated as organ-equivalent doses per air kerma, K_a, in Sv/Gy. For this transformation, conversion coefficients for air kerma per fluence were applied (Seltzer, 1993).

(125) As described in Section 3.4, the active marrow and endosteum doses were estimated as the absorbed dose to spongiosa in each individual bone site. Skeletal-averaged absorbed doses to these two target tissues were taken as the mass-weighted average of the regional spongiosa and medullary cavity dose.

(126) The calculation of the effective dose was performed as described in Section 2.2.4.

4.1.3. Differences among results of Monte Carlo codes for photons

(127) The data sets generated from the EGSnrc, MCNPX 2.6, and GEANT4 codes show very good agreement. As an example, Fig. 4.2 shows the absorbed dose conversion coefficients generated by the three transport codes for a colon target

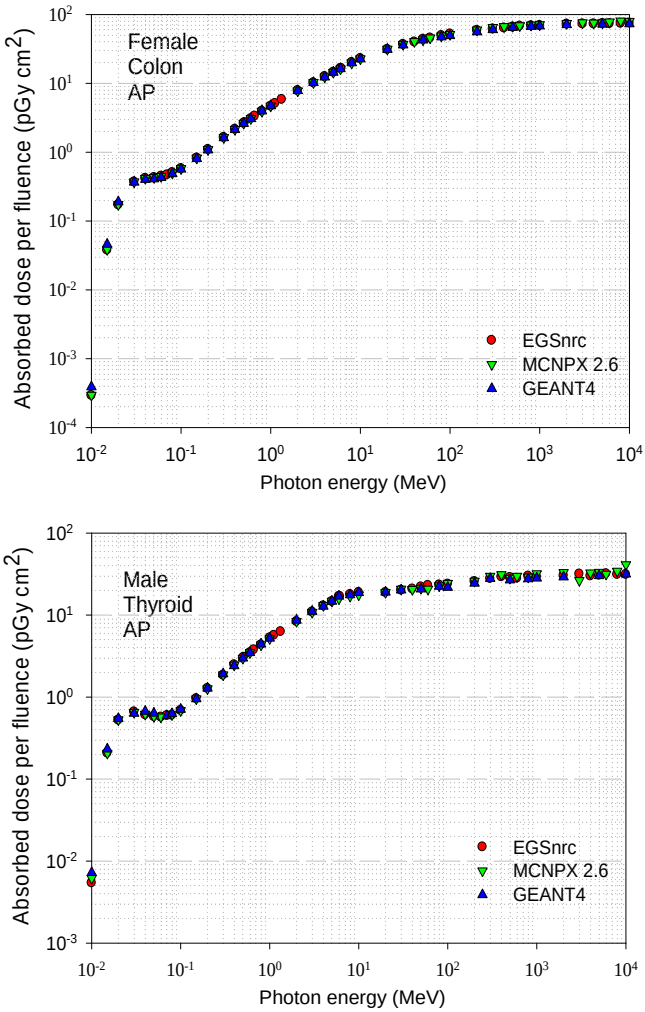

Fig. 4.2. Comparison of dose conversion coefficients of colon (female) and thyroid (male) for antero-posterior (AP) geometry, calculated by three Monte Carlo programs.

within the female phantom and a thyroid target within the male phantom, both under AP irradiation geometry.

(128) The reference absorbed dose conversion coefficients were evaluated from the data of all calculators by applying data averaging, smoothing, and fitting. The reference effective dose conversion coefficients are given in Annex A and shown graphically in Fig. 4.4. Annex B presents lists of the reference organ absorbed dose conversion coefficients for photons for all organs contributing to the effective dose and the remainder tissues. Conversion coefficients for the lens of the eye can be found in Annex F.

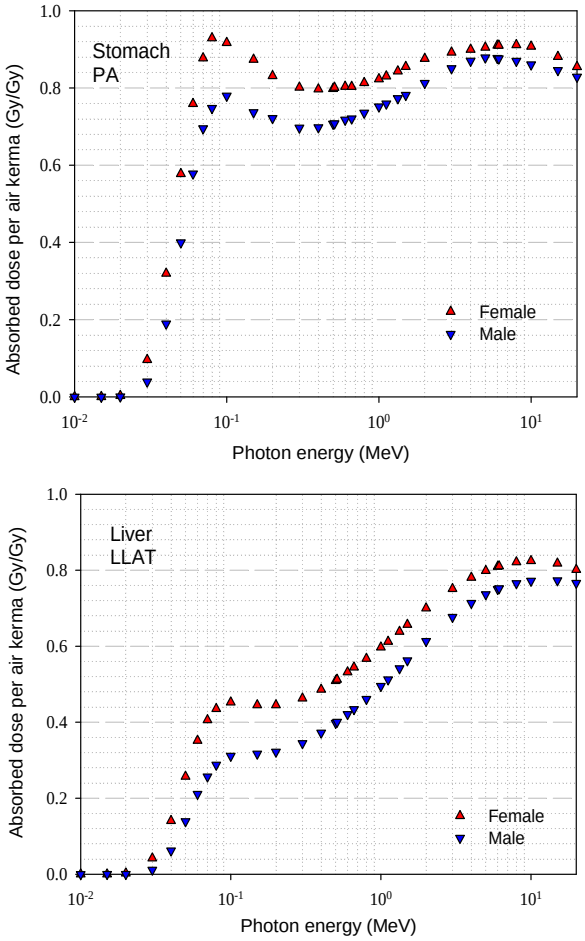

Fig. 4.3. Comparison of stomach postero-anterior (PA) and liver left lateral (LLAT) organ dose conversion coefficients for photons of the male and female reference phantoms.

4.1.4. Analysis of organ dose conversion coefficients for photons

(129) The organ absorbed dose conversion coefficients show a noticeable difference between the sexes of the phantoms (Schlattl et al., 2007). The smaller stature of Reference Female leads to higher values (30–50% or more) in several organs than those found in Reference Male. In contrast, under AP geometry and for low photon energies, the shielding by the female breast causes the conversion coefficients to be lower compared with the male phantoms for several organs in the upper torso. The organ dose conversion coefficients for the male and female phantoms show their largest differences at photon energies from ~40 to 80 keV. The relative differences are largest for unidirectional irradiation (i.e. AP, PA, LLAT, and RLAT), and can approach

50%. In most cases, these differences increase with decreasing photon energy. With decreasing photon energy, the depth of an organ within the human body becomes an increasingly important parameter, strongly influencing the value of the organ dose conversion coefficient. This can lead to high relative differences of 100% or more for conversion coefficients below ~20–30 keV photon energy.

(130) Fig. 4.3 shows dose conversion coefficients for the stomach and liver under PA and LLAT irradiation geometries, respectively. For ROT and ISO photon sources, the organ dose conversion coefficients are nearly the same for all organs of the male and female phantoms.

4.1.5. Analysis of effective dose conversion coefficients for photons

(131) Fig. 4.4 shows the effective dose per fluence for photon exposures and the idealised geometries considered. For energies up to 4 MeV, AP irradiation geometry results in the highest values of effective dose. However, above 30 MeV, AP geometry shows the lowest values.

4.1.6. Comparison with ICRP *Publication 74* (ICRP, 1996) for photons

(132) The data of ICRP *Publication 74* (ICRP, 1996) for photons were calculated using the mathematical phantoms Adam and Eva (Kramer et al., 1982), derived from the Medical Internal Radiation Dose (MIRD) Committee phantom (Snyder et al., 1969, 1978). The GSF code was used (Kramer et al., 1982; Veit et al., 1989), a successor of the ALGAM code (Warner and Craig, 1968) developed at Oak Ridge National Laboratory. The cross sections used were those of the DLC99/HUGO library (Roussin et al., 1983).

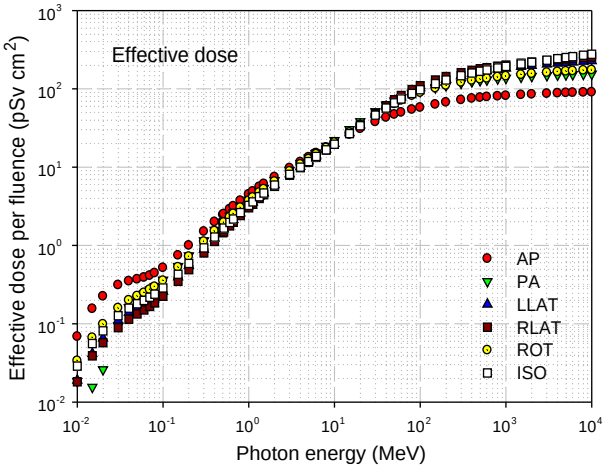

Fig. 4.4. Effective dose per fluence for photon exposures for various geometries. AP, antero-posterior; PA, postero-anterior; LLAT, left lateral; RLAT, right lateral; ROT, rotational; ISO, isotropic.

(133) In ICRP *Publication 74* (ICRP, 1996), the energy transferred at the point of a photon interaction was assumed to be deposited at that point (i.e. secondary electrons were not followed). This simplification is called the 'kerma approximation'. The kerma approximation is valid as long as there is approximate secondary particle equilibrium in the volume of interest, an acceptable assumption for all points located

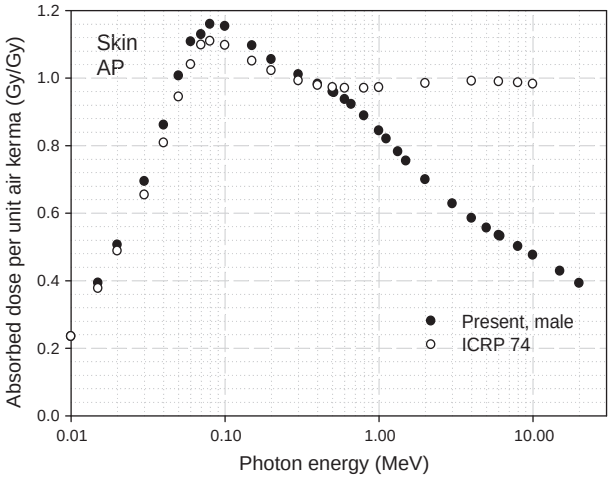

Fig. 4.5. Comparison of skin absorbed dose conversion coefficients for the male phantom for antero-posterior geometry as calculated for the present report and those of ICRP *Publication 74* (ICRP, 1996).

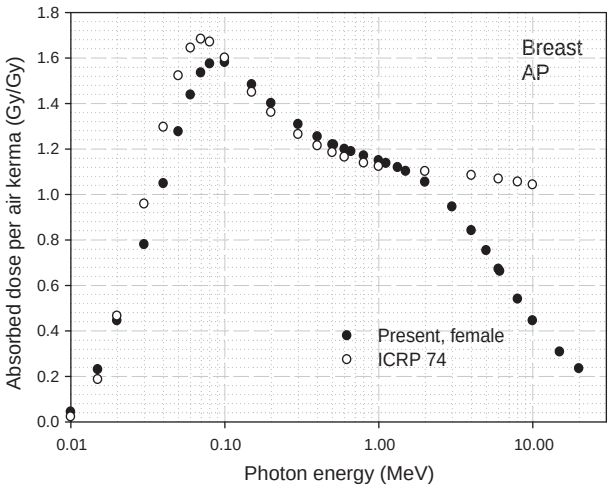

Fig. 4.6. Comparison of the breast absorbed dose conversion coefficients of the female phantom for antero-posterior geometry as calculated for the present report and those of ICRP *Publication 74* (ICRP, 1996).

well within the body. However, for superficial organs (e.g. skin, breast, and testes), the kerma approximation leads to overestimations of absorbed dose of up to a factor of two at a photon energy of 10 MeV. For the superficial organs, the kerma approximation is only valid below ~1 MeV. In the present report, all secondary electrons were followed regardless of the incident photon energy. It should be noted that in external irradiation by photons, the exposure is always accompanied by exposure from associated secondary electrons (and positrons) for which conversion coefficients must be included to estimate absorbed doses.

(134) In ICRP *Publication 74* (ICRP, 1996), simplified elemental compositions were assumed in the Adam and Eva stylised phantoms. In the present report, a more comprehensive list of tissue elemental compositions is considered as documented in ICRP *Publication 110* (ICRP, 2009).

Organ absorbed doses

(135) The largest differences between the organ dose conversion coefficients computed for the present report and those given in ICRP *Publication 74* (ICRP, 1996) can be attributed to the different anatomy of the models employed, confirming earlier findings of other authors (Jones, 1997; Chao et al., 2001; Zankl et al., 2002; Ferrari and Gualdrini, 2005; Kramer et al., 2005; Schlattl et al., 2007) who used their own voxel phantoms in comparison with ICRP *Publication 74* (ICRP, 1996). Some of the observed differences in the dose conversion coefficients can be explained by the shape of the thorax of the stylised mathematical models, which is composed of an extended ellipsoid with embedded arm bones. This shape is somewhat different from real human anatomy in which the thorax is more rectangular in cross section.

(136) Secondly, an important difference between the present report and ICRP *Publication 74* (ICRP, 1996) is that the transport of secondary electrons is considered for the calculations of the present report, instead of the use of the kerma approximation for which secondary electrons are deposited locally. This influences the absorbed dose conversion coefficients of superficial organs (e.g. skin and breast) at incident photon energies exceeding 400 keV and 1 MeV, respectively (Figs. 4.5 and 4.6). For these energies, not all electrons released in superficial, thin organs are absorbed locally and thus the resulting dose conversion coefficients are lower compared with those calculated under the kerma approximation.

(137) Also, Schlattl et al. (2007) concluded that below 40 keV, variations in transport codes, cross sections, and organ composition can influence the values of the dose conversion coefficients, showing relative differences of up to 20%. As a result of the differences between the mathematical and voxel phantoms, higher dose conversion coefficients for RLAT exposures are observed in the reference computational phantoms, particularly for colon, pancreas, and stomach. Lower dose conversion coefficients are obtained for active marrow and thyroid. Furthermore, the lungs and thymus are better shielded by the rib cage of the reference computational phantoms, and thus their absorbed dose conversion coefficients are smaller than in the stylised mathematical phantoms. For example, the absorbed dose conversion coefficient for the lungs at 100 keV is ~30% less than the corresponding value given in ICRP *Publication 74* (ICRP, 1996). As noted by Lee et al. (2006), the somewhat

simplified location of the arms in the stylised phantoms also contributes to the overestimation of the lung dose for LAT exposures. Except for the pancreas, the same trends are apparent for LLAT irradiation. In this case, the dose conversion coefficients for the pancreas are similar in mathematical and voxel phantoms. Higher conversion coefficients emerge for the liver, which is less shielded in the reference computational phantoms from LLAT irradiation compared with the mathematical phantoms. Under AP irradiation, the stomach and thymus receive a lower absorbed dose in the reference voxel phantoms, but the dose conversion coefficients for active marrow and, especially, the oesophagus are underestimated by the values given in ICRP *Publication 74* (ICRP, 1996). In the stylised mathematical phantoms Adam and Eva, the oesophagus is located more towards the posterior of the body than in reality, which explains the rather large conversion coefficient in PA geometry for this phantom type.

(138) In comparison with ICRP *Publication 74* (ICRP, 1996), higher dose conversion coefficients are obtained for the thymus and thyroid for PA geometry. These organs are shielded more by the spine in the stylised mathematical phantoms. In contrast, lower conversion coefficients are obtained for the active marrow, small and large intestines, kidneys, and pancreas. This indicates that the distance of the intestine, kidneys, and pancreas to the back of the body is underestimated by the stylised mathematical phantoms, and/or the organs are located more towards the front of the phantoms.

(139) In conclusion, for most organs, the new dose conversion coefficients deviate by up to 20% from the reference values given in ICRP *Publication 74* (ICRP, 1996). However, for some organs, including many that make large contributions to the effective dose, the relative differences are ~30% or even higher under certain

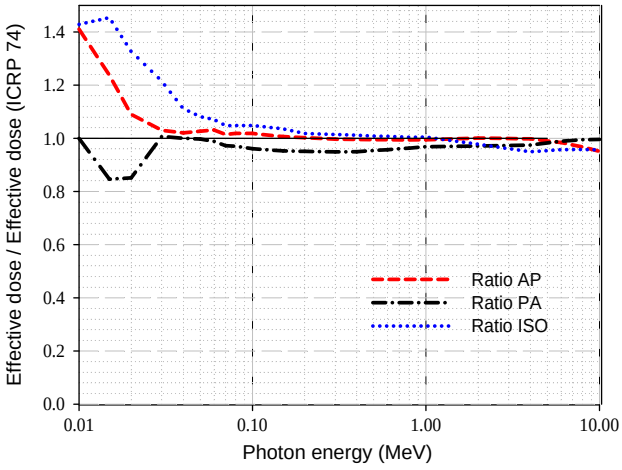

Fig. 4.7. Ratios of effective dose per air kerma conversion coefficients for photons from the present report to values given in ICRP *Publication 74* (ICRP, 1996). AP, antero-posterior; PA, postero-anterior; ISO, isotropic.

irradiation geometries. Overall, the main differences between organ dose conversion coefficients in ICRP *Publication 74* (ICRP, 1996) and those of the present report can be attributed to the more realistic anatomy represented by the reference phantoms from ICRP *Publication 110* (ICRP, 2009).

Effective dose

(140) Fig. 4.7 shows the ratios of the effective dose per air kerma in the present report to those given in ICRP *Publication 74* (ICRP, 1996) and ICRU Report 57 (ICRU, 1998) for photon irradiation for AP, PA, and ISO geometries. For AP and ISO geometries, the effective dose per air kerma conversion coefficients are very similar to those given in ICRP *Publication 74* (ICRP, 1996) at incident photon energies between 0.1 and 6 MeV. For AP geometry and for photons of energies between 6 and 10 MeV, the present values of effective dose per air kerma are lower than the previous values due to overestimation of the breast dose under the kerma approximation. The largest differences were observed for PA and LAT irradiations, although above 0.1 MeV, the differences in the values of the sets of conversion coefficients are, at most, a few percent of a Sv/Gy. In these cases, the modifications to tissue weighting factors in ICRP *Publication 103* (ICRP, 2007) have had the largest impact. The lower effective dose conversion coefficients for PA irradiation are mainly caused by the smaller conversion coefficients of highly weighted organs (e.g. active marrow, lung, and large intestine). For LAT exposures, organ dose conversion coefficients for some organs are lower than given in ICRP *Publication 74* (ICRP, 1996) (lungs, active marrow, oesophagus, and thyroid), while they are higher for other organs (colon and stomach). These competing differences are averaged out and result in a moderate increase in the effective dose conversion coefficient for LAT irradiation. Nevertheless, the increased tissue weighting factor for the breast and the remainder tissues, and the decreased tissue weighting factor for the gonads in ICRP *Publication 103* (ICRP, 2007) yields an effective dose conversion coefficient for LAT irradiation that is somewhat higher than that given previously in ICRP *Publication 74* (ICRP, 1996). In conclusion, the relative changes in the effective dose conversion coefficients are small (below 20%). Therefore, the impact of the changes of the dosimetric procedure brought by the new phantoms and the revised weighting factors of ICRP *Publication 103* (ICRP, 2007) is moderate for external photon exposures.

4.2. Electrons and positrons

4.2.1. Characteristics of energy deposition by electrons and positrons in the human body

(141) The simulation of electron and positron transport is more complicated than that of photons, primarily because the average energy loss of an electron in a single interaction is very small (of the order of a few tens of eV). As a consequence, high-energy electrons suffer a large number of interactions before being effectively absorbed in the medium. In common radiation transport codes, these interactions

are typically not modelled explicitly and particle energy loss is handled through multiple-scattering theories.

(142) Along their path in the human body, electrons and positrons undergo numerous scattering events, at times producing secondary electrons (delta rays), in which the particles lose their energy. Bremsstrahlung photons can be produced in the scattering process. For energies below ~100 MeV, the primary energy-loss processes for electrons in soft tissue are due to ionisation and excitation of the constituent atoms, while bremsstrahlung production is the dominant process for higher energies.

(143) In soft tissue, the electron and positron range for energies below ~300 keV is less than 1 mm, so they can only penetrate the skin of the voxel phantom. For positrons, the annihilation photons can also cause absorbed dose in deeper organs. For electrons, only photons released by the bremsstrahlung process are able to traverse the skin. For low-energy electrons and positrons in soft tissue, only a very small fraction of the energy is transferred to bremsstrahlung photons; therefore, the absorbed doses in deeper organs are also very small for these low-energy particles.

(144) The cross sections for electron–electron (Møller scattering) and positron–electron (Bhabha scattering) interactions are fairly similar, so their penetration depths in the human body are almost equal. Nevertheless, positrons do also annihilate with electrons present within the tissue, creating two photons of 511 keV which can contribute a large fraction of the dose, particularly for positron energies below a few MeV.

4.2.2. Calculation conditions for electrons and positrons

(145) The primary calculations were performed with MCNPX Version 2.6.0 (Pelowitz, 2008). For more details on the code used, see Section 3.3.4. CEM03 physics was used to ensure that photonuclear reactions were included, although they represent a very small contribution to the total absorbed doses. The electron and positron organ dose conversion coefficient uncertainties varied strongly with energy and orientation in the parallel beams, so a complete description of their magnitude is not included in this discussion. Most of the calculated organ doses for particles below 150 keV, with the exception of skin, had extremely high statistical uncertainties. This is expected due to the short ranges of the particles at low energies, and the amount of intervening tissue between the surface of the body and most internal organs. For sufficiently penetrating electron/positron energies, the organ dose relative uncertainties were below 2%. For less penetrating energies, the internal organs had relative uncertainties of up to 10%. In the worst cases for very short-range electrons and positrons, the uncertainties approached 70–100% for small organs, although almost of all of these high uncertainties were for energies below 150 keV. All effective dose relative uncertainties were less than 2% for energies above 100 keV. The large relative uncertainties in organ absorbed dose for incident particles at lower energies and for organs at deeper depths in the phantoms are a consequence of the deposition of energy of the few bremsstrahlung photons produced at shallow tissue depths. It should be noted that the MCNP codes have traditionally ignored electron/positron

differences in particle transport, except for the obvious issues of annihilation, charge deposition, and magnetic field tracking.

(146) A secondary set of calculations for external electron irradiations was performed with the EGSnrc code. For electron energies below 200 keV, a variance-reduction technique called 'bremsstrahlung splitting' (Rogers and Bielajew, 1990; Rogers et al., 1995) has been applied to decrease the relative statistical uncertainty of absorbed dose in internal organs that are beyond the range of the externally incident electrons.

(147) Validation calculations were performed with the GEANT4 code for AP irradiation. For electron and positron transport, the GEANT4 code includes the processes of bremsstrahlung, ionisation/excitation, delta-ray production, and positron annihilation. For electrons, the relative statistical uncertainties were below 4% for incident energies of 600 keV for larger organs and 10% for smaller organs. Due to annihilation events, the relative statistical uncertainties for positrons were below 2% at 10 keV for all internal organs.

(148) Dose conversion coefficients for AP, PA, and ISO exposures were computed as absorbed dose per particle fluence. The computation of the effective dose was performed as described in Section 2.2.4.

4.2.3. Differences among Monte Carlo codes for electrons and positrons

(149) The conversion coefficients calculated with the MCNPX 2.6, EGSnrc, and GEANT4 codes showed very good agreement. As an example, Fig. 4.8 shows the absorbed dose per fluence in the thyroid of Reference Female irradiated by external electrons in AP geometry. Exceptions to this good agreement are the MCNPX results at positron energies of a few MeV, as shown in Fig. 4.9. Here, the absorbed

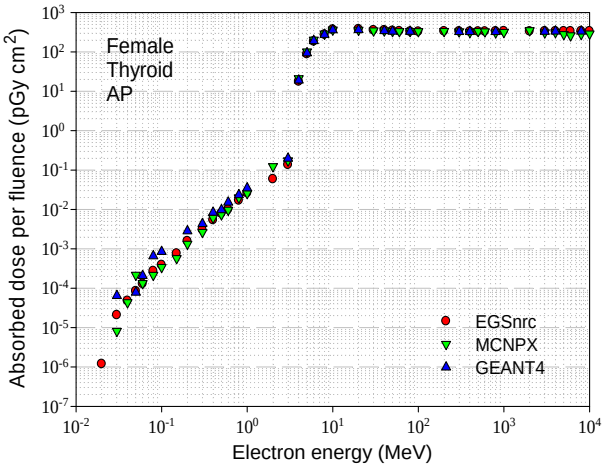

Fig. 4.8. Comparison of dose conversion coefficients of thyroid (female) for antero-posterior geometry, calculated by different Monte Carlo codes.

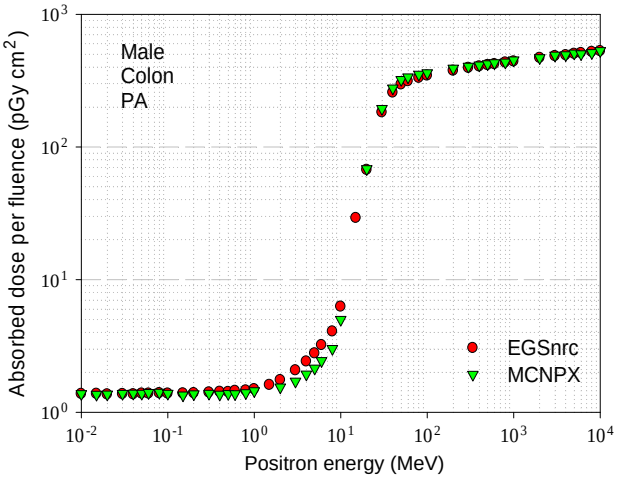

Fig. 4.9. Comparison of dose conversion coefficients of colon (male) for postero-anterior geometry, calculated by different Monte Carlo codes.

dose per fluence for the male colon is shown for incident positrons in PA geometry. These discrepancies are attributed to the fact that, in contrast to the EGSnrc and GEANT4 codes, the MCNPX code uses electron physics models to transport positrons (H. Grady Hughes, Los Alamos National Laboratory, personal communication). Consequently, the MCNPX results for positron energies between 1 and 20 MeV are disregarded in this report, and are not utilised for establishing reference conversion coefficients.

4.2.4. Analysis of organ dose conversion coefficients for electrons and positrons

(150) The reference absorbed dose conversion coefficients were evaluated from the data of all calculators by applying methods of data averaging, smoothing, and fitting. Lists of the reference organ absorbed dose conversion coefficients for electrons and positrons for all organs contributing to the effective dose, the remainder tissues and the lens of the eye, can be found in the CD accompanying this report.

(151) As described in Section 3.4, the active marrow and endosteum absorbed doses were estimated as the absorbed dose to spongiosa for each individual bone site. Skeletal-averaged absorbed doses to these two target tissues were then taken as the mass-weighted average of their corresponding regional spongiosa absorbed dose.

(152) The dose conversion coefficients for electrons and positrons are very similar for particle energies above 100 MeV as their interaction cross sections are similar. This is demonstrated in Fig. 4.10, which shows the conversion coefficients for pancreas within the male phantom for both externally incident electrons and positrons.

(153) At lower energies, electrons and positrons cannot penetrate the body to reach deeper organs; consequently, the absorbed doses to these deeper organs are due solely to secondary photons. In the case of electrons, the photons are only

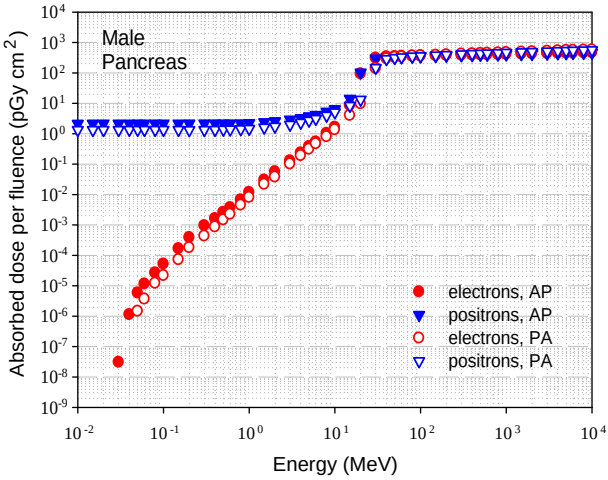

Fig. 4.10. Comparison of pancreas (male) dose per fluence for antero-posterior (AP) and postero-anterior (PA) geometries for electrons and positrons.

emitted through the bremsstrahlung processes in which both the photon yield and mean photon energy increase with increasing electron energy. This leads to very low dose conversion coefficients on the order of 10^{-6} pGy cm^2 or less at 10 keV. Above 10 keV, the dose conversion coefficients increase as an almost quadratic function of the incident electron energy. Low-energy positrons annihilate within the skin and two annihilation photons of 511 keV are created which are able to reach deeper organs. The absorbed dose to the deeper organs due to the annihilation photons is much higher than that due to the bremsstrahlung photons generated for external electrons. Consequently, for many organs and for positron energies between 10 keV and ~1 MeV, the organ dose conversion coefficients for positrons are rather constant.

(154) For energies between ~1 and 10 MeV, positrons and electrons start to reach deeper organs directly, and the dose conversion coefficients rise in this energy interval by more than three orders of magnitude. The onset of this rise strongly depends on the effective depth of the organ, which depends on the irradiation direction and phantom sex. For some organs (e.g. ovaries), this leads to a noticeable difference in the shape and relative position of the curve, and the corresponding values of the conversion coefficients in this energy range (see Fig. 4.11). For larger organs (e.g. lungs), the differences between irradiation geometries and phantom sex are less prominent.

(155) The conversion coefficients for external electrons and positrons incident upon the female phantom are mostly larger than those of the male phantom for deeper organs, as can be seen in Fig. 4.12. Exceptions are the gonads, for which the dose conversion coefficients of the male are larger than those of the female, as shown in Fig. 4.13. This is an effect of the differences in the depth and position of the testes in the male and the ovaries in the female.

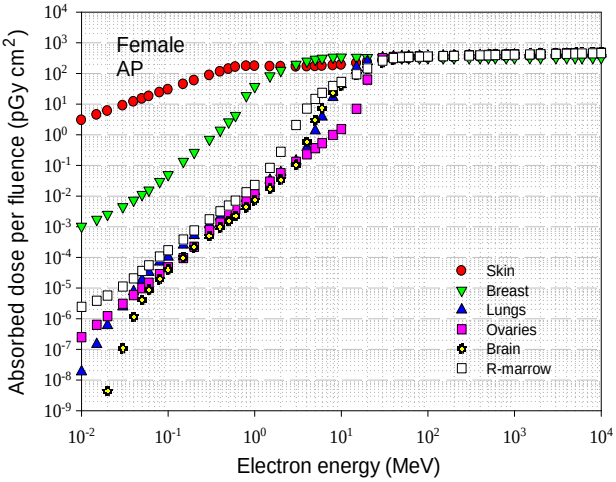

Fig. 4.11. Organ dose conversion coefficients per electron fluence for the female phantom for antero-posterior geometry. R-marrow, red bone marrow.

(156) The skin is always directly exposed to primary particles. The skin thickness of the male and females phantoms is ~2.1 mm and ~1.8 mm, respectively. The continuous-slowing-down approximation (CSDA) range of electrons with energies below 600 keV in skin is 2.1 mm. Therefore, for energies below 600 keV, almost all the energy is deposited in the skin of both phantoms. For energies above 600 keV, the electrons and positrons can traverse the skin voxels; thus, the values of the dose conversion coefficients are not determined by particle energy and mass of the skin

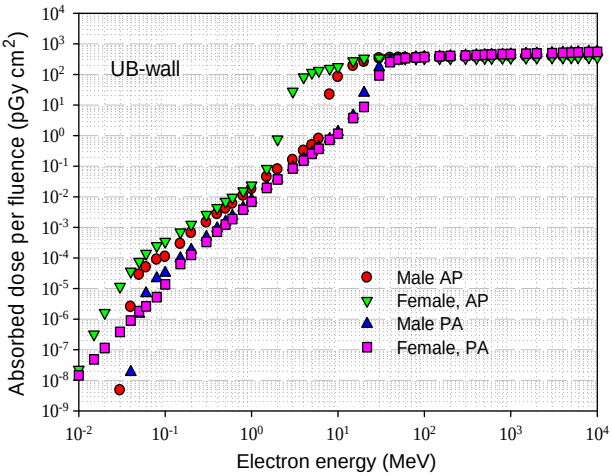

Fig. 4.12. Comparison of male and female urinary bladder wall dose per electron fluence for antero-posterior (AP) and postero-anterior (PA) geometries.

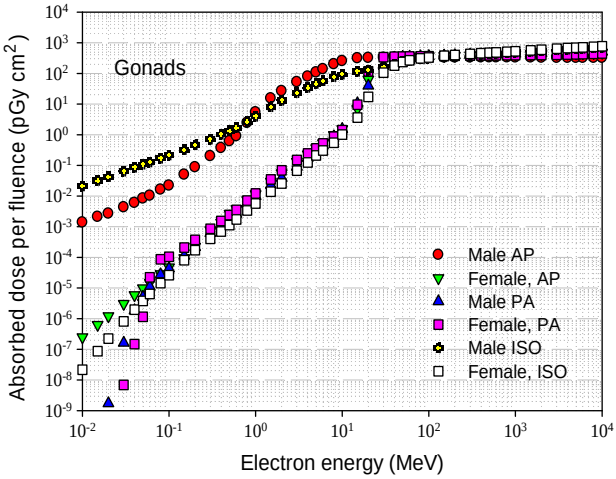

Fig. 4.13. Comparison of gonad dose per electron fluence for antero-posterior (AP), postero-anterior (PA), and isotropic (ISO) geometries.

alone. For incident energies above ~60 MeV, the electrons and positrons can traverse the entire thorax, and from this energy upwards, the dose conversion coefficients increase almost linearly with electron or positron energy. Fig. 4.14 shows the skin dose per fluence for electrons and positrons for the male and female phantoms. The differences between the male and female conversion coefficients are primarily due to their different skin masses (see also Section 3.5.1).

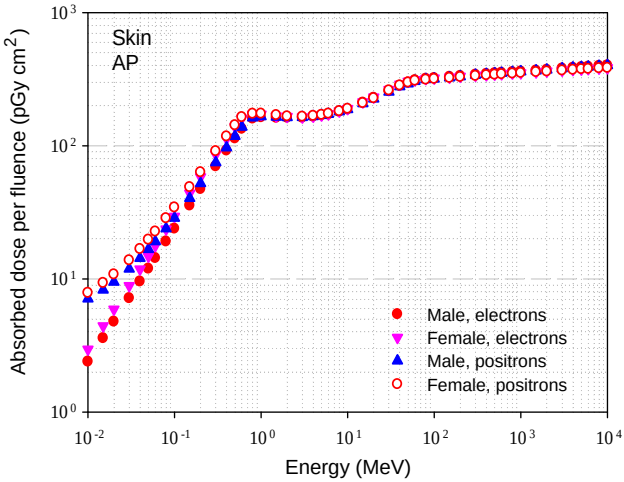

Fig. 4.14. Skin dose per fluence for electrons and positrons for the male and female phantoms for antero-posterior geometry.

4.2.5. Analysis of effective dose conversion coefficients for electrons and positrons

(157) Fig. 4.15 shows the values of effective dose conversion coefficients per fluence for electrons and positrons as a function of energy for the idealised geometries considered. It can be seen that the values of effective dose for both particles increase with energy, as deeper organs are progressively reached by the incident particles. For energies up to ~1 MeV, the absorbed dose to skin is the largest contributor to the effective dose. The reference effective dose conversion coefficients are given in tabular form in Annex A and in the CD accompanying this report.

4.2.6. Comparison with ICRP *Publication 74* (ICRP, 1996) for electrons and positrons

(158) Fig. 4.16 shows the present reference values of the effective dose per fluence in comparison with the values presented in ICRP *Publication 74* (ICRP, 1996). The ICRP *Publication 74* values were calculated in the energy range 100 keV–10 MeV. Below 600 keV, almost all the incident particle energy is deposited within the skin. The skin of the stylised phantoms employed for the electron calculations in ICRP *Publication 74* (ICRP, 1996) included a 70-μm insensitive layer, which was not included in the present voxel model. This insensitive layer results in lower values for effective dose per fluence at the lowest energy of 100 keV. At 400 keV, the agreement is good; however, from ~1 to 4 MeV, the ICRP *Publication 74* values are lower than the recommended results given in this report. These differences are due to the corresponding differences in the models of the breasts and gonads (testes and ovaries), as seen in the stylised models of ICRP *Publication 74* (ICRP, 1996) and the voxel phantoms of ICRP *Publication 110* (ICRP, 2009). Above 4 MeV, the agreement between the dose conversion coefficients from ICRP *Publication 74* and the present recommendations is very good.

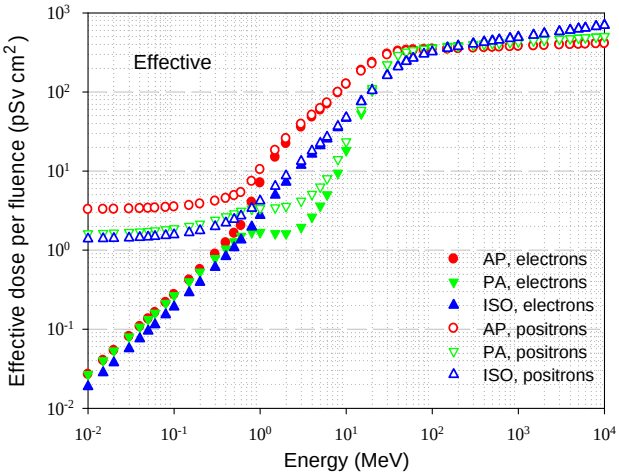

Fig. 4.15. Effective dose per fluence for electrons and positrons for antero-posterior (AP), postero-anterior (PA) and isotropic (ISO) geometries.

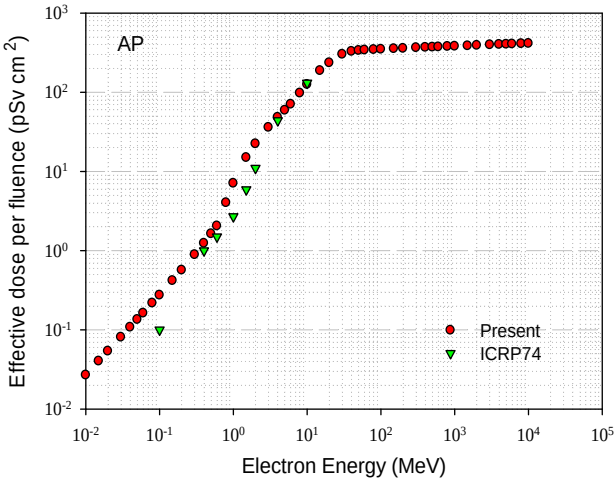

Fig. 4.16. Comparison of the effective dose per electron fluence between the present report and the values given in ICRP *Publication 74* (ICRP, 1996) for antero-posterior geometry.

4.3. Neutrons

4.3.1. Characteristics of energy deposition by neutrons in the human body

(159) Neutrons undergo many interactions in the human body in which many different types of secondary particles are produced. The deposition of energy is a complex process, and generally fluence to absorbed dose conversion coefficients are strongly energy dependent.

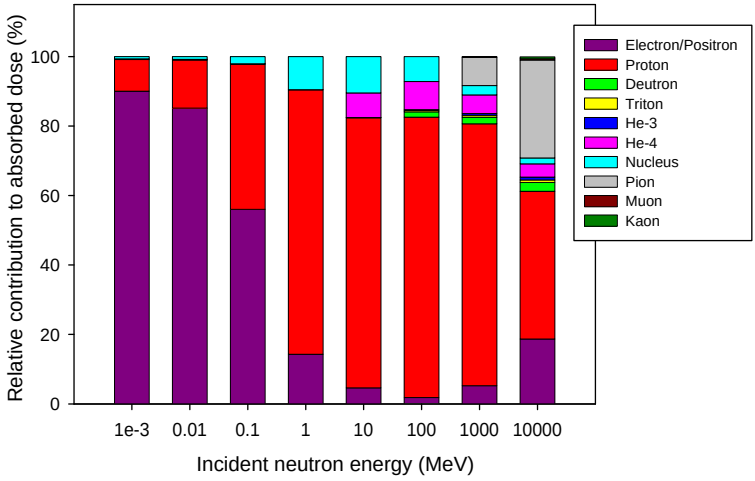

Fig. 4.17. Calculated relative absorbed dose contribution of various secondary charged particles, produced by neutron-induced reactions or elastic scattering.

(160) Fig. 4.17 shows the relative absorbed dose contribution of secondary charged particles in the whole body of the male voxel phantom in ISO geometry as a function of incident neutron energy. For neutrons with incident energies up to ~10 keV, secondary photons contribute the major fraction of the absorbed dose deep within the body, and ~90% of the absorbed dose comes from 2.2 MeV photons emitted during neutron capture by hydrogen. As photons deposit their energy via electrons and positrons, the photon contribution is classified in Fig. 4.17 under 'Electron/Positron'. The rest of the absorbed dose (~10%) originates from the $^{14}N(n,p)^{14}C$ reaction; protons and ^{14}C recoil nuclei deposit their energy and are classified into 'Proton' and 'Nucleus', respectively. Photons contribute 90% of the absorbed dose from irradiation by thermal- and epithermal neutrons; at neutron energies above 10 keV, the contribution to absorbed dose from photons falls sharply and is less than 20% at 1 MeV. At energies above ~1 keV, the energy deposited by recoil protons from elastic scattering with hydrogen becomes important, while at energies above a few MeV, the production of charged particles by nuclear reactions becomes an increasingly important mechanism for the deposition of incident neutron energy. As the incident energy of the neutrons increases, various secondary particles emitted in inelastic nuclear reactions play an important part in the distribution of absorbed dose to internal organs.

(161) To compute organ absorbed doses by the Monte Carlo method, every secondary charged particle is tracked and the resulting energy deposition in each organ is summed. However, at neutron energies below 20 MeV, the absorbed dose is usually computed by means of kerma approximation. In fact, the ranges of the secondary charged particles are very small [the range of 20-MeV protons is about 4 mm in tissue (ICRU, 1993)] compared with most organ dimensions, and thus charged-particle equilibrium is approximately achieved for many organs. For a given neutron energy, the organ absorbed dose is simply determined by the neutron fluence in that organ multiplied by the appropriate kerma coefficient. Above 20 MeV, fewer of the body's organs and tissues can be considered to be in charged-particle equilibrium, and thus detailed transport calculations of the secondary charged particles must be performed.

4.3.2. Calculation conditions for neutrons

(162) Four different codes were used to calculate the data reported here (Table 4.1). The energies considered ranged from 0.001 eV to 10 GeV, and the geometries simulated were AP, PA, LLAT, RLAT, ROT, and ISO.

(163) Primary calculations were obtained with the PHITS code. For neutron energies below 20 MeV, this code employs the kerma approximation using the evaluated nuclear data files ENDF/B-VI. Nuclear reactions induced by neutrons from 20 MeV to 3.5 GeV were simulated by the JQMD model, while those induced by higher-energy particles were dealt with using the JAM model. For the PHITS simulations, the relative standard deviations of the conversion coefficients for these organs were generally small, less than 5%, but those for smaller organs (e.g. thyroid) were up to 15%.

More details on these simulations with the PHITS code can be found in Sato et al. (2009).

(164) Secondary calculations were performed with the FLUKA code. Below 20 MeV, absorbed doses in organs were calculated using the kerma approximation employing a neutron cross section library consisting of 260 groups. For energies between 20 MeV and 5 GeV, hadron–nucleon and hadron–nucleus interactions were simulated by the PEANUT package, which includes a Generalised Intra-nuclear Cascade model and a Pre-equilibrium model. The Dual Parton model was employed for energies above 5 GeV. The relative statistical uncertainties for the larger organs were mainly between 0.8% and 3% depending on neutron energy. For smaller organs (e.g. thyroid), however, the range of relative statistical uncertainties was between 0.8% and 8%.

(165) Validation calculations were performed using MCNPX Version 2.5.0 and GEANT4 codes. In the MCNPX calculation, the absorbed dose in each organ was calculated using the kerma approximation and the ENDF/B-VI and LA-150 libraries. For nuclides available from the LA-150 library, tabulated cross sections were used up to 150 MeV. For nuclides not included in the LA-150 library, the ENDF/B-VI data was used up to 20 MeV. In the absence of tabulated data, the Bertini Intra-nuclear Cascade model was employed up to 3.5 GeV, and the FLUKA89 (Aarnio et al., 1990) high-energy generator was used above 3.5 GeV.

(166) The GEANT4 validation calculation was performed for AP geometry. For neutrons below 20 MeV, the absorbed dose in each organ was calculated using the kerma approximation and the ENDF/B-VI library. From 20 MeV to 3 GeV, processes were simulated using the Bertini Intra-nuclear Cascade model (GEANT4, 2006). Above 3 GeV, the Low Energy Parameterized (LEP) and High Energy Parameterized (HEP) models (GEANT4, 2006) were used, which are improved versions of the well-known GEISHA package of GEANTA3 (Fesefeldt, 1985). Relative statistical uncertainties were below 5% for all organs over the entire energy range.

(167) As the secondary particles produced from nuclear reactions play a dominant role in the energy-deposition processes for high-energy irradiations, the dependence of the nuclear reaction model employed in the codes for simulating high-energy nuclear reactions was investigated. PHITS employed the JQMD model combined with the Generalised Evaporation Model (GEM) for energies between 20 MeV and 3.5 GeV, and the JAM model with the GEM for energies above 3.5 GeV. The FLUKA code used the PEANUT (Cascade Pre-equilibrium model) up to 5 GeV and the Dual Parton model above 5 GeV. The MCNPX code used the Bertini Intra-nuclear Cascade model below 3.5 GeV with a switch to the FLUKA89 (Aarnio et al., 1990) high-energy generator above 3.5 GeV. The GEANT4 code employed the Bertini Intra-nuclear Cascade model up to 3 GeV, and used the LEP model above 3 GeV, which is suitable for energies up to 20 GeV.

4.3.3. Differences among Monte Carlo codes for neutrons

(168) Comparisons of organ absorbed dose data produced by different codes revealed that the variations among the results were, in almost all cases, much smaller

than the estimated relative statistical uncertainties. The reference dose conversion coefficients were obtained from all calculation results by averaging and smoothing with a cubic spline function (de Boor, 1978). The agreement among the codes is very good, as can be seen in Fig. 4.18 which shows the gonad absorbed dose conversion coefficients of the female phantom and the lung absorbed dose conversion coefficients of the male phantom. The data points obtained from each code are shown together with the final reference values.

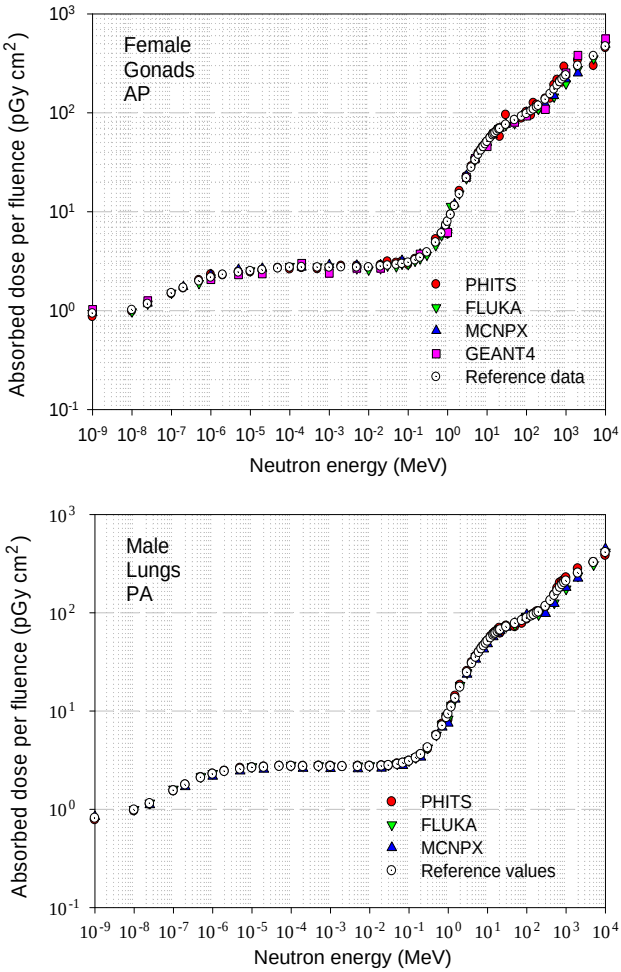

Fig. 4.18. Reference and original data for neutrons for the absorbed dose to the gonads (female) and lungs (male) for antero-posterior geometry.

4.3.4. Analysis of organ dose conversion coefficients

(169) Tables C.1–C.30 in Annex C present the evaluated conversion coefficients for those specific organs (i.e. red (active) bone marrow, colon, lung, stomach, breast, ovaries, testes, urinary bladder wall, oesophagus, liver, thyroid, endosteum, brain, salivary glands, and skin) for which ICRP recommends tissue weighting factors as well as for the remainder tissues. Conversion coefficients for the lens of the eye can be found in Annex F. Data are given separately for the male and female phantoms, and for all irradiation geometries considered (i.e. AP, PA, LLAT, RLAT, ROT, and ISO). In the CD accompanying this report, conversion coefficients of those organs contributing to the remainder tissues are also shown (i.e. adrenals, extrathoracic region, gall bladder, heart, kidneys, lymphatic nodes, muscle, oral mucosa, pancreas, prostate, small intestine, spleen, thymus, and uterus/cervix), as well as the dose conversion coefficients for the organs mentioned above.

(170) As examples of the evaluated reference organ dose conversion coefficients, absorbed dose conversion coefficients for the thyroid and stomach of the reference male phantom are shown in Fig. 4.19 for all the geometries considered. It can be seen that AP irradiation gives the highest and lowest values of the dose conversion coefficients for lower- and higher-energy neutrons, respectively, and this tendency holds for organs located close to the front surface of the phantoms (e.g. thyroid and stomach). This tendency is also observed in PA irradiation geometry for organs close to the back surface (e.g. active bone marrow within the spine and pelvis). The conversion coefficients for LLAT and RLAT irradiations have generally similar values except for organs that are positioned asymmetrically, such as the stomach which is located on the left side of the body (Sato et al., 2009). These results indicate that the organ dose conversion coefficients depend strongly on the distance of the organ to the irradiation surface; the conversion coefficients for organs close to the irradiation surface are larger compared with the other organs for incident energies less than 20 MeV, while this relationship is reversed for the higher-energy cases. These effects can be explained by the fact that the primary particles play a dominant role in the energy-deposition processes for low-energy neutron irradiations, while the secondary particles play a dominant role for high-energy neutron irradiations. The fluence of the primary particles decreases with increasing distance from the irradiation surface, while the fluence of the secondary particles increases. Note that high-energy neutrons can trigger a cascade of secondary particles by inducing complex nuclear reactions successively in the human body (Sato et al., 2009).

(171) The sex dependence of the organ dose conversion coefficients was not found to be significant, except for the gonads. This can be explained by the significant difference in the distance between the organ and the irradiation surface for the testes and ovaries.

4.3.5. Effective dose for neutrons

(172) The effective dose conversion coefficients for neutrons in different irradiation geometries are shown in Annex A and Fig. 4.20 as a function of incident neutron

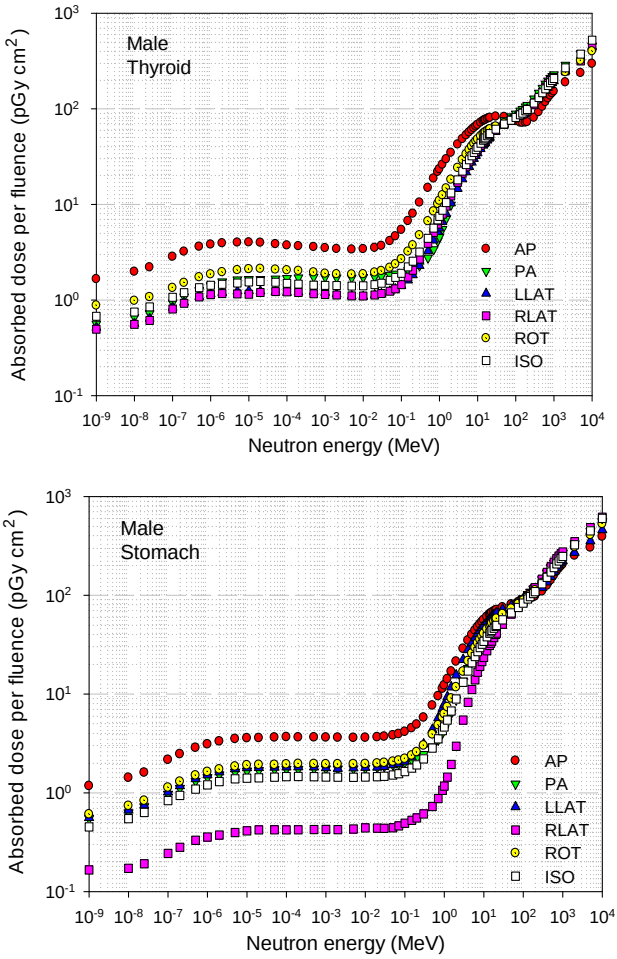

Fig. 4.19. Reference absorbed dose per neutron fluence for the thyroid and stomach wall of the male reference phantom. AP, antero-posterior; PA, postero-anterior; LLAT, left lateral; RLAT, right lateral; ROT, rotational; ISO, isotropic.

energy. As several organs of importance in determining the value of the effective dose (i.e. those organs with the larger tissue weighting factors) are located near the front of the body, the energy dependence of the effective dose for AP irradiation geometry at high energies is different from that of other irradiation geometries. Above 10 MeV, the effective dose continues to increase with neutron energy for PA, LAT, ROT, and ISO irradiation geometries, but for AP irradiation geometry, the effective dose actually shows a small decrease.

(173) In Fig. 4.20, values of effective dose conversion coefficients for AP irradiation are seen to be highest among all irradiation geometries for neutrons below 50 MeV. For neutrons of 50 MeV–2 GeV, the conversion coefficients for PA irradiation give the highest values, and ISO values are the highest above 2 GeV.

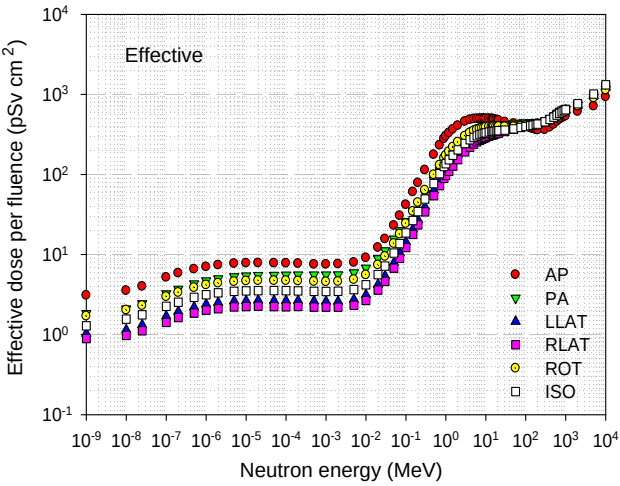

Fig. 4.20. Effective dose per neutron fluence. AP, antero-posterior; PA, postero-anterior; LLAT, left lateral; RLAT, right lateral; ROT, rotational; ISO, isotropic.

4.3.6. Comparison with ICRP *Publication 74* (ICRP, 1996) for neutrons

(174) Fig. 4.21 shows the ratios of effective dose as evaluated for the present report to values given in ICRP *Publication 74* (ICRP, 1996). It can be seen that the present values are lower than those given in ICRP *Publication 74* for neutron energies below

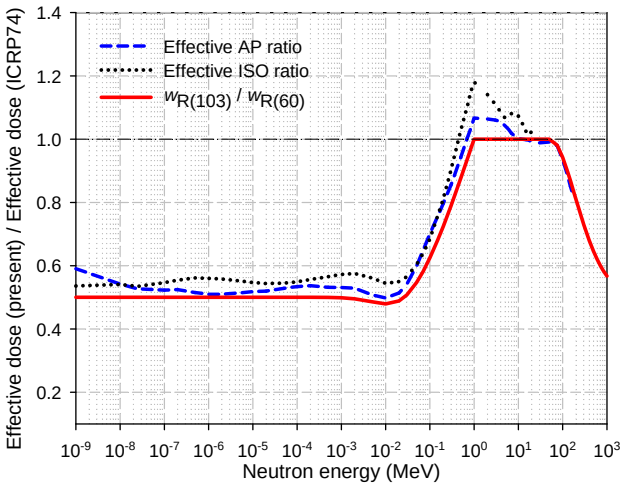

Fig. 4.21. Ratios of neutron fluence to effective dose conversion coefficients from the present report to fluence to effective dose conversion coefficients from ICRP *Publication 74* (ICRP, 1996) for antero-posterior (AP) and isotropic (ISO) irradiation geometries. Also shown is the ratio of the ICRP *Publication 103* (ICRP, 2007) w_R values to the ICRP *Publication 60* w_R values (ICRP, 1991).

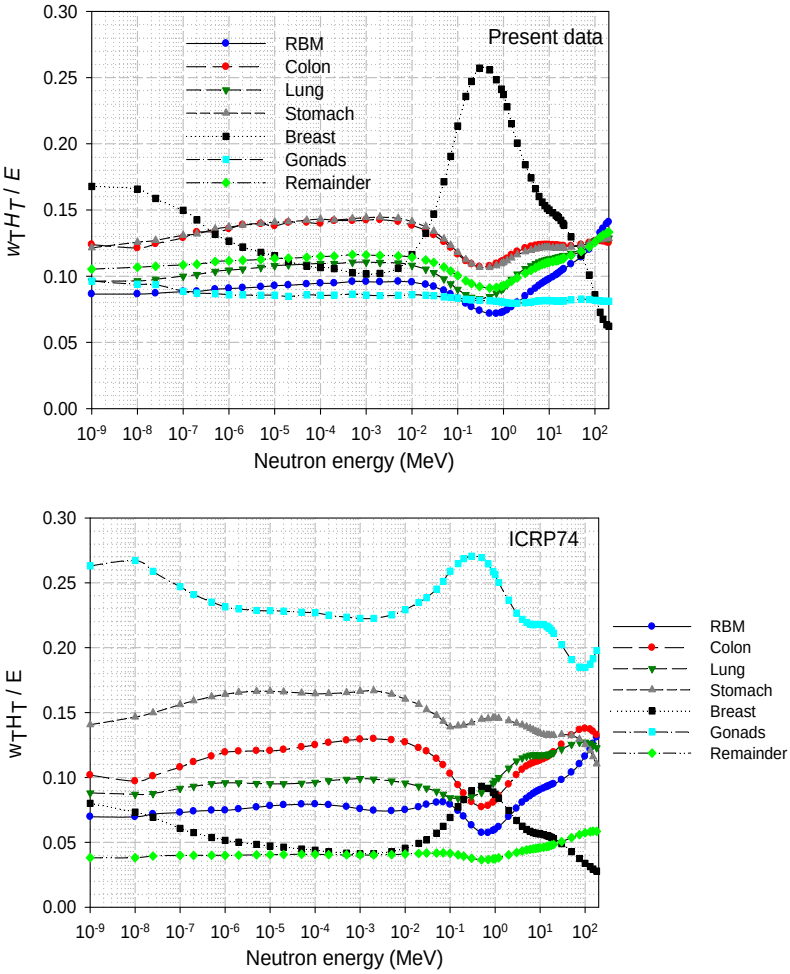

Fig. 4.22. Organs with the highest contribution to the effective dose for neutrons incident in the antero-posterior direction. The top graph shows the contributions estimated for the present calculations, and the bottom graph shows those of ICRP *Publication 74* (ICRP, 1996). RBM, red bone marrow.

400 keV and above 50 MeV, while they show fairly good agreement at the intermediate energies. The differences are mainly due to the use of the new values of w_R as recommended in ICRP *Publication 103* (ICRP, 2007). Fig. 4.21 also shows the ratio of w_R values given in ICRP *Publication 103* (ICRP, 2007) to the ICRP *Publication 60* (ICRP, 1991) values. Note that the values of w_R for lower- and intermediate-energy neutrons were modified downwards from 5 to 2.5 in ICRP *Publication 103* (ICRP, 2007). In the energy range with w_R ratio smaller than unity ($E_n < 1$ MeV), the effective dose decreases less than expected based simply on the ratio of w_R values. This is mainly attributed to anatomical differences between the stylised and reference voxel

phantoms. In the energy range with w_R ratio equal to unity (1 MeV < E_n < 100 MeV), the effective doses from the present report tend to be higher than those in ICRP *Publication 74* (ICRP, 1996), except for PA irradiation. This is due to the combined effect of the transition from a stylised to a voxel phantom, and to the higher w_T values recommended for the breast (0.12 instead of 0.05); this is indicated in Fig. 4.22 which shows contributions to the effective dose as a function of neutron energy for AP irradiation.

4.4. Protons

4.4.1. Characteristics of energy deposition by protons in the human body

(175) Protons mainly lose their energy through Coulomb interactions in multiple-scattering events. Above a certain energy, protons can also undergo inelastic nuclear reactions in soft tissue, producing various secondary particles and photons. The deposition of energy by protons as a function of the distance travelled shows a characteristic maximum at the end of the range called the 'Bragg peak'. Low levels of bremsstrahlung are produced by electron secondary particles. Low-energy protons have a short range in soft tissue. For example, protons incident with energies below 10 MeV deposit almost all their energy in the skin for all irradiation geometries. For the breast in AP irradiation, protons with energies between 20 and 100 MeV will deposit nearly all their energy in this organ. Hence, the organ dose conversion coefficients for low-energy protons depend significantly on the morphology of the phantom (see also Section 4.4.5). In contrast, high-energy protons induce hadronic cascades that generate various secondary particles, including neutrons and photons. These secondary particles, whose fluence increases as a function of increasing depth from the irradiated surface, play a dominant role in the energy-deposition processes for incident high-energy protons.

4.4.2. Calculation conditions for protons

(176) Similarly to the neutron calculations, four different codes were used to calculate the organ and effective dose conversion coefficients for external protons for the male and female adult reference computational phantoms (see Table 4.1). General features of the transport codes used for the calculations are discussed in Section 3.3. Energies from 1 MeV to 10 GeV were considered, and the geometries simulated were AP, PA, LLAT, RLAT, ROT, and ISO.

(177) The primary data sets were obtained with the PHITS code. Nuclear reactions induced by protons with energies from 10 MeV to 3.5 GeV were simulated by the JQMD model, while those induced by higher-energy particles used the JAM model. For the PHITS simulations, the relative standard deviations of the conversion coefficients for these organs are generally small, less than 5%, but those for smaller organs (e.g. thyroid) approached 15%. More details on these simulations with the PHITS code can be found in Sato et al. (2009).

(178) Secondary calculations were performed with the FLUKA code for AP and ISO irradiation geometries. The models employed are described in Section 3.3.

(179) Validation calculations were performed with the GEANT4 code for AP irradiation. Inelastic processes were simulated by several models. Below 3 GeV, the Bertini Intra-nuclear Cascade model, coupled with excitons, pre-equilibrium, nucleus explosion, fission, and evaporation models, was utilised. Above 3 GeV, the LEP model (GEANT4, 2006) based on the GEANT3-GHEISHA (Fesefeldt, 1985) package was applied, which is suitable for energies up to 20 GeV. Relative statistical uncertainties were less than 4% for all organs above 20 MeV, and reached a maximum of 11% at energies below 20 MeV.

(180) Validation calculations were performed with MCNPX Version 2.6.0 (Pelowitz, 2008). The MCNPX simulations were performed for AP, PA, and ISO irradiation geometries and some selected energies. The Bertini Intra-nuclear Cascade model was used for proton energies up to 3.5 GeV, and for energies above 3.5 GeV, FLUKA89 (Aarnio et al., 1990) was employed, which is an older version of FLUKA, taken directly from the LAHET code (Prael and Lichtenstein, 1989). The organ absorbed doses were tallied using a collision heating tally that scores energy deposition from all particles.

4.4.3. Differences among Monte Carlo codes for protons

(181) Comparisons of organ absorbed dose data produced by different codes revealed that the variation was, in almost all cases, much lower than the estimated statistical uncertainty. The reference dose conversion coefficients were obtained separately for the male and female phantoms from all calculation results by averaging then smoothing with a combination of cubic spline, least-square B-spline, and non-uniform rational B-spline methods, depending on the shape of curves (de Boor, 1978; Hewitt and Yip, 1992). Above 10 MeV, the agreement among the codes is very good, as can be seen from Fig. 4.23. The figure shows, for example, the lung absorbed dose conversion coefficients of the female phantom and the gonad absorbed dose conversion coefficients of the male phantom. The data points obtained from each code are shown together with the reference values.

(182) It can be seen that the gonad absorbed dose conversion coefficients of the male phantom differ between the FLUKA/MCNPX and PHITS/GEANT4 codes for 10-MeV protons incident in AP geometry. The discrepancy is caused by the difference of transport models for protons used in the codes: the FLUKA and MCNPX codes consider elastic-scattering angular deflections, while the PHITS and GEANT4 codes do not take this effect into account. In AP irradiation geometry, primary protons are incident perpendicularly on the skin voxels; some of the skin voxels adjoin the gonad voxels, and some protons incident near the boundary of these voxels enter the gonad voxels through angle straggling of these low-energy protons. Special consideration is needed for treatment of low-energy protons, and this will be discussed in Section 4.4.5.

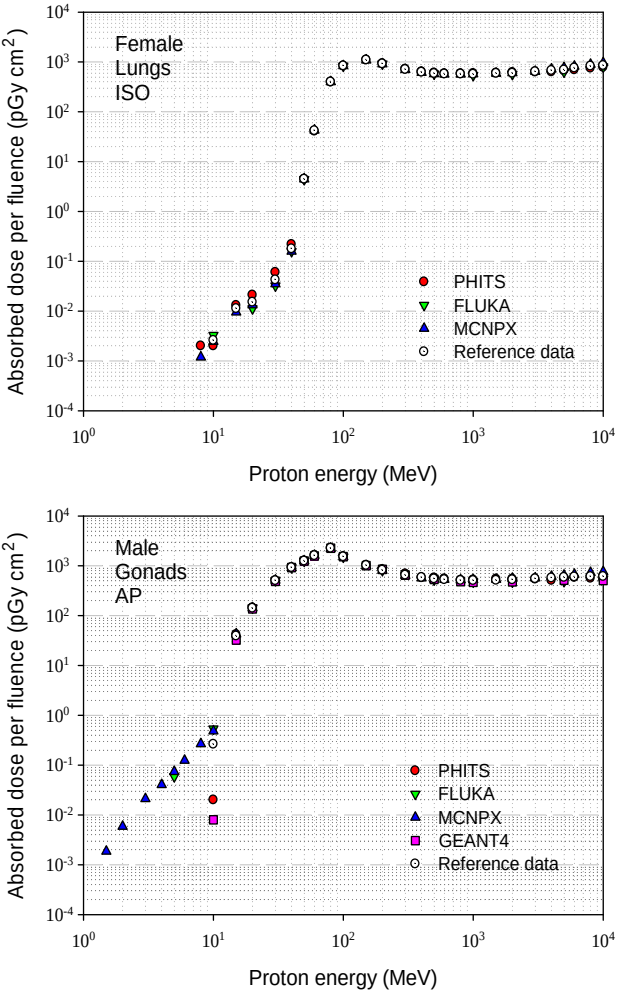

Fig. 4.23. Evaluated reference and original data for the absorbed dose per proton fluence for the female lungs for isotropic (ISO) geometry and for the male gonads for antero-posterior (AP) geometry.

4.4.4. Analysis of organ dose conversion coefficients for protons

(183) As examples of the calculated organ absorbed dose, Fig. 4.24 shows a comparison of the conversion coefficients of red bone marrow, colon (male), breast, and skin (female) for the various geometries as a function of proton energy.

(184) As for neutrons, the sex dependence of the organ dose conversion coefficients was not found to be significant, except for the case of the gonads. This again can be explained by the difference in the distances from the skin surface to the testes and the ovaries; the testes are located much closer to the skin than the ovaries.

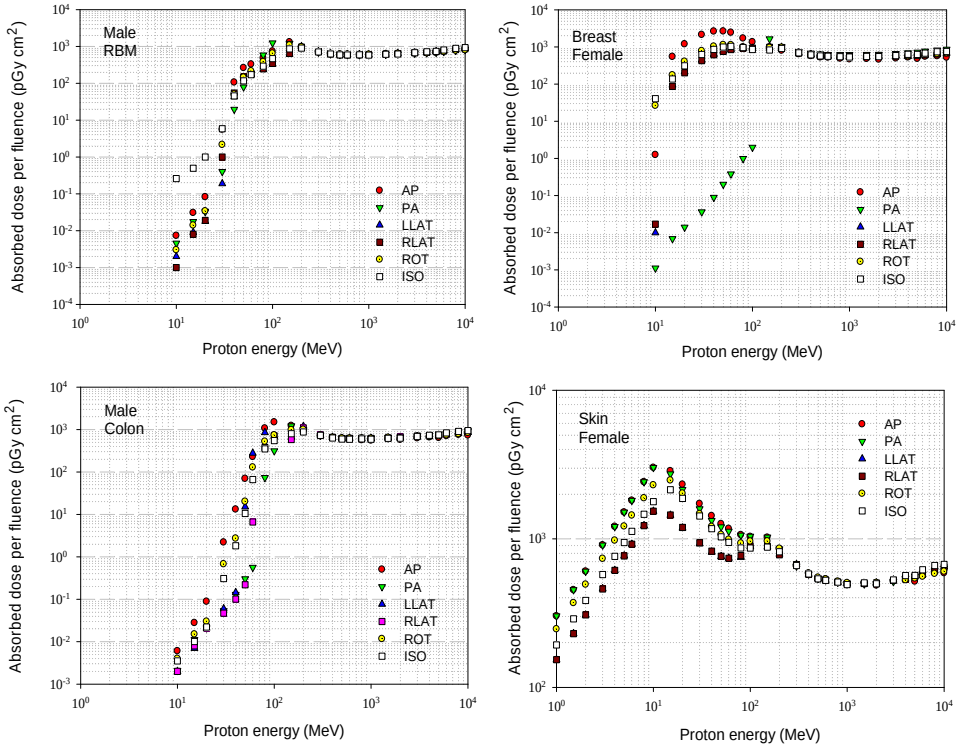

Fig. 4.24. Organ doses per fluence of protons as a function of energy for the male reference phantom [red bone marrow (RBM), colon] and the female reference phantom (breast, skin). AP, antero-posterior; PA, postero-anterior; LLAT, left lateral; RLAT, right lateral; ROT, rotational; ISO, isotropic.

4.4.5. Special considerations for low-energy protons

(185) The range of 10 MeV protons in muscle is 0.12 cm, and protons with energies less than 10 MeV cannot penetrate the skin represented in the ICRP reference voxel phantoms because the voxel in-plane resolutions are 0.2137 cm and 0.1775 cm in the male and female phantoms, respectively. As shown in Fig. 4.25, it was observed that absorbed doses to the breast differ significantly between AP and ISO geometries for low-energy protons (less than 10 MeV), despite the fact that primary protons of this energy should not be able to reach the breast directly.

(186) This difference in the absorbed dose to the male breast in AP and ISO geometries is due to a limitation in the geometry of the reference voxel phantoms. The skin of the reference voxel phantoms is a one-voxel-thick layer on the phantoms' exterior. However, some internal organs or tissues are directly exposed to the primary radiation in ISO geometry in several positions. Fig. 4.26 shows a cross-sectional view (sagittal plane) of the reference male phantom, passing through the breast, and shows that one of the breast tissue voxels is in direct contact with outer region (vacuum)

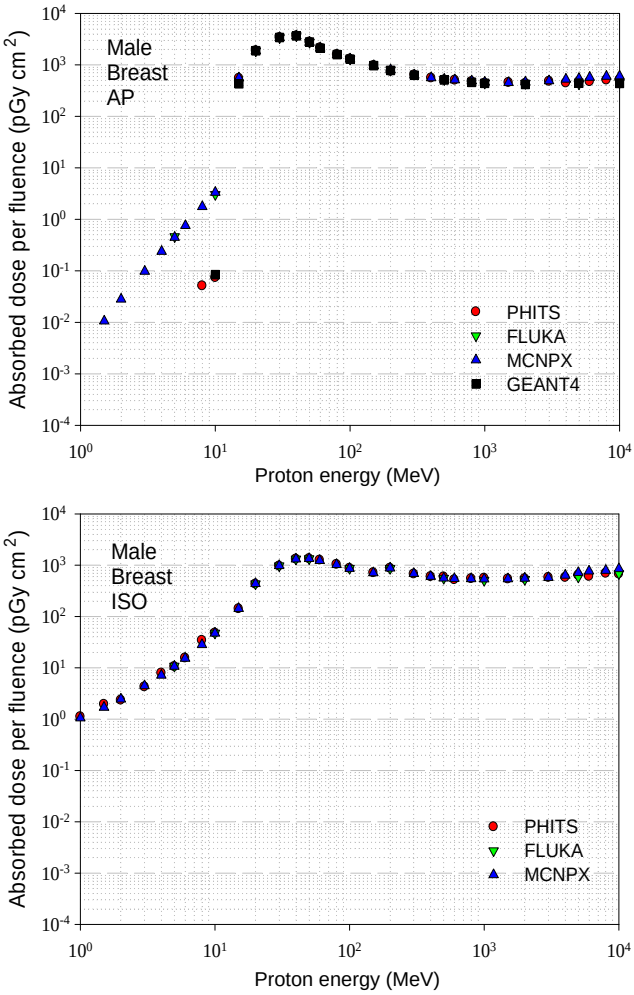

Fig. 4.25. Breast dose of the male phantom for antero-posterior (AP) and isotropic (ISO) geometries.

voxels. In AP irradiation geometry, low-energy protons are incident perpendicularly on the skin voxels and are absorbed by them. In ISO geometry, some primary protons are incident directly on the breast voxels, which are exposed to the outer regions of the phantom voxel array. Therefore, a significant dose to the breast is scored even for 1 MeV protons. However, this is an artefact of the computational phantoms and not a realistic phenomenon, as the human body is uniformly covered by skin, and protons of energies less than 10 MeV cannot penetrate this tissue layer.

(187) The relevance of these observed artefacts for practical radiological protection is small. For the effective dose, the breast will contribute up to 1% for AP geometry. For ISO geometry, the breast dose is higher but still only contributes 2% to the

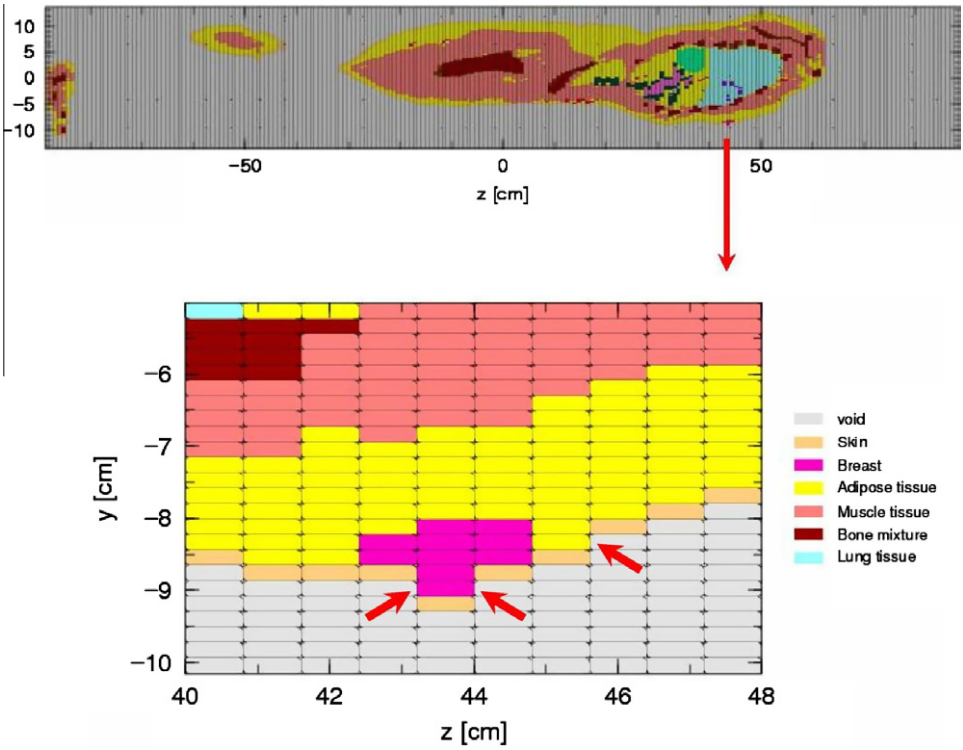

Fig. 4.26. Cross-sectional views around the breast of the male phantom.

effective dose. Irradiation by low-energy protons is unlikely to happen, except for local applications of protons (e.g. to the eye). Particles that cannot penetrate the skin are also shielded in practice by clothing; therefore, the practical relevance of this issue is limited.

(188) In summary, protons with energies less than 10 MeV cannot penetrate the skin. The energy deposition in internal organs is caused by secondary particles and is very small compared with the skin dose. Furthermore, the relative statistical uncertainties of the Monte Carlo calculations were large below this energy. Therefore, absorbed doses of all organs except for skin have been set to zero for incident protons of less than 10 MeV. This argument is also applied to helium ions, as discussed in Section 4.7.4.

4.4.6. Effective dose for protons

(189) The effective dose conversion coefficients for protons for the standard irradiation geometries are shown in Annex A and Fig. 4.27 as a function of proton energy. It is evident from Fig. 4.27 that the effective dose conversion coefficients for AP geometry have the highest values for incident energies below 100 MeV. Above

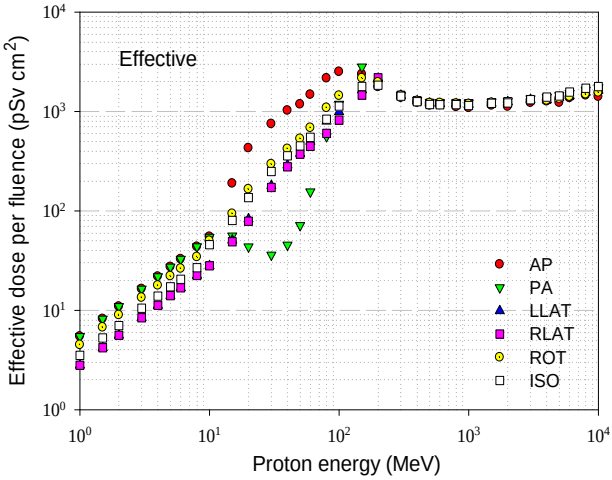

Fig. 4.27. Effective dose per proton fluence for the standard geometries. AP, antero-posterior; PA, postero-anterior; LLAT, left lateral; RLAT, right lateral; ROT, rotational; ISO, isotropic.

3 GeV, ISO irradiation geometry gives the highest values. Between these two energies, the dose conversion coefficients are very similar for the different irradiation geometries.

4.5. Positive and negative muons

4.5.1. Characteristics of energy deposition by muons in the human body

(190) In the energy range of interest (i.e. 1 MeV–10 GeV), energy loss by muons in the human body is dominated by ionisation (and excitation). Other energy-loss mechanisms such as pair production, bremsstrahlung emission, and photonuclear interactions are unimportant until ~10 GeV (Groom et al., 2001). Additionally, the short lifetime of muons should be taken into account in the calculation of dose conversion coefficients.

(191) Muons are unstable particles and decay to an electron and two neutrinos ($\mu^{\pm} \rightarrow e^{\pm} + \nu_e + \nu_\mu$) with a lifetime at rest of 2.2×10^{-6} s. Electrons and positrons originating from the decay process have relatively high energies and produce electron–photon cascades in the human body. Production of delta rays begins to be significant above a few hundred MeV. The production cross section and the energy of delta rays produced increases with muon energy, and therefore the transport of delta rays should be considered.

(192) When a negative muon comes to rest in matter, it is captured in the Coulomb field of a nucleus, and a muonic atom is formed. The captured muon de-excites to the 1s state through Auger-electron and muonic characteristic x-ray emissions. The muon further decays to an electron and two neutrinos or is captured by the nucleus; the capture results in the production of neutrons and neutrinos.

4.5.2. Calculation conditions for muons

(193) Dose conversion coefficients were calculated for both negative and positive externally incident muons. The primary calculations were performed with the FLUKA code in the energy range from 1 MeV to 10 GeV for AP, PA, and ISO geometries. In most organs, absorbed doses were determined with relative statistical uncertainties of less than 0.5%. For small organs (e.g. adrenals and ovaries), statistical uncertainties were less than 1%.

(194) A second set of calculations was obtained with MCNPX Version 2.6.0 using the CEM model for both negative and positive muons for some selected energies for AP, PA, and ISO geometries. In most organs, absorbed doses were determined with relative statistical uncertainties of less than 2%.

(195) Validation calculations were performed with the GEANT4 code for both negative and positive muons in AP geometry; with the FLUKA code for both negative and positive muons in ISO geometry; and with the MCNPX 2.6.0 code using the Bertini model for negative muons in AP, PA, and ISO geometries.

4.5.3. Differences among Monte Carlo codes for muons

(196) Fig. 4.28 shows an example of the differences in calculated organ dose data from the four Monte Carlo codes. The FLUKA and GEANT4 codes include all muon energy-deposition processes that are considered to be important for energy deposition in the human body, and show excellent agreement over the entire energy range. The MCNPX code with two physics models, CEM and Bertini, shows good agreement with the FLUKA and GEANT4 codes up to 1 GeV. However, the MCNPX code shows higher values than the FLUKA and GEANT4 codes above 1 GeV, and this discrepancy increases with increasing incident muon energy.

(197) As described in Section 4.5.1, the production of delta rays becomes significant above 1 GeV, and the energy of the delta rays increases with the incident muon energy. The energetic delta rays have ranges larger than the organ dimensions in the reference voxel phantoms, and therefore they tend to escape from the organs in which they are produced. The MCNPX code does not consider the production and transport of delta rays for muons, and this neglect leads to overestimation of organ doses at incident muon energies above 1 GeV. The same tendency is found in all organs for both negative and positive muons. It was, therefore, decided to disregard the organ doses calculated by the MCNPX code above 1 GeV for its evaluation of the reference organ dose data sets for muons.

4.5.4. Analysis of organ dose conversion coefficients for muons

(198) Fig. 4.29 shows the absorbed dose conversion coefficients in AP geometry for selected organs located at different depths from the front surface of the body. The absorbed doses reach their maximum values at energies between 5 and 60 MeV depending on the organ depth, while the absorbed doses become energy and organ

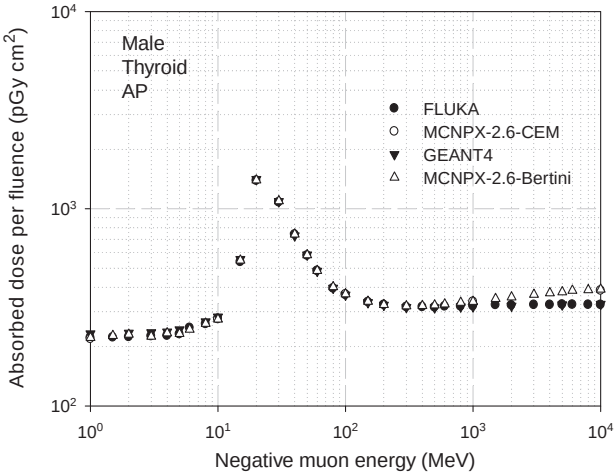

Fig. 4.28. Thyroid absorbed dose per fluence of negative muons for the male phantom for antero-posterior geometry, calculated with different Monte Carlo codes.

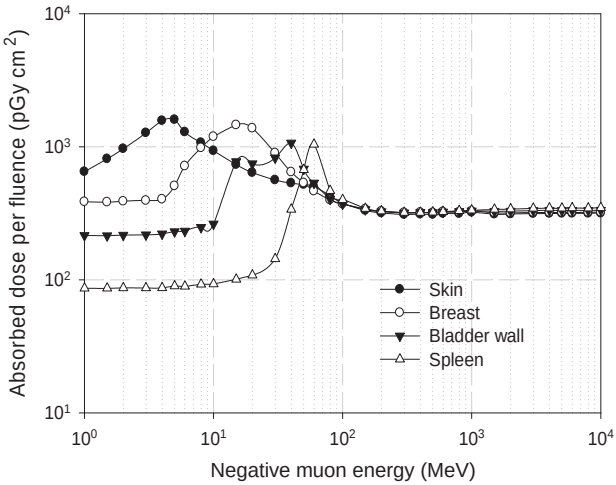

Fig. 4.29. Organ dose conversion coefficients per fluence of negative muons for the female phantom for antero-posterior geometry.

independent at incident muon energies above 200 MeV, and then decrease to approach a uniform value.

(199) The CSDA ranges of muons in soft tissue at 5, 10, and 100 MeV are 0.193, 0.695, and 31.1 g/cm^2, respectively (Groom et al., 2001). The organ doses increase and reach their maximum values at the energy for which many Bragg peaks are formed in the given organs. The absorbed doses to the bladder wall, for example,

have two peaks at around 15 and 40 MeV. Depths from the front body surface to the voxels delineating the bladder wall in the female phantom range from 0.8 to 8.4 cm, and the distribution of depths has two peaks at ~1.3 and 5.8 cm (ICRP, 2009). These distances correspond to the CSDA ranges of 14- and 34-MeV muons respectively. The energy dependence of the absorbed dose in the bladder wall, as well as in other organs, can thus be explained by the relationship between organ position and the range of the incident muons.

(200) Above 200 MeV, the muons penetrate through the body completely in AP, PA, and ISO irradiation geometries. From 300 MeV to 500 GeV, the stopping power of muons in soft tissue increases slightly with muon energy (Groom et al., 2001). However, the energetic delta rays escape from the human body to offset these increases and make the absorbed dose nearly constant.

4.5.5. Analysis of effective dose conversion coefficients for muons

(201) Fig. 4.30 shows the effective dose conversion coefficients as a function of negative muon energy for AP, PA, and ISO irradiation geometries. The effective doses increase with increasing muon energy, and reach their maximum values at 50 MeV in AP geometry, 60 MeV in PA geometry, and 80 MeV in ISO geometry. As discussed in Section 4.5.4, these differences in peak energies are a function of the organ depth, irradiation direction, and muon range. Above 200 MeV, the muons penetrate the human body completely and energetic delta rays escape from the body. Consequently, at these higher incident energies, the effective doses depend less on the incident direction and become independent of incident muon energy.

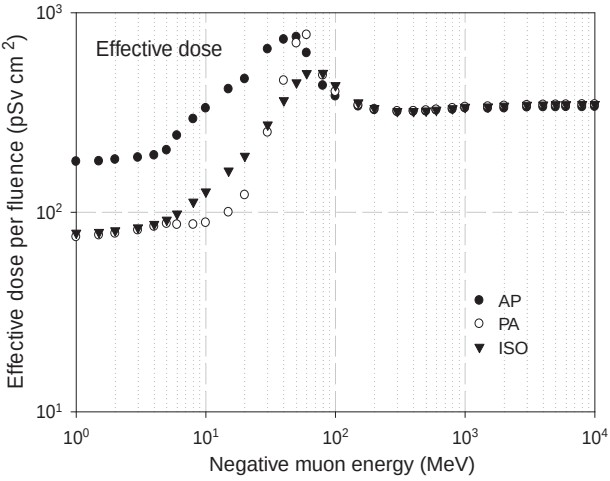

Fig. 4.30. Effective dose conversion coefficients per fluence of negative muon energy. AP, antero-posterior; PA, postero-anterior; ISO, isotropic.

4.5.6. Dependence on muon charge

(202) Fig. 4.31 shows a comparison of effective dose conversion coefficients between negative and positive muons for ISO geometry. The dose conversion coefficients above 100 MeV are practically the same, while positive muons give slightly higher values than negative muons at lower energies. This difference is because positrons produced from positive muon decay give a higher dose compared with electrons produced from negative muon decay. The analysis of energy deposition events showed that, at 10 MeV, the relative contribution to energy deposited by nuclear recoils, produced by negative muon capture, is less than 0.1% of the primary energy.

4.5.7. Comparison with previous calculations performed for muons using a stylised phantom

(203) Ferrari et al. (1997) calculated organ dose and effective dose conversion coefficients of negative and positive muons using the FLUKA code and the MIRD phantom. The effective doses were calculated using w_T and w_R ($w_R = 1$ for muons), as defined in ICRP *Publication 60* (ICRP, 1991).

(204) Fig. 4.32 compares the present data and Ferrari et al.'s results for negative muons. It can be seen that there is generally good agreement between these values over the entire energy range. Relative differences of ~10–20% are observed for energies from 10 to 20 MeV. These differences are due to the different anatomy of the models employed, especially the differences of the position and shape of organs such as the breast. Furthermore, the value of w_T was substantially changed for this organ, as defined in ICRP *Publications 60* (ICRP, 1991) and *103* (ICRP, 2007).

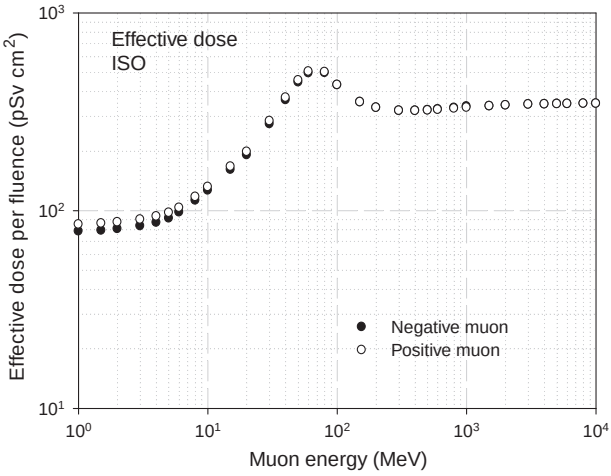

Fig. 4.31. Comparison of effective dose conversion coefficients per muon fluence for negative and positive muons for isotropic geometry.

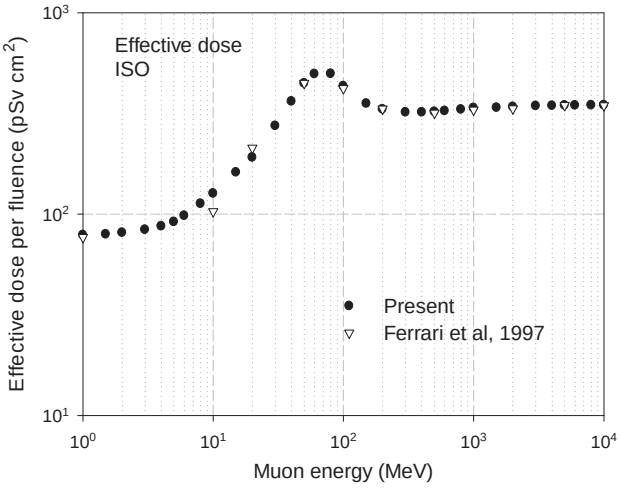

Fig. 4.32. Comparison of effective dose conversion coefficients between the present data and those of Ferrari et al. (1997) for isotropic geometry.

(205) Above 200 MeV, muons penetrate the human body completely and all organs are irradiated uniformly. Therefore, the effective doses are less sensitive to anatomical differences in human phantoms and both phantoms give similar values, as shown in Fig. 4.32.

4.6. Positive and negative pions

4.6.1. Characteristics of energy deposition by pions in the human body

(206) Charged pions mainly lose their energy through Coulomb interactions. At higher energies, hadron–nucleon and hadron–nucleus interactions produce various secondary particles contributing to the energy deposition in the human body. In addition, the following characteristics of charged pions are important to calculate dose conversion coefficients. Charged pions are unstable particles and decay with mean lifetimes of 2.6×10^{-8} s to a muon and a muon neutrino ($\pi^{\pm} \rightarrow \mu^{\pm} + \nu_{\mu}$). The muons originating from the decay process interact with the human body as described in Section 4.5.1. When a negative pion comes to rest in the human body, it is usually captured by a nucleus which then disintegrates, emitting a variety of high-LET particles (so-called 'star fragmentation').

4.6.2. Calculation conditions for pions

(207) Dose conversion coefficients were calculated for both positive and negative pions. Calculation for neutral pions was not included because of their short mean lifetime (8.7×10^{-17} s). Calculations were performed using two Monte Carlo codes,

FLUKA and PHITS, over the energy range of 1 MeV–200 GeV for AP, PA, and ISO irradiation geometries.

(208) In the calculations using the FLUKA code, absorbed doses were determined with relative statistical uncertainties of less than 0.5% in most organs. For small organs (e.g. adrenals and ovaries), relative statistical uncertainties were less than 1%. In the calculations using the PHITS code, absorbed doses were determined with relative statistical uncertainties of less than 5% in most organs. For small organs and low incident energies, the statistical uncertainties were as high as 10%.

4.6.3. Differences among Monte Carlo codes for pions

(209) Fig. 4.33 shows an example in the differences of the calculated organ absorbed dose data determined using FLUKA and PHITS codes. Relative differences amounting to a maximum of 20% were found for incident pion energies between 3 and 100 GeV. As described in Section 3.3.2, the FLUKA code uses the PEANUT package which includes a Generalised Intra-nuclear Cascade model and a Pre-equilibrium model up to 5 GeV, followed by the Dual Parton model above 5 GeV. The PHITS code uses the JQMD model for hadron–nucleon and hadron–nucleus interactions below 2.5 GeV, and the JAM model above 2.5 GeV. Small discontinuities were found at 5 and 3 GeV in the results from the FLUKA and PHITS codes, respectively, due to the switching between the interaction models in the respective codes. It was found that the difference above 3 GeV comes from the different nuclear reaction models employed by the FLUKA and PHITS codes. It was therefore decided that the reference data should be calculated by averaging the FLUKA and PHITS results, followed by data smoothing.

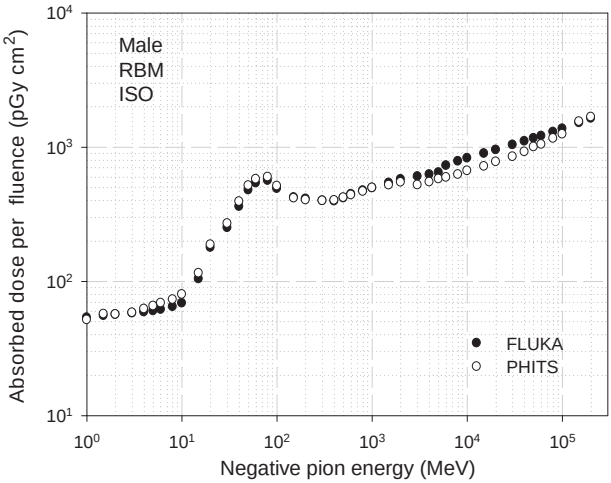

Fig. 4.33. Red bone marrow absorbed dose to the male phantom per fluence for isotropic geometry, calculated with different Monte Carlo codes, as a function of negative pion energy.

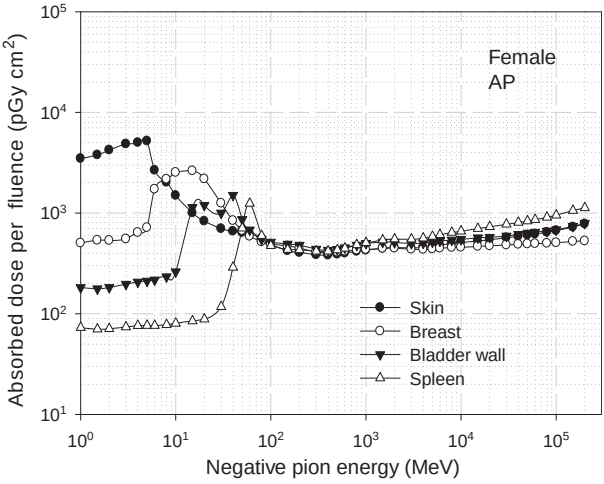

Fig. 4.34. Organ dose conversion coefficients per fluence for negative pions for the female phantom for antero-posterior geometry.

4.6.4. Analysis of organ dose conversion coefficients for pions

(210) Fig. 4.34 shows absorbed dose conversion coefficients for negative pions and for AP irradiation geometry for selected organs located at different depths from the front surface of the body. In general, the organ absorbed doses increase with increasing incident pion energy, reach a maximum value, and then decrease thereafter. Above 500 MeV, the organ absorbed doses increase again. Below 100 MeV, the energy dependence of organ absorbed doses is similar to that of muons, as indicated in Fig. 4.29, and is influenced by many factors including organ depth, incident pion energy, and corresponding range in tissue.

(211) The increase in organ absorbed dose above 500 MeV, as shown in Fig. 4.34, is most noticeable in the spleen, which is located deep inside the body. High-energy pions produce hadronic cascades of secondary particles through complex nuclear reactions. These secondary particles deposit more energy in organs located deeper within the body.

4.6.5. Analysis of effective dose conversion coefficients for pions

(212) Fig. 4.35 shows the effective dose conversion coefficients as a function of negative pion energy for AP, PA, and ISO irradiations. Below 100 MeV, the energy dependence of the effective dose conversion coefficients can be explained by comparing organ depth, particle direction, and pion energy and corresponding range in tissue.

(213) Up to 50 MeV, the effective dose conversion coefficients for AP geometry are higher than those for PA and ISO geometries because incident pions reach

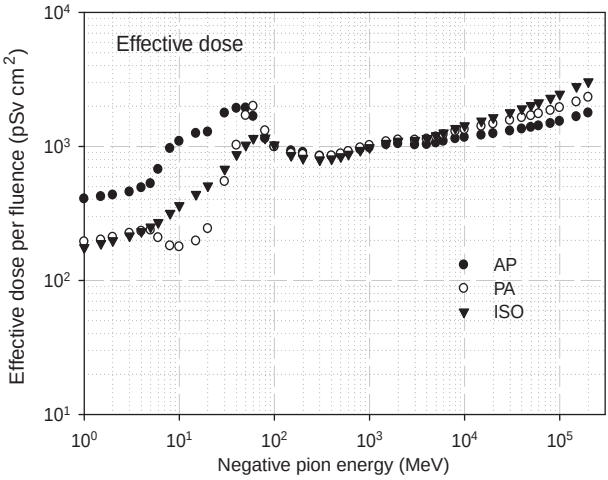

Fig. 4.35. Effective dose conversion coefficients per pion fluence. AP, antero-posterior; PA, postero-anterior; ISO, isotropic.

organs contributing largely to the effective dose in AP geometry (e.g. breasts). In PA geometry, on the other hand, skin dose is the main contributor to the effective dose for energies up to 5 MeV. Above 5 MeV, the incident pions penetrate the skin but cannot reach sensitive organs, and the effective dose subsequently decreases. With further increases in the incident pion energy, the effective dose increases again as these particles are able to reach additional internal organs. In the higher-energy region, ISO geometry gives higher conversion coefficients than AP and PA geometries due to secondary particles produced through the hadronic cascade, as discussed in Section 4.6.1. This is a common phenomenon for charged particles, and a similar energy dependence is found for protons (Fig. 4.27) and helium ions (Fig. 4.40).

4.6.6. Dependence on pion charge

(214) Fig. 4.36 shows a comparison of effective dose conversion coefficients for negative and positive pions incident upon the body in ISO geometry. When negative and positive pions come to rest, the former are usually captured by nuclei which then disintegrate to emit a variety of secondary particles, while the latter generally decay to a muon and a neutrino. The energy deposited by high-LET secondary particles from negative pions with energies below 80 MeV is much larger than the corresponding energy deposited by the same fluence of the positive pions, as shown in Fig. 4.36. On the other hand, at ~200 MeV, the dose conversion coefficients of positive pions are higher than those of negative pions due to the difference in tissue cross sections by delta resonance in this energy region.

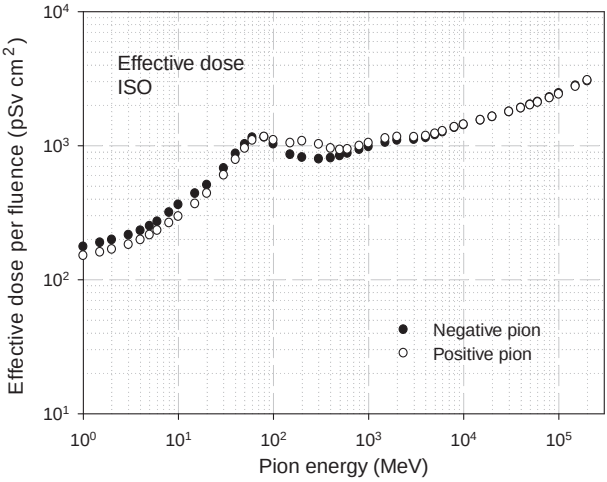

Fig. 4.36. Comparison of effective dose conversion coefficients between negative and positive pions as a function of pion energy.

4.6.7. Comparison with previous work for pions

(215) Ferrari et al. (1998) calculated organ dose conversion coefficients for negative and positive pions using the FLUKA code and the stylised MIRD phantom, according to the definitions in ICRP *Publication 60* (ICRP, 1991). As ICRP *Publication 60* gave no w_R values for pions, Ferrari et al. (1998) calculated

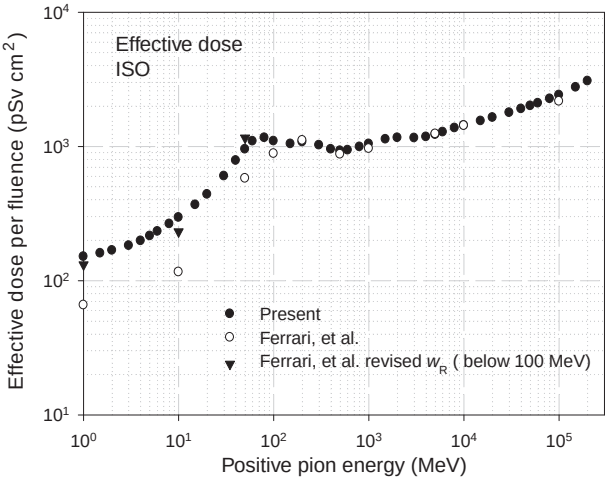

Fig. 4.37. Comparison of effective dose conversion coefficients of positive pions between the present data and those of Ferrari et al. (1998) for isotropic irradiation.

effective quality factors at 10-mm depth in the ICRU sphere, and estimated w_R for negative and positive pions as a function of energy. Based on these calculations, the following w_R values were derived depending on the energy and charge of pions: for positive pions, $w_R = 1$ for pion energies <100 MeV and $w_R = 2$ for energies $\geqslant$100 MeV; for negative pions, $w_R = 5$ for energies <50 MeV and $w_R = 2$ for energies $\geqslant$50 MeV.

(216) Fig. 4.37 compares the effective dose conversion coefficients for positive pions from the present data with those calculated by Ferrari et al. (1998). Significant differences are observed below 100 MeV because different w_R values were applied in these calculations compared with $w_R = 2$ used in the present calculation for pions over the entire energy range. To compare the two data sets, the data below 100 MeV calculated by Ferrari et al. (1998) have been replotted with the application of $w_R = 2$. It can thus be seen in Fig. 4.37 that the differences between the present data and the replotted data become minor. These results indicate that anatomical differences between the phantoms and updates of w_T have had little influence on the dose conversion coefficients for incident charged pions.

4.7. Helium ions

4.7.1. Characteristics of energy deposition of helium ions in human body

(217) For helium ions with energies greater than 1 MeV/u, the dominant process of energy loss in the human body is the electronic excitation and ionisation of the atoms of the tissues. At higher energies, nuclear reactions of helium ions contribute to energy loss. Energy loss by the radiative processes (i.e. bremmstrahlung) is negligible up to very high energies.

(218) Recent developments in several Monte Carlo codes (e.g. PHITS and FLUKA codes) have made it possible to analyse various aspects of the complex interactions of heavy ions using sophisticated models to describe the fragmentation reactions at high energies.

4.7.2. Calculation conditions for helium ions

(219) The primary calculations of absorbed dose conversion coefficients for helium ions were performed with the PHITS code for energies of 1 MeV/u–100 GeV/u for AP, PA, and ISO geometries (Sato et al., 2010). The absorbed dose conversion coefficients for most organs were generally determined with relative statistical deviations of less than 5%, but for smaller organs (e.g. thyroid), they amounted to up to 15%.

(220) The secondary calculations were performed with the FLUKA code for AP, PA, and ISO geometries. These calculations were carried out from 10 MeV/u to 100 GeV/u, since the lowest energy treated in the FLUKA code for heavy ions is 10 MeV/u. Absorbed doses were determined with statistical uncertainties of less than 5% in most organs.

4.7.3. Differences among transport codes for helium ions

(221) Fig. 4.38 shows an example of the differences in the calculated organ dose conversion coefficients. The PHITS and FLUKA codes give satisfactory agreement over the entire energy range. In calculations using the PHITS code, nuclear reactions induced by particles below 3.5 GeV/u are simulated by the JQMD model, while those induced by higher-energy particles are dealt with using the JAM model for protons and neutrons, and by the combination of the JQMD and JAM models for heavy ions. The FLUKA code treats nuclear interactions with the RQMD model up to 5 GeV/u, and uses the DPMJET model above this energy. Although the PHITS and FLUKA codes use different nuclear reaction models above 5 GeV/u, the results of both codes show good agreement. For evaluation of the reference data, the Task Group decided to average the organ absorbed doses calculated by the PHITS and FLUKA codes, followed by the application of data-smoothing techniques.

4.7.4. Analysis of organ dose conversion coefficients for helium ions

(222) Fig. 4.39 shows absorbed dose conversion coefficients for helium ions in AP irradiation geometry for selected organs, located at different distances from the front surface of the body within the female reference phantom. It can be seen that the organ absorbed doses in different organs show large variations for energies less than 100 MeV/u, while they are in fairly good agreement above this energy. At low incident energies, helium ions have very short ranges and mainly deposit their energy towards the end of their path in the characteristic Bragg peak. The energy of the helium ion, and therefore its range, is the main factor that determines the distribution of absorbed dose within internal organs and tissues. For example, at helium

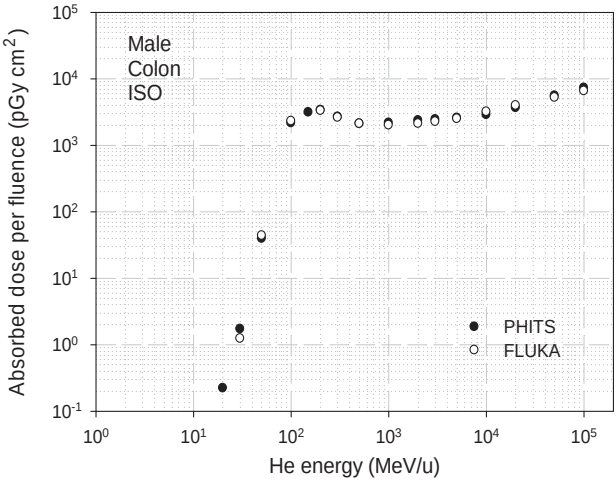

Fig. 4.38. Colon absorbed dose per fluence of the male phantom for isotropic geometry, calculated with different Monte Carlo codes.

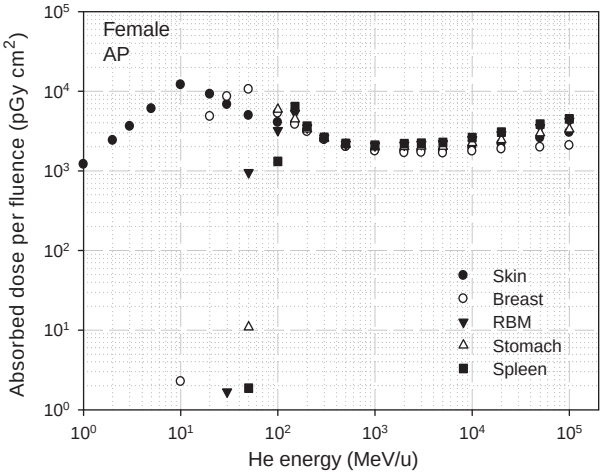

Fig. 4.39. Organ absorbed doses per fluence of helium ions for selected organs of the female phantom for antero-posterior irradiation. RBM, red bone marrow.

ion energies below 10 MeV/u, almost all the energy is imparted to the skin. The energy dependence of the absorbed dose conversion coefficients shows a maximal value with the peak energy differing for each organ. The range of the helium ions corresponding to the peak energies for each organ coincides with the average depth from the skin to the relevant organ. For example, energy of ~50 MeV/u corresponds to the range of a few centimetres in tissue, which corresponds approximately to the average depth of the female breast. For bone marrow, the peak is found at ~100–150 MeV/u, which corresponds to an approximate depth of 8–16 cm.

(223) On the other hand, at high incident energies, helium ions have such long ranges that they can completely traverse the human body without producing a Bragg peak. Consequently, the absorbed doses are more uniformly distributed inside the human body. However, the organ depth dependence of the conversion coefficients can still be observed even in the high-energy region. The conversion coefficients for organs located deep inside the body (e.g. stomach and spleen) rise rapidly with increasing incident energy, in comparison with those for organs located near the surface of the body (e.g. skin and breast). This tendency is due to the fact that high-energy helium ions can trigger a cascade of secondary particles through complex nuclear reactions, and these secondary particles deposit more energy in locations deeper inside the human body.

(224) As discussed in Section 4.4.5 for low-energy protons, helium ions below 10 MeV/u cannot penetrate the skin (the range of 10 MeV/u helium ions in muscle is 0.13 cm). Therefore, organ doses except for skin were not considered to be relevant below 10 MeV/u.

4.7.5. Analysis of effective dose conversion coefficients for helium ions

(225) Fig. 4.40 shows the effective dose conversion coefficients as a function of helium ion energy for the standard AP, PA, and ISO irradiation geometries. Up to 20 MeV/u, the effective dose is mainly determined by the skin dose, and the absorbed dose conversion coefficients for AP and PA geometries are slightly higher compared with ISO geometry. At intermediate energies, from 20 to 100 MeV/u, the effective dose conversion coefficients for AP and PA geometries are much higher and lower than those for ISO irradiation, respectively. This tendency is attributed to the fact that the incident particles generally stop in radiobiologically sensitive organs (e.g. breast) for AP irradiation, while they cannot reach radiobiologically sensitive organs for PA irradiation. Above 20 GeV/u, ISO geometry gives higher effective dose conversion coefficients than AP and PA geometries because of the cascade of secondary particles produced by high-energy helium ions, which then deposit energy in the deeper organs.

4.7.6. Comparison with previous work for helium ions

(226) Fig. 4.41 compares the effective dose conversion coefficients calculated as defined in ICRP *Publication 60* (ICRP, 1991) using the PHITS code with the MIRD phantom (Sato et al., 2003) with those based on the present calculations, as given in Fig. 4.40. Note that the maximum helium ion energy for the calculation of effective dose conversion coefficients in the former study was limited to 3 GeV/u.

(227) It is evident from Fig. 4.41 that the effective dose conversion coefficients calculated following the concepts given in the different ICRP publications are very

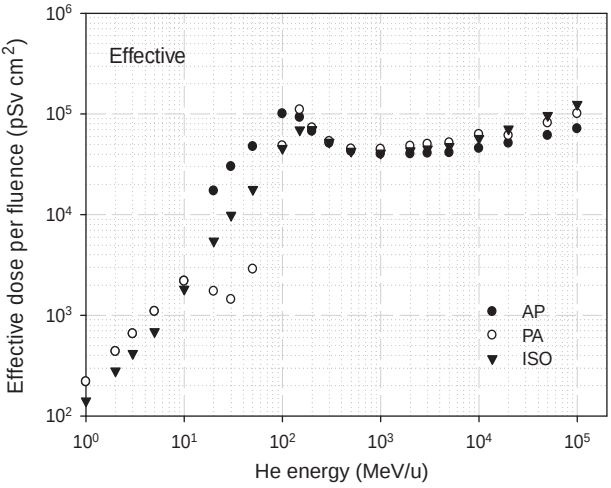

Fig. 4.40. Effective dose conversion coefficients as a function of the energy of helium ions. AP, antero-posterior; PA, postero-anterior; ISO, isotropic.

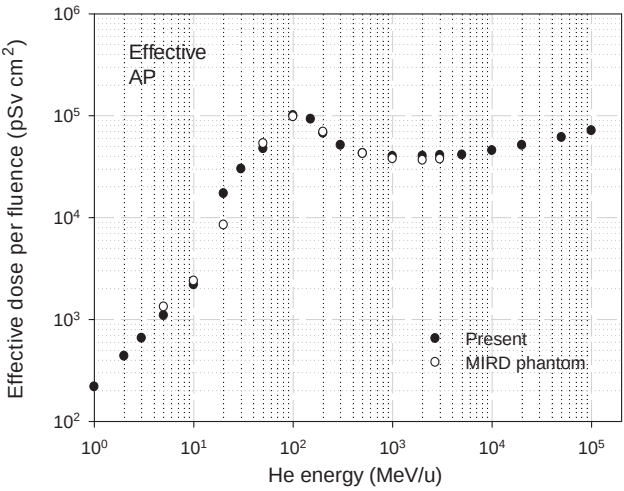

Fig. 4.41. Comparison between the present data for effective dose per fluence and values calculated using the MIRD phantom (Sato et al., 2003) for antero-posterior geometry.

similar, except in the intermediate-energy region, from ~20 to 100 MeV/u. This agreement indicates that the revisions in ICRP *Publication 103* (ICRP, 2007) for the effective dose conversion coefficients are not significant for helium ion irradiation, in contrast to neutrons, as discussed in Section 4.3.6. This is because the numerical values of w_R for heavy ions were not modified in ICRP *Publication 103* (ICRP, 2007), while those for neutrons were revised. The differences at the intermediate incident energies are mainly attributed to the revision of w_T assigned to the breast, the value of which was increased from 0.05 to 0.12 in ICRP *Publication 103* (ICRP, 2007). As shown in Fig. 4.39, the absorbed dose conversion coefficients for the breast are larger than those for other organs in the intermediate incident energy region, as the ranges of the incident particles are close to the average depth from the skin surface to this organ of interest (i.e. a few cm). Thus, effective doses in this energy region depend largely on the absorbed dose in the breast tissues which have a relatively large w_T value.

4.8. References

Aarnio, P.A., Miihring, H.J., Ranft, J., et al., 1990. FLUKA89. Conseil Européen pour la Recherche Nucléaire informal report, Geneva.

Chao, T.C., Bozkurt, A., Xu, X.G., 2001. Conversion coefficients based on the VIP-Man anatomical model and EGS4-VLSI code for external monoenergetic photons from 10 keV to 10 MeV. Health Phys. 81, 163–183.

de Boor, C., 1978. A Practical Guide to Splines. Springer Verlag, New York.

Ferrari, A., Pelliccioni, M., Pillon, M., 1997. Fluence to effective dose conversion coefficients for muons. Radiat. Prot. Dosim. 74, 227–233.

Ferrari, A., Pelliccioni, M., Pillon, M., 1998. Fluence to effective dose conversion coefficients for negatively and positively charged pions. Radiat. Prot. Dosim. 80, 361–370.

Ferrari, P., Gualdrini, G., 2005. An improved MCNP version of the NORMAN voxel phantom for dosimetry studies. Phys. Med. Biol. 50, 4299–4316.

Fesefeldt, H.C., 1985. Simulation of Hadronic Showers, Physics and Application. Technical Report PITHA 85-02.

GEANT4, 2006. GEANT4: Physics Reference Manual. Available at: http://geant4.web.cern.ch/geant4/UserDocumentation/UsersGuides/PhysicsReferenceManual/fo/PhysicsReferenceManual.pdf.

Groom, D.E., Mokhov, N.V., Striganov, S.I., 2001. Muon stopping power and range tables 10 MeV–100 TeV. Atom Data Nucl. Data Tables 78, 183–356.

Hewitt, W.T., Yip, D., 1992. The NURBS Procedure Library. Technical Report CGU76. Manchester Computing Centre, Manchester.

ICRP, 1991. 1990 Recommendations of the International Commission on Radiological Protection. ICRP Publication 60. Ann. ICRP 21(1–3).

ICRP, 1996. Conversion coefficients for use in radiological protection against external radiation. ICRP Publication 74. Ann. ICRP 26(3/4).

ICRP, 2002. Basic anatomical and physiological data for use in radiological protection: reference values. ICRP Publication 89. Ann. ICRP 32(3/4).

ICRP, 2007. The 2007 Recommendations of the International Commission on Radiological Protection. ICRP Publication 103. Ann. ICRP 37(2–4).

ICRP, 2009. Adult reference computational phantoms. ICRP Publication 110. Ann. ICRP 39(2).

ICRU, 1993. Stopping Power and Ranges for Protons and Alpha Particles. ICRU Report 49. International Commission on Radiation Units and Measurements, Bethesda, MD.

ICRU, 1998. Conversion Coefficients for use in Radiological Protection Against External Radiation. ICRU Report 57. International Commission on Radiation Units and Measurements, Bethesda, MD.

Jones, D.G., 1997. A realistic anthropomorphic phantom for calculating organ doses arising from external photon irradiation. Radiat. Prot. Dosim. 72, 21–29.

Kawrakow, I., Mainegra-Hing, E., Rogers, D.W.O., et al., 2009. The EGSnrc Code System: Monte Carlo Simulation of Electron and Photon Transport. PIRS Report 701. National Research Council of Canada, Ottawa.

Kramer, R., Zankl, M., Williams, G., et al., 1982. The Calculation of Dose from External Photon Exposures Using Reference Human Phantoms and Monte Carlo Methods, Part I: the Male (Adam) and Female (Eva) Adult Mathematical Phantoms. GSF Report S-885. GSF – National Research Centre for Environment and Health, Neuherberg.

Kramer, R., Khoury, H.J., Vieira, J.W., 2005. Comparison between effective doses for voxel-based and stylized exposure models from photon and electron irradiation. Phys. Med. Biol. 50, 5105–5126.

Lee, C., Lee, C., Lee, J.-K., 2006. On the need to revise the arm structure in stylized anthropomorphic phantoms in lateral photon irradiation geometry. Phys. Med. Biol. 51, N393–N402.

Pelowitz, D.B., 2008. MCNPX User's Manual, Version 2.6.0. LA-CP-07-1473. Los Alamos National Laboratory, Los Alamos, NM.

Prael, R.E., Lichtenstein, H., 1989. User Guide to LCS: the LAHET Code System LA-UR-89-3014 (1989), Los Alamos National Laboratory Los Alamos, NM, USA.

Rogers, D.W.O., Bielajew, A.F., 1990. Monte Carlo Techniques of Electron and Photon Transport for Radiation Dosimetry. In: Kase, K.R., Bjärngard, B.E., Attix, F.H. (Eds.), The Dosimetry of Ionizing Radiation. Vol. 3. Academic Press, San Diego, CA, pp. 427–539.

Rogers, D.W.O., Faddegon, B.A., Ding, G.X., et al., 1995. BEAM: a Monte Carlo code to simulate radiotherapy treatment units. Med. Phys. 22, 503–524.

Roussin, R.W., Knight, J.R., Hubbell, J.H., et al., 1983. Description of the DLC-99/HUGO Package of Photon Interaction Data in ENDF/B-V Format. ORNL Report RSIC-46 (ENDF-335). Radiation Shielding Information Center, Oak Ridge National Laboratory, Oak Ridge, TN.

Sato, T., Tsuda, S., Sakamoto, Y., et al., 2003. Conversion coefficients from fluence to effective dose for heavy ions with energies up to 3 GeV/A. Radiat. Prot. Dosim. 106, 137–144.

Sato, T., Endo, A., Zankl, M., et al., 2009. Fluence-to-dose conversion coefficients for neutrons and protons calculated using the PHITS code and ICRP/ICRU adult reference computational phantoms. Phys. Med. Biol. 54, 1997–2014.

Sato, T., Endo, A., Niita, K., 2010. Fluence-to-dose conversion coefficients for heavy ions calculated using the PHITS code and the ICRP/ICRU adult reference computational phantoms. Phys. Med. Biol. 55, 2235–2246.

Schlattl, H., Zankl, M., Petoussi-Henss, N., 2007. Organ dose conversion coefficients for voxel models of the reference male and female from idealized photon exposures. Phys. Med. Biol. 52, 2123–2145.

Seltzer, S.M., 1993. Calculation of photon mass energy-transfer and mass energy-absorption coefficients. Radiat. Res. 136, 147–170.

Snyder, W.S., Ford, M.R., Warner, G.G., et al., 1969. Estimates of absorbed fractions for monoenergetic photon sources uniformly distributed in various organs of a heterogeneous phantom. Medical Internal Radiation Dose Committee Pamphlet No. 5. J. Nucl. Med. 10 (Suppl. 3).

Snyder, W.S., Ford, M.R., Warner, G.G., 1978. Estimates of Specific Absorbed Fractions for Monoenergetic Photon Sources Uniformly Distributed in Various Organs of a Heterogeneous Phantom. Medical Internal Radiation Dose Committee Pamphlet 5 Revised. Society of Nuclear Medicine, New York, NY.

Veit, R., Zankl, M., Petoussi, N., et al., 1989. Tomographic Anthropomorphic Models. Part I: Construction Technique and Description of Models of an 8 Week Old Baby and a 7 Year Old Child. GSF Report 3/89. GSF – National Research Center for Environment and Health, Neuherberg.

Warner, G.G., Craig, A.M., 1968. ALGAM, a Computer Program for Estimating Internal Dose from Gamma-ray Sources in a Man Phantom. ORNL Report TM-2250. Oak Ridge National Laboratory, Oak Ridge, TN.

Zankl, M., Fill, U., Petoussi-Henss, N., et al., 2002. Organ dose conversion coefficients for external photon irradiation of male and female voxel models. Phys. Med. Biol. 47, 2367–2385.

5. RELATIONSHIPS BETWEEN DOSE CONVERSION COEFFICIENTS FOR OPERATIONAL AND PROTECTION QUANTITIES

(228) This section examines the impact of the changes in the 2007 Recommendations (ICRP, 2007) for protection quantities with respect to the ICRU operational quantities.

(229) ICRU defined a set of operational quantities for external radiations in Report 39 (ICRU, 1985) for use in assessment of the ICRP protection quantities in radiation protection measurements. This set of operational quantities was developed further in ICRU Report 51 (ICRU, 1993). ICRU published three reports on practical applications of these quantities: Reports 43, 47, and 66 (ICRU, 1988, 1992, 2001). In ICRP *Publication 74* (ICRP, 1996) and ICRU Report 57 (ICRU, 1998), reference values for the conversion coefficients for operational quantities for photons, neutrons, and electrons for limited particle energy ranges were reported, and comparisons of the conversion coefficients for protection and operational quantities were presented.

(230) The protection quantities are defined for the particles incident in the medium in which the body or phantom is located, while operational quantities are defined at the point at which the phantom is located. The values of the conversion coefficients for the photon protection and operational quantities recommended in ICRP *Publication 74* (ICRP, 1996) and ICRU Report 57 (ICRU, 1998) were calculated using the kerma approximation. This approximation, under certain circumstances, can give a reasonably good estimate of absorbed dose. The kerma approximation assumes that all energy transferred from the incident particle in an interaction is deposited locally. The numerical value of kerma approaches that of the absorbed dose, to the degree that charged-particle equilibrium exists, that radiative losses are negligible, and that the kinetic energy of the uncharged particles is large compared with the binding energy of the liberated charged particles.

(231) In ICRP *Publication 74* (ICRP, 1996) and ICRU Report 57 (ICRU, 1998), the neutron protection and operational quantities were computed using the kerma approximation for neutrons incident on the various phantoms for energies up to 20 MeV. For incident neutrons over 20 MeV, secondary charged particles ($A \leqslant 4$) were tracked and their energy deposition was scored. Once the incident neutrons were moderated to energies up to 20 MeV inside the phantom, the kerma approximation was applied at their next interaction.

(232) In a comparison of the results of the calculations of the protection quantities for the reference phantoms *in vacuo* presented in this publication, and those given in ICRP *Publication 74* (ICRP, 1996) and ICRU Report 57 (ICRU, 1998) for photons and neutrons, the differences observed for ratios of the protection quantities for photons are mainly due to the differences between the phantoms used and the values of the tissue weighting factors employed (see Section 4.1.6). The differences for

neutrons are mainly a result of the change in radiation weighting factors (see Section 4.3.6).

(233) The kerma approximation is not generally acceptable at all energies for the calculation of conversion coefficients for the operational quantities. For photons, information on the influence of air outside the phantom was available at the time of the preparation of ICRU Report 39 (Dimbylow and Francis, 1979, 1983, 1984; ICRU, 1985). However, up to now, for radiation protection calibrations and measurements in an air medium, the recommended values of the conversion coefficients for the operational quantities for photons using the kerma approximation were considered to give an acceptable approximation to the protection quantities for broad distributions of particle energies and directions, and to be suitable for practical application for most radiation protection practices for the range of particle energies in the radiation fields considered.

(234) In general for instrument measurements and calibrations, the definitions of the operational quantities and consideration of the calculations of the corresponding operational quantities need to be considered further. This work is presently under review by ICRU.

(235) The comparisons of values of the reference conversion coefficients for operational quantities (ICRP, 1996; ICRU, 1998) demonstrate how well they serve as predictors of the protection quantities for broad particle energy and directional distributions for most radiation protection applications over the range of particle energies in the radiation fields considered.

5.1. Changes in protection quantities

(236) In this section, the dose conversion coefficients for protection quantities recommended in this publication are compared with the previously recommended conversion coefficients for operational quantities. In several cases, they are also compared with operational quantity values reported since the release of ICRP *Publication 74* (ICRP, 1996) and ICRU Report 57 (ICRU, 1998), principally to extend the comparisons to the higher energies considered in this publication. When the values of operational quantities that are not extracted from ICRP *Publication 74* (ICRP, 1996) and ICRU Report 57 (ICRU, 1998) are used in comparisons, their use does not in any way constitute an endorsement of those values as recommended values, as an extensive evaluation process was not employed to select them from the existing refereed literature on conversion coefficients for operational quantities.

(237) It is important to note that all of the recommended conversion coefficients for photon operational quantities, namely those in ICRP *Publication 74* (ICRP, 1996) and ICRU Report 57 (ICRU, 1998), used to construct the ratios in this section were based on the kerma approximation to absorbed dose, and the presently recommended protection quantities are not. The use of the kerma approximation to compute conversion coefficients for operational quantities does not strictly comply with

the definitions of those quantities (Ferrari and Pelliccioni, 1994a; Bartlett and Dietze, 2010), but that approach has been maintained here for consistency with reference values for photon operational quantities in ICRP *Publication 74* (ICRP, 1996) and ICRU Report 57 (ICRU, 1998).

5.2. Photons

(238) Photon effective dose conversion coefficients are compared with the $H^*(10)$ conversion coefficients (ICRP, 1996; ICRU, 1998) in Fig. 5.1. The ratios indicate that $H^*(10)$ computed under the kerma approximation conservatively overestimates effective dose at all energies up to 10 MeV. To provide an evaluation of the effective dose conversion coefficients at energies above 10 MeV, ambient dose equivalent values (Ferrari and Pelliccioni, 1994a; Pelliccioni, 2000) are compared with the effective dose conversion coefficients up to 10 GeV in Fig. 5.2. Both quantities are calculated with the body and sphere *in vacuo*, and are absorbed dose computations in which secondary electrons were tracked. Above ~3 MeV, the ambient dose equivalent increasingly underestimates the effective dose, an effect not observed when the kerma approximation is used, as in Fig. 5.1. This departure from the effective dose at 3 MeV is amplified in the top graph of Fig. 5.2 in which the data are only plotted to 10 MeV. Similar calculations have been performed for the personal dose equivalent (Veinot and Hertel, 2010) and yield essentially the same results.

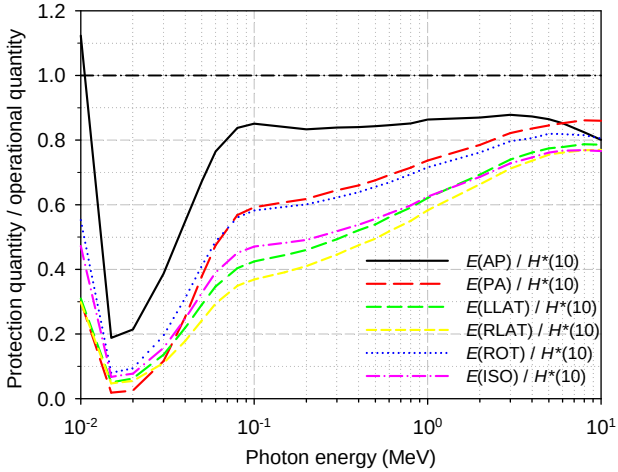

Fig. 5.1. Ratios of photon effective dose (present report) to ambient dose equivalent under charged-particle equilibrium (ICRP, 1996) for mono-energetic photons. AP, antero-posterior; PA, postero-anterior; LLAT, left lateral; RLAT, right lateral; ROT, rotational; ISO, isotropic.

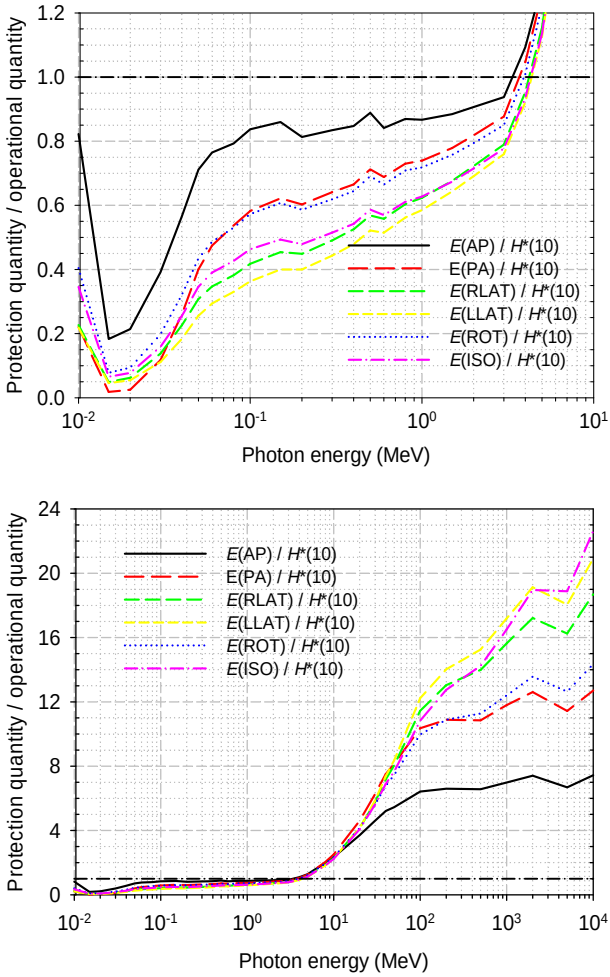

Fig. 5.2. Ratios of photon effective dose (present report) to ambient dose equivalent (Ferrari and Pelliccioni, 1994a; Pelliccioni, 2000) for mono-energetic photons. It should be noted that for the calculation of the ambient dose equivalent, the secondary particles were tracked (i.e. there is no kerma approximation). To facilitate comparison with Fig. 5.1, the upper figure shows values up to energies of 10 MeV. AP, antero-posterior; PA, postero-anterior; LLAT, left lateral; RLAT, right lateral; ROT, rotational; ISO, isotropic.

5.3. Electrons

(239) The electron effective dose conversion coefficients of this publication are compared with the ambient dose equivalent conversion coefficients (ICRP, 1996; ICRU, 1998) in Fig. 5.3. (The ambient dose equivalent is not specifically reported in ICRP *Publication 74* and ICRU Report 57, but the directional dose equivalent $H'(10,0)$ is reported. These two quantities are numerically equal when the ICRU sphere is used as the phantom.) It can be seen that ambient dose equivalent overestimates effective dose up to 10 MeV. In Fig. 5.4, effective dose conversion coefficients are compared with the

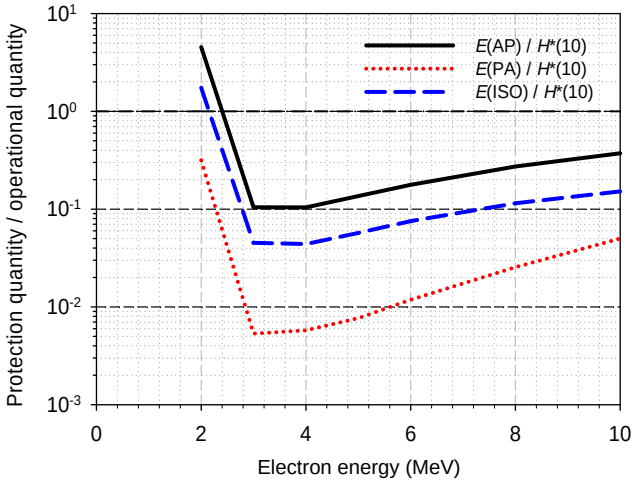

Fig. 5.3. Ratios of electron effective dose (present report) to ambient dose equivalent, $H^*(10)$, from ICRP *Publication 74* (ICRP, 1996) for mono-energetic electrons. AP, antero-posterior; PA, postero-anterior; ISO, isotropic.

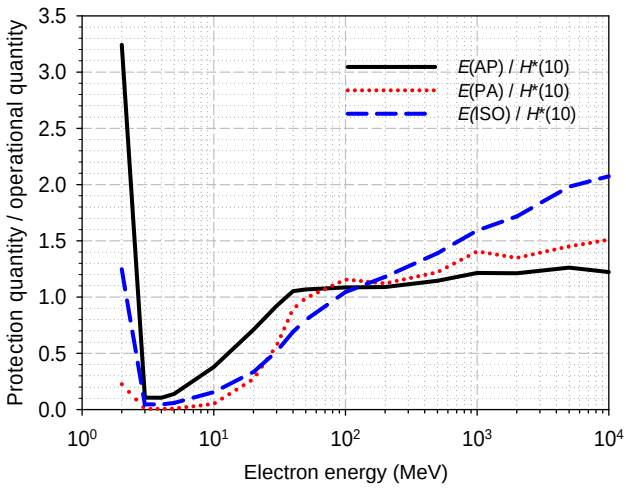

Fig. 5.4. Ratios of electron effective dose (present report) to ambient dose equivalent, $H^*(10)$, from Ferrari and Pelliccioni (1994b) for mono-energetic electrons. AP, antero-posterior; PA, postero-anterior; ISO, isotropic.

dose conversion coefficients reported at higher energies (Ferrari and Pelliccioni, 1994a). Note that above 100 MeV, all ratios are greater than 1, thereby indicating that the ambient dose equivalent does not provide a conservative estimate for effective dose.

5.4. Neutrons

(240) In Fig. 5.5, neutron effective dose conversion coefficients for AP, PA, RLAT, LLAT, ISO, and ROT geometries by neutrons with energies up to 200 MeV are

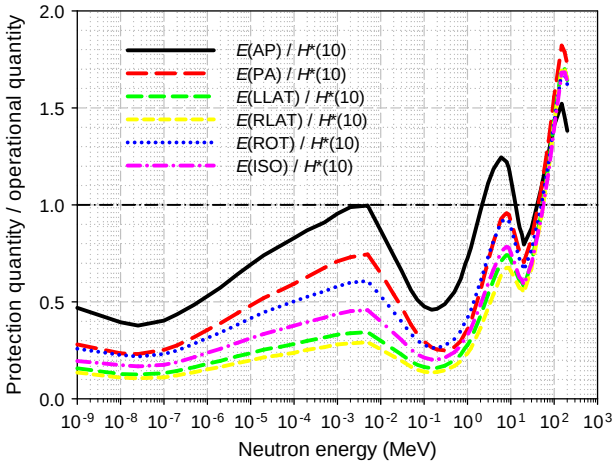

Fig. 5.5. Ratios of neutron effective dose (present report) to ambient dose equivalent (ICRP, 1996) for mono-energetic neutrons. AP, antero-posterior; PA, postero-anterior; LLAT, left lateral; RLAT, right lateral; ROT, rotational; ISO, isotropic.

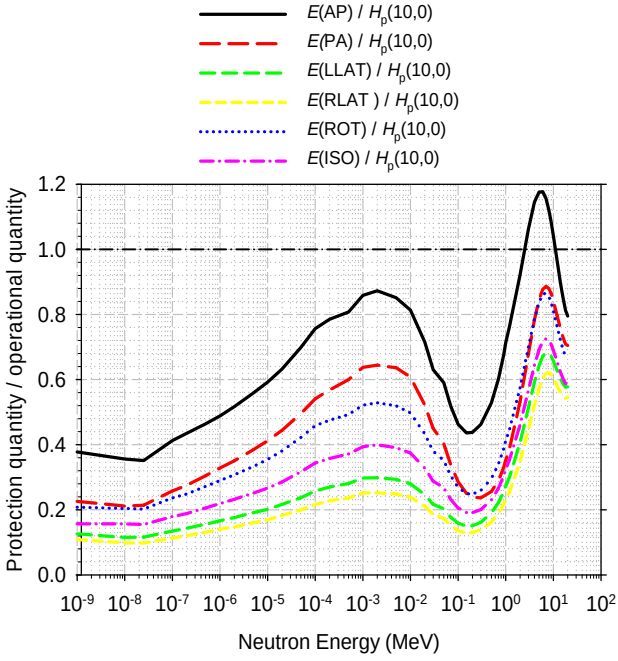

Fig. 5.6. Ratio of neutron effective dose (present report) to personal dose equivalent (ICRP, 1996) for mono-energetic neutrons. AP, antero-posterior; PA, postero-anterior; LLAT, left lateral; RLAT, right lateral; ROT, rotational; ISO, isotropic.

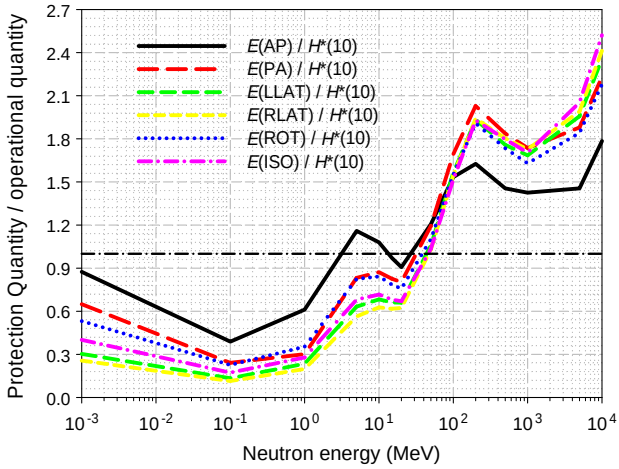

Fig. 5.7. Ratios of neutron effective dose (present report) to ambient dose equivalent (Ferrari and Pelliccioni, 1998) for mono-energetic neutrons. AP, antero-posterior; PA, postero-anterior; LLAT, left lateral; RLAT, right latral; ROT, rotational; ISO, isotropic.

compared with values of $H^*(10)$ (ICRP, 1996; ICRU, 1998). The conversion coefficients for the operational quantities are conservative overestimates of the effective dose for all irradiation geometries up to 3 MeV. They underestimate the effective dose slightly for AP radiation geometry between 3 and 12 MeV. At 50 MeV, the conversion coefficients for effective dose for AP and PA irradiation geometries are underestimated by those for $H^*(10)$, and above 75 MeV, the conversion coefficients for effective doses for all irradiation geometries are underestimated by those given by $H^*(10)$. In the energy region from 75 to 200 MeV, the underestimates range from factors of 1.5–1.8 at their maximum, and all decrease above 200 MeV.

(241) In Fig. 5.6, the neutron effective dose conversion coefficients for AP, PA, RLAT, LLAT, ISO, and ROT irradiation geometries are compared with reference values for the personal dose equivalent conversion coefficients, $H_p(10,0)$ (ICRP, 1996; ICRU, 1998). It can be seen that there is a slight underestimate of the effective dose for the AP irradiation geometry from 4 to 12 MeV.

(242) The neutron effective dose conversion coefficients were also compared with the ambient dose equivalent conversion coefficients of Ferrari and Pelliccioni (1998) for higher energies. The ratios of the recommended protection quantities to these values of $H^*(10)$ are shown in Fig. 5.7. The magnitude of the underestimation of the effective dose by $H^*(10)$ decreases above 200 MeV, and then continues to increase above 1 GeV, approaching factors of 2.5 and 1.8 for ISO and AP irradiation geometries, respectively, at 10 GeV.

5.5. Comparison of dose to the lens of the eye with the operational quantities

(243) A comparison of equivalent dose to the lens of the eye with the operational quantities warrants a discussion with regard to which operational quantity is most

appropriate for the assessment of equivalent dose to this specific radiosensitive tissue. However, this discussion is beyond the scope of the current report. At the time of its preparation, studies are underway concerning the suitability of existing operational quantities, their calibration procedures, and appropriate calibration phantoms for dosimeters that can be used to monitor and assess the operational quantities.

(244) Due to the position of the lens of the eye at the front of the head, the organ dose is strongly dependent upon the direction of radiation incidence, especially for radiations of low or intermediate energy, while for very high radiation energies, absorption in the head is less important compared with the radiation built up in the material traversed anteriorly to the lens. At low radiation energies, frontal radiation (AP) incidence deserves the most attention. Generally, the quantities for area and individual monitoring are nearly equal for AP exposure values of $H^*(3)$ and $H_p(3)$, but this is not the case for other directions of radiation incidence. For such geometries, it might be more appropriate to consider $H_p(3)$ and $H_p(0.07)$. Data for $H_p(3)$ and $H_p(0.07)$ on suitable calibration phantoms, however, are not presently available.

(245) In Fig. 5.8, the equivalent dose to the lens of the eye is compared with $H^*(3)$ based on the data reported in ICRP *Publication 51* (ICRP, 1987) for photon energies up to 10 MeV. It should be noted that the equivalent dose (Sv) is numerically the same as the absorbed dose (Gy) for photons and electrons. Although $H^*(3)$ was not reported explicitly in ICRP *Publication 51* (ICRP, 1987), the dose for parallel irradiation at a depth of 3 mm on the principal axis is equivalent to $H^*(3)$. It should be noted that the $H^*(3)$ data were computed using the kerma approximation. It can be seen that

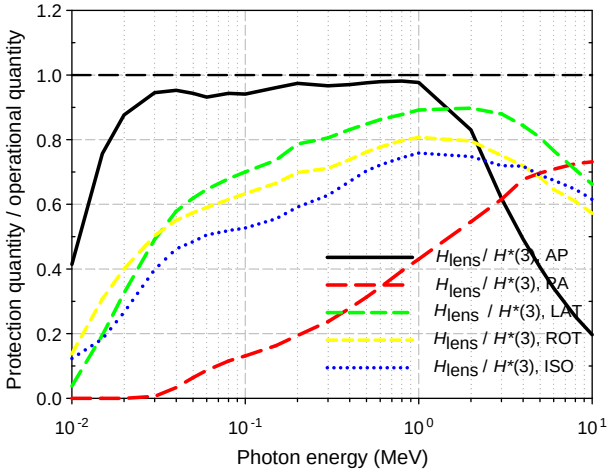

Fig. 5.8. Ratios of equivalent dose to the lens of the eye (present report) to $H^*(3)$ for photons, based on data from ICRP *Publication 51* (ICRP, 1987). AP, antero-posterior; PA, postero-anterior; LLAT, left lateral; RLAT, right lateral; ROT, rotational; ISO, isotropic.

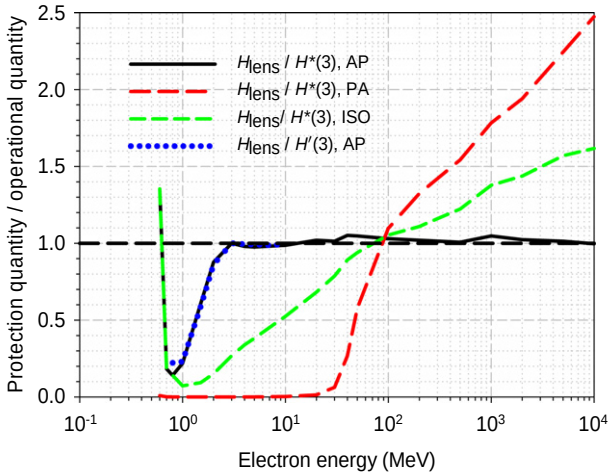

Fig. 5.9. Ratios of equivalent dose to the lens of the eye (present report) to $H'(3)$ for electrons from ICRP *Publication 74* (ICRP, 1996), and to $H^*(3)$ based on data from Ferrari and Pelliccioni (1994b). AP, antero-posterior; PA, postero-anterior; ISO, isotropic.

$H^*(3)$ is a conservative approximation to the equivalent dose to the lens of the eye in this energy range for all directions of radiation incident on the head.

(246) In Fig. 5.9, the equivalent dose to the lens of the eye is compared with $H'(3)$ from ICRP *Publication 74* (ICRP, 1996; ICRU, 1998) for electron energies up to 10 MeV. For AP exposure of the phantom, however, $H'(3)$ is always equal to $H^*(3)$. In addition, the doses to the lens of the eye are compared with $H^*(3)$ from Ferrari and Pelliccioni (1994b) as these data were computed to higher energies. It can be seen that $H^*(3)$ conservatively estimates the dose to the lens of the eye for AP irradiation and electron energies above ~0.7 MeV. Above ~70 MeV, $H^*(3)$ underestimates the equivalent dose to the lens of the eye for both the PA and ISO irradiation geometries because of the dose build-up effect near the surface of the ICRU sphere phantom, compared with the position of the eye in the head for PA and ISO exposure. Hence, $H^*(3)$ can only assess the equivalent dose to the lens of the eye sufficiently for AP exposure. However, precise data for $H_p(3)$ on a head phantom are not yet available.

5.6. Conclusions

(247) In this section, the conversion coefficients for effective dose, calculated according to the recommendations of ICRP *Publication 103* (ICRP, 2007), were compared with recommended conversion coefficients for operational quantities (ICRP, 1996; ICRU, 1998). From those comparisons, it can be deduced that the operational quantities for photons, neutrons, and electrons (ICRP, 1996; ICRU,

1998) continue to provide a good approximation for broad particle energy and direction distributions, and to be of practical application for most radiation protection practices for the range of particle energies in the radiation fields considered (ICRP, 1996; ICRU, 1998), but not at the higher energies considered in this publication.

(248) For operational quantities at these higher energies, comparisons with a small sample of the data published since 1996 demonstrate that there is a need to further examine the relationship of the operational and protection quantities. In 2010, ICRU undertook the task to re-evaluate the definitions of the operational quantities.

5.7. References

Bartlett, D.T., Dietze, G., 2010. ICRU operational quantities. Radiat. Prot. Dosim. 139, 475–476.

Dimbylow, P.J., Francis, T.M., 1979. A Calculation of the Photon Depth-Dose Distributions in the ICRU Sphere for a Broad Parallel Beam, a Point Source and an Isotropic Field. National Radialogical Protection Board-R92. NRPB, London..

Dimbylow, P.J., Francis, T.M., 1983. The effect of photon scatter and consequent electron build-up in air on the calculation of dose equivalent quantities in the ICRU sphere for photon energies from 0.662 to 10 MeV. Phys. Med. Biol. 28, 817–828.

Dimbylow, P.J., Francis, T.M., 1984. The calculation of dose equivalent quantities in the ICRU sphere for photon energies from 0.01 to 10 MeV. Radiat. Prot. Dosim. 9, 49–53.

Ferrari, A., Pelliccioni, M., 1994a. On ambient dose equivalent. J. Radiol. Prot. 14, 331–335.

Ferrari, A., Pelliccioni, M., 1994b. Dose equivalents for monoenergetic electrons incident on the ICRU sphere. Radiat. Prot. Dosim. 55, 207–210.

Ferrari, A., Pelliccioni, M., 1998. Fluence to effective dose conversion data and effective quality factors of high energy neutrons. Radiat. Prot. Dosim. 76, 215–224.

ICRP, 1987. Data for use in protection against external radiation. ICRP Publication 51. Ann. ICRP 17(2/3).

ICRP, 1996. Conversion coefficients for use in radiological protection against external radiation. ICRP Publication 74. Ann. ICRP 26(3/4).

ICRP, 2007. The 2007 Recommendations of the International Commission on Radiological Protection. ICRP Publication 103. Ann. ICRP 37(2–4).

ICRU, 1985. Determination of Dose Equivalents Resulting from External Radiation Sources. ICRU Report 39. International Commission on Radiation Units and Measurements, Bethesda, MD.

ICRU, 1988. Measurement of Dose Equivalents from External Radiation Sources. Part 2. ICRU Report 43. International Commission on Radiation Units and Measurements, Bethesda, MD.

ICRU, 1992. Measurement of Dose Equivalents from External Photon and Electron Radiations. ICRU Report 47. International Commission on Radiation Units and Measurements, Bethesda, MD.

ICRU, 1993. Quantities and Units in Radiation Protection Dosimetry. ICRU Report 51. International Commission on Radiation Units and Measurements, Bethesda, MD.

ICRU, 1998. Conversion Coefficients for use in Radiological Protection Against External Radiation. ICRU Report 57. International Commission on Radiation Units and Measurements, Bethesda, MD.

ICRU, 2001. Determination of Operational Dose Equivalent Quantities for Neutrons. ICRU Report 66. International Commission on Radiation Units and Measurements, Bethesda, MD.

Pelliccioni, M., 2000. Overview of fluence-to-effective dose and fluence-to-ambient dose equivalent conversion coefficients for high energy radiation calculated using the FLUKA code. Radiat. Prot. Dosim. 88, 279–297.

Veinot, K., Hertel, N., 2010. Personal dose equivalent conversion coefficients for photons to 1 GeV. Radiat. Prot. Dosim. 145, 28–35.

ANNEX A. EFFECTIVE DOSE CONVERSION COEFFICIENTS

(A1) This annex lists reference values for effective dose conversion coefficients for photons, electrons, positrons, neutrons, negative and positive muons, negative and positive pions, and helium ions, each for the specific irradiation geometries considered. These tables can also be found in the CD accompanying this report.

(A2) The specific irradiation geometries considered are unidirectional broad parallel beams along the antero-posterior, postero-anterior, left and right lateral axes, and rotational and fully isotropic directions of incidence (see Section 3.2).

(A3) The effective doses are normalised to incident particle fluence, Φ, and are given in units of pSv cm^2. For photons of energies up to 10 MeV, the conversion coefficients are also tabulated as the effective dose per air kerma free-in-air, K_a, in units of Sv/Gy. For this transformation, conversion coefficients for air kerma per particle fluence were applied (Seltzer, 1993).

(A4) The following table entries are reference values and were derived from the organ dose conversion coefficients calculated using the ICRP/ICRU reference computational phantoms coupled to various Monte Carlo radiation transport codes (see Sections 3.1 and 3.3). All reference values for effective dose are given following its definition in the 2007 Recommendations (ICRP, 2007).

Table A.1. Photons: effective dose per fluence, in units of pSv cm^2, for mono-energetic particles incident in various geometries.

Energy (MeV)	AP	PA	LLAT	RLAT	ROT	ISO
0.01	0.0685	0.0184	0.0189	0.0182	0.0337	0.0288
0.015	0.156	0.0155	0.0416	0.0390	0.0664	0.0560
0.02	0.225	0.0260	0.0655	0.0573	0.0986	0.0812
0.03	0.313	0.0940	0.110	0.0891	0.158	0.127
0.04	0.351	0.161	0.140	0.114	0.199	0.158
0.05	0.370	0.208	0.160	0.133	0.226	0.180
0.06	0.390	0.242	0.177	0.150	0.248	0.199
0.07	0.413	0.271	0.194	0.167	0.273	0.218
0.08	0.444	0.301	0.214	0.185	0.297	0.239
0.1	0.519	0.361	0.259	0.225	0.355	0.287
0.15	0.748	0.541	0.395	0.348	0.528	0.429
0.2	1.00	0.741	0.552	0.492	0.721	0.589
0.3	1.51	1.16	0.888	0.802	1.12	0.932
0.4	2.00	1.57	1.24	1.13	1.52	1.28
0.5	2.47	1.98	1.58	1.45	1.92	1.63
0.511	2.52	2.03	1.62	1.49	1.96	1.67
0.6	2.91	2.38	1.93	1.78	2.30	1.97
0.662	3.17	2.62	2.14	1.98	2.54	2.17
0.8	3.73	3.13	2.59	2.41	3.04	2.62
1.0	4.49	3.83	3.23	3.03	3.72	3.25
1.117	4.90	4.22	3.58	3.37	4.10	3.60
1.33	5.59	4.89	4.20	3.98	4.75	4.20
1.5	6.12	5.39	4.68	4.45	5.24	4.66
2.0	7.48	6.75	5.96	5.70	6.55	5.90
3.0	9.75	9.12	8.21	7.90	8.84	8.08
4.0	11.7	11.2	10.2	9.86	10.8	10.0
5.0	13.4	13.1	12.0	11.7	12.7	11.8
6.0	15.0	15.0	13.7	13.4	14.4	13.5
6.129	15.1	15.2	13.9	13.6	14.6	13.7
8.0	17.8	18.6	17.0	16.6	17.6	16.6
10.0	20.5	22.0	20.1	19.7	20.6	19.6
15.0	26.1	30.3	27.4	27.1	27.7	26.8
20.0	30.8	38.2	34.4	34.4	34.4	33.8
30.0	37.9	51.4	47.4	48.1	46.1	46.1
40.0	43.1	62.0	59.2	60.9	56.0	56.9
50.0	47.1	70.4	69.5	72.2	64.4	66.2
60.0	50.1	76.9	78.3	82.0	71.2	74.1
80.0	54.5	86.6	92.4	97.9	82.0	87.2
100	57.8	93.2	103	110	89.7	97.5
150	63.3	104	121	130	102	116
200	67.3	111	133	143	111	130
300	72.3	119	148	161	121	147
400	75.5	124	158	172	128	159
500	77.5	128	165	180	133	168
600	78.9	131	170	186	136	174
800	80.5	135	178	195	142	185
1000	81.7	138	183	201	145	193
1500	83.8	142	193	212	152	208
2000	85.2	145	198	220	156	218
3000	86.9	148	206	229	161	232
4000	88.1	150	212	235	165	243
5000	88.9	152	216	240	168	251
6000	89.5	153	219	244	170	258
8000	90.2	155	224	251	172	268
10,000	90.7	155	228	255	175	276

AP, antero-posterior; PA, postero-anterior; LLAT, left lateral; RLAT, right lateral; ROT, rotational; ISO, isotropic.

Table A.2. Photons: effective dose per air kerma free-in-air, in units of Sv/Gy, for mono-energetic particles incident in various geometries.

Energy (MeV)	AP	PA	LLAT	RLAT	ROT	ISO
0.01	0.0090	0.0024	0.0025	0.0024	0.0044	0.0038
0.015	0.0485	0.0048	0.0130	0.0122	0.0207	0.0175
0.02	0.130	0.0151	0.0379	0.0332	0.0571	0.0470
0.03	0.423	0.127	0.149	0.121	0.214	0.171
0.04	0.801	0.369	0.319	0.261	0.455	0.361
0.05	1.13	0.633	0.487	0.406	0.688	0.548
0.06	1.33	0.827	0.604	0.513	0.850	0.680
0.07	1.42	0.935	0.668	0.574	0.939	0.751
0.08	1.44	0.974	0.693	0.599	0.963	0.773
0.1	1.39	0.970	0.694	0.605	0.953	0.769
0.15	1.25	0.901	0.658	0.581	0.880	0.715
0.2	1.17	0.865	0.644	0.574	0.842	0.687
0.3	1.09	0.836	0.643	0.580	0.812	0.675
0.4	1.06	0.831	0.653	0.595	0.806	0.678
0.5	1.04	0.833	0.665	0.611	0.807	0.684
0.511	1.03	0.833	0.667	0.613	0.807	0.685
0.6	1.02	0.837	0.678	0.626	0.810	0.692
0.662	1.02	0.839	0.685	0.635	0.813	0.697
0.8	1.01	0.846	0.699	0.652	0.821	0.708
1.0	1.00	0.855	0.720	0.676	0.830	0.725
1.117	0.999	0.861	0.730	0.688	0.836	0.734
1.33	0.996	0.870	0.748	0.709	0.846	0.748
1.5	0.996	0.878	0.761	0.724	0.853	0.759
2.0	0.990	0.894	0.788	0.754	0.867	0.781
3.0	0.977	0.914	0.823	0.792	0.886	0.810
4.0	0.960	0.923	0.839	0.812	0.893	0.824
5.0	0.943	0.927	0.846	0.822	0.893	0.831
6.0	0.924	0.927	0.848	0.825	0.889	0.832
6.129	0.921	0.926	0.848	0.825	0.888	0.832
8.0	0.886	0.922	0.842	0.824	0.874	0.825
10.0	0.848	0.913	0.831	0.816	0.856	0.814
15.0	0.756	0.880	0.794	0.786	0.804	0.778
20.0	0.679	0.843	0.759	0.758	0.759	0.744

AP, antero-posterior; PA, postero-anterior; LLAT, left lateral; RLAT, right lateral; ROT, rotational; ISO, isotropic.

Table A.3. Electrons: effective dose per fluence, in units of pSv cm^2, for mono-energetic particles incident in various geometries.

Energy (MeV)	AP	PA	ISO
0.01	0.0269	0.0268	0.0188
0.015	0.0404	0.0402	0.0283
0.02	0.0539	0.0535	0.0377
0.03	0.0810	0.0801	0.0567
0.04	0.108	0.107	0.0758
0.05	0.135	0.133	0.0948
0.06	0.163	0.160	0.114
0.08	0.218	0.213	0.152
0.1	0.275	0.267	0.191
0.15	0.418	0.399	0.291
0.2	0.569	0.530	0.393
0.3	0.889	0.787	0.606
0.4	1.24	1.04	0.832
0.5	1.63	1.28	1.08
0.6	2.05	1.50	1.35
0.8	4.04	1.68	1.97
1.0	7.10	1.68	2.76
1.5	15.0	1.62	4.96
2.0	22.4	1.62	7.24
3.0	36.1	1.95	11.9
4.0	48.2	2.62	16.4
5.0	59.3	3.63	21.0
6.0	70.6	5.04	25.5
8.0	97.9	9.46	35.5
10.0	125	18.3	46.7
15.0	188	53.1	76.9
20.0	236	104	106
30.0	302	220	164
40.0	329	297	212
50.0	337	331	249
60.0	341	344	275
80.0	346	358	309
100	349	366	331
150	355	379	363
200	359	388	383
300	365	399	410
400	369	408	430
500	372	414	445
600	375	419	457
800	379	428	478
1000	382	434	495
1500	387	446	525
2000	391	455	549
3000	397	468	583
4000	401	477	608
5000	405	484	628
6000	407	490	646
8000	411	499	675
10,000	414	507	699

AP, antero-posterior; PA, postero-anterior; ISO, isotropic.

Table A.4. Positrons: effective dose per fluence, in units of pSv cm^2, for mono-energetic particles incident in various geometries.

Energy (MeV)	AP	PA	ISO
0.01	3.28	1.62	1.39
0.015	3.29	1.64	1.40
0.02	3.30	1.65	1.41
0.03	3.33	1.68	1.43
0.04	3.36	1.71	1.45
0.05	3.39	1.73	1.47
0.06	3.42	1.76	1.49
0.08	3.47	1.82	1.53
0.1	3.53	1.87	1.57
0.15	3.67	2.01	1.67
0.2	3.84	2.14	1.77
0.3	4.16	2.40	1.98
0.4	4.52	2.65	2.21
0.5	4.90	2.90	2.45
0.6	5.36	3.12	2.72
0.8	7.41	3.32	3.38
1.0	10.5	3.37	4.20
1.5	18.3	3.44	6.42
2.0	25.7	3.59	8.70
3.0	39.1	4.19	13.3
4.0	51.0	5.11	18.0
5.0	61.7	6.31	22.4
6.0	72.9	8.03	26.9
8.0	99.0	14.0	36.7
10.0	126	23.6	47.6
15.0	184	59.0	75.5
20.0	229	111	104
30.0	294	221	162
40.0	320	291	209
50.0	327	321	243
60.0	333	334	268
80.0	339	349	302
100	342	357	323
150	349	371	356
200	354	381	377
300	362	393	405
400	366	402	425
500	369	409	440
600	372	415	453
800	376	424	474
1000	379	430	491
1500	385	443	522
2000	389	451	545
3000	395	465	580
4000	399	473	605
5000	402	480	627
6000	404	486	645
8000	408	495	674
10,000	411	503	699

AP, antero-posterior; PA, postero-anterior; ISO, isotropic.

Table A.5. Neutrons: effective dose per fluence, in units of pSv cm^2, for mono-energetic particles incident in various geometries.

Energy (MeV)	AP	PA	LLAT	RLAT	ROT	ISO
1.0E−9	3.09	1.85	1.04	0.893	1.70	1.29
1.0E−8	3.55	2.11	1.15	0.978	2.03	1.56
2.5E−8	4.00	2.44	1.32	1.12	2.31	1.76
1.0E−7	5.20	3.25	1.70	1.42	2.98	2.26
2.0E−7	5.87	3.72	1.94	1.63	3.36	2.54
5.0E−7	6.59	4.33	2.21	1.86	3.86	2.92
1.0E−6	7.03	4.73	2.40	2.02	4.17	3.15
2.0E−6	7.39	5.02	2.52	2.11	4.40	3.32
5.0E−6	7.71	5.30	2.64	2.21	4.59	3.47
1.0E−5	7.82	5.44	2.65	2.24	4.68	3.52
2.0E−5	7.84	5.51	2.68	2.26	4.72	3.54
5.0E−5	7.82	5.55	2.66	2.24	4.73	3.55
1.0E−4	7.79	5.57	2.65	2.23	4.72	3.54
2.0E−4	7.73	5.59	2.66	2.24	4.67	3.52
5.0E−4	7.54	5.60	2.62	2.21	4.60	3.47
0.001	7.54	5.60	2.61	2.21	4.58	3.46
0.002	7.61	5.62	2.60	2.20	4.61	3.48
0.005	7.97	5.95	2.74	2.33	4.86	3.66
0.01	9.11	6.81	3.13	2.67	5.57	4.19
0.02	12.2	8.93	4.21	3.60	7.41	5.61
0.03	15.7	11.2	5.40	4.62	9.46	7.18
0.05	23.0	15.7	7.91	6.78	13.7	10.4
0.07	30.6	20.0	10.5	8.95	18.0	13.7
0.1	41.9	25.9	14.4	12.3	24.3	18.6
0.15	60.6	34.9	20.8	17.9	34.7	26.6
0.2	78.8	43.1	27.2	23.4	44.7	34.4
0.3	114	58.1	39.7	34.2	63.8	49.4
0.5	177	85.9	63.7	54.4	99.1	77.1
0.7	232	112	85.5	72.6	131	102
0.9	279	136	105	89.3	160	126
1.0	301	148	115	97.4	174	137
1.2	330	167	130	110	193	153
1.5	365	195	150	128	219	174
2.0	407	235	179	153	254	203
3.0	458	292	221	192	301	244
4.0	483	330	249	220	331	271
5.0	494	354	269	240	351	290
6.0	498	371	284	255	365	303
7.0	499	383	295	267	374	313
8.0	499	392	303	276	381	321
9.0	500	398	310	284	386	327
10.0	500	404	316	290	390	332
12.0	499	412	325	301	395	339
14.0	495	417	333	310	398	344
15.0	493	419	336	313	398	346
16.0	490	420	338	317	399	347
18.0	484	422	343	323	399	350
20.0	477	423	347	328	398	352
21.0	474	423	348	330	398	353
30.0	453	422	360	345	395	358
50.0	433	428	380	370	395	371
75.0	420	439	399	392	402	387
100	402	444	409	404	406	397
130	382	446	416	413	411	407
150	373	446	420	418	414	412
180	363	447	425	425	418	421
200	359	448	427	429	422	426
300	363	464	441	451	443	455
400	389	496	472	483	472	488
500	422	533	510	523	503	521
600	457	569	547	563	532	553

Table A.5. (*continued*)

Energy (MeV)	AP	PA	LLAT	RLAT	ROT	ISO
700	486	599	579	597	558	580
800	508	623	603	620	580	604
900	524	640	621	638	598	624
1000	537	654	635	651	614	642
2000	612	740	730	747	718	767
5000	716	924	963	979	906	1.01E+3
10,000	933	1.17E+3	1.23E+3	1.26E+3	1.14E+3	1.32E+3

AP, antero-posterior; PA, postero-anterior; LLAT, left lateral; RLAT, right lateral; ROT, rotational; ISO, isotropic.

Table A.6. Protons: effective dose per fluence, in units of pSv cm^2, for mono-energetic particles incident in various geometries.

Energy (MeV)	AP	PA	LLAT	RLAT	ROT	ISO
1.0	5.46	5.47	2.81	2.81	4.50	3.52
1.5	8.20	8.21	4.21	4.20	6.75	5.28
2.0	10.9	10.9	5.61	5.62	8.98	7.02
3.0	16.4	16.4	8.43	8.41	13.4	10.5
4.0	21.9	21.9	11.2	11.2	17.8	13.9
5.0	27.3	27.3	14.0	14.0	22.1	17.3
6.0	32.8	32.8	16.8	16.8	26.3	20.5
8.0	43.7	43.7	22.4	22.4	34.5	26.8
10.0	54.9	54.6	28.1	28.1	50.1	45.8
15.0	189	56.1	50.7	48.9	93.7	80.1
20.0	428	43.6	82.8	78.8	165	136
30.0	750	36.1	180	172	296	249
40.0	1.02E+3	45.5	290	278	422	358
50.0	1.18E+3	71.5	379	372	532	451
60.0	1.48E+3	156	500	447	687	551
80.0	2.16E+3	560	799	602	1.09E+3	837
100	2.51E+3	1.19E+3	994	818	1.44E+3	1.13E+3
150	2.38E+3	2.82E+3	1.64E+3	1.46E+3	2.16E+3	1.79E+3
200	1.77E+3	1.93E+3	2.15E+3	2.18E+3	1.96E+3	1.84E+3
300	1.38E+3	1.45E+3	1.44E+3	1.45E+3	1.44E+3	1.42E+3
400	1.23E+3	1.30E+3	1.27E+3	1.28E+3	1.28E+3	1.25E+3
500	1.15E+3	1.24E+3	1.21E+3	1.21E+3	1.22E+3	1.18E+3
600	1.16E+3	1.23E+3	1.20E+3	1.20E+3	1.22E+3	1.17E+3
800	1.11E+3	1.23E+3	1.19E+3	1.20E+3	1.20E+3	1.17E+3
1000	1.09E+3	1.23E+3	1.18E+3	1.20E+3	1.19E+3	1.15E+3
1500	1.15E+3	1.25E+3	1.21E+3	1.23E+3	1.23E+3	1.21E+3
2000	1.12E+3	1.28E+3	1.25E+3	1.25E+3	1.23E+3	1.22E+3
3000	1.23E+3	1.34E+3	1.32E+3	1.32E+3	1.30E+3	1.31E+3
4000	1.27E+3	1.40E+3	1.31E+3	1.33E+3	1.29E+3	1.40E+3
5000	1.23E+3	1.45E+3	1.39E+3	1.41E+3	1.35E+3	1.43E+3
6000	1.37E+3	1.53E+3	1.44E+3	1.45E+3	1.41E+3	1.57E+3
8000	1.45E+3	1.65E+3	1.56E+3	1.59E+3	1.49E+3	1.71E+3
10,000	1.41E+3	1.74E+3	1.63E+3	1.67E+3	1.56E+3	1.78E+3

AP, antero-posterior; PA, postero-anterior; LLAT, left lateral; RLAT, right lateral; ROT, rotational; ISO, isotropic.

Table A.7. Negative muons: effective dose per fluence, in units of pSv cm^2, for mono-energetic particles incident in various geometries.

Energy (MeV)	AP	PA	ISO
1.0	180	75.2	78.7
1.5	180	76.8	79.5
2.0	184	78.3	80.9
3.0	188	81.4	83.7
4.0	193	84.8	87.1
5.0	205	87.7	91.5
6.0	242	86.7	98.1
8.0	293	86.8	113
10.0	332	88.6	127
15.0	414	100	161
20.0	465	122	191
30.0	657	251	275
40.0	735	457	363
50.0	755	703	446
60.0	628	775	496
80.0	431	485	498
100	382	402	432
150	340	345	354
200	326	329	332
300	319	321	321
400	320	321	321
500	321	324	323
600	325	326	326
800	327	332	331
1000	333	337	337
1500	331	338	338
2000	333	341	341
3000	336	344	344
4000	337	345	346
5000	337	346	347
6000	337	346	347
8000	337	347	348
10,000	338	347	348

AP, antero-posterior; PA, postero-anterior; ISO, isotropic.

Table A.8. Positive muons: effective dose per fluence, in units of pSv cm^2, for mono-energetic particles incident in various geometries.

Energy (MeV)	AP	PA	ISO
1.0	194	82.6	85.2
1.5	196	84.1	86.2
2.0	198	85.7	87.5
3.0	202	88.9	90.3
4.0	207	92.1	93.6
5.0	216	94.3	97.7
6.0	251	92.5	103
8.0	300	92.8	117
10.0	340	94.8	132
15.0	425	108	167
20.0	481	133	199
30.0	674	265	284
40.0	751	473	373
50.0	768	721	456
60.0	635	787	506
80.0	431	483	502
100	381	399	432
150	339	345	354
200	326	328	332
300	318	320	320
400	319	321	320
500	320	323	322
600	322	325	324
800	325	330	329
1000	327	333	333
1500	331	339	338
2000	333	341	341
3000	336	344	344
4000	337	345	346
5000	337	346	347
6000	337	346	347
8000	337	347	348
10,000	339	347	348

AP, antero-posterior; PA, postero-anterior; ISO, isotropic.

Table A.9. Negative pions: effective dose per fluence, in units of pSv cm^2, for mono-energetic particles incident in various geometries.

Energy (MeV)	AP	PA	ISO
1.0	406	194	176
1.5	422	201	189
2.0	433	210	198
3.0	458	225	215
4.0	491	233	232
5.0	528	237	251
6.0	673	208	271
8.0	965	181	317
10.0	1.09E+3	178	361
15.0	1.25E+3	197	439
20.0	1.28E+3	244	508
30.0	1.77E+3	547	676
40.0	1.92E+3	1.02E+3	868
50.0	1.93E+3	1.70E+3	1.02E+3
60.0	1.68E+3	1.99E+3	1.15E+3
80.0	1.14E+3	1.31E+3	1.15E+3
100	995	991	1.03E+3
150	927	889	857
200	902	871	815
300	848	843	794
400	844	850	807
500	869	880	838
600	901	917	875
800	947	976	935
1000	977	1.02E+3	979
1500	1.03E+3	1.08E+3	1.05E+3
2000	1.05E+3	1.12E+3	1.09E+3
3000	1.03E+3	1.11E+3	1.11E+3
4000	1.03E+3	1.13E+3	1.15E+3
5000	1.06E+3	1.18E+3	1.20E+3
6000	1.09E+3	1.22E+3	1.26E+3
8000	1.14E+3	1.29E+3	1.36E+3
10,000	1.17E+3	1.34E+3	1.43E+3
15,000	1.21E+3	1.41E+3	1.55E+3
20,000	1.24E+3	1.47E+3	1.64E+3
30,000	1.30E+3	1.56E+3	1.79E+3
40,000	1.35E+3	1.63E+3	1.91E+3
50,000	1.39E+3	1.70E+3	2.02E+3
60,000	1.42E+3	1.75E+3	2.11E+3
80,000	1.48E+3	1.86E+3	2.29E+3
100,000	1.54E+3	1.95E+3	2.46E+3
150,000	1.67E+3	2.15E+3	2.80E+3
200,000	1.78E+3	2.33E+3	3.04E+3

AP, antero-posterior; PA, postero-anterior; ISO, isotropic.

Table A.10. Positive pions: effective dose per fluence, in units of pSv cm^2, for mono-energetic particles incident in various geometries.

Energy (MeV)	AP	PA	ISO
1.0	314	121	151
1.5	324	125	160
2.0	340	133	168
3.0	379	151	183
4.0	429	170	198
5.0	489	183	216
6.0	540	185	233
8.0	717	177	265
10.0	819	179	296
15.0	1000	201	367
20.0	1.10E+3	247	439
30.0	1.52E+3	494	602
40.0	1.75E+3	906	787
50.0	1.83E+3	1.48E+3	953
60.0	1.66E+3	1.82E+3	1.09E+3
80.0	1.22E+3	1.38E+3	1.16E+3
100	1.13E+3	1.12E+3	1.10E+3
150	1.22E+3	1.15E+3	1.05E+3
200	1.25E+3	1.23E+3	1.08E+3
300	1.07E+3	1.10E+3	1.02E+3
400	969	998	953
500	943	970	930
600	952	980	938
800	999	1.04E+3	993
1000	1.04E+3	1.09E+3	1.05E+3
1500	1.10E+3	1.16E+3	1.13E+3
2000	1.10E+3	1.19E+3	1.16E+3
3000	1.06E+3	1.16E+3	1.16E+3
4000	1.06E+3	1.16E+3	1.18E+3
5000	1.07E+3	1.20E+3	1.23E+3
6000	1.10E+3	1.24E+3	1.28E+3
8000	1.14E+3	1.31E+3	1.37E+3
10,000	1.17E+3	1.35E+3	1.43E+3
15,000	1.22E+3	1.42E+3	1.55E+3
20,000	1.25E+3	1.48E+3	1.64E+3
30,000	1.30E+3	1.57E+3	1.79E+3
40,000	1.34E+3	1.64E+3	1.90E+3
50,000	1.38E+3	1.70E+3	2.01E+3
60,000	1.42E+3	1.75E+3	2.10E+3
80,000	1.48E+3	1.84E+3	2.27E+3
100,000	1.54E+3	1.94E+3	2.42E+3
150,000	1.67E+3	2.14E+3	2.76E+3
200,000	1.78E+3	2.33E+3	3.07E+3

AP, antero-posterior; PA, postero-anterior; ISO, isotropic.

Table A.11. Helium ions: effective dose per fluence, in units of pGy cm^2, for mono-energetic particles incident in various geometries.

Energy (MeV/u)	AP	PA	ISO
1.0	219	219	141
2.0	438	438	281
3.0	656	657	419
5.0	1.09E+3	1.09E+3	689
10.0	2.19E+3	2.19E+3	1.82E+3
14.0	4.61E+3	2.56E+3	2.81E+3
20.0	1.72E+4	1.74E+3	5.46E+3
30.0	3.01E+4	1.44E+3	9.86E+3
50.0	4.75E+4	2.88E+3	1.78E+4
75.0	8.05E+4	1.75E+4	3.00E+4
100	1.01E+5	4.84E+4	4.55E+4
150	9.25E+4	1.10E+5	6.95E+4
200	6.74E+4	7.29E+4	7.01E+4
300	5.14E+4	5.33E+4	5.25E+4
500	4.27E+4	4.49E+4	4.27E+4
700	4.11E+4	4.60E+4	4.19E+4
1000	4.00E+4	4.47E+4	4.09E+4
2000	4.02E+4	4.80E+4	4.31E+4
3000	4.08E+4	5.01E+4	4.50E+4
5000	4.12E+4	5.17E+4	4.76E+4
10,000	4.56E+4	6.26E+4	5.73E+4
20,000	5.12E+4	6.10E+4	7.10E+4
50,000	6.12E+4	8.14E+4	9.67E+4
100,000	7.14E+4	1.01E+5	1.24E+5

AP, antero-posterior; PA, postero-anterior; ISO, isotropic.

A.1. References

ICRP, 2007. The 2007 Recommendations of the International Commission on Radiological Protection. ICRP Publication 103. Ann. ICRP 37(2–4).

Seltzer, S.M., 1993. Calculation of photon mass energy-transfer and mass energy-absorption coefficients. Radiat. Res. 136, 147–170.

ANNEX B. ORGAN ABSORBED DOSE CONVERSION COEFFICIENTS FOR PHOTONS

(B1) This annex lists reference values for organ absorbed dose conversion coefficients for photons and the specific irradiation geometries considered for the following organs: red (active) bone marrow, colon, lung, stomach, breast, ovaries, testes, urinary bladder wall (UB-wall), oesophagus, liver, thyroid, bone surface, brain, salivary glands, skin, and remainder tissues. Data are given separately for the male and female phantoms. Data for the lens of the eye can be found in Annex F. In the CD accompanying this report, these dose conversion coefficients are given in electronic form along with those for the individual remainder tissues, which include: adrenals, extrathoracic region, gall bladder, heart, kidneys, lymphatic nodes, muscle, oral mucosa, pancreas, prostate, small intestine, spleen, thymus, and uterus/cervix.

(B2) The specific irradiation geometries considered are broad parallel beams along the antero-posterior, postero-anterior, left and right lateral axes, and rotational and isotropic directions (see Section 3.2).

(B3) The organ absorbed doses are normalised to particle fluence, and are given in units of pGy cm^2. The following table entries are reference values and were derived from dose conversion coefficients calculated using the ICRP/ICRU reference phantoms and various Monte Carlo radiation transport codes (see Sections 3.1 and 3.3) following the application of averaging and smoothing techniques (see Annex I).

Table B.1. Photons, female: brain absorbed dose per fluence, in units of pGy cm^2, for mono-energetic particles incident in various geometries.

Energy (MeV)	AP	PA	LLAT	RLAT	ROT	ISO
0.01	–	–	–	2.8E−8	–	9.8E−7
0.015	4.8E−5	8.0E−5	9.0E−5	9.0E−5	1.2E−4	2.5E−4
0.02	0.0022	0.0043	0.0060	0.0061	0.0059	0.0063
0.03	0.0453	0.0710	0.0901	0.0919	0.0806	0.0714
0.04	0.108	0.148	0.180	0.183	0.162	0.143
0.05	0.152	0.191	0.226	0.231	0.207	0.183
0.06	0.185	0.219	0.257	0.261	0.235	0.209
0.07	0.199	0.243	0.288	0.291	0.262	0.236
0.08	0.229	0.268	0.311	0.315	0.287	0.257
0.1	0.284	0.329	0.376	0.381	0.347	0.311
0.15	0.444	0.506	0.574	0.580	0.538	0.481
0.2	0.628	0.702	0.796	0.803	0.745	0.671
0.3	1.01	1.12	1.25	1.26	1.18	1.07
0.4	1.41	1.54	1.71	1.72	1.62	1.48
0.5	1.81	1.95	2.16	2.16	2.06	1.88
0.511	1.85	2.00	2.20	2.21	2.10	1.93
0.6	2.19	2.36	2.58	2.59	2.47	2.28
0.662	2.42	2.60	2.84	2.85	2.72	2.51
0.8	2.92	3.12	3.38	3.39	3.25	3.01
1.0	3.62	3.84	4.13	4.13	3.98	3.71
1.117	4.01	4.23	4.54	4.55	4.38	4.10
1.33	4.69	4.92	5.24	5.25	5.07	4.78
1.5	5.21	5.44	5.79	5.81	5.61	5.29
2.0	6.58	6.82	7.21	7.23	7.01	6.64
3.0	8.98	9.26	9.66	9.68	9.43	8.99
4.0	11.1	11.5	11.9	11.9	11.6	11.1
5.0	13.1	13.5	13.9	13.9	13.6	13.1
6.0	15.0	15.5	15.8	15.8	15.6	15.0
6.129	15.3	15.7	16.1	16.1	15.8	15.3
8.0	18.7	19.0	19.5	19.4	19.2	18.6
10.0	22.2	22.4	22.9	22.8	22.6	21.9
15.0	30.4	30.1	30.4	30.1	30.0	29.6
20.0	37.8	36.7	36.6	36.4	36.5	36.5
30.0	50.2	47.4	45.9	45.7	46.4	47.6
40.0	59.7	55.6	52.6	52.1	53.9	55.6
50.0	67.2	61.8	57.7	57.0	59.6	62.1
60.0	73.1	66.8	61.6	60.7	64.0	67.4
80.0	82.2	74.5	67.5	66.4	70.8	75.6
100	88.6	79.7	71.8	70.6	75.5	82.1
150	99.8	88.3	78.9	77.6	83.0	94.0
200	107	93.7	83.7	82.3	88.0	102
300	116	101	89.6	88.1	94.3	113
400	120	105	93.0	91.4	98.3	120
500	124	108	95.2	93.5	101	126
600	127	111	96.9	95.2	103	130
800	131	115	99.4	97.6	106	136
1000	134	117	101	99.5	108	141
1500	140	121	104	103	110	150
2000	142	122	106	104	112	156
3000	145	125	107	106	114	166
4000	147	127	108	107	117	174
5000	148	128	109	107	118	180
6000	149	129	110	107	119	185
8000	151	131	111	108	121	192
10,000	152	132	112	109	122	198

AP, antero-posterior; PA, postero-anterior; LLAT, left lateral; RLAT, right lateral; ROT, rotational; ISO, isotropic.

Table B.2. Photons, female: breast absorbed dose per fluence, in units of pGy cm^2, for mono-energetic particles incident in various geometries.

Energy (MeV)	AP	PA	LLAT	RLAT	ROT	ISO
0.01	0.323	–	0.0617	0.0575	0.120	0.100
0.015	0.720	1.1E−5	0.175	0.167	0.282	0.233
0.02	0.751	4.7E−4	0.228	0.220	0.322	0.279
0.03	0.569	0.0187	0.222	0.216	0.272	0.246
0.04	0.457	0.0502	0.197	0.191	0.231	0.213
0.05	0.416	0.0753	0.188	0.183	0.221	0.201
0.06	0.416	0.0956	0.195	0.190	0.229	0.206
0.07	0.444	0.118	0.212	0.206	0.249	0.221
0.08	0.479	0.139	0.235	0.229	0.276	0.247
0.1	0.577	0.186	0.294	0.288	0.343	0.305
0.15	0.878	0.328	0.477	0.470	0.546	0.490
0.2	1.19	0.489	0.683	0.674	0.769	0.686
0.3	1.81	0.849	1.11	1.10	1.22	1.10
0.4	2.38	1.23	1.55	1.53	1.67	1.51
0.5	2.91	1.62	1.97	1.96	2.10	1.92
0.511	2.98	1.66	2.02	2.01	2.15	1.96
0.6	3.42	2.00	2.39	2.38	2.52	2.30
0.6627	3.72	2.23	2.64	2.63	2.77	2.53
0.8	4.35	2.74	3.16	3.16	3.31	3.03
1.0	5.17	3.44	3.91	3.90	4.04	3.73
1.117	5.59	3.83	4.31	4.31	4.43	4.11
1.33	6.30	4.50	5.02	5.00	5.10	4.74
1.5	6.79	5.02	5.53	5.51	5.61	5.21
2.0	7.96	6.40	6.85	6.85	6.89	6.43
3.0	9.43	8.75	8.95	8.97	8.91	8.37
4.0	10.2	10.8	10.7	10.7	10.5	9.92
5.0	10.7	12.7	12.2	12.3	11.8	11.3
6.0	10.9	14.5	13.5	13.6	12.9	12.4
6.129	10.9	14.7	13.7	13.8	13.1	12.6
8.0	10.9	17.8	15.8	15.9	14.9	14.5
10.0	10.7	21.0	17.8	18.0	16.7	16.3
15.0	10.6	29.4	22.4	22.7	20.9	20.6
20.0	10.7	38.2	26.7	27.0	24.9	24.7
30.0	10.9	54.7	34.4	34.8	32.5	32.4
40.0	11.3	68.3	41.4	41.9	39.9	39.7
50.0	11.7	79.0	47.4	48.1	46.4	46.4
60.0	12.0	87.1	52.2	53.2	51.8	52.2
80.0	12.4	98.9	60.2	61.2	60.5	61.6
100	12.7	107	65.8	66.9	66.7	69.0
150	13.4	119	75.5	76.8	76.4	81.9
200	14.2	127	82.2	83.4	82.9	91.0
300	15.2	137	90.7	91.9	91.2	104
400	15.8	143	95.7	97.3	96.4	113
500	16.1	147	99.0	101	99.9	119
600	16.2	151	101	103	103	124
800	16.2	156	105	107	107	132
1000	16.3	159	107	109	109	138
1500	16.5	164	112	114	114	149
2000	16.6	167	114	116	118	157
3000	16.7	171	117	119	122	168
4000	16.8	174	119	121	125	175
5000	16.9	176	121	123	127	183
6000	16.9	178	122	124	129	188
8000	17.1	179	125	127	131	197
10,000	17.1	180	127	128	133	203

AP, antero-posterior; PA, postero-anterior; LLAT, left lateral; RLAT, right lateral; ROT, rotational; ISO, isotropic.

Table B.3. Photons, female: colon absorbed dose per fluence, in units of pGy cm^2, for mono-energetic particles incident in various geometries.

Energy (MeV)	AP	PA	LLAT	RLAT	ROT	ISO
0.01	3.3E−4	–	9.9E−8	2.0E−7	5.1E−5	2.0E−5
0.015	0.0407	9.8E−4	0.0012	0.0010	0.0092	0.0057
0.02	0.178	0.0115	0.0177	0.0180	0.0542	0.0352
0.03	0.369	0.0757	0.0800	0.0832	0.153	0.111
0.04	0.412	0.139	0.120	0.123	0.203	0.152
0.05	0.423	0.183	0.144	0.144	0.228	0.173
0.06	0.441	0.215	0.163	0.161	0.249	0.192
0.07	0.468	0.242	0.180	0.178	0.272	0.209
0.08	0.496	0.274	0.198	0.195	0.295	0.229
0.1	0.575	0.332	0.242	0.236	0.349	0.275
0.15	0.818	0.502	0.372	0.365	0.524	0.407
0.2	1.09	0.689	0.524	0.515	0.715	0.559
0.3	1.63	1.09	0.849	0.838	1.11	0.888
0.4	2.14	1.48	1.19	1.17	1.50	1.23
0.5	2.63	1.88	1.53	1.51	1.89	1.56
0.511	2.68	1.93	1.57	1.55	1.93	1.59
0.6	3.08	2.26	1.87	1.84	2.27	1.89
0.662	3.35	2.50	2.08	2.05	2.50	2.09
0.8	3.92	2.99	2.53	2.50	3.00	2.53
1.0	4.70	3.68	3.16	3.12	3.68	3.13
1.117	5.11	4.06	3.52	3.47	4.05	3.48
1.33	5.82	4.71	4.14	4.10	4.68	4.06
1.5	6.37	5.20	4.62	4.57	5.17	4.51
2.0	7.80	6.54	5.91	5.88	6.52	5.79
3.0	10.3	8.94	8.19	8.17	8.88	8.07
4.0	12.4	11.0	10.2	10.2	11.0	10.1
5.0	14.4	12.9	12.1	12.0	12.9	12.0
6.0	16.4	14.7	13.9	13.9	14.8	13.7
6.129	16.6	14.9	14.1	14.1	15.0	13.9
8.0	19.8	18.2	17.4	17.3	18.2	17.0
10.0	22.7	21.7	20.8	20.7	21.4	20.2
15.0	27.6	30.6	28.7	28.5	28.5	27.6
20.0	31.4	39.0	36.4	35.9	35.6	34.8
30.0	36.5	53.6	50.1	49.5	47.3	47.5
40.0	40.3	65.6	62.4	62.0	57.4	58.8
50.0	43.2	75.2	73.3	73.1	66.0	68.5
60.0	45.3	82.5	82.6	82.6	73.0	77.0
80.0	48.7	93.8	97.7	97.7	84.2	90.9
100	51.1	101	109	109	92.2	102
150	55.2	113	127	128	104	123
200	58.4	120	139	140	112	137
300	62.3	130	154	156	123	157
400	65.0	136	164	166	130	169
500	66.6	140	171	173	135	179
600	67.6	143	176	179	139	187
800	68.8	148	184	187	145	199
1000	69.8	151	189	192	148	207
1500	71.3	157	199	202	154	222
2000	72.5	161	204	209	159	232
3000	73.9	164	212	216	165	248
4000	74.6	167	217	221	168	259
5000	75.2	168	220	225	171	268
6000	75.6	169	223	228	173	275
8000	76.2	171	228	233	175	286
10,000	76.6	173	233	237	177	294

AP, antero-posterior; PA, postero-anterior; LLAT, left lateral; RLAT, right lateral; ROT, rotational; ISO, isotropic.

Table B.4. Photons, female: bone surface (endosteum) absorbed dose per fluence, in units of pGy cm^2, for mono-energetic particles incident in various geometries.

Energy (MeV)	AP	PA	LLAT	RLAT	ROT	ISO
0.01	2.0E−4	6.1E−5	1.2E−4	1.1E−4	2.0E−4	0.0012
0.015	0.0107	0.0067	0.0072	0.0070	0.0102	0.0156
0.02	0.0717	0.0566	0.0495	0.0506	0.0617	0.0601
0.03	0.277	0.243	0.179	0.182	0.233	0.192
0.04	0.392	0.363	0.251	0.254	0.335	0.274
0.05	0.434	0.412	0.279	0.282	0.374	0.307
0.06	0.451	0.432	0.290	0.293	0.391	0.322
0.07	0.464	0.447	0.298	0.300	0.401	0.332
0.08	0.479	0.463	0.308	0.310	0.415	0.342
0.1	0.524	0.509	0.338	0.340	0.455	0.375
0.15	0.699	0.682	0.459	0.461	0.612	0.507
0.2	0.914	0.894	0.612	0.615	0.805	0.671
0.3	1.36	1.35	0.952	0.956	1.22	1.04
0.4	1.83	1.80	1.30	1.31	1.65	1.41
0.5	2.27	2.24	1.66	1.66	2.07	1.78
0.511	2.31	2.29	1.70	1.70	2.11	1.82
0.6	2.69	2.67	2.00	2.00	2.47	2.15
0.662	2.96	2.92	2.22	2.22	2.71	2.36
0.8	3.50	3.47	2.67	2.67	3.22	2.84
1.0	4.24	4.20	3.31	3.31	3.93	3.50
1.117	4.64	4.60	3.67	3.67	4.32	3.86
1.33	5.33	5.30	4.30	4.30	5.01	4.51
1.5	5.85	5.82	4.77	4.78	5.52	4.99
2.0	7.30	7.24	6.07	6.08	6.91	6.32
3.0	9.74	9.71	8.37	8.37	9.35	8.66
4.0	11.9	11.9	10.4	10.4	11.5	10.7
5.0	13.9	13.8	12.3	12.3	13.5	12.6
6.0	15.7	15.7	14.1	14.1	15.3	14.4
6.129	16.0	15.9	14.3	14.3	15.5	14.6
8.0	19.1	19.2	17.3	17.3	18.7	17.8
10.0	22.2	22.5	20.3	20.3	21.8	20.9
15.0	28.7	29.5	27.1	27.2	28.7	28.0
20.0	34.0	35.3	33.5	33.4	34.4	34.3
30.0	41.9	43.8	44.6	44.4	43.6	45.0
40.0	47.8	50.0	54.4	54.1	51.0	53.8
50.0	52.2	54.6	62.9	62.5	57.2	61.1
60.0	55.6	58.3	70.1	69.8	62.1	67.3
80.0	60.9	64.0	82.1	81.8	69.9	77.3
100	64.7	67.9	91.3	91.1	75.3	85.2
150	71.1	74.4	108	107	84.4	99.8
200	75.6	78.5	119	119	90.3	110
300	81.2	83.5	133	133	97.9	124
400	84.5	86.7	143	143	103	133
500	86.7	88.9	150	149	106	139
600	88.2	90.5	155	155	109	145
800	90.4	93.0	162	162	113	153
1000	91.9	94.5	168	168	115	159
1500	94.5	97.1	178	178	120	171
2000	95.9	98.6	184	184	122	178
3000	97.7	100	193	193	126	189
4000	98.8	102	200	199	129	197
5000	99.7	102	204	204	131	204
6000	100	103	208	208	132	210
8000	101	104	213	214	134	219
10,000	102	104	217	218	135	227

AP, antero-posterior; PA, postero-anterior; LLAT, left lateral; RLAT, right lateral; ROT, rotational; ISO, isotropic.

Table B.5. Photons, female: liver absorbed dose per fluence, in units of pGy cm^2, for mono-energetic particles incident in various geometries.

Energy (MeV)	AP	PA	LLAT	RLAT	ROT	ISO
0.01	2.9E−5	1.1E−6	2.4E−7	8.4E−6	1.3E−5	6.6E−6
0.015	0.0131	0.0022	3.9E−4	0.0068	0.0055	0.0031
0.02	0.0859	0.0235	0.0046	0.0488	0.0388	0.0248
0.03	0.257	0.110	0.0308	0.164	0.138	0.0984
0.04	0.335	0.182	0.0614	0.227	0.201	0.149
0.05	0.367	0.230	0.0839	0.255	0.235	0.177
0.06	0.391	0.264	0.102	0.275	0.259	0.198
0.07	0.420	0.295	0.117	0.297	0.283	0.217
0.08	0.445	0.325	0.132	0.318	0.309	0.236
0.1	0.516	0.389	0.165	0.375	0.367	0.283
0.15	0.736	0.575	0.264	0.554	0.538	0.420
0.2	0.977	0.779	0.379	0.759	0.730	0.573
0.3	1.47	1.20	0.641	1.19	1.14	0.905
0.4	1.95	1.63	0.924	1.62	1.54	1.25
0.5	2.41	2.04	1.22	2.05	1.93	1.59
0.511	2.46	2.08	1.25	2.09	1.97	1.62
0.6	2.85	2.44	1.52	2.46	2.32	1.92
0.662	3.11	2.68	1.71	2.70	2.55	2.12
0.8	3.67	3.19	2.11	3.22	3.04	2.56
1.0	4.42	3.89	2.69	3.95	3.73	3.17
1.117	4.82	4.27	3.01	4.35	4.11	3.52
1.33	5.52	4.93	3.60	5.05	4.77	4.12
1.5	6.04	5.43	4.05	5.58	5.26	4.58
2.0	7.44	6.80	5.29	6.97	6.59	5.84
3.0	9.89	9.18	7.49	9.39	8.95	8.07
4.0	12.1	11.3	9.49	11.5	11.1	10.1
5.0	14.1	13.2	11.3	13.5	13.1	12.0
6.0	16.0	15.1	13.1	15.4	14.9	13.8
6.129	16.2	15.4	13.3	15.7	15.2	14.0
8.0	19.6	18.8	16.5	19.1	18.4	17.2
10.0	22.9	22.2	19.9	22.5	21.8	20.6
15.0	29.8	30.4	28.2	30.3	29.6	28.4
20.0	35.2	38.3	36.5	37.1	36.7	35.6
30.0	43.0	51.0	52.6	48.4	48.7	48.6
40.0	48.7	61.2	68.0	57.2	58.8	60.1
50.0	52.8	69.4	82.0	64.2	67.1	70.0
60.0	55.9	75.6	94.1	69.6	73.8	78.3
80.0	60.5	85.3	114	77.9	84.5	92.0
100	63.9	91.7	129	83.6	92.0	103
150	69.6	102	153	93.4	105	122
200	74.0	108	170	100.0	113	135
300	79.6	117	190	108	123	153
400	83.1	122	204	113	129	165
500	85.1	125	213	116	134	174
600	86.7	128	221	118	137	181
800	88.1	133	231	121	142	191
1000	89.4	136	239	124	147	199
1500	91.6	140	252	128	153	213
2000	93.6	142	261	130	157	224
3000	95.6	144	273	133	162	237
4000	96.7	147	282	135	165	246
5000	97.3	149	288	137	167	254
6000	97.7	150	293	138	168	260
8000	98.1	152	300	140	171	271
10,000	98.3	154	305	142	173	279

AP, antero-posterior; PA, postero-anterior; LLAT, left lateral; RLAT, right lateral; ROT, rotational; ISO, isotropic.

Table B.6. Photons, female: lung absorbed dose per fluence, in units of pGy cm^2, for mono-energetic particles incident in various geometries.

Energy (MeV)	AP	PA	LLAT	RLAT	ROT	ISO
0.01	2.4E−5	4.9E−6	4.4E−6	3.5E−6	6.7E−6	7.7E−6
0.015	0.0065	0.0069	0.0030	0.0030	0.0045	0.0026
0.02	0.0593	0.0568	0.0172	0.0201	0.0376	0.0248
0.03	0.219	0.208	0.0554	0.0657	0.142	0.106
0.04	0.291	0.291	0.0884	0.0972	0.205	0.158
0.05	0.319	0.331	0.111	0.117	0.236	0.185
0.06	0.340	0.360	0.127	0.133	0.259	0.206
0.07	0.363	0.387	0.144	0.150	0.281	0.226
0.08	0.390	0.423	0.159	0.164	0.307	0.247
0.1	0.457	0.500	0.195	0.200	0.365	0.296
0.15	0.665	0.734	0.304	0.311	0.542	0.445
0.2	0.897	0.993	0.433	0.440	0.744	0.614
0.3	1.37	1.51	0.722	0.730	1.17	0.979
0.4	1.84	2.01	1.03	1.03	1.59	1.35
0.5	2.29	2.50	1.34	1.34	2.00	1.71
0.511	2.34	2.55	1.38	1.38	2.05	1.75
0.6	2.72	2.95	1.66	1.65	2.40	2.06
0.662	2.98	3.23	1.85	1.84	2.64	2.28
0.8	3.53	3.80	2.28	2.26	3.16	2.75
1.0	4.27	4.56	2.88	2.86	3.87	3.41
1.117	4.68	4.98	3.23	3.20	4.26	3.78
1.33	5.39	5.71	3.84	3.80	4.95	4.41
1.5	5.92	6.26	4.32	4.26	5.45	4.90
2.0	7.36	7.70	5.61	5.52	6.84	6.22
3.0	9.85	10.2	7.88	7.80	9.31	8.55
4.0	12.1	12.4	9.95	9.90	11.5	10.7
5.0	14.2	14.5	11.9	11.8	13.6	12.6
6.0	16.2	16.6	13.8	13.6	15.5	14.5
6.129	16.5	16.8	14.0	13.9	15.8	14.8
8.0	20.1	20.5	17.4	17.3	19.3	18.2
10.0	23.7	24.2	20.9	20.8	23.0	21.8
15.0	31.4	31.3	29.5	29.2	31.2	30.0
20.0	37.6	36.6	38.0	37.5	38.3	37.6
30.0	46.2	43.4	54.2	53.1	49.9	50.5
40.0	52.1	48.1	68.9	67.3	59.1	60.8
50.0	56.4	51.5	81.4	79.5	66.5	69.3
60.0	59.7	54.3	91.9	89.9	72.5	76.4
80.0	64.9	58.6	108	107	81.9	87.8
100	68.5	61.4	120	119	88.6	96.4
150	74.9	65.9	140	140	99.1	112
200	79.4	69.0	154	154	106	123
300	85.0	73.0	171	172	114	138
400	88.3	75.3	181	183	119	147
500	90.3	76.9	188	191	123	155
600	91.6	78.1	193	197	126	160
800	93.5	79.8	201	206	130	169
1000	94.9	80.9	208	212	133	175
1500	97.0	82.6	218	223	137	187
2000	98.6	83.4	224	230	140	194
3000	100	84.6	232	239	143	206
4000	101	85.5	237	246	146	214
5000	102	86.1	241	251	147	220
6000	103	86.6	245	255	149	225
8000	104	86.7	250	261	151	233
10,000	104	86.8	253	265	152	240

AP, antero-posterior; PA, postero-anterior; LLAT, left lateral; RLAT, right lateral; ROT, rotational; ISO, isotropic.

Table B.7. Photons, female: oesophagus absorbed dose per fluence, in units of pGy cm^2, for mono-energetic particles incident in various geometries.

Energy (MeV)	AP	PA	LLAT	RLAT	ROT	ISO
0.01	–	–	–	–	–	–
0.015	0.0010	–	2.5E−5	1.5E−5	1.5E−4	8.3E−5
0.02	0.0353	7.5E−4	0.0030	0.0031	0.0090	0.0051
0.03	0.215	0.0380	0.0582	0.0537	0.0871	0.0573
0.04	0.318	0.106	0.122	0.112	0.159	0.113
0.05	0.366	0.162	0.159	0.148	0.205	0.146
0.06	0.397	0.205	0.185	0.173	0.238	0.170
0.07	0.432	0.245	0.209	0.196	0.262	0.190
0.08	0.460	0.277	0.231	0.217	0.292	0.213
0.1	0.540	0.349	0.281	0.265	0.346	0.256
0.15	0.769	0.535	0.431	0.410	0.530	0.392
0.2	1.02	0.728	0.599	0.578	0.729	0.535
0.3	1.52	1.14	0.971	0.939	1.11	0.851
0.4	2.00	1.55	1.36	1.31	1.50	1.17
0.5	2.47	1.95	1.74	1.68	1.89	1.50
0.511	2.52	1.99	1.79	1.72	1.95	1.53
0.6	2.90	2.33	2.12	2.06	2.29	1.82
0.662	3.16	2.56	2.35	2.28	2.51	2.03
0.8	3.71	3.10	2.84	2.77	3.03	2.46
1.0	4.46	3.81	3.52	3.46	3.73	3.04
1.117	4.88	4.21	3.88	3.83	4.11	3.37
1.33	5.57	4.87	4.51	4.49	4.78	3.91
1.5	6.10	5.38	4.98	4.99	5.27	4.35
2.0	7.53	6.70	6.33	6.33	6.56	5.55
3.0	10.1	8.95	8.73	8.61	8.81	7.73
4.0	12.3	11.1	10.8	10.7	10.9	9.75
5.0	14.2	13.0	12.8	12.5	12.9	11.6
6.0	16.1	14.8	14.7	14.4	14.8	13.4
6.129	16.4	15.1	14.9	14.6	15.0	13.6
8.0	19.9	18.5	18.4	18.1	18.4	16.8
10.0	23.6	22.0	22.0	21.7	21.8	20.1
15.0	31.8	30.9	30.9	30.5	29.9	28.3
20.0	38.4	40.2	39.6	39.6	38.1	36.4
30.0	45.9	56.2	54.8	54.9	52.4	51.3
40.0	51.0	69.2	67.1	67.8	63.4	63.8
50.0	54.5	79.3	77.0	78.4	72.3	74.5
60.0	57.1	86.5	84.7	86.7	79.5	83.4
80.0	61.3	96.9	96.4	99.6	90.0	98.3
100	64.3	102	104	109	98.0	110
150	69.3	113	118	123	112	131
200	73.7	123	126	132	120	147
300	78.9	132	138	144	129	167
400	82.0	137	146	152	135	180
500	83.8	140	151	157	139	189
600	84.9	142	154	162	142	196
800	86.0	146	158	167	147	207
1000	87.4	150	162	171	150	217
1500	88.6	155	167	176	158	233
2000	90.0	159	171	180	163	244
3000	91.9	165	174	186	170	260
4000	92.6	168	178	190	171	269
5000	93.8	169	181	192	171	275
6000	94.3	170	182	193	172	281
8000	94.9	170	184	196	173	293
10,000	95.1	170	186	198	173	301

AP, antero-posterior; PA, postero-anterior; LLAT, left lateral; RLAT, right lateral; ROT, rotational; ISO, isotropic.

Table B.8. Photons, female: ovaries absorbed dose per fluence, in units of pGy cm^2, for mono-energetic particles incident in various geometries.

Energy (MeV)	AP	PA	LLAT	RLAT	ROT	ISO
0.01	–	–	–	–	–	–
0.015	6.4E−6	1.1E−4	–	–	–	7.8E−5
0.02	0.0034	0.0126	2.9E−5	5.8E−5	0.0037	0.0018
0.03	0.0843	0.145	0.0042	0.0055	0.0535	0.0366
0.04	0.180	0.241	0.0242	0.0300	0.121	0.0857
0.05	0.247	0.311	0.0493	0.0586	0.161	0.128
0.06	0.295	0.359	0.0717	0.0832	0.199	0.154
0.07	0.331	0.392	0.0828	0.106	0.246	0.183
0.08	0.370	0.425	0.105	0.125	0.267	0.204
0.1	0.439	0.490	0.142	0.159	0.322	0.246
0.15	0.652	0.700	0.230	0.254	0.468	0.366
0.2	0.892	0.942	0.333	0.368	0.634	0.502
0.3	1.36	1.40	0.564	0.611	1.000	0.807
0.4	1.79	1.85	0.807	0.883	1.37	1.13
0.5	2.21	2.30	1.06	1.17	1.73	1.45
0.511	2.27	2.34	1.10	1.20	1.77	1.48
0.6	2.62	2.71	1.35	1.46	2.09	1.77
0.662	2.87	2.97	1.54	1.64	2.32	1.96
0.8	3.42	3.55	1.93	2.03	2.80	2.41
1.0	4.18	4.32	2.49	2.63	3.45	3.02
1.117	4.60	4.75	2.79	2.97	3.82	3.35
1.33	5.31	5.41	3.36	3.54	4.46	3.93
1.5	5.89	5.94	3.77	3.95	4.95	4.38
2.0	7.23	7.28	4.95	5.17	6.22	5.58
3.0	9.52	9.66	7.10	7.36	8.56	7.72
4.0	11.5	11.8	9.09	9.34	10.7	9.72
5.0	13.4	13.8	10.9	11.2	12.6	11.6
6.0	15.2	15.9	12.7	13.0	14.5	13.4
6.129	15.4	16.1	13.0	13.2	14.7	13.7
8.0	18.8	19.7	16.0	16.4	18.0	17.0
10.0	22.5	23.5	19.3	19.7	21.5	20.5
15.0	31.8	32.4	27.9	28.0	29.8	28.8
20.0	39.8	40.6	36.8	36.5	38.5	37.4
30.0	53.9	50.9	54.2	54.7	54.3	52.7
40.0	63.4	57.5	71.7	72.4	66.7	66.5
50.0	70.4	63.0	88.1	87.4	76.7	78.5
60.0	75.4	67.0	102	100	85.6	89.0
80.0	82.0	74.1	127	121	98.4	104
100	87.2	79.4	144	136	109	117
150	94.9	87.1	171	163	127	139
200	100	91.4	189	182	137	153
300	108	96.3	212	205	150	174
400	112	98.8	229	217	158	191
500	115	100	241	228	163	201
600	118	102	250	235	166	207
800	120	104	264	245	173	221
1000	122	105	272	254	178	230
1500	124	108	290	268	185	246
2000	124	110	300	277	190	258
3000	124	112	310	289	198	272
4000	125	113	316	298	203	283
5000	127	114	322	305	206	292
6000	128	114	328	310	209	299
8000	129	114	335	320	213	310
10,000	131	114	341	326	216	320

AP, antero-posterior; PA, postero-anterior; LLAT, left lateral; RLAT, right lateral; ROT, rotational; ISO, isotropic.

Table B.9. Photons, female: red (active) bone marrow absorbed dose per fluence, in units of pGy cm^2, for mono-energetic particles incident in various geometries.

Energy (MeV)	AP	PA	LLAT	RLAT	ROT	ISO
0.01	3.5E−4	2.8E−5	2.0E−4	1.5E−4	2.2E−4	6.9E−4
0.015	0.0169	0.0080	0.0092	0.0082	0.0106	0.0114
0.02	0.0669	0.0542	0.0344	0.0342	0.0469	0.0414
0.03	0.202	0.211	0.0972	0.100	0.156	0.125
0.04	0.305	0.333	0.148	0.154	0.243	0.191
0.05	0.362	0.398	0.180	0.187	0.295	0.231
0.06	0.395	0.437	0.200	0.207	0.326	0.257
0.07	0.423	0.465	0.217	0.224	0.350	0.278
0.08	0.447	0.492	0.232	0.239	0.371	0.294
0.1	0.502	0.552	0.265	0.272	0.419	0.333
0.15	0.678	0.743	0.372	0.381	0.574	0.460
0.2	0.882	0.963	0.501	0.512	0.754	0.609
0.3	1.32	1.43	0.792	0.807	1.14	0.936
0.4	1.75	1.88	1.10	1.12	1.54	1.28
0.5	2.17	2.32	1.41	1.43	1.93	1.61
0.511	2.22	2.37	1.45	1.47	1.97	1.65
0.6	2.58	2.75	1.72	1.74	2.31	1.95
0.662	2.83	3.01	1.92	1.94	2.54	2.15
0.8	3.35	3.55	2.34	2.36	3.03	2.59
1.0	4.07	4.28	2.93	2.96	3.70	3.21
1.117	4.47	4.68	3.27	3.30	4.08	3.56
1.33	5.14	5.37	3.87	3.89	4.74	4.17
1.5	5.65	5.89	4.32	4.36	5.23	4.63
2.0	7.02	7.29	5.57	5.61	6.58	5.90
3.0	9.44	9.73	7.80	7.84	8.97	8.17
4.0	11.6	11.9	9.81	9.85	11.1	10.2
5.0	13.6	13.9	11.7	11.7	13.1	12.1
6.0	15.4	15.8	13.5	13.5	14.9	13.9
6.129	15.6	16.1	13.7	13.8	15.1	14.1
8.0	18.9	19.5	16.9	16.9	18.4	17.3
10.0	22.2	22.9	20.1	20.1	21.8	20.6
15.0	30.0	30.4	28.0	27.9	29.8	28.5
20.0	37.1	36.8	35.6	35.7	37.0	35.9
30.0	48.4	46.3	50.1	49.9	49.1	49.1
40.0	56.8	53.1	63.3	62.9	59.0	60.3
50.0	63.1	58.2	74.8	74.3	67.3	69.8
60.0	67.9	62.1	84.6	83.9	73.8	77.9
80.0	75.1	68.2	101	99.8	84.1	91.0
100	80.3	72.4	113	112	91.4	101
150	89.1	79.2	134	132	103	120
200	95.0	83.5	148	146	111	133
300	102	89.0	166	164	121	150
400	107	92.6	177	175	127	161
500	110	95.1	185	183	132	170
600	112	96.9	192	189	135	176
800	115	99.5	201	198	140	187
1000	117	101	208	205	143	194
1500	120	104	220	217	149	208
2000	122	105	227	224	152	218
3000	125	107	238	234	158	231
4000	127	108	245	241	161	240
5000	128	109	250	247	163	248
6000	128	110	254	251	165	254
8000	130	111	261	258	168	264
10,000	131	111	267	263	169	271

AP, antero-posterior; PA, postero-anterior; LLAT, left lateral; RLAT, right lateral; ROT, rotational; ISO, isotropic.

Table B.10. Photons, female: remainder tissues absorbed dose per fluence, in units of pGy cm^2, for mono-energetic particles incident in various geometries.

Energy (MeV)	AP	PA	LLAT	RLAT	ROT	ISO
0.01	0.0023	8.0E−4	0.0011	0.0012	0.0014	0.0017
0.015	0.0370	0.0113	0.0131	0.0119	0.0177	0.0135
0.02	0.0967	0.0348	0.0360	0.0271	0.0467	0.0346
0.03	0.209	0.113	0.0974	0.0673	0.119	0.0898
0.04	0.271	0.179	0.142	0.104	0.174	0.134
0.05	0.304	0.224	0.171	0.128	0.210	0.164
0.06	0.332	0.257	0.193	0.148	0.234	0.186
0.07	0.365	0.287	0.215	0.169	0.260	0.207
0.08	0.391	0.318	0.239	0.189	0.286	0.230
0.1	0.464	0.387	0.292	0.232	0.347	0.280
0.15	0.679	0.581	0.447	0.366	0.522	0.424
0.2	0.915	0.792	0.623	0.519	0.717	0.586
0.3	1.40	1.23	1.000	0.848	1.13	0.930
0.4	1.86	1.66	1.38	1.19	1.54	1.28
0.5	2.31	2.08	1.76	1.53	1.93	1.63
0.511	2.36	2.13	1.80	1.56	1.98	1.67
0.6	2.73	2.49	2.13	1.86	2.32	1.97
0.662	2.98	2.73	2.35	2.07	2.56	2.18
0.8	3.53	3.26	2.84	2.52	3.07	2.63
1.0	4.27	3.97	3.51	3.16	3.77	3.27
1.117	4.67	4.36	3.87	3.51	4.16	3.62
1.33	5.37	5.04	4.52	4.13	4.83	4.25
1.5	5.90	5.56	5.02	4.61	5.33	4.71
2.0	7.30	6.95	6.36	5.90	6.69	6.01
3.0	9.70	9.33	8.70	8.19	9.05	8.31
4.0	11.8	11.5	10.8	10.2	11.1	10.3
5.0	13.8	13.4	12.7	12.1	13.1	12.2
6.0	15.6	15.2	14.6	13.9	14.9	14.0
6.129	15.8	15.5	14.8	14.1	15.2	14.2
8.0	19.0	18.8	18.1	17.3	18.5	17.3
10.0	22.2	22.2	21.5	20.6	21.9	20.6
15.0	29.3	30.5	29.4	28.7	29.8	28.4
20.0	35.4	38.6	36.8	36.4	37.1	36.1
30.0	44.5	51.3	49.6	50.6	49.4	49.5
40.0	51.0	60.8	60.7	63.3	59.4	60.6
50.0	55.9	68.1	69.8	74.3	67.7	70.0
60.0	59.6	73.5	77.4	83.7	74.3	77.9
80.0	65.3	82.0	89.2	98.6	84.4	90.9
100	69.5	87.6	97.7	110	91.5	101
150	76.5	96.9	112	128	103	119
200	81.5	103	121	141	111	131
300	88.0	110	134	157	120	147
400	92.2	115	141	167	126	158
500	94.7	118	146	175	130	165
600	96.6	120	150	180	134	172
800	98.8	124	156	188	138	181
1000	101	127	160	194	141	188
1500	104	131	167	204	146	201
2000	106	133	171	211	150	210
3000	109	136	177	219	155	223
4000	111	138	180	225	158	232
5000	112	139	183	230	160	239
6000	113	139	185	233	161	245
8000	114	140	188	238	163	254
10,000	114	141	191	242	165	261

AP, antero-posterior; PA, postero-anterior; LLAT, left lateral; RLAT, right lateral; ROT, rotational; ISO, isotropic.

Table B.11. Photons, female: salivary glands absorbed dose per fluence, in units of pGy cm^2, for mono-energetic particles incident in various geometries.

Energy (MeV)	AP	PA	LLAT	RLAT	ROT	ISO
0.01	7.9E−5	5.3E−4	0.0302	0.0224	0.0121	0.0075
0.015	0.0094	0.0255	0.220	0.202	0.120	0.0787
0.02	0.0583	0.101	0.330	0.326	0.214	0.154
0.03	0.161	0.207	0.324	0.329	0.260	0.192
0.04	0.209	0.234	0.293	0.296	0.256	0.190
0.05	0.228	0.241	0.282	0.287	0.260	0.194
0.06	0.249	0.261	0.290	0.291	0.274	0.206
0.07	0.275	0.284	0.307	0.305	0.297	0.219
0.08	0.305	0.308	0.336	0.338	0.325	0.248
0.1	0.372	0.387	0.408	0.407	0.396	0.299
0.15	0.578	0.612	0.632	0.628	0.614	0.475
0.2	0.814	0.858	0.878	0.871	0.851	0.672
0.3	1.30	1.37	1.36	1.37	1.32	1.07
0.4	1.77	1.87	1.86	1.85	1.81	1.47
0.5	2.24	2.34	2.33	2.32	2.28	1.86
0.511	2.29	2.39	2.38	2.37	2.33	1.90
0.6	2.69	2.78	2.76	2.77	2.73	2.23
0.662	2.95	3.05	3.03	3.02	3.01	2.45
0.8	3.52	3.62	3.60	3.59	3.58	2.95
1.0	4.28	4.44	4.39	4.34	4.33	3.62
1.117	4.69	4.90	4.83	4.76	4.76	4.02
1.33	5.40	5.67	5.56	5.47	5.47	4.66
1.5	5.92	6.28	6.12	6.00	6.05	5.18
2.0	7.34	7.74	7.50	7.46	7.49	6.52
3.0	9.82	10.2	9.82	9.88	10.0	8.79
4.0	12.0	12.4	11.8	11.9	12.0	10.8
5.0	14.0	14.3	13.3	13.5	13.7	12.5
6.0	15.9	16.2	14.8	14.8	15.4	14.1
6.129	16.1	16.4	14.9	15.0	15.5	14.2
8.0	19.3	19.5	17.0	17.1	18.2	16.9
10.0	22.4	22.6	19.1	19.1	20.9	19.6
15.0	29.1	29.2	24.3	23.9	26.3	26.0
20.0	35.0	34.5	28.7	28.4	31.7	31.7
30.0	42.6	41.2	36.4	36.2	38.8	42.2
40.0	47.8	45.2	42.4	41.9	44.4	50.8
50.0	51.5	48.0	46.7	46.5	49.5	57.7
60.0	54.0	50.9	50.2	49.8	52.7	63.2
80.0	58.1	55.7	55.5	55.1	57.2	72.5
100	61.0	59.9	58.8	59.1	60.1	79.1
150	65.3	63.9	65.1	65.1	66.4	92.6
200	69.1	65.8	69.0	69.2	70.3	102
300	74.0	69.3	74.4	74.9	75.0	115
400	76.6	71.7	77.9	78.4	77.2	123
500	78.6	73.5	79.9	80.1	79.1	128
600	79.5	74.7	81.5	81.9	80.7	132
800	81.3	76.1	83.0	84.1	82.8	140
1000	81.9	77.2	84.1	85.6	84.0	145
1500	84.2	78.1	86.0	86.1	86.5	156
2000	85.6	78.7	87.4	87.1	88.1	162
3000	85.6	80.2	90.1	88.0	89.1	171
4000	85.6	80.8	91.8	89.3	90.2	174
5000	85.7	81.1	92.6	90.4	91.2	179
6000	86.0	81.2	93.2	91.4	92.0	184
8000	86.9	81.4	93.7	93.0	93.6	193
10,000	87.3	81.4	93.5	94.3	95.2	199

AP, antero-posterior; PA, postero-anterior; LLAT, left lateral; RLAT, right lateral; ROT, rotational; ISO, isotropic.

Table B.12. Photons, female: skin absorbed dose per fluence, in units of pGy cm^2, for mono-energetic particles incident in various geometries.

Energy (MeV)	AP	PA	LLAT	RLAT	ROT	ISO
0.01	1.95	1.92	0.998	1.00	1.59	1.31
0.015	1.30	1.27	0.688	0.692	1.10	0.971
0.02	0.894	0.874	0.494	0.497	0.768	0.696
0.03	0.531	0.529	0.312	0.314	0.460	0.419
0.04	0.392	0.397	0.237	0.238	0.342	0.308
0.05	0.340	0.343	0.208	0.209	0.296	0.266
0.06	0.328	0.331	0.203	0.204	0.286	0.256
0.07	0.339	0.339	0.212	0.212	0.294	0.264
0.08	0.360	0.362	0.228	0.229	0.315	0.282
0.1	0.429	0.429	0.277	0.279	0.375	0.338
0.15	0.658	0.652	0.439	0.442	0.581	0.526
0.2	0.910	0.902	0.623	0.627	0.809	0.734
0.3	1.41	1.39	1.00	1.01	1.27	1.16
0.4	1.88	1.85	1.37	1.38	1.70	1.56
0.5	2.30	2.26	1.71	1.72	2.09	1.93
0.511	2.34	2.30	1.74	1.76	2.13	1.97
0.6	2.66	2.63	2.02	2.03	2.43	2.26
0.662	2.87	2.83	2.20	2.22	2.63	2.45
0.8	3.27	3.22	2.56	2.57	3.01	2.83
1.0	3.72	3.66	3.00	3.02	3.46	3.28
1.117	3.94	3.87	3.23	3.25	3.70	3.52
1.33	4.27	4.22	3.61	3.62	4.04	3.88
1.5	4.51	4.47	3.87	3.88	4.30	4.13
2.0	5.10	5.06	4.53	4.56	4.97	4.75
3.0	6.09	6.03	5.73	5.74	6.03	5.84
4.0	6.92	6.91	6.76	6.79	6.97	6.78
5.0	7.70	7.75	7.73	7.75	7.83	7.67
6.0	8.45	8.56	8.67	8.66	8.67	8.51
6.129	8.54	8.66	8.79	8.78	8.77	8.60
8.0	9.85	10.1	10.5	10.4	10.3	10.1
10.0	11.2	11.4	12.2	12.2	11.8	11.6
15.0	14.4	14.7	16.4	16.4	15.5	15.3
20.0	17.3	17.7	20.5	20.5	18.9	18.9
30.0	22.5	22.9	28.1	28.1	25.1	25.5
40.0	26.8	27.2	34.8	34.7	30.4	31.4
50.0	29.8	30.8	40.9	40.7	35.0	36.3
60.0	33.4	34.2	46.5	46.4	39.5	40.9
80.0	36.6	38.1	55.5	55.3	45.4	48.3
100	39.4	41.1	62.8	62.5	49.8	54.3
150	44.5	46.0	76.1	75.6	57.7	65.2
200	47.5	49.2	85.3	84.8	62.8	73.2
300	52.0	53.1	97.7	97.0	69.1	84.3
400	54.9	55.6	106	105	73.4	91.5
500	56.7	57.4	112	111	76.5	96.8
600	57.6	58.8	116	115	78.9	101
800	59.6	60.7	123	122	82.4	108
1000	60.2	61.9	128	127	84.9	113
1500	62.2	64.1	137	136	89.0	122
2000	63.7	65.6	143	141	91.6	129
3000	66.4	67.2	151	149	95.4	138
4000	66.9	68.3	156	154	97.7	144
5000	67.9	68.9	160	158	99.6	149
6000	68.9	69.5	164	162	101	154
8000	69.6	70.6	169	167	103	161
10,000	69.8	71.0	172	172	105	168

AP, antero-posterior; PA, postero-anterior; LLAT, left lateral; RLAT, right lateral; ROT, rotational; ISO, isotropic.

Table B.13. Photons, female: stomach wall absorbed dose per fluence, in units of pGy cm^2, for mono-energetic particles incident in various geometries.

Energy (MeV)	AP	PA	LLAT	RLAT	ROT	ISO
0.01	1.9E−5	–	8.9E−6	–	3.7E−6	–
0.015	0.0243	2.0E−5	0.0109	1.3E−5	0.0079	0.0046
0.02	0.137	0.0049	0.0829	7.3E−4	0.0516	0.0331
0.03	0.321	0.0701	0.246	0.0153	0.155	0.111
0.04	0.381	0.140	0.309	0.0408	0.209	0.156
0.05	0.402	0.188	0.331	0.0613	0.240	0.181
0.06	0.420	0.220	0.344	0.0784	0.262	0.201
0.07	0.450	0.254	0.365	0.0945	0.286	0.218
0.08	0.473	0.283	0.391	0.109	0.309	0.237
0.1	0.547	0.335	0.458	0.140	0.372	0.285
0.15	0.780	0.517	0.672	0.228	0.542	0.420
0.2	1.04	0.708	0.916	0.336	0.737	0.574
0.3	1.55	1.11	1.42	0.588	1.15	0.909
0.4	2.06	1.52	1.91	0.859	1.55	1.25
0.5	2.53	1.91	2.38	1.15	1.95	1.59
0.511	2.58	1.96	2.43	1.18	2.00	1.63
0.6	2.97	2.30	2.83	1.45	2.34	1.92
0.662	3.24	2.52	3.10	1.64	2.57	2.13
0.8	3.80	3.02	3.67	2.05	3.09	2.56
1.0	4.57	3.70	4.44	2.63	3.77	3.18
1.117	4.99	4.09	4.86	2.96	4.14	3.53
1.33	5.72	4.75	5.58	3.56	4.78	4.18
1.5	6.25	5.27	6.13	4.01	5.24	4.69
2.0	7.69	6.61	7.58	5.25	6.51	5.96
3.0	10.2	8.90	10.1	7.43	8.99	8.15
4.0	12.3	10.9	12.2	9.40	11.2	10.2
5.0	14.3	12.9	14.3	11.3	13.2	12.0
6.0	16.2	14.7	16.3	13.1	15.0	13.8
6.129	16.4	15.0	16.5	13.2	15.2	14.0
8.0	19.7	18.4	19.9	16.6	18.3	17.1
10.0	22.7	21.9	23.2	19.9	21.5	20.2
15.0	28.5	30.4	30.2	28.1	28.6	27.5
20.0	32.9	38.9	36.0	36.7	35.7	35.0
30.0	38.8	53.0	44.2	53.6	47.0	48.1
40.0	43.1	64.6	49.8	70.0	56.6	59.0
50.0	46.2	73.9	53.8	84.9	65.0	68.3
60.0	48.4	80.6	56.9	97.7	71.9	76.2
80.0	52.2	91.2	61.6	119	82.6	89.8
100	54.8	98.4	65.0	134	90.4	100
150	59.4	109	70.9	158	102	120
200	63.0	116	75.0	174	109	134
300	67.5	125	80.2	195	120	152
400	70.4	130	82.8	208	126	163
500	72.1	135	84.8	217	131	171
600	73.3	138	86.1	224	134	178
800	74.5	143	88.0	234	140	188
1000	75.5	147	89.7	242	144	197
1500	77.1	150	92.1	255	150	212
2000	77.7	152	93.1	264	154	222
3000	79.2	155	94.6	276	159	238
4000	79.9	158	95.2	284	161	249
5000	80.4	160	96.1	290	163	258
6000	80.7	161	96.7	294	165	264
8000	81.3	164	98.0	300	167	273
10,000	81.8	165	99.2	304	167	278

AP, antero-posterior; PA, postero-anterior; LLAT, left lateral; RLAT, right lateral; ROT, rotational; ISO, isotropic.

Table B.14. Photons, female: thyroid absorbed dose per fluence, in units of pGy cm^2, for mono-energetic particles incident in various geometries.

Energy (MeV)	AP	PA	LLAT	RLAT	ROT	ISO
0.01	0.0129	–	2.0E−6	–	0.0019	9.8E−4
0.015	0.308	–	2.7E−4	0.0015	0.0773	0.0414
0.02	0.644	6.4E−4	0.0029	0.0173	0.205	0.119
0.03	0.698	0.0279	0.0250	0.0674	0.287	0.186
0.04	0.684	0.0972	0.0512	0.107	0.300	0.206
0.05	0.624	0.157	0.0737	0.129	0.301	0.223
0.06	0.592	0.201	0.0930	0.147	0.312	0.239
0.07	0.597	0.226	0.111	0.167	0.330	0.250
0.08	0.619	0.254	0.126	0.183	0.353	0.274
0.1	0.699	0.310	0.154	0.217	0.413	0.318
0.15	0.962	0.483	0.233	0.324	0.607	0.471
0.2	1.28	0.662	0.333	0.452	0.825	0.645
0.3	1.88	1.05	0.560	0.746	1.26	1.04
0.4	2.47	1.44	0.792	1.05	1.69	1.41
0.5	3.02	1.82	1.05	1.35	2.13	1.78
0.511	3.08	1.86	1.07	1.39	2.16	1.82
0.6	3.52	2.19	1.30	1.67	2.53	2.15
0.662	3.80	2.41	1.45	1.85	2.79	2.39
0.8	4.39	2.88	1.81	2.26	3.32	2.88
1.0	5.25	3.52	2.33	2.88	4.02	3.55
1.117	5.70	3.88	2.65	3.21	4.40	3.95
1.33	6.50	4.55	3.19	3.85	5.06	4.63
1.5	7.08	5.05	3.58	4.36	5.52	5.15
2.0	8.58	6.42	4.77	5.64	6.89	6.53
3.0	11.1	8.80	7.05	7.91	9.45	8.86
4.0	13.1	10.9	9.11	9.98	11.5	10.8
5.0	14.9	12.9	11.0	11.9	13.4	12.5
6.0	16.1	14.8	12.7	13.8	15.1	14.2
6.129	16.2	15.1	12.9	14.1	15.4	14.5
8.0	16.9	18.6	16.0	17.3	18.0	17.6
10.0	17.0	22.2	19.1	20.6	20.6	20.9
15.0	17.0	31.2	26.4	27.7	26.0	27.6
20.0	17.4	40.5	34.3	34.2	31.1	33.5
30.0	18.0	56.3	49.3	45.8	40.5	45.2
40.0	18.9	67.8	63.6	57.0	48.7	55.0
50.0	19.5	76.9	76.3	66.4	55.8	62.8
60.0	19.9	83.2	87.3	75.2	61.0	69.7
80.0	20.5	93.6	106	90.5	69.5	80.3
100	21.3	101	120	102	75.7	89.0
150	22.5	112	145	120	85.9	104
200	24.0	120	163	132	93.2	115
300	25.3	130	186	146	102	128
400	26.2	136	200	156	108	135
500	26.3	140	211	162	110	143
600	26.6	142	219	168	113	150
800	26.8	147	232	177	117	160
1000	27.2	149	239	183	120	169
1500	27.5	154	252	193	125	183
2000	27.6	157	260	197	129	190
3000	28.3	160	275	202	132	197
4000	28.3	162	285	208	134	203
5000	28.3	164	290	211	136	209
6000	28.2	165	290	214	137	214
8000	28.4	167	282	218	139	226
10,000	28.5	170	268	222	141	237

AP, antero-posterior; PA, postero-anterior; LLAT, left lateral; RLAT, right lateral; ROT, rotational; ISO, isotropic.

Table B.15. Photons, female: UB (urinary bladder) wall absorbed dose per fluence, in units of pGy cm^2, for mono-energetic particles incident in various geometries.

Energy (MeV)	AP	PA	LLAT	RLAT	ROT	ISO
0.01	0.0154	–	8.8E−7	–	0.0025	0.0015
0.015	0.234	–	2.3E−5	9.3E−6	0.0574	0.0388
0.02	0.415	5.4E−4	8.0E−4	6.1E−4	0.120	0.0866
0.03	0.501	0.0306	0.0161	0.0144	0.166	0.132
0.04	0.498	0.0797	0.0399	0.0411	0.195	0.154
0.05	0.496	0.128	0.0646	0.0638	0.212	0.171
0.06	0.505	0.166	0.0840	0.0857	0.236	0.190
0.07	0.532	0.187	0.104	0.0993	0.252	0.207
0.08	0.555	0.217	0.120	0.118	0.281	0.226
0.1	0.645	0.273	0.154	0.154	0.327	0.273
0.15	0.915	0.425	0.253	0.255	0.501	0.404
0.2	1.20	0.590	0.371	0.370	0.675	0.554
0.3	1.77	0.951	0.636	0.639	1.05	0.875
0.4	2.30	1.33	0.921	0.920	1.44	1.20
0.5	2.80	1.69	1.22	1.21	1.82	1.53
0.511	2.88	1.72	1.24	1.24	1.85	1.57
0.6	3.31	2.04	1.50	1.50	2.18	1.87
0.662	3.62	2.25	1.68	1.67	2.39	2.09
0.8	4.19	2.71	2.09	2.07	2.86	2.52
1.0	4.97	3.36	2.71	2.66	3.51	3.15
1.117	5.39	3.73	3.06	3.01	3.88	3.49
1.33	6.16	4.37	3.64	3.61	4.54	4.11
1.5	6.71	4.85	4.12	4.10	5.06	4.56
2.0	8.21	6.15	5.38	5.35	6.38	5.80
3.0	10.7	8.47	7.57	7.53	8.65	7.95
4.0	12.6	10.4	9.56	9.49	10.7	9.82
5.0	14.4	12.4	11.4	11.3	12.7	11.6
6.0	15.8	14.2	13.2	13.1	14.5	13.2
6.129	15.9	14.4	13.4	13.3	14.8	13.4
8.0	18.1	17.7	16.6	16.5	17.6	16.4
10.0	20.0	21.0	19.9	19.9	20.6	19.4
15.0	23.9	29.6	28.1	28.1	27.9	26.6
20.0	26.8	38.6	36.4	36.1	34.5	33.5
30.0	30.5	55.3	53.2	52.7	46.5	46.6
40.0	32.7	70.6	68.6	68.8	57.3	58.6
50.0	34.5	82.6	82.1	82.6	67.3	68.6
60.0	35.8	92.2	93.8	94.5	75.4	77.9
80.0	38.3	105	112	112	88.6	92.4
100	39.8	114	125	125	98.5	104
150	42.7	127	147	147	114	126
200	44.7	137	161	162	124	141
300	47.8	149	178	180	136	160
400	49.4	156	188	191	141	173
500	50.1	160	196	199	145	183
600	51.0	164	202	204	150	190
800	51.7	172	212	213	157	201
1000	51.9	176	220	220	163	208
1500	53.3	182	229	228	174	224
2000	54.3	185	233	234	179	236
3000	55.0	189	240	245	184	249
4000	56.2	193	246	253	189	257
5000	56.3	196	248	258	191	267
6000	56.1	199	252	263	193	273
8000	56.3	203	259	269	197	283
10,000	56.0	208	267	271	202	291

AP, antero-posterior; PA, postero-anterior; LLAT, left lateral; RLAT, right lateral; ROT, rotational; ISO, isotropic.

Table B.16. Photons, male: brain absorbed dose per fluence, in units of pGy cm^2, for mono-energetic particles incident in various geometries.

Energy (MeV)	AP	PA	LLAT	RLAT	ROT	ISO
0.01	3.6E−7	–	–	2.5E−8	2.8E−8	7.9E−7
0.015	9.7E−5	3.1E−5	6.0E−5	7.2E−5	1.1E−4	2.8E−4
0.02	0.0022	0.0023	0.0046	0.0048	0.0040	0.0060
0.03	0.0400	0.0580	0.0805	0.0834	0.0661	0.0662
0.04	0.0988	0.135	0.169	0.173	0.144	0.136
0.05	0.141	0.181	0.218	0.224	0.193	0.177
0.06	0.170	0.210	0.250	0.255	0.224	0.204
0.07	0.188	0.236	0.276	0.282	0.249	0.228
0.08	0.219	0.262	0.306	0.313	0.279	0.253
0.1	0.274	0.321	0.371	0.377	0.337	0.308
0.15	0.432	0.496	0.566	0.574	0.522	0.476
0.2	0.612	0.691	0.784	0.795	0.726	0.661
0.3	0.990	1.10	1.24	1.25	1.15	1.06
0.4	1.38	1.52	1.69	1.70	1.59	1.46
0.5	1.77	1.93	2.12	2.13	2.01	1.85
0.511	1.81	1.97	2.17	2.18	2.05	1.89
0.6	2.15	2.32	2.54	2.56	2.41	2.23
0.662	2.38	2.57	2.79	2.81	2.65	2.45
0.8	2.87	3.09	3.33	3.36	3.18	2.95
1.0	3.56	3.79	4.07	4.10	3.91	3.65
1.117	3.94	4.18	4.48	4.50	4.30	4.04
1.33	4.61	4.85	5.18	5.20	5.00	4.70
1.5	5.12	5.37	5.70	5.73	5.53	5.21
2.0	6.50	6.76	7.14	7.15	6.93	6.56
3.0	8.89	9.18	9.62	9.63	9.37	8.92
4.0	11.0	11.4	11.8	11.8	11.5	11.1
5.0	13.0	13.4	13.8	13.8	13.6	13.0
6.0	14.9	15.4	15.8	15.8	15.5	14.9
6.129	15.1	15.6	16.0	16.0	15.8	15.2
8.0	18.5	19.1	19.5	19.4	19.1	18.6
10.0	22.0	22.5	22.9	22.9	22.5	22.0
15.0	30.3	30.3	30.2	30.3	30.6	29.9
20.0	38.1	37.5	37.1	36.8	37.4	36.9
30.0	51.6	48.7	47.1	46.5	48.3	48.1
40.0	61.8	57.3	54.2	53.2	56.5	56.6
50.0	70.4	64.1	59.5	58.5	62.9	63.4
60.0	76.8	69.5	63.7	62.3	67.8	69.0
80.0	86.3	78.1	70.1	68.4	75.0	77.9
100	92.2	84.0	74.7	72.8	80.3	84.8
150	104	93.2	82.6	80.2	88.7	96.9
200	111	98.7	87.7	85.2	94.5	105
300	121	105	93.8	91.5	102	116
400	128	110	97.2	95.0	106	124
500	132	114	99.7	97.3	109	130
600	135	116	101	99.2	111	134
800	138	120	104	102	114	141
1000	141	122	106	103	116	147
1500	146	126	109	107	119	156
2000	149	128	111	108	122	163
3000	153	131	113	110	124	174
4000	156	134	114	111	126	182
5000	158	135	115	112	128	189
6000	159	136	116	112	128	194
8000	161	137	117	113	129	203
10,000	163	138	117	114	130	210

AP, antero-posterior; PA, postero-anterior; LLAT, left lateral; RLAT, right lateral; ROT, rotational; ISO, isotropic.

Table B.17. Photons, male: breast absorbed dose per fluence, in units of pGy cm^2, for mono-energetic particles incident in various geometries.

Energy (MeV)	AP	PA	LLAT	RLAT	ROT	ISO
0.01	0.449	–	0.0802	0.0747	0.160	0.131
0.015	0.987	–	0.283	0.268	0.378	0.328
0.02	0.922	3.8E−6	0.346	0.331	0.390	0.366
0.03	0.613	0.0048	0.277	0.267	0.296	0.289
0.04	0.463	0.0211	0.215	0.206	0.230	0.224
0.05	0.417	0.0356	0.197	0.190	0.215	0.207
0.06	0.423	0.0525	0.197	0.190	0.217	0.207
0.07	0.428	0.0692	0.209	0.198	0.241	0.220
0.08	0.475	0.0861	0.233	0.225	0.265	0.245
0.1	0.571	0.120	0.290	0.279	0.332	0.305
0.15	0.886	0.228	0.462	0.448	0.533	0.494
0.2	1.21	0.365	0.656	0.639	0.754	0.687
0.3	1.82	0.667	1.04	1.01	1.18	1.10
0.4	2.40	0.997	1.44	1.39	1.62	1.50
0.5	2.95	1.34	1.83	1.78	2.05	1.89
0.511	3.00	1.39	1.88	1.83	2.09	1.93
0.6	3.45	1.72	2.23	2.16	2.45	2.28
0.662	3.76	1.94	2.46	2.38	2.71	2.50
0.8	4.39	2.45	2.93	2.85	3.25	2.99
1.0	5.23	3.11	3.59	3.50	3.98	3.64
1.117	5.67	3.47	3.93	3.86	4.37	3.99
1.33	6.36	4.14	4.56	4.49	5.06	4.59
1.5	6.81	4.65	5.03	4.95	5.58	5.03
2.0	7.80	6.04	6.26	6.12	6.75	6.07
3.0	8.72	8.41	8.20	8.02	8.45	7.73
4.0	8.80	10.4	9.66	9.50	9.69	9.03
5.0	8.56	12.1	10.8	10.8	10.7	10.3
6.0	8.21	13.8	11.8	11.7	11.6	11.3
6.129	8.17	14.0	11.9	11.8	11.7	11.4
8.0	7.68	17.1	13.5	13.4	13.2	12.7
10.0	7.28	20.3	15.0	14.9	14.5	14.1
15.0	6.93	28.6	18.5	18.5	17.7	17.7
20.0	6.79	37.2	21.9	22.1	20.7	21.6
30.0	6.75	54.8	28.7	29.3	28.1	28.4
40.0	6.91	71.5	35.6	37.0	35.6	34.4
50.0	7.12	85.6	42.2	44.1	42.3	40.4
60.0	7.30	97.8	48.1	50.3	48.0	45.8
80.0	7.53	114	58.2	61.2	57.5	55.4
100	7.87	125	66.2	69.3	63.7	63.5
150	8.29	144	80.9	84.4	76.3	77.9
200	8.81	154	91.1	95.5	84.7	88.3
300	9.59	166	104	111	96.2	103
400	10.1	174	112	121	103	113
500	10.3	179	118	128	108	120
600	10.4	184	122	133	112	127
800	10.4	189	129	142	118	137
1000	10.6	194	133	147	122	145
1500	10.6	201	143	158	129	158
2000	10.6	206	148	164	134	166
3000	10.6	211	155	169	140	177
4000	10.6	214	157	174	143	186
5000	10.6	218	160	178	147	195
6000	10.7	220	162	182	150	202
8000	10.7	222	167	188	155	212
10,000	10.8	223	172	195	158	218

AP, antero-posterior; PA, postero-anterior; LLAT, left lateral; RLAT, right lateral; ROT, rotational; ISO, isotropic.

Table B.18. Photons, male: colon absorbed dose per fluence, in units of pGy cm^2, for mono-energetic particles incident in various geometries.

Energy (MeV)	AP	PA	LLAT	RLAT	ROT	ISO
0.01	3.2E−4	–	2.1E−6	1.1E−7	3.3E−5	3.3E−5
0.015	0.0168	6.6E−5	0.0051	9.5E−4	0.0050	0.0030
0.02	0.0926	0.0044	0.0499	0.0197	0.0386	0.0259
0.03	0.269	0.0634	0.151	0.0951	0.136	0.101
0.04	0.340	0.130	0.190	0.138	0.194	0.146
0.05	0.372	0.178	0.204	0.159	0.225	0.170
0.06	0.396	0.210	0.218	0.175	0.245	0.188
0.07	0.412	0.245	0.233	0.190	0.267	0.209
0.08	0.447	0.270	0.253	0.208	0.292	0.226
0.1	0.521	0.333	0.298	0.251	0.350	0.269
0.15	0.749	0.501	0.445	0.377	0.514	0.404
0.2	0.997	0.690	0.610	0.525	0.702	0.550
0.3	1.50	1.09	0.964	0.841	1.09	0.868
0.4	1.99	1.49	1.33	1.17	1.47	1.19
0.5	2.46	1.88	1.68	1.49	1.85	1.52
0.511	2.50	1.92	1.71	1.53	1.89	1.55
0.6	2.90	2.26	2.02	1.82	2.22	1.84
0.662	3.16	2.50	2.23	2.02	2.46	2.03
0.8	3.71	2.99	2.69	2.45	2.95	2.47
1.0	4.44	3.67	3.33	3.07	3.61	3.07
1.117	4.84	4.06	3.70	3.41	3.98	3.41
1.33	5.53	4.72	4.31	4.01	4.61	4.00
1.5	6.06	5.22	4.79	4.48	5.07	4.44
2.0	7.48	6.59	6.09	5.74	6.39	5.67
3.0	9.94	8.97	8.42	7.97	8.72	7.89
4.0	12.1	11.0	10.5	9.99	10.8	9.88
5.0	14.1	12.9	12.3	11.8	12.7	11.7
6.0	16.0	14.7	14.1	13.6	14.5	13.5
6.129	16.3	14.9	14.3	13.8	14.7	13.7
8.0	19.6	18.2	17.5	17.0	18.0	16.7
10.0	22.8	21.7	20.6	20.3	21.0	19.9
15.0	29.5	29.8	27.4	27.9	28.1	27.5
20.0	34.7	37.9	33.5	35.1	35.1	34.8
30.0	42.2	52.3	45.0	47.8	47.6	47.5
40.0	47.4	64.3	55.8	59.6	58.2	58.7
50.0	51.3	73.9	65.5	70.3	67.0	68.6
60.0	54.3	81.3	74.1	79.8	74.1	77.3
80.0	58.7	92.5	88.2	96.4	85.6	92.2
100	62.0	100	99.0	109	93.9	104
150	67.5	112	117	131	108	126
200	71.6	120	129	145	118	142
300	76.8	131	145	164	130	163
400	79.9	138	156	175	138	175
500	82.0	143	163	184	143	185
600	83.4	146	169	191	147	193
800	85.1	150	177	201	154	206
1000	86.3	153	183	208	158	217
1500	88.4	157	193	219	165	235
2000	89.7	161	199	227	169	247
3000	91.2	166	207	237	176	263
4000	92.8	170	214	243	181	275
5000	93.7	172	219	247	184	285
6000	94.2	173	223	251	186	292
8000	94.6	174	228	258	190	305
10,000	94.4	174	231	265	193	316

AP, antero-posterior; PA, postero-anterior; LLAT, left lateral; RLAT, right lateral; ROT, rotational; ISO, isotropic.

Table B.19. Photons, male: bone surface (endosteum) absorbed dose per fluence, in units of pGy cm^2, for mono-energetic particles incident in various geometries.

Energy (MeV)	AP	PA	LLAT	RLAT	ROT	ISO
0.01	3.5E−4	4.3E−5	1.1E−4	1.4E−4	2.3E−4	0.0016
0.015	0.0098	0.0030	0.0051	0.0056	0.0082	0.0152
0.02	0.0586	0.0356	0.0384	0.0410	0.0493	0.0542
0.03	0.238	0.196	0.153	0.158	0.198	0.170
0.04	0.346	0.313	0.219	0.223	0.292	0.245
0.05	0.389	0.365	0.246	0.250	0.333	0.277
0.06	0.408	0.392	0.258	0.262	0.351	0.293
0.07	0.425	0.411	0.268	0.273	0.367	0.307
0.08	0.442	0.433	0.281	0.285	0.384	0.320
0.1	0.491	0.484	0.315	0.319	0.428	0.358
0.15	0.669	0.665	0.440	0.444	0.588	0.494
0.2	0.882	0.878	0.593	0.599	0.782	0.659
0.3	1.33	1.33	0.928	0.935	1.20	1.02
0.4	1.79	1.78	1.27	1.28	1.62	1.40
0.5	2.22	2.22	1.62	1.63	2.03	1.76
0.511	2.27	2.26	1.65	1.67	2.07	1.81
0.6	2.64	2.64	1.96	1.97	2.42	2.13
0.662	2.89	2.89	2.16	2.18	2.66	2.35
0.8	3.43	3.43	2.62	2.63	3.18	2.82
1.0	4.16	4.16	3.24	3.26	3.88	3.47
1.117	4.56	4.56	3.59	3.61	4.27	3.83
1.33	5.25	5.25	4.20	4.22	4.95	4.47
1.5	5.77	5.79	4.66	4.69	5.46	4.96
2.0	7.19	7.20	5.95	5.97	6.83	6.28
3.0	9.66	9.65	8.23	8.25	9.22	8.61
4.0	11.8	11.8	10.3	10.3	11.3	10.7
5.0	13.7	13.8	12.1	12.1	13.3	12.6
6.0	15.5	15.7	13.9	13.9	15.1	14.3
6.129	15.8	16.0	14.1	14.1	15.3	14.6
8.0	18.8	19.3	17.1	17.1	18.5	17.6
10.0	21.8	22.6	20.1	20.0	21.6	20.7
15.0	28.3	29.7	26.9	26.8	28.4	27.7
20.0	33.7	35.7	33.1	32.9	34.2	34.0
30.0	42.2	44.6	44.0	43.8	43.8	44.7
40.0	48.9	51.2	53.9	53.6	51.7	53.7
50.0	54.0	56.2	62.7	62.2	58.3	61.2
60.0	58.1	60.2	70.4	69.8	63.6	67.6
80.0	64.3	66.4	83.3	82.5	72.0	78.2
100	68.7	70.6	93.4	92.4	78.0	86.6
150	76.2	77.2	111	110	88.1	102
200	81.3	81.5	124	123	94.7	113
300	87.8	87.0	141	140	103	128
400	91.5	90.5	152	151	109	138
500	94.0	93.1	160	159	113	145
600	95.8	95.0	166	165	116	151
800	98.1	97.6	176	175	120	160
1000	99.9	99.4	183	182	123	167
1500	103	102	195	194	128	180
2000	105	104	203	203	131	189
3000	107	106	215	214	136	203
4000	109	108	224	223	138	213
5000	110	108	230	229	141	221
6000	111	109	235	234	143	228
8000	112	110	243	241	145	239
10,000	113	110	249	246	147	247

AP, antero-posterior; PA, postero-anterior; LLAT, left lateral; RLAT, right lateral; ROT, rotational; ISO, isotropic.

Table B.20. Photons, male: liver absorbed dose per fluence, in units of pGy cm^2, for mono-energetic particles incident in various geometries.

Energy (MeV)	AP	PA	LLAT	RLAT	ROT	ISO
0.01	1.5E−6	–	–	1.8E−6	1.7E−6	–
0.015	0.0040	2.9E−4	4.7E−6	0.0037	0.0018	0.0010
0.02	0.0406	0.0070	3.0E−4	0.0339	0.0188	0.0119
0.03	0.169	0.0618	0.0084	0.136	0.0906	0.0660
0.04	0.255	0.127	0.0270	0.208	0.152	0.115
0.05	0.304	0.178	0.0454	0.246	0.192	0.148
0.06	0.337	0.219	0.0610	0.272	0.223	0.173
0.07	0.359	0.253	0.0743	0.298	0.249	0.195
0.08	0.396	0.285	0.0875	0.323	0.275	0.217
0.1	0.466	0.350	0.114	0.383	0.330	0.263
0.15	0.668	0.526	0.188	0.566	0.491	0.392
0.2	0.889	0.719	0.274	0.772	0.669	0.538
0.3	1.34	1.12	0.477	1.20	1.04	0.850
0.4	1.78	1.52	0.708	1.63	1.40	1.17
0.5	2.21	1.91	0.952	2.05	1.77	1.49
0.511	2.26	1.95	0.979	2.09	1.81	1.52
0.6	2.62	2.29	1.20	2.45	2.13	1.81
0.662	2.87	2.52	1.36	2.69	2.35	2.00
0.8	3.39	3.01	1.71	3.21	2.82	2.42
1.0	4.10	3.69	2.23	3.93	3.47	3.01
1.117	4.49	4.06	2.52	4.32	3.83	3.34
1.33	5.16	4.71	3.05	5.01	4.46	3.92
1.5	5.67	5.21	3.47	5.52	4.94	4.37
2.0	7.04	6.54	4.63	6.90	6.24	5.60
3.0	9.44	8.82	6.75	9.29	8.57	7.82
4.0	11.6	10.8	8.67	11.4	10.6	9.81
5.0	13.6	12.8	10.5	13.4	12.6	11.7
6.0	15.5	14.7	12.1	15.3	14.4	13.4
6.129	15.7	14.9	12.4	15.5	14.6	13.7
8.0	19.1	18.3	15.4	18.9	17.9	16.8
10.0	22.5	21.9	18.6	22.3	21.3	20.1
15.0	30.3	30.1	26.7	30.0	29.2	28.0
20.0	37.1	38.2	34.9	37.2	36.7	35.8
30.0	47.8	52.6	51.1	49.0	50.0	49.8
40.0	56.3	64.8	67.5	58.5	61.8	62.2
50.0	62.6	74.8	82.8	66.1	71.8	73.1
60.0	67.5	82.5	96.7	72.0	80.0	82.4
80.0	74.6	94.5	121	81.0	93.2	98.1
100	79.7	103	139	87.4	102	110
150	87.8	116	171	98.2	119	132
200	94.0	124	193	105	129	148
300	102	135	221	114	143	169
400	107	142	240	120	152	183
500	110	147	253	123	158	192
600	112	151	264	126	163	200
800	115	156	279	130	169	213
1000	117	160	291	133	174	222
1500	120	166	310	137	183	239
2000	123	170	323	140	189	251
3000	126	175	342	144	196	266
4000	128	178	354	146	201	278
5000	129	180	363	148	205	288
6000	130	182	371	150	208	295
8000	131	184	383	151	211	308
10,000	133	186	393	152	213	318

AP, antero-posterior; PA, postero-anterior; LLAT, left lateral; RLAT, right lateral; ROT, rotational; ISO, isotropic.

Table B.21. Photons, male: lung absorbed dose per fluence, in units of pGy cm^2, for mono-energetic particles incident in various geometries.

Energy (MeV)	AP	PA	LLAT	RLAT	ROT	ISO
0.01	7.1E−6	–	1.3E−7	1.8E−7	8.0E−7	2.2E−6
0.015	0.0100	3.5E−4	6.8E−4	2.6E−4	0.0021	0.0017
0.02	0.0761	0.0094	0.0075	0.0054	0.0222	0.0165
0.03	0.230	0.0833	0.0373	0.0371	0.0985	0.0758
0.04	0.290	0.168	0.0678	0.0681	0.157	0.124
0.05	0.319	0.226	0.0909	0.0906	0.193	0.154
0.06	0.342	0.268	0.109	0.109	0.220	0.178
0.07	0.361	0.305	0.126	0.125	0.246	0.201
0.08	0.396	0.340	0.142	0.141	0.271	0.223
0.1	0.468	0.415	0.177	0.176	0.329	0.273
0.15	0.691	0.629	0.279	0.278	0.500	0.417
0.2	0.936	0.859	0.397	0.395	0.688	0.577
0.3	1.43	1.32	0.662	0.655	1.08	0.919
0.4	1.91	1.78	0.941	0.936	1.48	1.27
0.5	2.38	2.23	1.23	1.22	1.87	1.62
0.511	2.43	2.28	1.26	1.25	1.91	1.66
0.6	2.82	2.65	1.52	1.51	2.25	1.97
0.662	3.09	2.90	1.70	1.69	2.48	2.18
0.8	3.64	3.44	2.10	2.08	2.98	2.62
1.0	4.39	4.17	2.67	2.64	3.67	3.26
1.117	4.80	4.58	2.99	2.95	4.04	3.61
1.33	5.51	5.28	3.57	3.52	4.69	4.24
1.5	6.04	5.82	4.01	3.96	5.18	4.72
2.0	7.47	7.24	5.24	5.17	6.52	5.99
3.0	9.94	9.67	7.45	7.37	8.90	8.24
4.0	12.1	11.8	9.46	9.38	11.0	10.3
5.0	14.3	13.8	11.4	11.3	13.0	12.3
6.0	16.2	15.8	13.2	13.1	14.9	14.2
6.129	16.5	16.0	13.5	13.3	15.1	14.4
8.0	20.0	19.7	16.8	16.7	18.6	17.8
10.0	23.4	23.6	20.3	20.1	22.3	21.3
15.0	30.6	32.7	28.8	28.6	30.8	29.8
20.0	36.5	40.8	37.2	37.0	38.9	37.8
30.0	44.4	51.9	53.4	52.9	51.7	51.7
40.0	50.2	60.1	68.6	67.7	62.5	63.3
50.0	54.4	66.2	82.1	81.0	71.2	72.9
60.0	57.6	70.9	93.8	92.5	78.3	80.9
80.0	62.3	78.2	113	112	89.8	93.9
100	65.9	83.1	127	127	97.3	104
150	71.6	90.6	152	153	111	123
200	75.8	95.4	168	170	119	136
300	81.1	101	189	191	130	153
400	84.6	105	202	206	137	164
500	86.8	108	211	216	142	172
600	88.3	110	218	224	146	179
800	89.9	113	229	236	151	189
1000	91.2	114	236	244	155	196
1500	93.3	118	249	259	162	211
2000	95.0	120	258	269	166	221
3000	96.9	123	270	283	170	235
4000	98.5	124	277	291	174	245
5000	99.4	125	283	298	176	252
6000	99.8	126	288	304	178	258
8000	100	126	296	313	181	268
10,000	100	126	302	319	183	278

AP, antero-posterior; PA, postero-anterior; LLAT, left lateral; RLAT, right lateral; ROT, rotational; ISO, isotropic.

Table B.22. Photons, male: oesophagus absorbed dose per fluence, in units of pGy cm^2, for mono-energetic particles incident in various geometries.

Energy (MeV)	AP	PA	LLAT	RLAT	ROT	ISO
0.01	9.8E−5	–	–	–	8.2E−6	1.1E−5
0.015	0.0120	–	2.6E−4	1.2E−4	0.0026	0.0015
0.02	0.0626	4.8E−4	0.0080	0.0047	0.0193	0.0115
0.03	0.166	0.0237	0.0403	0.0312	0.0707	0.0460
0.04	0.229	0.0951	0.0703	0.0547	0.119	0.0838
0.05	0.273	0.157	0.0949	0.0781	0.156	0.116
0.06	0.304	0.209	0.116	0.0992	0.193	0.146
0.07	0.326	0.257	0.134	0.117	0.227	0.170
0.08	0.369	0.294	0.157	0.133	0.254	0.191
0.1	0.446	0.364	0.197	0.173	0.317	0.244
0.15	0.665	0.579	0.313	0.277	0.498	0.377
0.2	0.897	0.789	0.452	0.402	0.686	0.530
0.3	1.35	1.22	0.737	0.679	1.08	0.855
0.4	1.83	1.64	1.05	0.957	1.45	1.19
0.5	2.27	2.05	1.37	1.24	1.84	1.52
0.511	2.32	2.08	1.41	1.28	1.89	1.56
0.6	2.69	2.44	1.68	1.54	2.23	1.85
0.662	2.95	2.67	1.87	1.72	2.45	2.05
0.8	3.51	3.18	2.28	2.11	2.96	2.47
1.0	4.27	3.88	2.90	2.70	3.63	3.04
1.117	4.68	4.28	3.24	3.03	4.02	3.34
1.33	5.38	4.98	3.86	3.64	4.66	3.88
1.5	5.92	5.50	4.31	4.12	5.18	4.34
2.0	7.38	6.94	5.57	5.27	6.53	5.64
3.0	9.86	9.29	7.86	7.34	8.86	8.03
4.0	12.0	11.5	9.83	9.30	10.9	10.0
5.0	13.9	13.3	11.7	11.1	12.8	11.8
6.0	15.8	15.1	13.5	13.0	14.7	13.5
6.129	16.0	15.4	13.7	13.2	14.9	13.7
8.0	19.2	18.7	16.9	16.6	18.3	16.9
10.0	22.4	22.4	20.3	20.0	21.7	20.1
15.0	29.6	31.8	28.6	28.1	30.1	28.3
20.0	36.7	41.1	36.6	35.8	38.4	36.6
30.0	47.1	56.4	52.3	50.9	52.7	52.0
40.0	55.2	67.6	67.1	66.3	64.0	65.5
50.0	60.8	75.8	79.9	80.1	73.4	76.7
60.0	65.1	81.7	91.2	92.2	80.8	86.4
80.0	71.0	90.8	108	112	92.4	100
100	75.6	96.5	121	126	99.8	112
150	82.5	107	144	151	113	134
200	88.0	113	159	167	121	150
300	95.0	122	176	188	132	168
400	99.7	127	185	200	140	179
500	102	131	192	209	146	188
600	104	134	196	216	150	194
800	106	138	204	225	155	205
1000	107	141	210	233	159	213
1500	111	146	221	246	163	231
2000	114	148	228	255	167	244
3000	117	150	237	269	172	258
4000	118	152	245	280	175	270
5000	118	152	250	287	177	279
6000	119	153	254	291	180	286
8000	119	153	261	294	183	297
10,000	118	154	265	297	186	306

AP, antero-posterior; PA, postero-anterior; LLAT, left lateral; RLAT, right lateral; ROT, rotational; ISO, isotropic.

Table B.23. Photons, male: red (active) bone marrow absorbed dose per fluence, in units of pGy cm^2, for mono-energetic particles incident in various geometries.

Energy (MeV)	AP	PA	LLAT	RLAT	ROT	ISO
0.01	6.7E−4	1.6E−5	1.2E−4	1.5E−4	2.5E−4	6.8E−4
0.015	0.0178	0.0024	0.0071	0.0079	0.0088	0.0099
0.02	0.0597	0.0266	0.0295	0.0323	0.0371	0.0347
0.03	0.175	0.155	0.0863	0.0909	0.128	0.104
0.04	0.267	0.275	0.130	0.134	0.207	0.164
0.05	0.321	0.347	0.158	0.161	0.257	0.203
0.06	0.355	0.394	0.177	0.180	0.290	0.229
0.07	0.384	0.427	0.193	0.197	0.315	0.251
0.08	0.409	0.462	0.208	0.211	0.340	0.269
0.1	0.465	0.529	0.241	0.245	0.392	0.311
0.15	0.639	0.729	0.345	0.350	0.545	0.436
0.2	0.839	0.953	0.468	0.475	0.723	0.581
0.3	1.26	1.41	0.741	0.750	1.10	0.897
0.4	1.68	1.87	1.03	1.04	1.49	1.22
0.5	2.09	2.31	1.32	1.34	1.87	1.55
0.511	2.14	2.36	1.35	1.37	1.91	1.59
0.6	2.49	2.73	1.62	1.64	2.23	1.88
0.662	2.72	2.98	1.80	1.82	2.45	2.07
0.8	3.24	3.52	2.20	2.22	2.94	2.50
1.0	3.94	4.24	2.77	2.79	3.61	3.10
1.117	4.33	4.64	3.09	3.11	3.98	3.44
1.33	4.99	5.32	3.66	3.68	4.63	4.04
1.5	5.50	5.85	4.10	4.11	5.11	4.50
2.0	6.87	7.24	5.31	5.33	6.44	5.76
3.0	9.25	9.65	7.49	7.54	8.76	8.01
4.0	11.4	11.8	9.47	9.53	10.9	10.0
5.0	13.3	13.9	11.3	11.4	12.8	11.9
6.0	15.2	15.8	13.1	13.1	14.7	13.6
6.129	15.4	16.1	13.3	13.3	14.9	13.9
8.0	18.6	19.5	16.4	16.4	18.2	17.1
10.0	21.8	23.1	19.6	19.7	21.5	20.3
15.0	29.6	31.2	27.4	27.4	29.4	28.2
20.0	36.8	37.7	34.9	35.0	36.8	35.7
30.0	48.9	47.8	49.1	49.2	49.6	49.2
40.0	58.5	55.1	62.7	62.5	60.4	60.9
50.0	66.0	60.8	74.9	74.5	69.4	71.0
60.0	71.8	65.2	85.7	85.1	76.8	79.8
80.0	80.6	72.2	104	103	88.4	94.2
100	86.7	76.8	118	117	96.6	106
150	97.3	84.0	142	141	111	127
200	104	88.9	159	158	120	142
300	113	95.0	181	180	131	162
400	119	98.9	195	194	138	175
500	122	102	206	205	143	184
600	125	104	214	213	148	192
800	128	107	226	224	153	204
1000	131	109	235	233	158	214
1500	135	111	250	249	165	230
2000	138	113	260	259	170	242
3000	142	116	275	274	176	258
4000	144	118	285	283	179	271
5000	146	119	292	291	182	281
6000	147	119	298	297	185	288
8000	149	120	308	307	189	301
10,000	151	120	315	314	192	312

AP, antero-posterior; PA, postero-anterior; LLAT, left lateral; RLAT, right lateral; ROT, rotational; ISO, isotropic.

Table B.24. Photons, male: remainder tissues absorbed dose per fluence, in units of pGy cm^2, for mono-energetic particles incident in various geometries.

Energy (MeV)	AP	PA	LLAT	RLAT	ROT	ISO
0.01	0.0076	0.0021	0.0041	0.0039	0.0044	0.0051
0.015	0.0492	0.0134	0.0199	0.0186	0.0247	0.0201
0.02	0.100	0.0323	0.0341	0.0317	0.0493	0.0378
0.03	0.184	0.102	0.0679	0.0628	0.106	0.0798
0.04	0.240	0.163	0.103	0.0958	0.155	0.119
0.05	0.279	0.206	0.131	0.121	0.191	0.148
0.06	0.309	0.242	0.152	0.142	0.220	0.170
0.07	0.331	0.272	0.172	0.160	0.246	0.192
0.08	0.368	0.306	0.193	0.181	0.276	0.215
0.1	0.441	0.371	0.239	0.226	0.337	0.263
0.15	0.647	0.560	0.371	0.355	0.507	0.403
0.2	0.870	0.769	0.520	0.499	0.697	0.556
0.3	1.33	1.19	0.843	0.808	1.09	0.881
0.4	1.77	1.61	1.18	1.13	1.48	1.21
0.5	2.20	2.02	1.52	1.46	1.87	1.55
0.511	2.25	2.07	1.55	1.49	1.91	1.58
0.6	2.62	2.43	1.85	1.78	2.25	1.88
0.662	2.86	2.66	2.05	1.98	2.47	2.08
0.8	3.39	3.18	2.50	2.41	2.96	2.51
1.0	4.11	3.87	3.12	3.01	3.64	3.11
1.117	4.49	4.25	3.46	3.35	4.01	3.45
1.33	5.17	4.91	4.07	3.95	4.66	4.05
1.5	5.68	5.40	4.53	4.41	5.15	4.51
2.0	7.05	6.74	5.81	5.65	6.49	5.77
3.0	9.43	9.10	8.09	7.87	8.82	8.00
4.0	11.5	11.2	10.1	9.84	10.9	10.0
5.0	13.4	13.1	11.9	11.7	12.8	11.9
6.0	15.2	15.0	13.7	13.4	14.5	13.6
6.129	15.4	15.2	13.9	13.6	14.7	13.8
8.0	18.5	18.6	17.0	16.7	17.9	16.9
10.0	21.5	21.9	20.3	20.0	21.2	20.1
15.0	28.5	30.1	28.1	27.7	29.0	27.8
20.0	34.9	38.0	35.9	35.3	36.5	35.2
30.0	45.3	51.1	50.0	49.1	49.1	48.7
40.0	53.4	61.5	62.7	61.7	60.0	60.5
50.0	59.6	69.9	73.9	73.2	69.0	70.6
60.0	64.4	76.6	83.4	83.1	76.5	79.2
80.0	71.5	86.6	98.7	99.4	88.1	93.4
100	76.7	93.5	110	112	96.4	105
150	85.3	105	130	134	110	125
200	91.5	112	142	149	119	139
300	99.4	120	159	168	130	159
400	104	126	170	181	137	172
500	108	130	177	190	142	181
600	110	133	183	198	146	188
800	112	137	192	208	152	200
1000	115	140	198	216	155	208
1500	118	146	208	229	163	225
2000	121	149	215	238	167	236
3000	124	153	223	249	173	252
4000	126	155	229	257	177	264
5000	128	156	233	263	180	273
6000	129	157	237	268	182	280
8000	130	158	242	276	186	291
10,000	131	159	246	282	187	299

AP, antero-posterior; PA, postero-anterior; LLAT, left lateral; RLAT, right lateral; ROT, rotational; ISO, isotropic.

Table B.25. Photons, male: salivary glands absorbed dose per fluence, in units of pGy cm^2, for mono-energetic particles incident in various geometries.

Energy (MeV)	AP	PA	LLAT	RLAT	ROT	ISO
0.01	7.0E−4	0.0058	0.0775	0.0544	0.0335	0.0231
0.015	0.0325	0.0700	0.328	0.284	0.191	0.138
0.02	0.136	0.178	0.420	0.392	0.296	0.225
0.03	0.251	0.256	0.360	0.345	0.294	0.238
0.04	0.262	0.247	0.303	0.294	0.267	0.214
0.05	0.264	0.245	0.283	0.278	0.258	0.210
0.06	0.273	0.254	0.283	0.280	0.266	0.214
0.07	0.291	0.278	0.295	0.292	0.289	0.228
0.08	0.325	0.307	0.323	0.318	0.313	0.248
0.1	0.400	0.374	0.390	0.384	0.377	0.305
0.15	0.621	0.602	0.599	0.587	0.589	0.482
0.2	0.867	0.859	0.823	0.820	0.810	0.674
0.3	1.37	1.38	1.28	1.29	1.30	1.07
0.4	1.87	1.88	1.76	1.76	1.79	1.47
0.5	2.36	2.38	2.22	2.20	2.25	1.87
0.511	2.41	2.42	2.26	2.24	2.29	1.92
0.6	2.82	2.83	2.64	2.63	2.67	2.26
0.662	3.10	3.11	2.89	2.88	2.92	2.49
0.8	3.68	3.69	3.43	3.43	3.46	3.00
1.0	4.48	4.47	4.18	4.15	4.24	3.69
1.117	4.92	4.91	4.59	4.54	4.66	4.06
1.33	5.65	5.62	5.29	5.24	5.40	4.72
1.5	6.22	6.17	5.82	5.79	5.94	5.23
2.0	7.69	7.62	7.17	7.24	7.33	6.62
3.0	10.1	10.3	9.32	9.46	9.50	8.67
4.0	12.1	12.6	10.9	11.1	11.3	10.4
5.0	14.0	14.4	12.2	12.5	13.0	12.1
6.0	15.9	16.1	13.4	13.5	14.4	13.6
6.129	16.1	16.4	13.5	13.7	14.6	13.8
8.0	19.0	19.1	15.3	15.4	16.5	16.5
10.0	21.6	21.8	17.2	17.3	18.5	19.0
15.0	27.0	27.7	21.9	22.2	24.0	24.7
20.0	31.1	32.4	26.5	26.8	29.0	30.0
30.0	37.0	39.2	35.0	35.2	37.2	39.6
40.0	40.7	43.6	42.2	42.6	44.0	48.0
50.0	43.3	47.0	48.0	48.5	49.4	55.0
60.0	45.3	48.8	52.6	53.5	53.4	60.9
80.0	47.7	52.3	59.7	60.8	59.6	70.4
100	49.7	53.9	64.6	66.2	63.5	77.7
150	53.3	59.0	73.7	75.2	70.3	91.9
200	56.0	62.6	79.6	81.5	75.7	102
300	59.2	65.9	86.5	88.7	81.4	114
400	61.4	68.2	91.4	93.1	84.8	123
500	62.6	69.6	94.6	96.1	87.3	130
600	63.5	70.6	96.9	98.4	89.4	135
800	65.0	71.9	100	102	91.8	142
1000	66.1	72.9	103	104	93.6	148
1500	66.7	74.2	107	109	96.5	158
2000	67.6	75.3	109	112	98.7	165
3000	69.3	77.3	113	114	101	177
4000	70.1	78.5	115	117	102	184
5000	70.7	79.4	116	118	103	190
6000	71.3	80.1	117	120	104	194
8000	72.1	81.3	117	122	105	201
10,000	72.8	82.4	117	124	106	205

AP, antero-posterior; PA, postero-anterior; LLAT, left lateral; RLAT, right lateral; ROT, rotational; ISO, isotropic.

Table B.26. Photons, male: skin absorbed dose per fluence, in units of pGy cm^2, for mono-energetic particles incident in various geometries.

Energy (MeV)	AP	PA	LLAT	RLAT	ROT	ISO
0.01	1.74	1.72	0.912	0.907	1.43	1.17
0.015	1.23	1.20	0.665	0.653	1.04	0.917
0.02	0.855	0.839	0.480	0.467	0.735	0.667
0.03	0.506	0.506	0.298	0.291	0.439	0.403
0.04	0.376	0.378	0.227	0.223	0.326	0.298
0.05	0.328	0.329	0.201	0.197	0.284	0.258
0.06	0.320	0.319	0.197	0.194	0.276	0.249
0.07	0.326	0.328	0.207	0.203	0.286	0.258
0.08	0.353	0.351	0.223	0.220	0.307	0.276
0.1	0.421	0.418	0.272	0.269	0.368	0.333
0.15	0.649	0.640	0.433	0.428	0.569	0.518
0.2	0.898	0.885	0.615	0.607	0.792	0.725
0.3	1.40	1.38	0.987	0.978	1.24	1.14
0.4	1.87	1.83	1.35	1.34	1.67	1.55
0.5	2.29	2.25	1.69	1.68	2.07	1.92
0.511	2.34	2.29	1.73	1.71	2.11	1.96
0.6	2.68	2.62	2.01	1.99	2.42	2.26
0.662	2.89	2.83	2.20	2.18	2.62	2.46
0.8	3.30	3.24	2.57	2.55	3.03	2.85
1.0	3.80	3.72	3.03	3.01	3.51	3.33
1.117	4.03	3.95	3.27	3.24	3.76	3.57
1.33	4.40	4.31	3.65	3.62	4.14	3.95
1.5	4.65	4.54	3.92	3.89	4.39	4.21
2.0	5.28	5.16	4.62	4.60	5.05	4.89
3.0	6.26	6.18	5.78	5.76	6.11	6.00
4.0	7.11	7.06	6.81	6.79	7.05	6.94
5.0	7.90	7.87	7.77	7.77	7.93	7.81
6.0	8.65	8.67	8.71	8.70	8.77	8.64
6.129	8.75	8.77	8.83	8.82	8.88	8.75
8.0	10.1	10.2	10.5	10.5	10.4	10.3
10.0	11.5	11.7	12.3	12.3	11.9	11.8
15.0	14.8	15.2	16.6	16.6	15.7	15.6
20.0	17.9	18.3	20.7	20.7	19.2	19.3
30.0	23.2	23.8	28.3	28.4	25.6	26.0
40.0	27.9	28.6	35.2	35.4	31.4	32.0
50.0	31.6	32.6	41.4	41.7	36.4	37.3
60.0	34.6	35.9	47.0	47.4	40.7	42.0
80.0	39.1	41.1	56.6	57.2	47.6	50.0
100	42.4	44.7	64.5	65.3	52.9	56.5
150	47.9	50.5	79.4	80.4	61.8	68.8
200	51.8	54.3	90.2	91.2	67.8	77.7
300	56.8	59.0	105	106	75.6	90.0
400	60.1	62.0	115	116	80.7	98.3
500	62.2	64.1	122	124	84.4	105
600	63.7	65.8	128	129	87.2	109
800	65.4	68.0	137	138	91.5	117
1000	67.0	69.7	143	145	94.6	123
1500	69.4	72.4	155	156	99.9	134
2000	71.5	74.2	163	165	104	142
3000	73.8	76.5	174	176	108	154
4000	75.3	77.9	182	184	111	163
5000	76.5	78.9	188	189	114	169
6000	77.3	79.6	193	194	116	175
8000	78.4	80.6	202	203	119	184
10,000	79.1	81.4	208	210	121	191

AP, antero-posterior; PA, postero-anterior; LLAT, left lateral; RLAT, right lateral; ROT, rotational; ISO, isotropic.

Table B.27. Photons, male: stomach wall absorbed dose per fluence, in units of pGy cm^2, for mono-energetic particles incident in various geometries.

Energy (MeV)	AP	PA	LLAT	RLAT	ROT	ISO
0.01	3.3E−6	–	–	–	–	–
0.015	0.0077	–	0.0014	6.9E−7	0.0019	0.0011
0.02	0.0767	8.5E−4	0.0258	5.4E−5	0.0240	0.0149
0.03	0.256	0.0285	0.144	0.0064	0.104	0.0738
0.04	0.336	0.0826	0.222	0.0265	0.162	0.121
0.05	0.375	0.130	0.261	0.0475	0.199	0.153
0.06	0.404	0.167	0.287	0.0655	0.227	0.176
0.07	0.422	0.201	0.311	0.0800	0.251	0.199
0.08	0.460	0.227	0.339	0.0951	0.277	0.218
0.1	0.536	0.285	0.398	0.123	0.331	0.261
0.15	0.763	0.436	0.593	0.202	0.492	0.388
0.2	1.01	0.615	0.806	0.298	0.664	0.530
0.3	1.50	0.965	1.26	0.521	1.03	0.838
0.4	1.98	1.33	1.71	0.769	1.39	1.17
0.5	2.45	1.69	2.14	1.03	1.75	1.49
0.511	2.50	1.73	2.19	1.06	1.80	1.52
0.6	2.89	2.05	2.56	1.30	2.11	1.80
0.662	3.15	2.26	2.81	1.47	2.33	1.98
0.8	3.70	2.73	3.35	1.84	2.80	2.42
1.0	4.44	3.38	4.09	2.38	3.46	3.03
1.117	4.85	3.74	4.49	2.68	3.83	3.37
1.33	5.55	4.35	5.18	3.24	4.48	3.97
1.5	6.10	4.82	5.71	3.67	4.95	4.42
2.0	7.50	6.13	7.14	4.87	6.25	5.62
3.0	9.91	8.48	9.61	7.03	8.52	7.78
4.0	12.1	10.6	11.8	8.96	10.5	9.74
5.0	14.1	12.5	13.7	10.7	12.4	11.7
6.0	16.0	14.2	15.5	12.4	14.3	13.4
6.129	16.2	14.4	15.8	12.7	14.5	13.6
8.0	19.6	17.5	19.2	15.8	17.8	16.7
10.0	23.0	20.8	22.7	19.0	21.1	20.0
15.0	30.0	29.2	30.5	26.9	28.8	27.8
20.0	35.5	37.7	37.5	35.1	36.2	35.4
30.0	43.4	53.9	48.8	52.0	49.3	48.7
40.0	49.2	68.2	57.1	68.7	61.1	61.0
50.0	53.5	80.2	63.5	84.3	71.0	71.7
60.0	56.8	90.0	68.4	98.0	79.5	80.9
80.0	61.3	104	75.9	121	92.6	96.2
100	64.8	115	81.1	138	102	108
150	70.4	131	90.9	167	118	130
200	74.8	141	97.3	185	128	146
300	80.2	154	105	210	142	167
400	83.4	162	109	226	150	180
500	85.2	168	112	238	155	190
600	86.8	172	114	247	160	197
800	88.6	178	117	259	165	209
1000	89.6	183	118	269	170	217
1500	92.2	191	122	284	180	234
2000	93.5	196	124	294	186	246
3000	95.1	202	126	310	194	263
4000	96.7	206	128	320	199	276
5000	97.3	208	130	328	203	286
6000	97.7	210	132	335	205	295
8000	97.9	212	134	345	210	309
10,000	98.2	213	137	352	213	320

AP, antero-posterior; PA, postero-anterior; LLAT, left lateral; RLAT, right lateral; ROT, rotational; ISO, isotropic.

Table B.28. Photons, male: testes absorbed dose per fluence, in units of pGy cm^2, for mono-energetic particles incident in various geometries.

Energy (MeV)	AP	PA	LLAT	RLAT	ROT	ISO
0.01	0.0569	–	2.2E−5	9.1E−6	0.0278	0.0439
0.015	0.268	6.1E−5	5.0E−4	8.0E−5	0.118	0.120
0.02	0.487	0.0050	0.0036	0.0010	0.205	0.188
0.03	0.620	0.0676	0.0269	0.0145	0.258	0.231
0.04	0.585	0.127	0.0559	0.0379	0.264	0.229
0.05	0.547	0.166	0.0767	0.0590	0.263	0.224
0.06	0.535	0.189	0.0940	0.0752	0.267	0.230
0.07	0.543	0.211	0.110	0.0890	0.283	0.237
0.08	0.571	0.236	0.124	0.102	0.297	0.253
0.1	0.650	0.287	0.152	0.131	0.352	0.304
0.15	0.904	0.436	0.252	0.215	0.528	0.450
0.2	1.20	0.616	0.371	0.324	0.730	0.617
0.3	1.77	1.02	0.644	0.575	1.10	0.975
0.4	2.33	1.41	0.945	0.855	1.51	1.34
0.5	2.83	1.80	1.25	1.15	1.91	1.68
0.511	2.88	1.84	1.29	1.19	1.95	1.72
0.6	3.30	2.18	1.57	1.46	2.30	2.04
0.662	3.59	2.41	1.77	1.64	2.53	2.25
0.8	4.17	2.94	2.20	2.04	3.04	2.69
1.0	4.96	3.63	2.83	2.64	3.72	3.33
1.117	5.37	4.02	3.18	2.98	4.09	3.67
1.33	6.07	4.68	3.81	3.58	4.76	4.25
1.5	6.64	5.16	4.30	4.04	5.26	4.68
2.0	8.04	6.44	5.56	5.29	6.59	5.87
3.0	10.3	8.75	7.84	7.56	8.83	7.98
4.0	12.1	10.9	9.92	9.58	10.7	9.91
5.0	13.4	12.9	11.7	11.4	12.4	11.6
6.0	14.6	14.7	13.5	13.1	13.8	13.1
6.129	14.7	15.0	13.7	13.3	14.1	13.3
8.0	16.6	18.2	16.7	16.4	16.6	16.1
10.0	18.2	21.7	19.8	19.6	19.1	18.5
15.0	20.0	30.3	27.2	27.3	24.7	24.2
20.0	21.1	39.1	35.1	35.1	30.2	29.5
30.0	22.8	54.5	50.4	51.0	40.8	40.0
40.0	24.3	66.3	65.0	66.6	51.2	50.3
50.0	25.5	75.1	77.1	79.9	59.8	58.6
60.0	26.5	81.9	87.5	90.8	67.0	66.4
80.0	27.6	91.9	102	107	77.3	78.6
100	28.6	98.7	113	119	84.8	88.1
150	30.4	109	131	138	97.9	107
200	32.0	116	142	151	107	121
300	34.0	125	156	168	118	140
400	36.0	131	165	178	124	154
500	36.9	135	172	184	128	163
600	37.4	138	177	190	132	171
800	37.6	142	184	198	138	181
1000	37.7	145	188	203	142	189
1500	38.0	150	197	212	150	203
2000	38.4	153	202	217	154	215
3000	39.1	156	207	222	158	232
4000	39.9	158	210	227	162	247
5000	40.5	159	214	231	165	260
6000	41.0	160	216	233	167	269
8000	41.5	162	218	235	170	280
10,000	41.6	164	220	237	172	287

AP, antero-posterior; PA, postero-anterior; LLAT, left lateral; RLAT, right lateral; ROT, rotational; ISO, isotropic.

Table B.29. Photons, male: thyroid absorbed dose per fluence, in units of pGy cm^2, for mono-energetic particles incident in various geometries.

Energy (MeV)	AP	PA	LLAT	RLAT	ROT	ISO
0.01	0.0063	–	2.2E−5	4.5E−5	0.0015	5.9E−4
0.015	0.216	3.1E−5	0.0116	0.0175	0.0627	0.0328
0.02	0.534	3.9E−4	0.0621	0.0873	0.186	0.107
0.03	0.649	0.0187	0.134	0.173	0.267	0.179
0.04	0.634	0.0757	0.160	0.195	0.284	0.197
0.05	0.596	0.126	0.175	0.202	0.294	0.204
0.06	0.578	0.166	0.185	0.209	0.301	0.220
0.07	0.595	0.202	0.200	0.222	0.325	0.243
0.08	0.613	0.229	0.218	0.243	0.349	0.265
0.1	0.693	0.281	0.266	0.289	0.408	0.317
0.15	0.955	0.443	0.396	0.431	0.600	0.450
0.2	1.27	0.627	0.551	0.603	0.797	0.627
0.3	1.88	1.01	0.874	0.970	1.25	0.985
0.4	2.45	1.40	1.22	1.34	1.69	1.35
0.5	2.99	1.80	1.55	1.70	2.12	1.71
0.511	3.05	1.84	1.59	1.74	2.17	1.74
0.6	3.48	2.18	1.88	2.06	2.52	2.05
0.662	3.77	2.40	2.07	2.27	2.77	2.27
0.8	4.39	2.89	2.51	2.74	3.28	2.72
1.0	5.19	3.57	3.16	3.39	3.98	3.38
1.117	5.63	3.93	3.54	3.76	4.36	3.74
1.33	6.37	4.56	4.18	4.42	5.01	4.39
1.5	6.90	5.01	4.68	4.94	5.51	4.87
2.0	8.42	6.31	5.98	6.29	6.88	6.16
3.0	11.0	8.62	8.28	8.69	9.35	8.53
4.0	13.1	10.7	10.4	10.8	11.5	10.4
5.0	14.9	12.7	12.4	12.8	13.5	12.3
6.0	16.4	14.7	14.1	14.5	15.2	14.0
6.129	16.4	15.0	14.3	14.7	15.4	14.2
8.0	17.8	18.6	17.3	17.5	17.7	17.1
10.0	18.5	22.4	20.1	20.4	20.3	20.0
15.0	18.9	31.6	26.9	27.2	26.3	26.9
20.0	19.3	40.6	33.2	33.3	31.6	33.1
30.0	20.1	56.7	44.7	44.6	41.2	44.5
40.0	20.8	69.2	56.0	55.0	49.5	54.0
50.0	21.4	78.9	66.7	65.0	56.2	62.5
60.0	21.9	86.3	75.8	73.1	62.0	69.7
80.0	22.7	96.8	91.9	86.2	70.2	81.5
100	23.3	105	103	96.1	76.1	91.4
150	25.0	118	122	113	86.4	109
200	26.3	126	135	124	93.4	121
300	27.6	135	150	140	103	137
400	28.3	141	160	148	110	147
500	29.0	146	166	155	114	154
600	29.2	149	172	161	117	160
800	29.6	153	180	168	120	169
1000	29.6	156	184	173	122	178
1500	30.0	161	194	183	127	192
2000	30.4	164	199	188	130	201
3000	31.0	167	207	195	134	218
4000	31.5	170	214	200	137	228
5000	31.9	171	219	204	140	236
6000	32.2	172	223	207	141	242
8000	32.7	174	229	211	144	251
10,000	33.1	175	235	214	146	258

AP, antero-posterior; PA, postero-anterior; LLAT, left lateral; RLAT, right lateral; ROT, rotational; ISO, isotropic.

Table B.30. Photons, male: urinary bladder wall absorbed dose per fluence, in units of pGy cm^2, for mono-energetic particles incident in various geometries.

Energy (MeV)	AP	PA	LLAT	RLAT	ROT	ISO
0.01	1.0E−6	–	–	–	–	–
0.015	0.0064	2.3E−5	1.0E−5	1.5E−5	0.0021	0.0010
0.02	0.0662	0.0021	5.7E−4	3.4E−4	0.0217	0.0135
0.03	0.203	0.0474	0.0109	0.0067	0.0892	0.0608
0.04	0.351	0.111	0.0359	0.0261	0.145	0.100
0.05	0.392	0.165	0.0623	0.0503	0.177	0.130
0.06	0.422	0.212	0.0827	0.0713	0.208	0.156
0.07	0.443	0.247	0.101	0.0902	0.240	0.180
0.08	0.486	0.278	0.119	0.109	0.272	0.201
0.1	0.574	0.357	0.159	0.144	0.327	0.247
0.15	0.822	0.528	0.259	0.236	0.483	0.366
0.2	1.09	0.725	0.374	0.347	0.656	0.506
0.3	1.62	1.12	0.641	0.592	1.03	0.803
0.4	2.12	1.50	0.929	0.863	1.41	1.11
0.5	2.58	1.90	1.22	1.15	1.79	1.41
0.511	2.63	1.94	1.25	1.18	1.83	1.45
0.6	3.02	2.27	1.51	1.44	2.13	1.72
0.662	3.28	2.50	1.70	1.61	2.35	1.91
0.8	3.85	3.01	2.09	2.00	2.81	2.31
1.0	4.66	3.71	2.66	2.57	3.45	2.90
1.117	5.10	4.08	2.99	2.90	3.81	3.22
1.33	5.85	4.75	3.58	3.46	4.45	3.82
1.5	6.41	5.25	4.02	3.91	4.92	4.27
2.0	7.81	6.60	5.26	5.13	6.19	5.49
3.0	10.2	8.88	7.49	7.24	8.50	7.59
4.0	12.4	11.0	9.39	9.12	10.6	9.52
5.0	14.5	12.9	11.2	11.0	12.6	11.3
6.0	16.4	14.8	13.0	12.8	14.5	13.0
6.129	16.6	15.0	13.2	13.0	14.7	13.2
8.0	20.0	18.4	16.3	16.3	18.1	16.4
10.0	23.2	21.8	19.6	19.5	21.5	19.7
15.0	29.8	30.3	27.5	27.7	29.3	27.5
20.0	35.2	38.9	36.0	36.1	37.1	35.3
30.0	42.2	54.8	53.9	53.4	51.1	49.9
40.0	46.9	68.0	70.6	70.3	63.5	63.2
50.0	50.4	77.9	85.5	85.8	73.8	74.6
60.0	52.9	86.1	98.2	98.7	82.3	84.6
80.0	57.2	97.0	118	120	95.8	101
100	60.1	104	132	135	106	114
150	65.1	116	156	161	121	138
200	68.6	122	172	178	130	155
300	72.6	131	191	199	143	178
400	75.6	138	205	213	152	193
500	77.3	143	213	222	158	205
600	78.7	147	220	230	163	213
800	80.4	152	230	240	170	227
1000	81.5	154	238	248	174	236
1500	82.7	159	250	261	183	254
2000	83.0	163	259	270	190	270
3000	83.3	166	268	284	196	287
4000	84.0	169	276	292	200	299
5000	84.6	171	283	299	203	307
6000	85.1	172	288	304	204	314
8000	85.8	174	296	311	207	323
10,000	86.4	175	302	317	208	330

AP, antero-posterior; PA, postero-anterior; LLAT, left lateral; RLAT, right lateral; ROT, rotational; ISO, isotropic.

ANNEX C. ORGAN ABSORBED DOSE CONVERSION COEFFICIENTS FOR NEUTRONS

(C1) This annex lists reference values for organ absorbed dose conversion coefficients for neutrons and the specific irradiation geometries considered for the following organs: red (active) bone marrow, colon, lung, stomach, breast, ovaries, testes, urinary bladder wall (UB-wall), oesophagus, liver, thyroid, bone surface (endosteum), brain, salivary glands, skin, and remainder tissues. Data are given separately for the male and female phantoms. Data for the lens of the eye can be found in Annex F. In the CD accompanying this report, these dose conversion coefficients are given in electronic form along with those for the individual remainder tissues, which include: adrenals, extrathoracic region, gall bladder, heart, kidneys, lymphatic nodes, muscle, oral mucosa, pancreas, prostate, small intestine, spleen, thymus, and uterus/cervix.

(C2) The specific irradiation geometries considered are broad parallel beams along the antero-posterior, postero-anterior, left and right lateral axes, and rotational and isotropic directions (see Section 3.2).

(C3) The organ absorbed doses are normalised to particle fluence, Φ, and are given in units of pGy cm^2. The following table entries are reference values and were derived from dose conversion coefficients calculated using the ICRP/ICRU reference phantoms and various Monte Carlo radiation transport codes (see Sections 3.1 and 3.3) following the application of averaging and smoothing techniques (see Annex I).

Table C.1. Neutrons, female: brain absorbed dose per fluence, in units of pGy cm^2, for mono-energetic particles incident in various geometries.

Energy (MeV)	AP	PA	LLAT	RLAT	ROT	ISO
1.0E−9	0.577	0.630	0.675	0.685	0.595	0.526
1.0E−8	0.636	0.686	0.804	0.798	0.736	0.641
2.5E−8	0.728	0.808	0.946	0.952	0.853	0.736
1.0E−7	0.942	1.06	1.26	1.26	1.13	0.972
2.0E−7	1.08	1.22	1.45	1.47	1.28	1.10
5.0E−7	1.21	1.40	1.67	1.69	1.49	1.27
1.0E−6	1.29	1.50	1.81	1.83	1.61	1.37
2.0E−6	1.35	1.56	1.89	1.91	1.69	1.45
5.0E−6	1.42	1.64	1.98	2.00	1.76	1.51
1.0E−5	1.44	1.66	1.99	2.01	1.79	1.53
2.0E−5	1.45	1.67	2.00	2.02	1.80	1.53
5.0E−5	1.44	1.64	1.98	1.99	1.79	1.52
1.0E−4	1.43	1.64	1.95	1.99	1.77	1.51
2.0E−4	1.39	1.63	1.94	1.96	1.72	1.46
5.0E−4	1.33	1.60	1.91	1.90	1.63	1.38
0.001	1.34	1.57	1.88	1.89	1.60	1.36
0.002	1.34	1.55	1.84	1.87	1.60	1.36
0.005	1.30	1.53	1.82	1.84	1.55	1.31
0.01	1.27	1.52	1.81	1.82	1.52	1.28
0.02	1.29	11.54	1.85	1.87	1.53	1.30
0.03	1.31	1.57	1.89	1.93	1.57	1.34
0.05	1.37	1.66	2.02	2.06	1.68	1.43
0.07	1.46	1.76	2.15	2.19	1.80	1.54
0.1	1.59	1.92	2.38	2.41	2.00	1.71
0.15	1.84	2.23	2.80	2.83	2.37	2.03
0.2	2.11	2.57	3.25	3.28	2.75	2.38
0.3	2.69	3.30	4.20	4.24	3.56	3.11
0.5	3.96	4.84	6.21	6.26	5.27	4.65
0.7	5.30	6.37	8.13	8.20	7.01	6.23
0.9	6.68	7.88	9.94	10.0	8.77	7.83
1.0	7.40	8.65	10.8	10.9	9.64	8.63
1.2	8.86	10.2	12.7	12.9	11.4	10.2
1.5	11.0	12.6	15.6	15.7	13.9	12.5
2.0	14.3	16.2	19.8	20.0	17.7	16.0
3.0	20.2	22.5	26.8	27.0	24.2	22.0
4.0	25.1	27.7	32.4	32.5	29.6	27.0
5.0	29.3	32.0	36.8	37.0	34.1	31.2
6.0	33.0	35.6	40.5	40.7	37.9	34.8
7.0	36.1	38.8	43.8	43.9	41.2	37.9
8.0	39.0	41.6	46.7	46.8	44.1	40.7
9.0	41.5	44.2	49.3	49.5	46.7	43.2
10.0	43.8	46.5	51.8	51.9	49.1	45.4
12.0	47.8	50.7	56.1	56.3	53.0	49.2
14.0	51.1	54.1	59.6	59.8	56.2	52.4
15.0	52.5	55.5	61.1	61.3	57.6	53.7
16.0	53.8	56.9	62.4	62.6	58.8	54.9
18.0	56.2	59.2	64.6	64.8	60.9	56.9
20.0	58.2	61.1	66.4	66.5	62.6	58.6
21.0	59.1	61.9	67.1	67.3	63.3	59.4
30.0	65.2	67.4	72.0	71.9	68.0	64.1
50.0	73.1	74.6	78.0	77.6	73.1	69.8
75.0	79.5	80.8	83.4	83.0	77.5	75.1
100	84.0	84.6	86.1	85.8	81.3	80.0
130	87.7	87.1	87.0	86.8	85.2	84.9
150	89.7	88.3	87.4	87.1	87.6	87.7
180	92.5	89.9	88.3	87.8	91.0	91.7
200	94.3	91.0	89.1	88.5	93.2	94.3
300	105	100	97.2	96.1	105	108
400	119	114	111	110	118	122
500	134	129	128	127	131	136
600	148	144	145	143	143	148
700	161	157	159	157	154	160
800	172	167	170	169	163	169
900	181	175	177	177	171	177
1000	188	181	183	184	178	184
2000	229	214	215	214	217	227
5000	286	271	266	254	268	293
10,000	382	366	362	358	321	379

AP, antero-posterior; PA, postero-anterior; LLAT, left lateral; RLAT, right lateral; ROT, rotational; ISO, isotropic.

Table C.2. Neutrons, female: breast absorbed dose per fluence, in units of pGy cm^2, for mono-energetic particles incident in various geometries.

Energy (MeV)	AP	PA	LLAT	RLAT	ROT	ISO
1.0E−9	1.71	0.430	0.472	0.440	0.733	0.581
1.0E−8	1.94	0.437	0.478	0.447	0.852	0.658
2.5E−8	2.12	0.516	0.584	0.539	0.948	0.739
1.0E−7	2.62	0.667	0.666	0.626	1.17	0.906
2.0E−7	2.90	0.757	0.806	0.740	1.27	0.989
5.0E−7	3.04	0.876	0.828	0.764	1.40	1.09
1.0E−6	3.13	0.959	0.928	0.853	1.47	1.14
2.0E−6	3.18	1.01	0.887	0.828	1.50	1.17
5.0E−6	3.22	1.07	0.968	0.896	1.52	1.18
1.0E−5	3.17	1.09	0.893	0.822	1.52	1.19
2.0E−5	3.14	1.11	0.951	0.868	1.51	1.16
5.0E−5	3.00	1.11	0.840	0.788	1.48	1.13
1.0E−4	2.96	1.11	0.829	0.779	1.45	1.12
2.0E−4	2.89	1.12	0.882	0.808	1.41	1.09
5.0E−4	2.63	1.12	0.799	0.735	1.34	1.03
0.001	2.65	1.12	0.833	0.766	1.31	1.02
0.002	2.68	1.11	0.790	0.723	1.32	1.04
0.005	2.69	1.12	0.846	0.764	1.33	1.04
0.01	2.83	1.13	0.861	0.779	1.40	1.09
0.02	3.31	1.14	0.978	0.912	1.60	1.26
0.03	3.78	1.16	1.10	1.02	1.80	1.43
0.05	4.64	1.18	1.35	1.28	2.20	1.78
0.07	5.49	1.20	1.60	1.51	2.58	2.11
0.1	6.83	1.23	1.99	1.87	3.13	2.58
0.15	8.76	1.28	2.61	2.46	3.97	3.32
0.2	10.4	1.34	3.16	3.04	4.76	4.01
0.3	13.5	1.46	4.27	4.12	6.18	5.29
0.5	18.5	1.79	6.28	6.08	8.67	7.55
0.7	22.5	2.25	8.03	7.83	10.8	9.55
0.9	26.2	2.81	9.61	9.39	12.8	11.4
1.0	27.9	3.14	10.4	10.1	13.7	12.2
1.2	30.7	3.92	11.9	11.7	15.5	13.9
1.5	34.0	5.29	14.1	13.8	17.8	16.1
2.0	38.7	7.88	17.4	17.1	21.3	19.3
3.0	46.6	13.4	23.0	22.8	27.1	24.7
4.0	52.7	18.5	28.0	27.7	31.9	29.2
5.0	56.7	23.3	32.0	31.6	36.0	33.1
6.0	59.9	27.5	35.4	35.0	39.6	36.4
7.0	62.7	31.3	38.4	38.0	42.8	39.4
8.0	65.5	34.7	41.0	40.7	45.7	42.2
9.0	68.2	37.9	43.6	43.4	48.4	44.7
10.0	70.8	40.8	46.1	45.9	50.8	47.1
12.0	75.2	46.0	50.7	50.5	55.1	51.3
14.0	78.5	50.7	54.7	54.4	58.6	54.8
15.0	79.7	52.8	56.4	56.2	60.0	56.3
16.0	80.6	54.8	57.9	57.7	61.4	57.6
18.0	81.8	58.4	60.4	60.3	63.5	59.9
20.0	82.3	61.5	62.4	62.4	65.2	61.7
21.0	82.4	62.9	63.2	63.3	65.9	62.4
30.0	81.9	72.1	69.0	69.3	69.8	66.4
50.0	78.0	82.5	74.5	75.6	71.9	68.8
75.0	71.8	90.8	79.1	79.3	73.1	70.9
100	63.5	98.0	80.9	80.9	74.7	73.8
130	55.6	106	79.8	80.6	77.3	77.9
150	52.6	111	80.6	81.3	79.3	80.7
180	50.7	117	84.3	83.6	82.5	84.8
200	50.4	121	86.4	85.4	84.9	87.5
300	55.5	139	93.6	95.5	97.6	101
400	64.7	158	107	110	112	114
500	74.8	176	122	126	125	128
600	85.0	193	140	144	138	141
700	93.6	208	154	158	149	153
800	100	220	164	168	158	163
900	105	230	172	175	165	171
1000	109	238	177	179	171	178
2000	129	287	211	207	210	221
5000	136	378	269	278	272	296
10,000	204	479	375	373	347	389

AP, antero-posterior; PA, postero-anterior; LLAT, left lateral; RLAT, right lateral; ROT, rotational; ISO, isotropic.

Table C.3. Neutrons, female: colon absorbed dose per fluence, in units of pGy cm^2, for mono-energetic particles incident in various geometries.

Energy (MeV)	AP	PA	LLAT	RLAT	ROT	ISO
1.0E−9	1.35	0.689	0.362	0.361	0.642	0.504
1.0E−8	1.48	0.774	0.390	0.377	0.806	0.614
2.5E−8	1.75	0.893	0.466	0.451	0.924	0.703
1.0E−7	2.37	1.19	0.597	0.580	1.22	0.910
2.0E−7	2.81	1.36	0.699	0.685	1.39	1.03
5.0E−7	3.09	1.56	0.816	0.790	1.62	1.20
1.0E−6	3.39	1.71	0.898	0.869	1.77	1.30
2.0E−6	3.70	1.81	0.950	0.916	1.88	1.37
5.0E−6	3.87	1.92	1.01	0.981	1.97	1.43
1.0E−5	3.82	1.97	1.03	0.981	2.02	1.46
2.0E−5	3.97	2.00	1.04	1.01	2.03	1.48
5.0E−5	3.93	2.01	1.04	1.00	2.05	1.49
1.0E−4	3.83	2.02	1.04	0.992	2.05	1.50
2.0E−4	3.90	2.05	1.05	1.01	2.03	1.50
5.0E−4	3.74	2.06	1.04	0.992	2.02	1.48
0.001	3.77	2.06	1.03	0.992	2.02	1.47
0.002	3.81	2.06	1.01	0.964	2.01	1.47
0.005	3.72	2.07	1.02	0.987	1.99	1.47
0.01	3.61	2.09	1.02	0.991	1.99	1.48
0.02	3.65	2.12	1.02	0.991	2.02	1.49
0.03	3.69	2.15	1.03	0.988	2.05	1.51
0.05	3.84	2.21	1.06	1.01	2.12	1.55
0.07	4.02	2.27	1.10	1.05	2.20	1.60
0.1	4.28	2.35	1.17	1.11	2.33	1.69
0.15	4.77	2.49	1.29	1.23	2.57	1.86
0.2	5.33	2.64	1.43	1.36	2.82	2.04
0.3	6.45	2.94	1.73	1.65	3.36	2.41
0.5	8.83	3.62	2.42	2.34	4.48	3.21
0.7	11.2	4.37	3.16	3.09	5.62	4.04
0.9	13.5	5.21	3.94	3.86	6.78	4.90
1.0	14.6	5.66	4.35	4.27	7.37	5.34
1.2	16.8	6.65	5.23	5.16	8.58	6.24
1.5	20.1	8.26	6.62	6.57	10.4	7.62
2.0	24.8	11.1	8.97	8.94	13.4	9.92
3.0	32.7	16.6	13.5	13.4	18.9	14.3
4.0	39.1	21.7	17.6	17.4	23.8	18.3
5.0	44.1	26.4	21.4	21.1	28.1	22.0
6.0	48.3	30.5	24.8	24.5	32.0	25.3
7.0	51.8	34.2	27.9	27.5	35.4	28.2
8.0	54.9	37.5	30.7	30.2	38.4	30.9
9.0	57.8	40.5	33.2	32.7	41.2	33.3
10.0	60.4	43.2	35.5	35.0	43.6	35.5
12.0	64.8	48.0	39.7	39.2	48.0	39.4
14.0	68.2	52.0	43.4	42.8	51.5	42.7
15.0	69.5	53.8	45.0	44.5	53.0	44.1
16.0	70.7	55.4	46.6	46.0	54.4	45.5
18.0	72.5	58.3	49.4	48.8	56.8	47.9
20.0	73.9	60.7	51.8	51.3	58.9	49.9
21.0	74.4	61.8	53.0	52.5	59.8	50.9
30.0	77.9	69.0	61.0	60.2	66.0	57.5
50.0	82.0	78.1	71.7	69.9	74.1	66.9
75.0	85.1	86.4	80.8	79.1	81.3	75.6
100	86.3	93.6	88.2	87.3	87.5	83.4
130	86.6	101	95.9	95.8	94.1	91.9
150	86.9	106	101	101	98.2	97.1
180	88.0	113	107	108	104	105
200	89.0	117	111	111	108	109
300	98.8	137	130	128	127	132
400	114	158	149	147	146	152
500	132	178	169	168	164	171
600	149	198	189	189	181	188
700	164	215	206	207	196	203
800	176	229	220	222	209	216
900	185	240	231	234	221	228
1000	193	250	241	244	230	238
2000	235	308	299	298	291	313
5000	286	407	400	424	388	443
10,000	381	521	514	536	503	594

AP, antero-posterior; PA, postero-anterior; LLAT, left lateral; RLAT, right lateral; ROT, rotational; ISO, isotropic.

Table C.4. Neutrons, female: bone surface (endosteum) absorbed dose per fluence, in units of pGy cm^2, for mono-energetic particles incident in various geometries.

Energy (MeV)	AP	PA	LLAT	RLAT	ROT	ISO
1.0E−9	0.970	0.878	0.451	0.454	0.687	0.546
1.0E−8	1.09	0.978	0.511	0.518	0.825	0.657
2.5E−8	1.23	1.14	0.596	0.601	0.936	0.741
1.0E−7	1.59	1.49	0.763	0.777	1.22	0.948
2.0E−7	1.79	1.70	0.874	0.886	1.37	1.06
5.0E−7	2.00	1.94	0.988	1.000	1.56	1.20
1.0E−6	2.13	2.09	1.06	1.07	1.67	1.28
2.0E−6	2.22	2.19	1.10	1.11	1.75	1.34
5.0E−6	2.31	2.30	1.13	1.15	1.81	1.39
1.0E−5	2.34	2.33	1.13	1.16	1.83	1.40
2.0E−5	2.34	2.34	1.13	1.15	1.83	1.40
5.0E−5	2.32	2.31	1.11	1.13	1.81	1.39
1.0E−4	2.30	2.30	1.09	1.11	1.79	1.37
2.0E−4	2.26	2.30	1.08	1.10	1.74	1.33
5.0E−4	2.15	2.26	1.05	1.07	1.66	1.27
0.001	2.15	2.23	1.03	1.05	1.64	1.26
0.002	2.15	2.20	1.01	1.03	1.64	1.26
0.005	2.09	2.19	1.00	1.02	1.59	1.22
0.01	2.06	2.19	0.997	1.01	1.58	1.21
0.02	2.10	2.22	1.03	1.05	1.61	1.23
0.03	2.16	2.26	1.07	1.09	1.66	1.27
0.05	2.29	2.38	1.16	1.18	1.78	1.36
0.07	2.46	2.51	1.27	1.29	1.91	1.47
0.1	2.71	2.72	1.44	1.46	2.12	1.64
0.15	3.16	3.10	1.73	1.76	2.50	1.94
0.2	3.63	3.51	2.03	2.07	2.89	2.24
0.3	4.59	4.35	2.64	2.68	3.69	2.87
0.5	6.54	6.08	3.85	3.88	5.32	4.16
0.7	8.45	7.77	4.96	5.00	6.92	5.45
0.9	10.3	9.40	6.00	6.08	8.50	6.73
1.0	11.2	10.2	6.53	6.62	9.28	7.36
1.2	13.0	11.9	7.61	7.71	10.8	8.62
1.5	15.6	14.4	9.22	9.32	13.0	10.4
2.0	19.3	18.2	11.8	11.9	16.3	13.2
3.0	25.7	24.7	16.3	16.4	22.0	18.1
4.0	30.8	29.9	20.1	20.2	26.7	22.3
5.0	34.9	34.1	23.4	23.5	30.7	25.8
6.0	38.5	37.6	26.2	26.4	34.2	29.0
7.0	41.6	40.7	28.8	28.9	37.2	31.8
8.0	44.4	43.6	31.2	31.3	40.0	34.3
9.0	47.0	46.2	33.3	33.5	42.5	36.6
10.0	49.3	48.6	35.4	35.5	44.8	38.7
12.0	53.5	52.9	39.2	39.2	48.7	42.4
14.0	57.0	56.5	42.5	42.5	52.0	45.5
15.0	58.4	58.0	43.9	44.0	53.4	46.8
16.0	59.8	59.3	45.3	45.3	54.6	48.1
18.0	62.0	61.6	47.7	47.7	56.8	50.3
20.0	63.8	63.4	49.8	49.8	58.6	52.1
21.0	64.5	64.1	50.7	50.8	59.3	52.9
30.0	69.3	68.9	56.9	57.3	64.3	58.5
50.0	75.0	74.9	65.6	66.2	70.0	65.7
75.0	79.5	80.6	73.9	74.1	75.1	72.2
100	82.4	84.6	80.3	80.0	79.7	77.9
130	84.8	87.4	85.8	85.4	84.6	84.2
150	86.2	88.7	88.7	88.4	87.6	88.0
180	88.4	90.6	92.4	92.4	91.9	93.5
200	90.0	91.9	94.6	94.9	94.8	97.0
300	101	102	107	108	109	114
400	116	117	123	124	124	130
500	132	134	141	142	139	146
600	147	150	160	159	154	160
700	161	164	176	174	166	173
800	172	175	188	186	177	184
900	182	183	197	196	186	193
1000	189	189	204	203	193	201
2000	230	223	245	247	239	254
5000	281	279	331	330	301	338
10,000	370	368	441	437	376	436

AP, antero-posterior; PA, postero-anterior; LLAT, left lateral; RLAT, right lateral; ROT, rotational; ISO, isotropic.

Table C.5. Neutrons, female: ovaries absorbed dose per fluence, in units of pGy cm^2, for mono-energetic particles incident in various geometries.

Energy (MeV)	AP	PA	LLAT	RLAT	ROT	ISO
1.0E−9	0.935	0.950	0.218	0.215	0.578	0.375
1.0E−8	1.01	1.09	0.199	0.252	0.661	0.490
2.5E−8	1.17	1.27	0.246	0.269	0.767	0.568
1.0E−7	1.50	1.72	0.366	0.314	0.962	0.757
2.0E−7	1.70	1.98	0.385	0.388	1.10	0.866
5.0E−7	1.98	2.36	0.405	0.407	1.35	0.997
1.0E−6	2.17	2.59	0.482	0.543	1.54	1.10
2.0E−6	2.31	2.73	0.555	0.524	1.63	1.21
5.0E−6	2.44	2.86	0.523	0.579	1.69	1.30
1.0E−5	2.51	2.90	0.545	0.628	1.74	1.28
2.0E−5	2.57	3.00	0.545	0.610	1.78	1.25
5.0E−5	2.67	3.03	0.545	0.548	1.84	1.28
1.0E−4	2.73	3.01	0.594	0.507	1.87	1.28
2.0E−4	2.76	3.07	0.567	0.623	1.82	1.31
5.0E−4	2.74	3.14	0.536	0.595	1.81	1.36
0.001	2.73	3.15	0.565	0.669	1.82	1.37
0.002	2.75	3.17	0.550	0.608	1.83	1.36
0.005	2.74	3.22	0.511	0.602	1.86	1.34
0.01	2.74	3.24	0.516	0.581	1.88	1.37
0.02	2.80	3.27	0.583	0.677	1.90	1.45
0.03	2.85	3.30	0.558	0.721	1.94	1.48
0.05	2.92	3.38	0.601	0.786	2.02	1.50
0.07	2.97	3.47	0.636	0.695	2.08	1.51
0.1	3.06	3.58	0.660	0.683	2.15	1.54
0.15	3.24	3.78	0.672	0.776	2.26	1.61
0.2	3.44	4.00	0.705	0.870	2.37	1.70
0.3	3.88	4.47	0.809	0.990	2.60	1.88
0.5	4.90	5.56	0.975	1.22	3.10	2.30
0.7	6.03	6.75	1.11	1.26	3.71	2.79
0.9	7.28	8.05	1.26	1.39	4.41	3.35
1.0	7.94	8.74	1.36	1.50	4.81	3.65
1.2	9.32	10.2	1.68	1.88	5.66	4.29
1.5	11.5	12.5	2.36	2.72	7.04	5.32
2.0	15.1	16.3	3.74	4.50	9.46	7.13
3.0	21.9	23.4	6.51	7.59	14.4	10.9
4.0	27.9	29.6	9.27	10.4	19.1	14.7
5.0	33.2	34.9	12.4	13.9	23.4	18.3
6.0	37.7	39.5	15.4	17.2	27.4	21.6
7.0	41.7	43.5	18.1	20.2	30.9	24.7
8.0	45.1	47.1	20.5	22.6	34.1	27.5
9.0	48.2	50.2	22.7	24.7	36.9	30.2
10.0	50.9	53.0	24.7	26.6	39.5	32.6
12.0	55.6	57.8	28.6	30.3	43.8	37.0
14.0	59.4	61.7	32.2	34.1	47.4	41.0
15.0	61.1	63.3	33.9	35.9	48.9	42.8
16.0	62.6	64.8	35.5	37.6	50.3	44.5
18.0	65.4	67.3	38.9	41.0	52.7	47.6
20.0	67.7	69.4	42.1	44.2	54.8	50.4
21.0	68.7	70.3	43.7	45.7	55.7	51.7
30.0	75.8	76.0	55.0	54.5	61.9	60.5
50.0	84.4	82.8	65.2	65.7	70.5	71.4
75.0	91.6	87.6	75.6	73.8	79.2	79.8
100	97.6	91.4	87.6	87.4	87.6	86.8
130	104	95.5	104	97.7	97.3	94.4
150	108	98.2	114	104	103	99.2
180	114	103	125	115	111	106
200	118	106	129	119	116	111
300	136	123	142	134	138	137
400	155	142	170	152	159	163
500	173	162	201	184	179	187
600	189	181	231	230	196	209
700	204	198	254	262	211	227
800	218	213	267	267	224	242
900	229	225	275	262	235	255
1000	239	235	278	256	244	266
2000	299	287	327	303	300	337
5000	375	349	490	395	406	462
10,000	468	434	611	593	568	618

AP, antero-posterior; PA, postero-anterior; LLAT, left lateral; RLAT, right lateral; ROT, rotational; ISO, isotropic.

Table C.6. Neutrons, female: liver absorbed dose per fluence, in units of pGy cm^2, for mono-energetic particles incident in various geometries.

Energy (MeV)	AP	PA	LLAT	RLAT	ROT	ISO
1.0E−9	1.24	0.868	0.224	0.583	0.688	0.520
1.0E−8	1.43	0.983	0.241	0.665	0.846	0.638
2.5E−8	1.63	1.14	0.277	0.779	0.973	0.728
1.0E−7	2.18	1.52	0.358	1.02	1.28	0.946
2.0E−7	2.49	1.74	0.411	1.19	1.46	1.07
5.0E−7	2.85	2.02	0.479	1.39	1.69	1.24
1.0E−6	3.07	2.20	0.521	1.51	1.84	1.35
2.0E−6	3.24	2.33	0.553	1.59	1.95	1.42
5.0E−6	3.42	2.48	0.585	1.68	2.06	1.50
1.0E−5	3.50	2.54	0.597	1.70	2.10	1.53
2.0E−5	3.54	2.57	0.606	1.73	2.12	1.55
5.0E−5	3.53	2.56	0.605	1.70	2.13	1.57
1.0E−4	3.54	2.59	0.605	1.71	2.14	1.58
2.0E−4	3.50	2.62	0.609	1.72	2.12	1.56
5.0E−4	3.40	2.61	0.609	1.69	2.07	1.52
0.001	3.41	2.60	0.610	1.68	2.06	1.51
0.002	3.43	2.58	0.609	1.66	2.06	1.51
0.005	3.36	2.60	0.609	1.65	2.02	1.49
0.01	3.30	2.62	0.608	1.63	2.00	1.49
0.02	3.33	2.65	0.617	1.65	2.02	1.50
0.03	3.36	2.68	0.626	1.67	2.04	1.51
0.05	3.47	2.75	0.649	1.75	2.11	1.55
0.07	3.60	2.83	0.672	1.82	2.18	1.60
0.1	3.81	2.95	0.707	1.95	2.31	1.68
0.15	4.20	3.16	0.768	2.20	2.55	1.83
0.2	4.63	3.39	0.831	2.48	2.80	2.00
0.3	5.54	3.87	0.966	3.07	3.34	2.37
0.5	7.48	4.91	1.27	4.38	4.48	3.17
0.7	9.45	6.00	1.63	5.69	5.69	4.04
0.9	11.4	7.14	2.03	7.00	6.93	4.96
1.0	12.4	7.75	2.26	7.68	7.56	5.43
1.2	14.4	9.05	2.75	9.12	8.84	6.40
1.5	17.2	11.1	3.57	11.4	10.7	7.86
2.0	21.4	14.5	5.07	14.9	13.8	10.2
3.0	28.4	20.6	8.31	21.2	19.3	14.7
4.0	34.2	25.9	11.6	26.4	24.2	18.8
5.0	39.0	30.5	14.7	30.9	28.5	22.4
6.0	43.0	34.5	17.7	34.7	32.3	25.7
7.0	46.5	37.9	20.4	38.1	35.6	28.6
8.0	49.7	41.1	23.0	41.1	38.6	31.3
9.0	52.5	43.9	25.3	43.9	41.3	33.7
10.0	55.0	46.5	27.5	46.4	43.7	35.9
12.0	59.4	51.2	31.5	50.9	47.8	39.7
14.0	62.9	55.0	35.1	54.7	51.2	43.0
15.0	64.3	56.7	36.7	56.3	52.7	44.5
16.0	65.5	58.2	38.3	57.8	54.1	45.8
18.0	67.6	60.8	41.1	60.4	56.4	48.3
20.0	69.3	62.9	43.8	62.5	58.4	50.4
21.0	70.0	63.9	45.0	63.5	59.3	51.4
30.0	74.6	70.0	53.9	69.5	65.2	58.2
50.0	80.0	77.7	66.6	76.5	72.7	67.7
75.0	84.3	85.4	77.7	83.6	79.7	76.3
100	86.9	92.0	87.0	89.5	86.1	83.7
130	89.1	98.5	96.8	94.8	93.0	91.7
150	90.5	102	103	97.5	97.3	96.6
180	92.7	107	111	101	103	103
200	94.4	110	117	103	107	108
300	107	126	140	115	126	128
400	123	145	162	132	144	148
500	141	165	182	152	161	166
600	158	185	201	171	176	183
700	174	201	217	188	190	198
800	186	215	232	201	203	211
900	196	225	244	211	213	222
1000	204	233	255	219	223	233
2000	249	279	328	260	284	300
5000	306	360	452	333	373	410
10,000	400	461	574	442	465	532

AP, antero-posterior; PA, postero-anterior; LLAT, left lateral; RLAT, right lateral; ROT, rotational; ISO, isotropic.

Table C.7. Neutrons, female: lung absorbed dose per fluence, in units of pGy cm^2, for mono-energetic particles incident in various geometries.

Energy (MeV)	AP	PA	LLAT	RLAT	ROT	ISO
1.0E−9	1.01	1.03	0.324	0.342	0.654	0.519
1.0E−8	1.15	1.22	0.352	0.366	0.808	0.628
2.5E−8	1.31	1.42	0.406	0.424	0.928	0.716
1.0E−7	1.73	1.93	0.519	0.537	1.22	0.934
2.0E−7	1.98	2.21	0.594	0.621	1.38	1.06
5.0E−7	2.26	2.58	0.681	0.715	1.60	1.23
1.0E−6	2.44	2.80	0.742	0.769	1.74	1.33
2.0E−6	2.58	2.94	0.785	0.804	1.84	1.41
5.0E−6	2.73	3.11	0.824	0.850	1.94	1.48
1.0E−5	2.80	3.19	0.829	0.861	1.99	1.51
2.0E−5	2.83	3.22	0.846	0.876	2.01	1.53
5.0E−5	2.84	3.20	0.847	0.871	2.02	1.54
1.0E−4	2.84	3.21	0.844	0.873	2.01	1.53
2.0E−4	2.80	3.21	0.844	0.879	1.99	1.52
5.0E−4	2.71	3.17	0.833	0.864	1.93	1.48
0.001	2.73	3.15	0.833	0.864	1.92	1.47
0.002	2.75	3.11	0.823	0.852	1.91	1.46
0.005	2.69	3.10	0.827	0.845	1.88	1.44
0.01	2.63	3.10	0.829	0.835	1.85	1.43
0.02	2.65	3.11	0.834	0.850	1.85	1.42
0.03	2.68	3.15	0.838	0.855	1.87	1.43
0.05	2.75	3.26	0.861	0.880	1.93	1.47
0.07	2.84	3.39	0.895	0.915	2.00	1.52
0.1	2.98	3.62	0.945	0.967	2.13	1.61
0.15	3.27	4.05	1.03	1.06	2.37	1.79
0.2	3.61	4.53	1.12	1.17	2.63	1.99
0.3	4.34	5.58	1.32	1.39	3.21	2.42
0.5	5.99	7.80	1.76	1.90	4.49	3.39
0.7	7.76	9.96	2.25	2.46	5.85	4.43
0.9	9.58	12.0	2.78	3.06	7.25	5.54
1.0	10.5	13.1	3.07	3.38	7.96	6.11
1.2	12.4	15.2	3.72	4.08	9.40	7.27
1.5	15.1	18.3	4.80	5.21	11.5	9.01
2.0	19.2	23.0	6.73	7.20	14.8	11.8
3.0	26.1	30.6	10.6	11.1	20.8	16.9
4.0	31.8	36.7	14.2	14.7	25.9	21.4
5.0	36.5	41.5	17.7	18.1	30.3	25.4
6.0	40.5	45.5	20.8	21.1	34.2	28.9
7.0	43.9	49.0	23.6	23.8	37.6	32.0
8.0	47.0	52.0	26.1	26.3	40.5	34.8
9.0	49.8	54.8	28.4	28.6	43.2	37.3
10.0	52.4	57.4	30.6	30.6	45.6	39.6
12.0	56.8	61.8	34.4	34.4	49.6	43.5
14.0	60.3	65.2	37.8	37.6	52.9	46.9
15.0	61.8	66.6	39.3	39.1	54.3	48.4
16.0	63.1	67.8	40.8	40.6	55.6	49.7
18.0	65.3	69.8	43.5	43.1	57.8	52.1
20.0	67.1	71.3	45.9	45.5	59.7	54.2
21.0	67.8	71.9	47.0	46.5	60.5	55.2
30.0	72.7	75.6	54.9	54.2	66.0	61.5
50.0	78.9	80.1	66.0	65.2	73.0	69.9
75.0	84.3	84.5	76.1	75.3	79.3	77.3
100	87.9	87.2	84.6	83.4	84.8	83.9
130	90.5	88.8	93.1	91.5	90.6	90.9
150	91.9	89.5	97.7	96.0	94.1	95.2
180	93.7	90.9	103	102	99.1	101
200	95.0	92.1	107	105	102	105
300	105	103	120	119	118	122
400	121	119	136	136	134	139
500	138	137	154	154	149	154
600	155	154	172	172	163	169
700	171	168	189	188	175	181
800	183	179	202	200	186	193
900	193	187	213	210	195	202
1000	201	193	221	219	203	211
2000	243	227	274	265	254	268
5000	292	280	378	360	326	359
10,000	390	364	488	478	401	457

AP, antero-posterior; PA, postero-anterior; LLAT, left lateral; RLAT, right lateral; ROT, rotational; ISO, isotropic.

Table C.8. Neutrons, female: oesophagus absorbed dose per fluence, in units of pGy cm^2, for mono-energetic particles incident in various geometries.

Energy (MeV)	AP	PA	LLAT	RLAT	ROT	ISO
1.0E−9	1.04	0.922	0.328	0.320	0.664	0.520
1.0E−8	1.22	1.12	0.380	0.331	0.820	0.621
2.5E−8	1.38	1.30	0.427	0.393	0.943	0.706
1.0E−7	1.85	1.74	0.519	0.506	1.24	0.919
2.0E−7	2.12	2.02	0.601	0.582	1.39	1.04
5.0E−7	2.44	2.38	0.710	0.675	1.61	1.20
1.0E−6	2.65	2.62	0.778	0.741	1.76	1.30
2.0E−6	2.75	2.81	0.823	0.781	1.86	1.39
5.0E−6	2.84	3.01	0.881	0.836	1.97	1.46
1.0E−5	2.98	3.11	0.908	0.853	2.02	1.52
2.0E−5	3.10	3.14	0.898	0.862	2.07	1.56
5.0E−5	3.12	3.14	0.882	0.869	2.12	1.60
1.0E−4	3.11	3.19	0.906	0.878	2.12	1.62
2.0E−4	3.07	3.23	0.913	0.883	2.08	1.61
5.0E−4	3.00	3.22	0.893	0.879	2.03	1.57
0.001	3.00	3.21	0.904	0.870	2.03	1.57
0.002	3.07	3.21	0.919	0.864	2.02	1.57
0.005	2.97	3.23	0.906	0.873	2.00	1.54
0.01	2.91	3.24	0.904	0.880	1.98	1.50
0.02	2.96	3.26	0.931	0.900	2.01	1.49
0.03	3.01	3.28	0.934	0.903	2.04	1.50
0.05	3.12	3.34	0.936	0.904	2.11	1.55
0.07	3.23	3.41	0.965	0.918	2.18	1.59
0.1	3.40	3.53	1.01	0.948	2.27	1.67
0.15	3.76	3.74	1.09	1.02	2.44	1.81
0.2	4.15	3.99	1.15	1.09	2.64	1.97
0.3	4.94	4.55	1.29	1.27	3.10	2.30
0.5	6.68	5.83	1.61	1.67	4.16	3.04
0.7	8.53	7.23	1.98	2.10	5.32	3.86
0.9	10.4	8.72	2.43	2.58	6.54	4.76
1.0	11.4	9.49	2.68	2.85	7.18	5.23
1.2	13.4	11.1	3.25	3.42	8.50	6.21
1.5	16.3	13.5	4.24	4.38	10.5	7.72
2.0	20.7	17.5	6.07	6.12	13.7	10.2
3.0	28.3	24.7	10.0	9.76	19.7	15.1
4.0	34.5	30.7	13.9	13.3	25.0	19.5
5.0	39.5	35.7	17.5	16.7	29.7	23.4
6.0	43.6	39.9	20.8	19.8	33.7	26.9
7.0	47.1	43.6	23.8	22.6	37.2	30.1
8.0	50.3	46.7	26.5	25.2	40.3	32.9
9.0	53.2	49.6	28.9	27.6	43.0	35.5
10.0	55.9	52.1	31.2	29.7	45.5	37.8
12.0	60.6	56.4	35.2	33.7	49.8	41.8
14.0	64.4	59.8	38.7	37.1	53.3	45.2
15.0	66.0	61.2	40.3	38.7	54.7	46.7
16.0	67.3	62.5	41.8	40.2	56.1	48.1
18.0	69.5	64.6	44.7	42.9	58.4	50.6
20.0	71.1	66.4	47.2	45.4	60.4	52.7
21.0	71.8	67.1	48.4	46.5	61.2	53.7
30.0	75.7	72.0	57.4	54.8	66.8	60.5
50.0	80.7	78.1	70.0	66.5	74.4	69.8
75.0	86.5	84.3	80.1	75.6	81.7	78.1
100	91.2	89.9	88.2	82.5	88.0	85.2
130	95.0	95.8	96.9	89.7	94.8	93.0
150	97.0	99.4	102	94.4	98.8	97.7
180	99.8	104	108	101	104	105
200	101	108	112	105	108	109
300	112	123	128	126	124	129
400	128	139	145	146	140	149
500	146	154	162	165	156	166
600	165	169	180	183	172	183
700	181	181	197	198	186	197
800	195	192	211	210	199	210
900	206	201	222	221	210	220
1000	215	209	232	230	219	230
2000	258	258	289	285	276	291
5000	304	332	381	377	357	385
10,000	415	411	493	518	434	480

AP, antero-posterior; PA, postero-anterior; LLAT, left lateral; RLAT, right lateral; ROT, rotational; ISO, isotropic.

Table C.9. Neutrons, female: red (active) bone marrow absorbed dose per fluence, in units of pGy cm^2, for mono-energetic particles incident in various geometries.

Energy (MeV)	AP	PA	LLAT	RLAT	ROT	ISO
1.0E−9	0.928	1.01	0.353	0.367	0.651	0.507
1.0E−8	1.06	1.16	0.394	0.408	0.789	0.614
2.5E−8	1.20	1.36	0.458	0.474	0.901	0.705
1.0E−7	1.58	1.83	0.587	0.608	1.18	0.911
2.0E−7	1.79	2.11	0.674	0.696	1.35	1.03
5.0E−7	2.04	2.45	0.769	0.800	1.56	1.18
1.0E−6	2.19	2.66	0.832	0.864	1.69	1.27
2.0E−6	2.32	2.80	0.870	0.909	1.78	1.35
5.0E−6	2.44	2.99	0.918	0.954	1.86	1.41
1.0E−5	2.50	3.04	0.931	0.967	1.91	1.44
2.0E−5	2.53	3.08	0.940	0.977	1.93	1.45
5.0E−5	2.54	3.05	0.933	0.970	1.94	1.46
1.0E−4	2.54	3.06	0.930	0.970	1.94	1.46
2.0E−4	2.53	3.08	0.933	0.971	1.91	1.45
5.0E−4	2.47	3.06	0.920	0.959	1.86	1.42
0.001	2.47	3.04	0.914	0.955	1.86	1.41
0.002	2.48	3.00	0.904	0.948	1.86	1.41
0.005	2.45	3.00	0.907	0.937	1.83	1.39
0.01	2.44	3.00	0.913	0.924	1.82	1.38
0.02	2.48	3.03	0.930	0.954	1.85	1.39
0.03	2.52	3.08	0.946	0.981	1.88	1.42
0.05	2.63	3.19	0.995	1.03	1.95	1.48
0.07	2.75	3.31	1.05	1.09	2.04	1.55
0.1	2.92	3.50	1.14	1.18	2.17	1.65
0.15	3.23	3.84	1.29	1.33	2.40	1.83
0.2	3.54	4.21	1.43	1.49	2.65	2.02
0.3	4.19	5.00	1.73	1.80	3.17	2.41
0.5	5.55	6.65	2.34	2.41	4.25	3.25
0.7	6.95	8.27	2.94	3.04	5.39	4.13
0.9	8.39	9.85	3.54	3.68	6.57	5.05
1.0	9.13	10.7	3.86	4.02	7.17	5.53
1.2	10.6	12.3	4.56	4.75	8.40	6.49
1.5	12.8	14.9	5.69	5.91	10.2	7.93
2.0	16.3	18.8	7.64	7.89	13.1	10.3
3.0	22.4	25.6	11.4	11.7	18.4	14.6
4.0	27.6	31.0	14.8	15.2	23.1	18.5
5.0	32.0	35.4	18.0	18.4	27.1	22.0
6.0	35.7	39.1	20.9	21.3	30.7	25.2
7.0	39.0	42.4	23.5	23.9	33.9	28.0
8.0	42.0	45.3	25.9	26.3	36.7	30.5
9.0	44.7	48.1	28.0	28.5	39.3	32.9
10.0	47.2	50.6	30.1	30.5	41.7	35.0
12.0	51.6	55.1	33.9	34.3	45.8	38.8
14.0	55.2	58.8	37.3	37.7	49.2	42.1
15.0	56.8	60.3	38.8	39.2	50.7	43.6
16.0	58.2	61.7	40.3	40.7	52.0	44.9
18.0	60.6	64.0	43.1	43.3	54.4	47.3
20.0	62.6	65.7	45.5	45.7	56.4	49.4
21.0	63.5	66.5	46.5	46.8	57.3	50.3
30.0	69.2	71.0	54.3	54.6	63.1	56.8
50.0	76.1	77.0	64.8	65.4	70.6	65.7
75.0	82.2	83.5	74.8	75.1	77.7	74.2
100	87.1	88.3	83.6	83.3	84.2	82.0
130	92.1	92.3	92.4	91.6	91.3	90.7
150	95.2	94.2	97.3	96.5	95.6	95.9
180	99.5	96.7	103	103	102	103
200	102	98.4	107	107	105	108
300	118	110	123	124	123	129
400	135	128	142	143	141	148
500	154	147	163	163	159	166
600	172	165	184	183	175	183
700	187	181	202	200	189	198
800	201	193	216	214	202	210
900	212	202	227	225	212	222
1000	221	209	236	234	222	231
2000	274	247	286	288	278	295
5000	344	312	392	392	359	402
10,000	444	407	513	510	455	527

AP, antero-posterior; PA, postero-anterior; LLAT, left lateral; RLAT, right lateral; ROT, rotational; ISO, isotropic.

Table C.10. Neutrons, female: remainder tissues absorbed dose per fluence, in units of pGy cm^2, for mono-energetic particles incident in various geometries.

Energy (MeV)	AP	PA	LLAT	RLAT	ROT	ISO
1.0E−9	1.13	0.846	0.397	0.353	0.674	0.515
1.0E−8	1.31	0.968	0.464	0.400	0.816	0.621
2.5E−8	1.48	1.13	0.535	0.464	0.936	0.709
1.0E−7	1.95	1.50	0.700	0.601	1.22	0.923
2.0E−7	2.21	1.72	0.795	0.695	1.39	1.05
5.0E−7	2.52	2.00	0.916	0.808	1.61	1.20
1.0E−6	2.71	2.18	1.00	0.874	1.75	1.30
2.0E−6	2.87	2.32	1.06	0.918	1.85	1.37
5.0E−6	3.02	2.47	1.12	0.973	1.96	1.45
1.0E−5	3.07	2.53	1.14	0.989	2.00	1.48
2.0E−5	3.09	2.57	1.16	1.00	2.02	1.48
5.0E−5	3.10	2.56	1.16	1.00	2.03	1.49
1.0E−4	3.09	2.58	1.15	1.00	2.03	1.49
2.0E−4	3.07	2.60	1.15	1.01	2.01	1.48
5.0E−4	2.99	2.60	1.14	1.01	1.96	1.45
0.001	3.00	2.59	1.13	1.000	1.94	1.45
0.002	3.01	2.57	1.12	0.987	1.94	1.44
0.005	2.95	2.59	1.11	0.984	1.93	1.42
0.01	2.92	2.60	1.12	0.985	1.92	1.42
0.02	2.97	2.63	1.14	1.00	1.94	1.43
0.03	3.02	2.66	1.16	1.02	1.97	1.45
0.05	3.14	2.74	1.22	1.07	2.05	1.51
0.07	3.29	2.83	1.29	1.12	2.13	1.57
0.1	3.50	2.97	1.38	1.21	2.27	1.67
0.15	3.90	3.20	1.55	1.36	2.51	1.85
0.2	4.33	3.46	1.74	1.51	2.76	2.03
0.3	5.21	4.00	2.12	1.85	3.31	2.43
0.5	7.06	5.19	2.96	2.55	4.49	3.27
0.7	8.92	6.44	3.83	3.29	5.74	4.18
0.9	10.8	7.73	4.73	4.07	7.04	5.13
1.0	11.7	8.41	5.20	4.48	7.70	5.62
1.2	13.6	9.83	6.19	5.34	9.04	6.62
1.5	16.2	12.0	7.73	6.69	11.0	8.13
2.0	20.2	15.6	10.3	8.99	14.2	10.6
3.0	27.2	22.2	15.2	13.4	20.0	15.2
4.0	33.0	27.8	19.6	17.5	25.2	19.5
5.0	37.7	32.7	23.6	21.2	29.6	23.2
6.0	41.8	36.8	27.2	24.6	33.5	26.6
7.0	45.3	40.5	30.4	27.6	37.0	29.6
8.0	48.4	43.7	33.2	30.3	40.1	32.3
9.0	51.2	46.6	35.8	32.8	42.8	34.8
10.0	53.8	49.3	38.2	35.1	45.3	37.0
12.0	58.1	53.9	42.4	39.1	49.6	41.0
14.0	61.6	57.7	46.0	42.7	53.1	44.3
15.0	63.0	59.3	47.6	44.2	54.6	45.7
16.0	64.3	60.8	49.1	45.7	55.9	47.1
18.0	66.4	63.2	51.7	48.4	58.3	49.5
20.0	68.1	65.3	54.0	50.8	60.2	51.6
21.0	68.9	66.2	55.0	51.9	61.1	52.5
30.0	73.6	72.0	62.1	59.4	66.8	59.1
50.0	79.2	79.3	71.8	69.7	73.6	68.3
75.0	83.8	85.8	80.4	78.8	80.0	76.6
100	87.2	91.0	87.4	86.4	86.0	83.8
130	90.4	96.2	94.4	94.3	92.8	91.6
150	92.3	99.4	98.5	99.0	97.0	96.5
180	95.2	104	104	106	103	104
200	97.2	107	108	110	107	108
300	110	123	125	128	125	129
400	126	142	143	147	143	148
500	143	160	162	167	160	166
600	160	178	180	185	176	182
700	175	192	196	201	190	196
800	187	204	209	214	201	209
900	197	214	220	225	212	220
1000	206	222	229	234	221	230
2000	253	270	284	288	278	295
5000	310	346	382	383	361	402
10,000	399	442	489	500	450	526

AP, antero-posterior; PA, postero-anterior; LLAT, left lateral; RLAT, right lateral; ROT, rotational; ISO, isotropic.

Table C.11. Neutrons, female: salivary glands absorbed dose per fluence, in units of pGy cm^2, for mono-energetic particles incident in various geometries.

Energy (MeV)	AP	PA	LLAT	RLAT	ROT	ISO
1.0E−9	0.971	0.638	0.906	0.904	0.836	0.612
1.0E−8	1.01	0.689	1.05	1.10	0.980	0.749
2.5E−8	1.12	0.779	1.23	1.24	1.11	0.849
1.0E−7	1.39	1.01	1.60	1.56	1.41	1.06
2.0E−7	1.56	1.16	1.78	1.76	1.57	1.17
5.0E−7	1.69	1.33	1.96	1.97	1.75	1.30
1.0E−6	1.80	1.47	2.03	2.05	1.84	1.38
2.0E−6	1.85	1.55	2.02	2.09	1.91	1.43
5.0E−6	1.91	1.64	2.10	2.13	1.97	1.46
1.0E−5	1.94	1.66	2.09	2.13	1.98	1.46
2.0E−5	1.98	1.66	2.05	2.10	1.97	1.45
5.0E−5	1.95	1.62	1.95	2.04	1.95	1.43
1.0E−4	1.92	1.61	1.92	2.02	1.91	1.42
2.0E−4	1.88	1.62	1.91	1.98	1.84	1.39
5.0E−4	1.80	1.59	1.82	1.90	1.76	1.32
0.001	1.78	1.58	1.78	1.85	1.72	1.29
0.002	1.80	1.56	1.76	1.80	1.70	1.28
0.005	1.70	1.54	1.74	1.83	1.66	1.24
0.01	1.61	1.52	1.71	1.89	1.66	1.23
0.02	1.65	1.55	1.86	1.97	1.73	1.28
0.03	1.69	1.60	2.05	2.08	1.83	1.36
0.05	1.76	1.70	2.39	2.37	2.05	1.52
0.07	1.86	1.82	2.74	2.70	2.29	1.68
0.1	2.01	2.01	3.27	3.19	2.66	1.93
0.15	2.31	2.39	4.10	3.99	3.27	2.35
0.2	2.68	2.80	4.87	4.75	3.87	2.77
0.3	3.48	3.69	6.32	6.18	5.07	3.60
0.5	5.27	5.60	9.01	8.79	7.39	5.23
0.7	7.21	7.53	11.4	11.1	9.62	6.81
0.9	9.19	9.43	13.5	13.3	11.7	8.35
1.0	10.2	10.4	14.5	14.3	12.8	9.10
1.2	12.2	12.4	16.4	16.2	14.7	10.6
1.5	15.1	15.4	19.1	18.9	17.5	12.6
2.0	19.3	20.0	23.1	22.8	21.6	15.8
3.0	26.4	27.8	29.9	29.5	28.4	21.3
4.0	32.1	33.9	35.3	34.9	34.0	25.9
5.0	36.8	38.8	39.7	39.3	38.7	29.9
6.0	40.7	42.8	43.4	43.1	42.6	33.3
7.0	44.1	46.3	46.6	46.4	46.1	36.3
8.0	47.1	49.5	49.6	49.4	49.0	39.0
9.0	49.9	52.4	52.3	52.1	51.7	41.4
10.0	52.3	55.1	54.8	54.6	54.0	43.5
12.0	56.6	59.8	59.2	58.8	57.9	47.0
14.0	60.1	63.7	62.8	62.3	60.9	49.9
15.0	61.5	65.3	64.2	63.7	62.1	51.2
16.0	62.8	66.7	65.5	65.0	63.2	52.3
18.0	64.9	69.0	67.6	67.2	64.9	54.3
20.0	66.7	70.8	69.2	68.9	66.3	56.0
21.0	67.4	71.5	69.8	69.6	66.8	56.7
30.0	72.4	75.7	73.5	73.6	70.1	62.1
50.0	78.4	81.3	77.9	77.3	73.1	69.2
75.0	82.3	86.7	82.5	79.5	76.2	75.1
100	83.3	89.3	84.4	80.9	79.3	80.0
130	83.3	89.8	84.8	82.4	83.0	85.1
150	83.4	90.0	85.1	83.7	85.3	88.1
180	84.2	90.9	86.0	86.1	88.9	92.3
200	85.0	91.9	87.1	87.9	91.4	95.0
300	93.2	102	97.3	99.6	104	109
400	106	117	112	114	117	122
500	120	133	127	129	130	136
600	134	148	142	143	143	149
700	146	161	155	155	153	160
800	156	171	167	165	163	170
900	164	179	176	173	171	179
1000	171	185	183	180	178	186
2000	206	217	217	225	222	236
5000	244	258	264	293	271	311
10,000	332	363	379	382	310	397

AP, antero-posterior; PA, postero-anterior; LLAT, left lateral; RLAT, right lateral; ROT, rotational; ISO, isotropic.

Table C.12. Neutrons, female: skin absorbed dose per fluence, in units of pGy cm^2, for mono-energetic particles incident in various geometries.

Energy (MeV)	AP	PA	LLAT	RLAT	ROT	ISO
1.0E−9	1.73	1.85	0.826	0.825	1.28	1.02
1.0E−8	1.43	1.46	0.648	0.647	1.11	0.880
2.5E−8	1.43	1.52	0.666	0.664	1.09	0.862
1.0E−7	1.50	1.57	0.663	0.661	1.15	0.897
2.0E−7	1.61	1.71	0.708	0.705	1.20	0.926
5.0E−7	1.62	1.73	0.722	0.720	1.25	0.960
1.0E−6	1.64	1.79	0.750	0.744	1.27	0.978
2.0E−6	1.66	1.79	0.746	0.739	1.29	0.992
5.0E−6	1.68	1.86	0.760	0.755	1.29	0.991
1.0E−5	1.65	1.81	0.738	0.736	1.27	0.973
2.0E−5	1.64	1.82	0.733	0.728	1.25	0.954
5.0E−5	1.57	1.70	0.688	0.680	1.22	0.927
1.0E−4	1.54	1.66	0.677	0.668	1.19	0.906
2.0E−4	1.52	1.69	0.680	0.674	1.15	0.879
5.0E−4	1.42	1.60	0.649	0.646	1.09	0.832
0.001	1.44	1.60	0.654	0.648	1.09	0.833
0.002	1.48	1.60	0.657	0.648	1.12	0.869
0.005	1.57	1.71	0.726	0.720	1.20	0.945
0.01	1.75	1.89	0.829	0.824	1.37	1.10
0.02	2.18	2.30	1.06	1.06	1.73	1.43
0.03	2.58	2.67	1.26	1.27	2.06	1.74
0.05	3.31	3.36	1.65	1.66	2.67	2.30
0.07	3.97	4.00	2.01	2.02	3.22	2.81
0.1	4.84	4.82	2.48	2.49	3.94	3.48
0.15	6.06	5.99	3.15	3.17	4.97	4.43
0.2	7.11	7.00	3.75	3.76	5.85	5.25
0.3	8.87	8.70	4.77	4.79	7.37	6.66
0.5	11.8	11.5	6.49	6.52	9.89	8.99
0.7	14.3	13.9	8.03	8.08	12.1	11.0
0.9	16.6	16.1	9.45	9.52	14.0	12.8
1.0	17.7	17.1	10.1	10.2	14.9	13.6
1.2	19.5	18.8	11.3	11.4	16.5	15.2
1.5	21.8	21.0	13.0	13.1	18.7	17.1
2.0	25.1	24.3	15.6	15.7	21.7	20.0
3.0	30.8	30.2	20.1	20.2	27.0	24.8
4.0	35.7	35.0	23.9	24.1	31.4	28.8
5.0	39.6	38.9	27.2	27.5	35.2	32.3
6.0	42.9	42.1	30.1	30.4	38.4	35.3
7.0	45.9	45.0	32.8	33.0	41.3	38.1
8.0	48.6	47.7	35.2	35.4	43.9	40.5
9.0	51.1	50.2	37.4	37.7	46.3	42.8
10.0	53.5	52.6	39.5	39.7	48.3	44.8
12.0	57.5	56.6	43.1	43.4	51.7	48.1
14.0	60.4	59.6	46.0	46.3	54.1	50.6
15.0	61.5	60.6	47.2	47.6	55.0	51.5
16.0	62.4	61.5	48.3	48.7	55.7	52.2
18.0	63.5	62.5	50.1	50.5	56.5	53.2
20.0	64.0	62.9	51.4	51.9	56.9	53.7
21.0	64.1	63.0	52.0	52.4	57.0	53.8
30.0	64.2	63.0	55.4	55.9	56.6	54.0
50.0	63.9	63.4	59.7	60.0	55.2	53.6
75.0	64.2	64.5	62.9	63.1	55.8	55.1
100	63.2	63.6	64.1	64.4	57.9	57.7
130	62.3	62.0	64.5	64.9	61.0	61.3
150	62.4	61.7	65.3	65.8	63.1	63.7
180	63.6	62.3	67.3	67.8	66.2	67.2
200	64.7	63.2	68.9	69.4	68.3	69.6
300	73.4	70.6	78.5	79.0	79.2	81.4
400	84.8	81.6	90.7	91.0	90.5	93.3
500	96.9	93.6	104	104	102	105
600	109	105	116	117	112	116
700	119	115	127	128	121	125
800	128	123	136	137	129	133
900	134	128	144	144	135	140
1000	140	133	149	149	140	145
2000	170	157	182	182	172	181
5000	205	197	245	245	219	243
10,000	280	272	338	339	277	317

AP, antero-posterior; PA, postero-anterior; LLAT, left lateral; RLAT, right lateral; ROT, rotational; ISO, isotropic.

Table C.13. Neutrons, female: stomach wall absorbed dose per fluence, in units of pGy cm^2, for mono-energetic particles incident in various geometries.

Energy (MeV)	AP	PA	LLAT	RLAT	ROT	ISO
1.0E−9	1.33	0.724	0.695	0.177	0.685	0.509
1.0E−8	1.55	0.792	0.798	0.173	0.840	0.629
2.5E−8	1.79	0.932	0.954	0.204	0.967	0.714
1.0E−7	2.37	1.23	1.26	0.266	1.27	0.924
2.0E−7	2.70	1.40	1.46	0.304	1.45	1.05
5.0E−7	3.10	1.62	1.69	0.354	1.68	1.24
1.0E−6	3.32	1.77	1.85	0.378	1.83	1.36
2.0E−6	3.50	1.88	1.96	0.392	1.94	1.42
5.0E−6	3.67	2.01	2.05	0.416	2.03	1.48
1.0E−5	3.76	2.07	2.07	0.431	2.07	1.52
2.0E−5	3.79	2.10	2.09	0.437	2.09	1.54
5.0E−5	3.78	2.10	2.08	0.441	2.11	1.55
1.0E−4	3.76	2.11	2.08	0.449	2.10	1.54
2.0E−4	3.69	2.13	2.08	0.452	2.08	1.52
5.0E−4	3.57	2.14	2.03	0.447	2.03	1.49
0.001	3.59	2.15	2.02	0.448	2.02	1.49
0.002	3.63	2.14	2.01	0.446	2.02	1.49
0.005	3.54	2.17	2.01	0.444	1.98	1.47
0.01	3.46	2.18	2.01	0.450	1.97	1.45
0.02	3.48	2.22	2.00	0.456	1.97	1.46
0.03	3.52	2.24	2.01	0.463	1.99	1.47
0.05	3.65	2.30	2.09	0.480	2.06	1.51
0.07	3.82	2.36	2.19	0.495	2.14	1.57
0.1	4.07	2.44	2.37	0.514	2.29	1.66
0.15	4.57	2.58	2.75	0.548	2.55	1.84
0.2	5.11	2.73	3.17	0.583	2.83	2.04
0.3	6.24	3.03	4.07	0.657	3.41	2.44
0.5	8.62	3.73	5.95	0.830	4.63	3.31
0.7	11.0	4.53	7.84	1.05	5.90	4.23
0.9	13.3	5.43	9.71	1.32	7.20	5.19
1.0	14.4	5.92	10.7	1.48	7.86	5.68
1.2	16.6	7.01	12.6	1.84	9.19	6.67
1.5	19.7	8.78	15.4	2.51	11.1	8.17
2.0	24.1	11.9	19.9	3.82	14.3	10.6
3.0	31.6	17.8	27.3	6.89	20.0	15.2
4.0	37.6	23.1	33.3	10.1	25.0	19.3
5.0	42.5	27.7	38.3	13.4	29.3	23.1
6.0	46.6	31.9	42.4	16.5	33.2	26.4
7.0	50.2	35.5	46.1	19.3	36.6	29.4
8.0	53.3	38.8	49.3	22.0	39.6	32.1
9.0	56.1	41.7	52.2	24.4	42.4	34.6
10.0	58.7	44.4	54.9	26.7	44.8	36.9
12.0	62.9	49.2	59.5	30.8	49.0	40.9
14.0	66.3	53.3	63.3	34.4	52.4	44.3
15.0	67.6	55.1	64.8	36.1	53.9	45.8
16.0	68.8	56.7	66.3	37.7	55.3	47.2
18.0	70.7	59.5	68.6	40.7	57.6	49.7
20.0	72.2	61.9	70.6	43.4	59.6	51.9
21.0	72.9	63.0	71.4	44.7	60.5	52.9
30.0	76.8	70.1	76.4	54.0	66.4	59.9
50.0	81.2	78.6	81.7	67.6	73.8	69.3
75.0	84.0	86.1	85.9	79.6	80.4	77.8
100	85.4	92.7	88.9	89.4	86.4	85.1
130	86.5	99.4	91.6	99.7	93.0	92.9
150	87.4	103	93.3	106	97.2	97.7
180	89.2	109	96.2	114	103	104
200	90.7	113	98.3	120	107	109
300	102	131	111	143	125	130
400	117	151	127	166	142	149
500	133	171	144	187	158	168
600	150	191	161	207	173	185
700	164	208	175	224	186	200
800	175	221	187	240	198	213
900	185	233	197	252	209	224
1000	192	242	205	263	218	234
2000	232	297	245	331	279	302
5000	277	383	313	452	370	414
10,000	361	486	407	578	462	544

AP, antero-posterior; PA, postero-anterior; LLAT, left lateral; RLAT, right lateral; ROT, rotational; ISO, isotropic.

Table C.14. Neutrons, female: thyroid absorbed dose per fluence, in units of pGy cm^2, for mono-energetic particles incident in various geometries.

Energy (MeV)	AP	PA	LLAT	RLAT	ROT	ISO
1.0E−9	1.66	0.671	0.395	0.504	0.816	0.561
1.0E−8	2.02	0.665	0.398	0.540	0.955	0.755
2.5E−8	2.32	0.820	0.457	0.574	1.07	0.805
1.0E−7	2.93	1.12	0.590	0.715	1.40	1.000
2.0E−7	3.31	1.28	0.670	0.855	1.61	1.11
5.0E−7	3.60	1.46	0.763	0.999	1.84	1.28
1.0E−6	3.74	1.64	0.802	1.04	1.95	1.41
2.0E−6	3.81	1.76	0.824	1.05	2.02	1.52
5.0E−6	3.88	1.88	0.848	1.11	2.08	1.57
1.0E−5	3.85	1.90	0.871	1.14	2.08	1.58
2.0E−5	3.83	1.95	0.898	1.14	2.05	1.59
5.0E−5	3.80	1.99	0.904	1.11	2.05	1.53
1.0E−4	3.68	1.97	0.894	1.13	2.04	1.50
2.0E−4	3.48	1.98	0.885	1.11	1.98	1.49
5.0E−4	3.17	1.97	0.876	1.06	1.85	1.46
0.001	3.17	1.99	0.876	1.09	1.79	1.42
0.002	3.23	1.96	0.859	1.10	1.77	1.38
0.005	3.11	1.96	0.820	1.13	1.76	1.32
0.01	3.08	2.04	0.806	1.19	1.78	1.31
0.02	3.27	2.04	0.847	1.17	1.84	1.34
0.03	3.49	2.05	0.865	1.13	1.93	1.39
0.05	4.03	2.08	0.872	1.09	2.13	1.51
0.07	4.63	2.11	0.874	1.10	2.33	1.65
0.1	5.53	2.15	0.877	1.15	2.63	1.85
0.15	7.01	2.20	0.903	1.29	3.15	2.19
0.2	8.42	2.30	0.949	1.43	3.67	2.54
0.3	11.0	2.57	1.06	1.73	4.70	3.24
0.5	15.7	3.18	1.31	2.31	6.67	4.60
0.7	19.6	3.89	1.59	2.85	8.54	5.91
0.9	23.1	4.70	1.91	3.41	10.3	7.19
1.0	24.6	5.18	2.08	3.71	11.2	7.82
1.2	27.4	6.28	2.46	4.35	12.8	9.06
1.5	30.8	8.17	3.10	5.38	15.1	10.8
2.0	35.5	11.4	4.30	7.18	18.5	13.6
3.0	43.0	17.5	6.96	10.8	24.3	18.6
4.0	48.7	22.8	9.67	14.2	29.2	22.9
5.0	53.2	27.3	12.3	17.4	33.4	26.8
6.0	56.9	31.1	14.8	20.3	37.0	30.2
7.0	60.1	34.6	17.2	22.9	40.2	33.2
8.0	63.1	37.6	19.3	25.3	43.0	36.0
9.0	65.9	40.4	21.3	27.5	45.5	38.5
10.0	68.4	43.0	23.2	29.5	47.8	40.8
12.0	72.6	47.6	26.5	33.0	51.7	44.8
14.0	75.7	51.3	29.4	36.0	54.8	48.3
15.0	76.8	52.9	30.8	37.4	56.2	49.8
16.0	77.8	54.4	32.1	38.6	57.4	51.2
18.0	79.3	56.9	34.5	40.8	59.5	53.7
20.0	80.3	59.0	36.8	42.7	61.3	55.8
21.0	80.7	59.9	37.8	43.6	62.0	56.8
30.0	82.3	66.6	45.8	50.1	66.6	63.2
50.0	81.6	73.8	58.2	60.7	70.6	71.1
75.0	78.1	81.3	69.2	70.7	73.8	76.8
100	73.4	89.1	77.6	77.8	77.3	81.3
130	69.5	97.1	85.6	84.3	82.0	86.3
150	68.4	100	90.3	87.8	85.2	89.7
180	68.7	103	96.4	92.6	90.0	94.8
200	69.6	104	100	95.6	93.2	98.3
300	79.1	113	117	110	109	115
400	93.2	128	132	125	124	132
500	109	148	147	140	138	147
600	124	168	160	155	151	160
700	136	186	172	167	162	172
800	144	200	182	177	172	181
900	151	210	191	185	181	190
1000	156	218	198	193	188	197
2000	182	260	239	238	236	245
5000	205	345	324	330	300	333
10,000	282	434	445	418	366	445

AP, antero-posterior; PA, postero-anterior; LLAT, left lateral; RLAT, right lateral; ROT, rotational; ISO, isotropic.

Table C.15. Neutrons, female: UB (urinary bladder) wall absorbed dose per fluence, in units of pGy cm^2, for mono-energetic particles incident in various geometries.

Energy (MeV)	AP	PA	LLAT	RLAT	ROT	ISO
1.0E−9	1.64	0.584	0.211	0.207	0.659	0.481
1.0E−8	1.91	0.635	0.216	0.221	0.813	0.615
2.5E−8	2.22	0.734	0.254	0.255	0.932	0.698
1.0E−7	2.96	0.956	0.314	0.318	1.23	0.899
2.0E−7	3.41	1.11	0.362	0.361	1.38	1.01
5.0E−7	3.79	1.28	0.411	0.418	1.56	1.16
1.0E−6	4.08	1.39	0.480	0.468	1.68	1.26
2.0E−6	4.20	1.48	0.520	0.508	1.77	1.33
5.0E−6	4.35	1.59	0.520	0.535	1.86	1.40
1.0E−5	4.37	1.64	0.499	0.539	1.89	1.43
2.0E−5	4.48	1.64	0.538	0.540	1.91	1.45
5.0E−5	4.37	1.62	0.545	0.533	1.92	1.42
1.0E−4	4.45	1.64	0.524	0.531	1.91	1.40
2.0E−4	4.43	1.67	0.545	0.542	1.87	1.38
5.0E−4	4.04	1.67	0.564	0.551	1.83	1.35
0.001	4.17	1.67	0.550	0.550	1.83	1.34
0.002	4.19	1.66	0.543	0.542	1.83	1.33
0.005	4.10	1.68	0.543	0.544	1.80	1.30
0.01	4.03	1.69	0.498	0.542	1.79	1.29
0.02	4.25	1.73	0.557	0.558	1.82	1.34
0.03	4.31	1.77	0.563	0.569	1.87	1.39
0.05	4.63	1.84	0.547	0.584	1.99	1.49
0.07	5.10	1.90	0.598	0.605	2.11	1.58
0.1	5.48	1.98	0.668	0.630	2.31	1.71
0.15	6.43	2.08	0.717	0.659	2.62	1.94
0.2	7.49	2.17	0.733	0.685	2.93	2.18
0.3	9.00	2.32	0.784	0.745	3.54	2.65
0.5	12.4	2.67	0.956	0.926	4.72	3.57
0.7	15.5	3.10	1.16	1.17	5.87	4.49
0.9	18.1	3.61	1.39	1.46	7.01	5.42
1.0	19.6	3.91	1.53	1.63	7.58	5.89
1.2	23.0	4.57	1.92	2.02	8.71	6.82
1.5	25.8	5.70	2.70	2.72	10.4	8.20
2.0	29.9	7.81	4.25	4.09	13.0	10.4
3.0	37.6	12.3	7.51	7.27	17.9	14.6
4.0	44.4	16.8	10.6	10.6	22.4	18.4
5.0	49.4	21.1	14.1	14.0	26.4	22.0
6.0	53.2	25.0	17.5	17.2	30.1	25.2
7.0	55.8	28.6	20.6	20.1	33.3	28.1
8.0	58.3	31.9	23.1	22.9	36.3	30.8
9.0	61.4	34.9	25.4	25.4	38.9	33.2
10.0	64.7	37.7	27.6	27.7	41.4	35.4
12.0	70.5	42.6	31.5	31.9	45.6	39.4
14.0	73.8	46.8	35.2	35.5	49.1	42.7
15.0	74.8	48.7	37.0	37.2	50.7	44.2
16.0	75.5	50.4	38.6	38.8	52.1	45.6
18.0	76.4	53.5	41.8	41.7	54.5	48.2
20.0	76.8	56.2	44.7	44.3	56.6	50.4
21.0	76.7	57.4	46.1	45.6	57.6	51.4
30.0	79.6	65.4	55.9	54.3	63.8	58.4
50.0	80.7	75.5	67.3	66.7	71.2	68.0
75.0	84.8	84.5	77.5	77.6	77.6	76.6
100	84.0	92.6	86.6	86.9	83.9	84.0
130	77.4	102	96.4	96.5	91.2	92.3
150	77.4	107	103	102	95.9	97.6
180	74.6	116	111	109	103	105
200	73.4	121	115	114	107	110
300	83.5	146	130	133	128	132
400	99.9	170	151	152	148	153
500	116	194	177	171	167	172
600	147	215	205	188	185	190
700	171	233	225	203	200	206
800	176	248	237	217	214	220
900	169	259	244	229	225	232
1000	165	269	249	239	236	243
2000	220	326	300	309	300	316
5000	243	428	420	426	394	444
10,000	349	557	562	538	498	596

AP, antero-posterior; PA, postero-anterior; LLAT, left lateral; RLAT, right lateral; ROT, rotational; ISO, isotropic.

Table C.16. Neutrons, male: brain absorbed dose per fluence, in units of pGy cm^2, for mono-energetic particles incident in various geometries.

Energy (MeV)	AP	PA	LLAT	RLAT	ROT	ISO
1.0E−9	0.518	0.629	0.663	0.708	0.605	0.526
1.0E−8	0.574	0.698	0.789	0.835	0.736	0.639
2.5E−8	0.646	0.810	0.918	0.965	0.847	0.730
1.0E−7	0.847	1.07	1.23	1.29	1.11	0.964
2.0E−7	0.963	1.21	1.42	1.49	1.27	1.09
5.0E−7	1.10	1.40	1.66	1.73	1.48	1.27
1.0E−6	1.17	1.51	1.81	1.88	1.61	1.38
2.0E−6	1.24	1.59	1.90	1.98	1.70	1.46
5.0E−6	1.29	1.66	1.97	2.06	1.78	1.52
1.0E−5	1.32	1.69	2.00	2.08	1.80	1.54
2.0E−5	1.32	1.69	2.01	2.09	1.81	1.55
5.0E−5	1.34	1.70	2.01	2.09	1.80	1.55
1.0E−4	1.35	1.70	2.00	2.07	1.79	1.54
2.0E−4	1.32	1.67	1.98	2.05	1.78	1.53
5.0E−4	1.31	1.66	1.96	2.02	1.76	1.52
0.001	1.29	1.63	1.93	1.99	1.74	1.50
0.002	1.28	1.61	1.91	1.97	1.72	1.48
0.005	1.26	1.60	1.87	1.95	1.71	1.46
0.01	1.27	1.60	1.86	1.97	1.71	1.46
0.02	1.28	1.61	1.89	1.98	1.72	1.47
0.03	1.31	1.64	1.94	2.01	1.75	1.49
0.05	1.37	1.70	2.05	2.11	1.83	1.57
0.07	1.44	1.78	2.16	2.24	1.94	1.66
0.1	1.55	1.93	2.35	2.46	2.11	1.82
0.15	1.75	2.20	2.71	2.85	2.43	2.10
0.2	1.97	2.49	3.11	3.25	2.78	2.41
0.3	2.46	3.14	3.96	4.12	3.50	3.06
0.5	3.55	4.54	5.73	5.96	5.02	4.42
0.7	4.68	5.94	7.46	7.72	6.57	5.82
0.9	5.85	7.36	9.16	9.45	8.12	7.23
1.0	6.46	8.08	10.0	10.3	8.90	7.94
1.2	7.75	9.58	11.8	12.1	10.5	9.37
1.5	9.76	11.8	14.4	14.8	12.8	11.5
2.0	13.0	15.4	18.5	19.0	16.5	14.9
3.0	18.9	21.6	25.3	25.8	23.0	20.8
4.0	23.8	26.8	30.9	31.3	28.4	25.8
5.0	28.0	31.1	35.4	35.7	33.0	30.0
6.0	31.7	34.8	39.2	39.5	36.9	33.7
7.0	34.9	38.1	42.5	42.8	40.2	36.8
8.0	37.7	40.9	45.4	45.7	43.2	39.6
9.0	40.3	43.5	48.0	48.3	45.8	42.1
10.0	42.6	45.9	50.4	50.7	48.2	44.3
12.0	46.7	49.9	54.6	55.0	52.2	48.1
14.0	50.0	53.2	58.1	58.4	55.4	51.1
15.0	51.5	54.7	59.5	59.9	56.8	52.5
16.0	52.9	55.9	60.8	61.1	58.0	53.6
18.0	55.3	58.2	63.1	63.3	60.1	55.7
20.0	57.3	60.0	64.9	65.0	61.8	57.5
21.0	58.2	60.8	65.6	65.7	62.6	58.2
30.0	64.4	66.3	70.5	70.2	67.4	63.5
50.0	72.4	73.8	76.4	76.1	73.0	70.6
75.0	79.5	80.6	81.8	81.6	77.9	76.7
100	85.0	85.4	85.7	85.5	82.2	81.9
130	90.2	89.0	88.6	88.4	86.7	87.2
150	92.9	90.6	90.2	89.7	89.5	90.4
180	96.2	92.7	92.3	91.5	93.4	95.0
200	98.3	93.9	93.8	92.7	96.0	98.1
300	109	103	104	102	109	113
400	124	116	119	116	123	128
500	140	131	134	132	137	143
600	155	146	150	148	149	156
700	169	159	163	162	160	168
800	181	169	174	173	170	178
900	190	177	183	182	178	187
1000	198	184	190	188	185	194
2000	242	219	228	224	227	241
5000	302	274	291	281	281	316
10,000	406	362	382	377	333	399

AP, antero-posterior; PA, postero-anterior; LLAT, left lateral; RLAT, right lateral; ROT, rotational; ISO, isotropic.

Table C.17. Neutrons, male: breast absorbed dose per fluence, in units of pGy cm^2, for mono-energetic particles incident in various geometries.

Energy (MeV)	AP	PA	LLAT	RLAT	ROT	ISO
1.0E−9	1.75	0.318	0.530	0.488	0.819	0.503
1.0E−8	1.98	0.330	0.570	0.521	0.868	0.685
2.5E−8	2.12	0.368	0.630	0.567	0.956	0.741
1.0E−7	2.57	0.478	0.713	0.701	1.11	0.848
2.0E−7	2.68	0.542	0.784	0.746	1.19	0.938
5.0E−7	2.74	0.633	0.874	0.795	1.30	1.04
1.0E−6	2.80	0.692	0.902	0.845	1.35	1.10
2.0E−6	2.84	0.738	0.912	0.855	1.37	1.13
5.0E−6	2.84	0.771	0.911	0.871	1.35	1.12
1.0E−5	2.85	0.793	0.887	0.875	1.33	1.11
2.0E−5	2.69	0.796	0.873	0.865	1.32	1.08
5.0E−5	2.61	0.814	0.840	0.818	1.30	1.02
1.0E−4	2.58	0.827	0.824	0.776	1.28	0.991
2.0E−4	2.56	0.811	0.810	0.773	1.26	0.964
5.0E−4	2.53	0.808	0.797	0.782	1.22	0.936
0.001	2.44	0.809	0.784	0.761	1.19	0.927
0.002	2.44	0.803	0.785	0.744	1.19	0.940
0.005	2.58	0.782	0.785	0.745	1.27	0.994
0.01	3.00	0.774	0.844	0.819	1.41	1.10
0.02	3.57	0.793	1.08	1.06	1.65	1.34
0.03	4.16	0.814	1.33	1.29	1.90	1.58
0.05	5.36	0.840	1.79	1.70	2.40	2.03
0.07	6.49	0.863	2.23	2.10	2.87	2.45
0.1	8.05	0.893	2.82	2.65	3.53	3.05
0.15	10.3	0.932	3.69	3.54	4.55	3.96
0.2	12.2	0.960	4.48	4.36	5.47	4.79
0.3	15.5	1.01	5.89	5.79	7.09	6.28
0.5	20.6	1.18	8.30	8.20	9.76	8.82
0.7	24.7	1.42	10.4	10.2	12.0	11.0
0.9	28.2	1.74	12.2	11.9	13.9	12.9
1.0	29.6	1.94	13.0	12.7	14.8	13.7
1.2	32.2	2.39	14.5	14.1	16.5	15.4
1.5	35.3	3.21	16.5	16.0	18.7	17.6
2.0	39.8	4.85	19.3	18.7	22.0	20.8
3.0	47.4	8.74	24.0	23.1	27.5	26.2
4.0	53.0	12.9	27.7	26.8	32.0	30.5
5.0	56.9	17.0	30.9	30.0	35.8	34.2
6.0	60.1	20.9	33.8	32.8	39.1	37.4
7.0	63.0	24.5	36.4	35.3	42.2	40.2
8.0	65.8	27.9	38.7	37.6	44.9	42.6
9.0	68.5	30.9	41.0	39.7	47.5	44.9
10.0	71.0	33.8	43.0	41.8	49.8	46.9
12.0	75.5	38.9	46.7	45.5	53.9	50.3
14.0	78.7	43.4	49.9	48.7	57.2	53.0
15.0	79.9	45.5	51.2	50.2	58.6	54.1
16.0	80.8	47.4	52.5	51.5	59.9	55.1
18.0	81.9	50.9	54.7	54.0	61.9	56.8
20.0	82.2	54.1	56.6	56.0	63.6	58.1
21.0	82.2	55.5	57.4	56.9	64.3	58.7
30.0	80.1	65.4	63.0	62.4	67.8	61.9
50.0	74.3	78.2	68.7	67.0	68.8	64.0
75.0	65.3	88.6	71.2	68.3	68.4	65.5
100	54.9	97.5	72.1	67.7	69.2	67.8
130	45.8	107	73.2	67.0	71.1	71.3
150	42.5	113	74.4	67.4	72.9	74.0
180	40.7	120	76.9	69.3	76.1	78.3
200	40.8	125	79.0	71.2	78.5	81.3
300	47.8	145	91.5	85.2	92.1	96.4
400	56.5	164	106	102	106	111
500	65.5	182	119	119	120	123
600	73.5	198	132	136	133	135
700	79.4	213	143	149	144	145
800	84.0	225	152	160	154	155
900	87.6	235	160	168	162	163
1000	90.7	244	167	173	170	170
2000	109	305	211	202	217	224
5000	129	416	284	274	291	304
10,000	190	520	347	369	377	381

AP, antero-posterior; PA, postero-anterior; LLAT, left lateral; RLAT, right lateral; ROT, rotational; ISO, isotropic.

Table C.18. Neutrons, male: colon absorbed dose per fluence, in units of pGy cm^2, for mono-energetic particles incident in various geometries.

Energy (MeV)	AP	PA	LLAT	RLAT	ROT	ISO
1.0E−9	1.20	0.633	0.528	0.394	0.673	0.497
1.0E−8	1.39	0.754	0.612	0.458	0.806	0.610
2.5E−8	1.57	0.858	0.713	0.524	0.925	0.699
1.0E−7	2.10	1.14	0.944	0.690	1.23	0.911
2.0E−7	2.41	1.28	1.08	0.803	1.40	1.04
5.0E−7	2.77	1.51	1.25	0.948	1.62	1.20
1.0E−6	2.97	1.66	1.36	1.04	1.77	1.30
2.0E−6	3.13	1.77	1.43	1.10	1.89	1.37
5.0E−6	3.30	1.85	1.51	1.16	1.98	1.44
1.0E−5	3.38	1.90	1.53	1.19	2.02	1.47
2.0E−5	3.38	1.93	1.53	1.20	2.05	1.49
5.0E−5	3.40	1.99	1.51	1.20	2.05	1.50
1.0E−4	3.43	2.00	1.49	1.21	2.04	1.51
2.0E−4	3.41	1.97	1.49	1.21	2.04	1.51
5.0E−4	3.39	1.99	1.48	1.20	2.02	1.49
0.001	3.36	2.00	1.46	1.20	2.02	1.48
0.002	3.34	2.00	1.44	1.19	2.00	1.48
0.005	3.31	2.00	1.42	1.18	1.99	1.48
0.01	3.32	2.02	1.40	1.17	1.99	1.49
0.02	3.35	2.06	1.40	1.18	2.01	1.50
0.03	3.39	2.10	1.42	1.19	2.04	1.51
0.05	3.51	2.16	1.50	1.24	2.12	1.56
0.07	3.64	2.21	1.59	1.28	2.21	1.61
0.1	3.85	2.30	1.74	1.35	2.34	1.70
0.15	4.25	2.44	2.02	1.50	2.58	1.87
0.2	4.69	2.58	2.31	1.67	2.82	2.04
0.3	5.64	2.89	2.92	2.04	3.35	2.41
0.5	7.63	3.55	4.15	2.84	4.44	3.19
0.7	9.58	4.28	5.36	3.67	5.56	4.02
0.9	11.5	5.10	6.54	4.53	6.69	4.87
1.0	12.4	5.55	7.12	4.98	7.27	5.30
1.2	14.4	6.52	8.28	5.89	8.44	6.20
1.5	17.2	8.09	9.97	7.29	10.2	7.57
2.0	21.6	10.9	12.6	9.59	13.1	9.85
3.0	29.1	16.3	17.4	13.9	18.5	14.2
4.0	35.1	21.4	21.6	17.8	23.3	18.1
5.0	40.0	26.0	25.2	21.3	27.5	21.6
6.0	44.2	30.1	28.5	24.4	31.3	24.8
7.0	47.8	33.8	31.4	27.3	34.6	27.7
8.0	51.0	37.0	34.1	29.8	37.6	30.3
9.0	53.9	40.0	36.5	32.2	40.3	32.7
10.0	56.5	42.7	38.7	34.4	42.8	34.8
12.0	60.9	47.4	42.7	38.3	47.0	38.7
14.0	64.4	51.4	46.0	41.8	50.6	42.1
15.0	65.8	53.1	47.5	43.3	52.1	43.6
16.0	67.0	54.7	48.9	44.8	53.6	45.0
18.0	69.0	57.5	51.4	47.4	56.1	47.5
20.0	70.5	59.9	53.6	49.8	58.2	49.7
21.0	71.2	61.0	54.6	50.9	59.2	50.8
30.0	75.4	68.1	61.5	58.7	65.6	58.0
50.0	80.5	77.1	70.8	69.6	73.5	67.9
75.0	84.8	85.5	78.9	79.3	80.5	76.9
100	87.7	92.9	85.8	87.5	86.9	84.7
130	90.0	101	93.3	96.3	94.1	93.2
150	91.2	106	97.9	102	98.6	98.6
180	93.2	113	105	109	105	106
200	94.7	118	109	114	109	111
300	106	139	129	135	129	134
400	122	160	150	156	149	155
500	139	181	169	176	168	176
600	157	200	187	195	185	195
700	173	217	203	211	200	211
800	185	231	217	225	214	226
900	196	242	229	236	225	238
1000	204	252	239	247	235	249
2000	249	309	307	311	299	322
5000	309	407	420	422	394	446
10,000	401	519	529	537	501	584

AP, antero-posterior; PA, postero-anterior; LLAT, left lateral; RLAT, right lateral; ROT, rotational; ISO, isotropic.

Table C.19. Neutrons, male: bone surface (endosteum) absorbed dose per fluence, in units of pGy cm^2, for mono-energetic particles incident in various geometries.

Energy (MeV)	AP	PA	LLAT	RLAT	ROT	ISO
1.0E−9	0.915	0.824	0.441	0.450	0.679	0.551
1.0E−8	1.04	0.952	0.506	0.517	0.814	0.653
2.5E−8	1.16	1.09	0.578	0.587	0.925	0.737
1.0E−7	1.50	1.44	0.750	0.762	1.20	0.946
2.0E−7	1.67	1.64	0.850	0.863	1.35	1.06
5.0E−7	1.88	1.89	0.970	0.981	1.53	1.20
1.0E−6	1.99	2.04	1.03	1.04	1.64	1.28
2.0E−6	2.09	2.14	1.08	1.09	1.71	1.33
5.0E−6	2.15	2.24	1.11	1.11	1.77	1.37
1.0E−5	2.18	2.28	1.11	1.12	1.79	1.38
2.0E−5	2.17	2.28	1.10	1.11	1.78	1.38
5.0E−5	2.16	2.28	1.09	1.09	1.76	1.37
1.0E−4	2.15	2.26	1.07	1.08	1.74	1.35
2.0E−4	2.11	2.24	1.05	1.06	1.72	1.33
5.0E−4	2.08	2.21	1.03	1.03	1.69	1.31
0.001	2.04	2.18	1.01	1.01	1.67	1.29
0.002	2.01	2.16	0.992	0.996	1.65	1.27
0.005	1.99	2.14	0.974	0.982	1.63	1.26
0.01	2.01	2.15	0.974	0.986	1.64	1.26
0.02	2.05	2.18	1.01	1.02	1.67	1.30
0.03	2.12	2.23	1.06	1.07	1.72	1.34
0.05	2.28	2.34	1.15	1.17	1.85	1.44
0.07	2.45	2.46	1.26	1.28	1.99	1.56
0.1	2.72	2.67	1.44	1.47	2.22	1.74
0.15	3.19	3.04	1.74	1.78	2.61	2.05
0.2	3.68	3.44	2.05	2.10	3.01	2.38
0.3	4.66	4.27	2.67	2.74	3.83	3.04
0.5	6.59	5.99	3.90	3.98	5.47	4.36
0.7	8.37	7.65	5.03	5.13	7.02	5.63
0.9	10.0	9.26	6.12	6.24	8.52	6.87
1.0	10.9	10.1	6.65	6.78	9.26	7.49
1.2	12.5	11.7	7.74	7.88	10.7	8.71
1.5	15.0	14.2	9.34	9.50	12.9	10.5
2.0	18.7	18.1	11.9	12.0	16.2	13.3
3.0	25.0	24.6	16.3	16.5	22.0	18.3
4.0	30.0	29.8	20.0	20.3	26.7	22.4
5.0	34.2	34.0	23.3	23.5	30.7	26.0
6.0	37.6	37.5	26.1	26.4	34.1	29.1
7.0	40.7	40.7	28.7	28.9	37.1	31.9
8.0	43.5	43.5	31.0	31.2	39.8	34.4
9.0	46.0	46.1	33.1	33.4	42.3	36.7
10.0	48.4	48.4	35.1	35.4	44.6	38.8
12.0	52.6	52.6	38.7	39.0	48.6	42.5
14.0	56.0	56.1	41.9	42.1	51.9	45.6
15.0	57.5	57.6	43.3	43.5	53.3	47.0
16.0	58.8	58.9	44.6	44.8	54.5	48.2
18.0	60.9	61.1	46.9	47.2	56.7	50.4
20.0	62.7	62.9	48.9	49.2	58.5	52.3
21.0	63.4	63.7	49.8	50.1	59.2	53.1
30.0	68.1	68.5	56.2	56.4	64.0	58.7
50.0	73.7	74.5	64.8	65.1	69.5	65.7
75.0	78.4	79.9	72.5	72.5	74.6	72.0
100	81.6	83.6	78.3	78.1	79.3	77.6
130	84.3	86.5	83.9	83.3	84.3	83.8
150	85.8	88.0	87.2	86.4	87.3	87.6
180	88.1	90.3	91.7	90.8	91.5	93.0
200	89.8	92.0	94.5	93.6	94.2	96.6
300	101	103	109	108	109	114
400	116	118	125	125	125	131
500	133	135	142	143	141	147
600	149	151	159	159	156	162
700	164	165	174	174	169	176
800	176	176	186	186	180	188
900	185	185	195	196	190	197
1000	193	191	203	204	197	206
2000	234	226	251	252	243	261
5000	286	282	343	343	307	352
10,000	383	371	456	445	386	460

AP, antero-posterior; PA, postero-anterior; LLAT, left lateral; RLAT, right lateral; ROT, rotational; ISO, isotropic.

Table C.20. Neutrons, male: testes absorbed dose per fluence, in units of pGy cm^2, for mono-energetic particles incident in various geometries.

Energy (MeV)	AP	PA	LLAT	RLAT	ROT	ISO
1.0E−9	2.04	0.579	0.250	0.182	0.823	0.645
1.0E−8	2.32	0.630	0.254	0.180	0.983	0.778
2.5E−8	2.58	0.712	0.295	0.224	1.09	0.849
1.0E−7	3.10	0.943	0.399	0.317	1.34	1.03
2.0E−7	3.41	1.05	0.423	0.346	1.45	1.15
5.0E−7	3.74	1.19	0.452	0.378	1.57	1.30
1.0E−6	3.88	1.31	0.490	0.408	1.67	1.36
2.0E−6	4.03	1.39	0.520	0.441	1.76	1.38
5.0E−6	4.16	1.45	0.514	0.454	1.83	1.37
1.0E−5	4.19	1.49	0.514	0.456	1.85	1.36
2.0E−5	4.07	1.52	0.534	0.448	1.83	1.36
5.0E−5	4.04	1.51	0.545	0.455	1.77	1.38
1.0E−4	3.94	1.50	0.543	0.446	1.74	1.38
2.0E−4	3.87	1.52	0.552	0.439	1.71	1.36
5.0E−4	3.78	1.56	0.553	0.430	1.69	1.32
0.001	3.71	1.54	0.527	0.436	1.68	1.30
0.002	3.67	1.53	0.527	0.436	1.69	1.28
0.005	3.64	1.52	0.516	0.446	1.73	1.30
0.01	3.72	1.52	0.513	0.454	1.77	1.35
0.02	3.88	1.56	0.545	0.445	1.85	1.45
0.03	4.05	1.61	0.554	0.439	1.94	1.53
0.05	4.46	1.67	0.540	0.440	2.13	1.70
0.07	4.95	1.70	0.537	0.447	2.33	1.86
0.1	5.67	1.75	0.548	0.459	2.63	2.12
0.15	6.78	1.83	0.599	0.483	3.12	2.55
0.2	7.84	1.92	0.654	0.510	3.59	2.97
0.3	9.93	2.10	0.745	0.566	4.46	3.75
0.5	13.8	2.54	0.932	0.698	6.04	5.17
0.7	17.1	3.08	1.14	0.853	7.48	6.47
0.9	19.9	3.72	1.39	1.05	8.84	7.68
1.0	21.2	4.08	1.54	1.17	9.49	8.26
1.2	23.7	4.89	1.93	1.45	10.8	9.41
1.5	27.0	6.27	2.66	1.99	12.6	11.0
2.0	31.7	8.77	4.15	3.12	15.4	13.6
3.0	39.3	14.0	7.46	5.91	20.6	18.0
4.0	45.3	19.0	10.8	9.02	25.1	22.0
5.0	49.9	23.6	14.2	12.2	29.1	25.5
6.0	53.6	27.8	17.5	15.3	32.6	28.7
7.0	56.8	31.5	20.5	18.2	35.8	31.5
8.0	59.7	34.8	23.2	20.8	38.7	34.1
9.0	62.3	37.9	25.6	23.3	41.2	36.5
10.0	64.7	40.8	27.9	25.5	43.5	38.7
12.0	68.7	45.8	31.9	29.6	47.5	42.4
14.0	71.5	50.2	35.5	33.1	50.8	45.6
15.0	72.6	52.1	37.1	34.8	52.2	47.0
16.0	73.4	53.8	38.7	36.3	53.4	48.2
18.0	74.7	56.9	41.5	39.1	55.6	50.4
20.0	75.6	59.6	44.0	41.7	57.4	52.3
21.0	76.0	60.8	45.2	42.8	58.2	53.1
30.0	78.0	68.6	53.0	51.0	63.2	58.7
50.0	78.5	78.7	62.9	61.6	68.8	66.0
75.0	76.1	88.5	72.0	71.1	74.1	73.8
100	71.4	97.9	79.7	79.2	79.7	80.6
130	65.8	108	87.7	88.0	86.4	87.9
150	63.2	114	92.6	93.4	90.6	92.3
180	61.1	121	98.7	101	96.5	98.5
200	60.6	125	102	105	100	102
300	65.3	141	117	124	118	121
400	75.2	160	135	142	135	140
500	87.4	181	154	159	150	159
600	100	201	173	176	164	177
700	111	218	190	192	176	193
800	121	232	203	205	187	207
900	129	243	213	216	197	218
1000	136	252	220	226	205	228
2000	173	309	276	280	265	288
5000	204	417	422	388	353	385
10,000	263	548	502	496	436	534

AP, antero-posterior; PA, postero-anterior; LLAT, left lateral; RLAT, right lateral; ROT, rotational; ISO, isotropic.

Table C.21. Neutrons, male: liver absorbed dose per fluence, in units of pGy cm^2, for mono-energetic particles incident in various geometries.

Energy (MeV)	AP	PA	LLAT	RLAT	ROT	ISO
1.0E−9	1.05	0.695	0.168	0.610	0.618	0.479
1.0E−8	1.25	0.823	0.177	0.725	0.768	0.583
2.5E−8	1.42	0.949	0.200	0.839	0.885	0.664
1.0E−7	1.89	1.26	0.254	1.13	1.16	0.872
2.0E−7	2.14	1.45	0.288	1.30	1.33	0.985
5.0E−7	2.49	1.70	0.334	1.52	1.55	1.15
1.0E−6	2.69	1.85	0.363	1.66	1.69	1.25
2.0E−6	2.86	1.97	0.386	1.77	1.79	1.33
5.0E−6	3.02	2.09	0.404	1.86	1.89	1.40
1.0E−5	3.10	2.15	0.412	1.90	1.94	1.44
2.0E−5	3.13	2.18	0.419	1.91	1.95	1.46
5.0E−5	3.17	2.21	0.426	1.92	1.97	1.47
1.0E−4	3.19	2.22	0.427	1.92	1.98	1.48
2.0E−4	3.18	2.24	0.428	1.91	1.98	1.48
5.0E−4	3.20	2.25	0.430	1.90	1.99	1.49
0.001	3.17	2.25	0.428	1.88	1.99	1.50
0.002	3.15	2.24	0.426	1.87	1.99	1.49
0.005	3.16	2.25	0.427	1.85	1.99	1.49
0.01	3.19	2.27	0.432	1.85	2.00	1.49
0.02	3.22	2.30	0.443	1.88	2.02	1.51
0.03	3.26	2.34	0.450	1.91	2.05	1.53
0.05	3.35	2.41	0.460	1.99	2.11	1.57
0.07	3.45	2.48	0.471	2.07	2.17	1.62
0.1	3.62	2.58	0.487	2.22	2.28	1.69
0.15	3.91	2.76	0.516	2.48	2.46	1.83
0.2	4.22	2.95	0.544	2.77	2.66	1.97
0.3	4.89	3.33	0.600	3.39	3.09	2.27
0.5	6.30	4.16	0.720	4.67	3.99	2.91
0.7	7.72	5.06	0.864	5.96	4.92	3.59
0.9	9.14	6.01	1.04	7.27	5.89	4.31
1.0	9.87	6.52	1.15	7.95	6.39	4.69
1.2	11.4	7.60	1.39	9.35	7.44	5.50
1.5	13.8	9.30	1.84	11.5	9.07	6.77
2.0	17.5	12.2	2.74	15.0	11.8	8.95
3.0	24.2	17.7	4.91	21.2	16.9	13.1
4.0	29.7	22.8	7.31	26.5	21.4	17.0
5.0	34.3	27.2	9.81	31.0	25.5	20.5
6.0	38.3	31.2	12.3	34.8	29.1	23.7
7.0	41.7	34.7	14.7	38.2	32.4	26.6
8.0	44.8	37.8	16.9	41.2	35.3	29.2
9.0	47.5	40.7	19.0	44.0	37.9	31.5
10.0	50.0	43.3	20.9	46.5	40.3	33.7
12.0	54.4	47.8	24.6	50.9	44.5	37.7
14.0	57.9	51.6	27.9	54.5	48.0	41.1
15.0	59.4	53.3	29.5	56.1	49.6	42.6
16.0	60.8	54.8	31.0	57.5	51.0	44.0
18.0	63.0	57.5	33.9	60.0	53.5	46.6
20.0	64.9	59.8	36.6	62.1	55.6	48.9
21.0	65.7	60.8	37.8	63.0	56.6	49.9
30.0	71.0	67.7	47.3	68.9	63.2	57.1
50.0	77.5	76.5	61.3	76.1	71.9	66.8
75.0	83.3	84.5	73.8	82.7	80.0	75.8
100	88.1	91.6	84.5	88.5	87.5	84.1
130	92.6	99.4	96.1	94.3	95.7	93.2
150	95.2	104	103	97.8	101	98.9
180	98.6	111	113	102	108	107
200	101	115	119	105	112	111
300	114	136	146	121	133	133
400	131	157	171	139	153	155
500	150	178	194	158	172	176
600	169	197	216	176	190	196
700	186	213	235	192	206	214
800	200	227	251	205	220	229
900	211	239	265	216	232	243
1000	221	249	276	225	242	254
2000	272	310	354	275	307	330
5000	338	410	504	362	410	451
10,000	442	514	649	459	528	597

AP, antero-posterior; PA, postero-anterior; LLAT, left lateral; RLAT, right lateral; ROT, rotational; ISO, isotropic.

Table C.22. Neutrons, male: lung absorbed dose per fluence, in units of pGy cm^2, for mono-energetic particles incident in various geometries.

Energy (MeV)	AP	PA	LLAT	RLAT	ROT	ISO
1.0E−9	0.976	0.811	0.325	0.315	0.611	0.482
1.0E−8	1.13	0.984	0.359	0.352	0.743	0.587
2.5E−8	1.29	1.14	0.410	0.395	0.853	0.665
1.0E−7	1.74	1.55	0.528	0.502	1.13	0.877
2.0E−7	1.98	1.77	0.600	0.571	1.28	0.999
5.0E−7	2.29	2.09	0.691	0.662	1.49	1.17
1.0E−6	2.47	2.28	0.746	0.721	1.62	1.27
2.0E−6	2.61	2.43	0.791	0.763	1.72	1.34
5.0E−6	2.75	2.56	0.830	0.801	1.81	1.42
1.0E−5	2.83	2.64	0.843	0.819	1.86	1.45
2.0E−5	2.85	2.67	0.855	0.831	1.88	1.47
5.0E−5	2.85	2.73	0.862	0.841	1.90	1.48
1.0E−4	2.86	2.74	0.867	0.842	1.91	1.48
2.0E−4	2.84	2.72	0.867	0.841	1.91	1.48
5.0E−4	2.85	2.73	0.867	0.841	1.91	1.48
0.001	2.82	2.72	0.861	0.839	1.90	1.48
0.002	2.78	2.72	0.856	0.834	1.89	1.47
0.005	2.78	2.71	0.851	0.836	1.88	1.47
0.01	2.79	2.73	0.848	0.842	1.88	1.47
0.02	2.82	2.75	0.865	0.840	1.90	1.49
0.03	2.87	2.79	0.882	0.844	1.93	1.51
0.05	2.97	2.87	0.907	0.862	1.99	1.56
0.07	3.09	2.95	0.928	0.884	2.05	1.60
0.1	3.29	3.08	0.965	0.923	2.16	1.69
0.15	3.68	3.33	1.04	0.997	2.36	1.84
0.2	4.10	3.61	1.12	1.08	2.58	2.01
0.3	5.02	4.23	1.30	1.26	3.07	2.38
0.5	6.95	5.62	1.69	1.65	4.12	3.20
0.7	8.82	7.07	2.12	2.10	5.24	4.08
0.9	10.6	8.57	2.59	2.60	6.40	5.02
1.0	11.6	9.36	2.85	2.87	7.00	5.51
1.2	13.4	11.0	3.42	3.46	8.24	6.53
1.5	16.2	13.5	4.38	4.43	10.1	8.11
2.0	20.6	17.5	6.10	6.15	13.3	10.7
3.0	27.8	24.6	9.56	9.63	18.9	15.7
4.0	33.7	30.4	12.9	12.9	23.9	20.0
5.0	38.5	35.3	16.0	16.1	28.2	23.9
6.0	42.5	39.4	18.9	18.9	31.9	27.3
7.0	45.9	43.0	21.6	21.5	35.2	30.3
8.0	49.0	46.1	24.0	23.9	38.2	33.0
9.0	51.9	48.9	26.2	26.0	40.8	35.5
10.0	54.4	51.4	28.2	28.0	43.2	37.7
12.0	58.8	55.7	31.8	31.6	47.3	41.6
14.0	62.3	59.2	35.1	34.8	50.7	45.0
15.0	63.7	60.7	36.6	36.3	52.2	46.4
16.0	65.0	62.0	38.0	37.6	53.6	47.8
18.0	67.1	64.2	40.6	40.2	56.0	50.2
20.0	68.7	66.0	42.9	42.5	58.0	52.2
21.0	69.4	66.8	44.0	43.5	58.9	53.2
30.0	73.8	71.8	51.8	51.3	64.8	59.6
50.0	79.1	77.8	63.2	62.7	72.3	68.1
75.0	83.5	83.5	73.9	73.1	79.3	76.2
100	86.7	88.2	83.0	81.7	85.6	83.4
130	89.2	92.8	92.2	90.5	92.5	91.0
150	90.5	95.6	97.5	95.6	96.6	95.7
180	92.4	99.4	104	102	102	102
200	93.9	102	108	107	106	106
300	105	116	124	125	123	126
400	121	133	142	144	140	144
500	139	151	162	163	157	163
600	157	167	180	181	173	180
700	173	181	197	197	187	195
800	186	193	211	210	199	208
900	196	202	221	222	209	219
1000	205	210	230	231	218	229
2000	250	254	284	296	274	294
5000	307	325	404	414	360	395
10,000	400	410	538	524	452	514

AP, antero-posterior; PA, postero-anterior; LLAT, left lateral; RLAT, right lateral; ROT, rotational; ISO, isotropic.

Table C.23. Neutrons, male: oesophagus absorbed dose per fluence, in units of pGy cm^2, for mono-energetic particles incident in various geometries.

Energy (MeV)	AP	PA	LLAT	RLAT	ROT	ISO
1.0E−9	0.984	0.777	0.362	0.299	0.593	0.451
1.0E−8	1.15	0.906	0.416	0.354	0.734	0.558
2.5E−8	1.30	1.06	0.464	0.393	0.854	0.640
1.0E−7	1.77	1.44	0.591	0.488	1.10	0.851
2.0E−7	2.02	1.66	0.676	0.560	1.26	0.967
5.0E−7	2.32	1.96	0.791	0.661	1.50	1.11
1.0E−6	2.50	2.18	0.860	0.721	1.64	1.22
2.0E−6	2.67	2.34	0.911	0.763	1.74	1.32
5.0E−6	2.82	2.49	0.947	0.811	1.82	1.46
1.0E−5	2.89	2.56	0.957	0.835	1.87	1.49
2.0E−5	2.90	2.63	0.966	0.846	1.92	1.46
5.0E−5	2.95	2.71	0.973	0.864	1.96	1.46
1.0E−4	2.97	2.74	0.980	0.887	1.98	1.49
2.0E−4	2.96	2.76	0.989	0.887	1.98	1.52
5.0E−4	2.96	2.78	1.00	0.873	1.98	1.53
0.001	2.96	2.77	1.01	0.861	1.96	1.53
0.002	2.97	2.77	0.999	0.866	1.94	1.52
0.005	2.96	2.79	0.986	0.884	1.94	1.52
0.01	2.91	2.84	0.990	0.893	1.97	1.53
0.02	2.92	2.89	1.02	0.883	2.02	1.54
0.03	2.99	2.93	1.05	0.879	2.05	1.56
0.05	3.14	3.01	1.08	0.890	2.11	1.61
0.07	3.26	3.06	1.11	0.914	2.17	1.66
0.1	3.44	3.14	1.15	0.959	2.27	1.74
0.15	3.78	3.30	1.24	1.04	2.46	1.85
0.2	4.16	3.48	1.33	1.13	2.66	1.96
0.3	4.96	3.88	1.54	1.31	3.07	2.23
0.5	6.56	4.81	2.02	1.70	3.97	2.84
0.7	8.10	5.88	2.53	2.13	4.92	3.51
0.9	9.64	7.05	3.09	2.61	5.93	4.25
1.0	10.4	7.68	3.39	2.87	6.46	4.64
1.2	12.0	9.01	4.03	3.42	7.57	5.48
1.5	14.5	11.1	5.07	4.33	9.30	6.81
2.0	18.4	14.7	6.91	5.97	12.2	9.09
3.0	25.4	21.3	10.7	9.40	17.8	13.6
4.0	31.3	27.1	14.3	12.8	22.9	17.7
5.0	36.2	32.1	17.8	16.0	27.4	21.5
6.0	40.4	36.4	21.0	19.0	31.4	24.8
7.0	44.0	40.1	23.9	21.7	34.9	27.9
8.0	47.3	43.4	26.5	24.2	38.0	30.6
9.0	50.2	46.3	29.0	26.5	40.7	33.0
10.0	52.8	48.9	31.3	28.7	43.2	35.2
12.0	57.4	53.4	35.4	32.5	47.5	39.1
14.0	61.1	57.1	39.0	35.9	51.0	42.4
15.0	62.7	58.6	40.6	37.4	52.5	43.9
16.0	64.1	60.0	42.2	38.8	53.9	45.2
18.0	66.5	62.4	45.0	41.5	56.4	47.7
20.0	68.5	64.4	47.6	43.9	58.4	49.9
21.0	69.4	65.3	48.8	45.0	59.3	50.9
30.0	74.6	70.9	57.3	53.0	65.6	58.6
50.0	80.6	77.8	68.7	65.0	73.8	69.9
75.0	86.2	84.2	77.9	75.4	81.6	78.9
100	91.0	89.7	85.2	83.7	88.9	85.6
130	95.9	95.6	92.8	92.5	96.9	92.7
150	98.8	99.3	97.6	97.8	102	97.2
180	103	105	105	105	109	104
200	106	108	109	110	113	108
300	121	126	131	130	133	130
400	140	144	152	150	153	153
500	159	163	172	170	171	175
600	177	180	191	189	188	195
700	193	195	208	206	203	213
800	207	208	222	220	216	228
900	218	219	234	233	227	241
1000	227	229	244	245	236	251
2000	282	290	311	323	295	322
5000	353	379	435	444	393	448
10,000	440	462	545	550	501	597

AP, antero-posterior; PA, postero-anterior; LLAT, left lateral; RLAT, right lateral; ROT, rotational; ISO, isotropic.

Table C.24. Neutrons, male: red (active) bone marrow absorbed dose per fluence, in units of pGy cm^2, for mono-energetic particles incident in various geometries.

Energy (MeV)	AP	PA	LLAT	RLAT	ROT	ISO
1.0E−9	0.856	0.940	0.356	0.361	0.630	0.500
1.0E−8	0.991	1.13	0.407	0.411	0.771	0.602
2.5E−8	1.12	1.31	0.462	0.465	0.885	0.685
1.0E−7	1.48	1.78	0.598	0.601	1.17	0.893
2.0E−7	1.67	2.04	0.679	0.685	1.32	1.01
5.0E−7	1.91	2.39	0.781	0.790	1.53	1.17
1.0E−6	2.06	2.61	0.843	0.852	1.66	1.26
2.0E−6	2.17	2.77	0.890	0.897	1.75	1.33
5.0E−6	2.28	2.93	0.928	0.932	1.84	1.39
1.0E−5	2.33	3.00	0.944	0.947	1.89	1.42
2.0E−5	2.34	3.02	0.949	0.953	1.90	1.44
5.0E−5	2.37	3.05	0.947	0.956	1.91	1.44
1.0E−4	2.37	3.06	0.943	0.953	1.91	1.44
2.0E−4	2.36	3.05	0.938	0.947	1.90	1.44
5.0E−4	2.35	3.04	0.931	0.939	1.90	1.43
0.001	2.34	3.02	0.923	0.930	1.89	1.43
0.002	2.32	3.01	0.917	0.923	1.88	1.42
0.005	2.32	3.00	0.909	0.918	1.88	1.42
0.01	2.35	3.01	0.912	0.924	1.89	1.42
0.02	2.39	3.05	0.934	0.944	1.92	1.45
0.03	2.45	3.10	0.961	0.970	1.95	1.48
0.05	2.57	3.20	1.01	1.02	2.03	1.54
0.07	2.69	3.32	1.07	1.08	2.12	1.61
0.1	2.88	3.50	1.15	1.17	2.26	1.72
0.15	3.19	3.84	1.30	1.33	2.50	1.90
0.2	3.51	4.19	1.45	1.48	2.75	2.09
0.3	4.16	4.94	1.75	1.79	3.25	2.48
0.5	5.44	6.52	2.35	2.40	4.29	3.28
0.7	6.67	8.08	2.95	3.02	5.35	4.09
0.9	7.89	9.65	3.57	3.65	6.41	4.91
1.0	8.52	10.4	3.89	3.98	6.96	5.34
1.2	9.83	12.1	4.54	4.65	8.10	6.22
1.5	11.8	14.6	5.57	5.71	9.83	7.57
2.0	15.1	18.5	7.31	7.50	12.7	9.80
3.0	20.9	25.2	10.7	11.0	17.9	14.0
4.0	25.9	30.7	13.9	14.2	22.4	17.8
5.0	30.1	35.2	16.9	17.2	26.4	21.2
6.0	33.8	39.0	19.6	19.9	29.9	24.2
7.0	37.0	42.3	22.1	22.4	33.0	26.9
8.0	39.9	45.2	24.4	24.7	35.8	29.4
9.0	42.6	48.0	26.5	26.8	38.4	31.7
10.0	45.1	50.4	28.4	28.8	40.7	33.8
12.0	49.5	54.8	32.0	32.4	44.8	37.6
14.0	53.1	58.3	35.2	35.6	48.2	40.8
15.0	54.7	59.8	36.6	37.0	49.7	42.3
16.0	56.1	61.1	38.0	38.4	51.1	43.6
18.0	58.6	63.3	40.5	40.9	53.5	46.1
20.0	60.6	65.1	42.8	43.2	55.5	48.2
21.0	61.5	65.8	43.9	44.2	56.3	49.1
30.0	67.1	70.6	51.5	51.9	62.2	55.7
50.0	74.2	76.6	62.8	63.0	69.7	64.5
75.0	80.9	82.5	73.1	73.0	77.1	72.8
100	86.8	87.2	81.6	81.3	83.9	80.6
130	93.0	91.5	90.7	89.9	91.5	89.2
150	96.5	94.0	96.1	95.2	96.0	94.6
180	101	97.6	104	102	102	102
200	104	100	108	107	106	107
300	120	114	129	128	126	129
400	138	132	149	148	145	150
500	158	151	169	168	164	170
600	178	169	187	187	182	188
700	195	185	203	203	198	205
800	210	198	216	217	211	219
900	222	207	228	229	222	231
1000	231	215	238	239	232	242
2000	288	258	306	306	292	315
5000	365	326	431	423	382	436
10,000	477	418	559	534	487	577

AP, antero-posterior; PA, postero-anterior; LLAT, left lateral; RLAT, right lateral; ROT, rotational; ISO, isotropic.

Table C.25. Neutrons, male: remainder tissues absorbed dose per fluence, in units of pGy cm^2, for mono-energetic particles incident in various geometries.

Energy (MeV)	AP	PA	LLAT	RLAT	ROT	ISO
1.0E−9	1.05	0.765	0.400	0.367	0.640	0.493
1.0E−8	1.22	0.897	0.453	0.423	0.774	0.599
2.5E−8	1.38	1.04	0.518	0.480	0.884	0.684
1.0E−7	1.82	1.39	0.677	0.625	1.17	0.880
2.0E−7	2.05	1.59	0.773	0.714	1.33	0.992
5.0E−7	2.36	1.86	0.891	0.827	1.54	1.14
1.0E−6	2.52	2.03	0.967	0.901	1.67	1.24
2.0E−6	2.65	2.14	1.03	0.959	1.77	1.31
5.0E−6	2.77	2.27	1.07	1.00	1.85	1.37
1.0E−5	2.84	2.34	1.09	1.02	1.89	1.40
2.0E−5	2.85	2.37	1.11	1.03	1.91	1.41
5.0E−5	2.86	2.39	1.12	1.04	1.92	1.43
1.0E−4	2.88	2.41	1.12	1.04	1.92	1.43
2.0E−4	2.86	2.41	1.11	1.03	1.92	1.44
5.0E−4	2.86	2.42	1.10	1.03	1.91	1.44
0.001	2.82	2.41	1.09	1.02	1.90	1.43
0.002	2.79	2.40	1.09	1.02	1.90	1.43
0.005	2.79	2.41	1.09	1.01	1.91	1.42
0.01	2.81	2.43	1.11	1.02	1.93	1.42
0.02	2.86	2.47	1.12	1.03	1.96	1.45
0.03	2.94	2.51	1.14	1.05	1.99	1.49
0.05	3.09	2.59	1.20	1.11	2.08	1.56
0.07	3.25	2.68	1.26	1.17	2.17	1.63
0.1	3.49	2.81	1.36	1.28	2.33	1.74
0.15	3.91	3.05	1.52	1.45	2.58	1.93
0.2	4.33	3.29	1.70	1.62	2.85	2.12
0.3	5.19	3.78	2.05	1.98	3.38	2.52
0.5	6.88	4.84	2.80	2.71	4.48	3.34
0.7	8.48	5.93	3.57	3.45	5.60	4.18
0.9	10.0	7.07	4.35	4.22	6.73	5.04
1.0	10.8	7.67	4.76	4.62	7.31	5.48
1.2	12.4	8.94	5.62	5.45	8.49	6.39
1.5	14.7	10.9	6.96	6.73	10.3	7.78
2.0	18.5	14.2	9.21	8.90	13.3	10.1
3.0	25.0	20.3	13.5	13.0	18.8	14.5
4.0	30.4	25.7	17.5	16.9	23.7	18.5
5.0	35.0	30.3	21.1	20.3	28.0	22.2
6.0	38.9	34.4	24.4	23.5	31.7	25.4
7.0	42.4	37.9	27.3	26.3	35.1	28.4
8.0	45.4	41.1	30.0	28.9	38.1	31.0
9.0	48.2	43.9	32.4	31.2	40.8	33.5
10.0	50.7	46.5	34.7	33.4	43.2	35.7
12.0	55.0	51.1	38.7	37.3	47.5	39.5
14.0	58.5	54.9	42.2	40.7	51.0	42.8
15.0	60.0	56.5	43.8	42.3	52.5	44.3
16.0	61.3	58.0	45.2	43.7	53.9	45.6
18.0	63.4	60.6	47.8	46.3	56.4	48.0
20.0	65.2	62.7	50.1	48.6	58.4	50.2
21.0	66.0	63.7	51.2	49.6	59.4	51.1
30.0	70.9	69.9	58.6	57.0	65.5	58.0
50.0	76.7	77.0	68.8	67.1	73.3	67.7
75.0	81.8	83.7	77.9	76.1	80.6	76.7
100	86.0	90.0	85.5	83.6	87.0	84.5
130	90.1	96.8	93.3	91.7	94.0	92.9
150	92.6	101	98.1	96.7	98.4	98.1
180	96.0	106	105	104	105	105
200	98.4	110	109	108	109	110
300	112	126	128	129	128	132
400	130	145	147	149	147	152
500	148	164	166	169	165	170
600	166	183	184	187	182	188
700	182	199	200	203	197	203
800	195	212	213	217	210	217
900	206	222	224	228	222	229
1000	215	231	234	238	231	239
2000	266	282	295	300	292	312
5000	332	367	408	409	380	430
10,000	431	468	527	520	484	565

AP, antero-posterior; PA, postero-anterior; LLAT, left lateral; RLAT, right lateral; ROT, rotational; ISO, isotropic.

Table C.26. Neutrons, male: salivary glands absorbed dose per fluence, in units of pGy cm^2, for mono-energetic particles incident in various geometries.

Energy (MeV)	AP	PA	LLAT	RLAT	ROT	ISO
1.0E−9	0.872	0.573	1.00	0.973	0.845	0.622
1.0E−8	0.976	0.613	1.17	1.15	0.960	0.741
2.5E−8	1.05	0.689	1.32	1.28	1.05	0.821
1.0E−7	1.29	0.888	1.63	1.53	1.34	1.04
2.0E−7	1.43	0.981	1.76	1.72	1.50	1.13
5.0E−7	1.59	1.12	1.91	1.89	1.66	1.24
1.0E−6	1.65	1.21	1.98	1.94	1.74	1.31
2.0E−6	1.70	1.26	2.03	1.97	1.77	1.37
5.0E−6	1.78	1.30	2.05	2.01	1.80	1.38
1.0E−5	1.80	1.32	2.03	1.99	1.79	1.37
2.0E−5	1.79	1.32	2.01	1.96	1.78	1.34
5.0E−5	1.76	1.31	1.97	1.92	1.74	1.32
1.0E−4	1.74	1.32	1.92	1.88	1.71	1.29
2.0E−4	1.71	1.29	1.86	1.82	1.69	1.27
5.0E−4	1.69	1.28	1.80	1.77	1.66	1.25
0.001	1.67	1.26	1.75	1.73	1.63	1.23
0.002	1.65	1.23	1.72	1.71	1.59	1.22
0.005	1.61	1.23	1.73	1.72	1.59	1.21
0.01	1.61	1.26	1.81	1.79	1.63	1.23
0.02	1.65	1.31	2.02	1.92	1.76	1.32
0.03	1.70	1.38	2.23	2.10	1.91	1.43
0.05	1.83	1.55	2.64	2.46	2.21	1.65
0.07	1.95	1.75	3.03	2.84	2.51	1.88
0.1	2.17	2.04	3.59	3.38	2.95	2.21
0.15	2.59	2.56	4.48	4.23	3.65	2.75
0.2	3.06	3.09	5.29	5.03	4.33	3.27
0.3	4.08	4.20	6.79	6.50	5.62	4.26
0.5	6.23	6.41	9.33	9.04	7.94	6.09
0.7	8.34	8.49	11.5	11.2	10.0	7.76
0.9	10.4	10.5	13.4	13.1	11.9	9.30
1.0	11.4	11.5	14.3	14.0	12.9	10.0
1.2	13.4	13.5	16.0	15.7	14.6	11.5
1.5	16.3	16.4	18.3	18.1	17.1	13.5
2.0	20.7	20.8	21.8	21.5	20.9	16.6
3.0	28.0	28.2	27.6	27.5	27.3	22.0
4.0	33.8	34.1	32.5	32.4	32.6	26.5
5.0	38.5	38.9	36.7	36.5	37.0	30.2
6.0	42.5	42.9	40.2	39.9	40.7	33.5
7.0	45.9	46.4	43.4	43.0	44.0	36.5
8.0	48.9	49.5	46.2	45.7	46.9	39.1
9.0	51.6	52.4	48.7	48.3	49.6	41.6
10.0	54.1	55.1	50.9	50.6	52.0	43.8
12.0	58.4	59.7	54.8	54.8	56.2	47.6
14.0	61.8	63.4	57.9	58.2	59.5	50.7
15.0	63.2	64.9	59.2	59.7	60.9	52.1
16.0	64.5	66.3	60.4	61.0	62.0	53.2
18.0	66.6	68.6	62.3	63.2	63.9	55.2
20.0	68.3	70.4	63.9	65.0	65.2	56.8
21.0	69.1	71.1	64.5	65.8	65.7	57.5
30.0	73.9	75.6	68.3	70.2	68.4	61.6
50.0	78.6	79.7	71.8	73.7	69.5	65.4
75.0	79.7	82.5	74.5	76.2	71.0	68.7
100	78.4	83.9	76.8	78.1	73.6	72.3
130	76.9	84.7	79.2	80.0	77.0	76.9
150	76.7	85.2	80.8	81.6	79.2	79.9
180	77.2	86.4	83.6	84.5	82.7	84.3
200	78.1	87.7	85.6	86.5	85.0	87.2
300	87.4	98.6	97.5	98.0	98.1	102
400	101	114	111	112	113	117
500	115	132	125	127	129	133
600	129	149	138	142	143	148
700	141	163	149	154	155	160
800	151	175	159	165	165	169
900	158	183	168	173	173	177
1000	165	190	175	179	180	184
2000	196	220	220	213	213	226
5000	240	267	291	280	254	300
10,000	306	352	373	391	326	417

AP, antero-posterior; PA, postero-anterior; LLAT, left lateral; RLAT, right lateral; ROT, rotational; ISO, isotropic.

Table C.27. Neutrons, male: skin absorbed dose per fluence, in units of pGy cm^2, for mono-energetic particles incident in various geometries.

Energy (MeV)	AP	PA	LLAT	RLAT	ROT	ISO
1.0E−9	1.62	1.71	0.792	0.786	1.25	0.993
1.0E−8	1.40	1.43	0.655	0.653	1.11	0.881
2.5E−8	1.38	1.45	0.653	0.652	1.10	0.870
1.0E−7	1.48	1.55	0.667	0.667	1.16	0.910
2.0E−7	1.55	1.63	0.698	0.697	1.20	0.942
5.0E−7	1.60	1.70	0.726	0.725	1.26	0.978
1.0E−6	1.62	1.75	0.739	0.740	1.28	0.996
2.0E−6	1.64	1.77	0.739	0.743	1.30	1.00
5.0E−6	1.65	1.80	0.743	0.745	1.30	0.999
1.0E−5	1.63	1.77	0.733	0.732	1.28	0.986
2.0E−5	1.60	1.75	0.719	0.719	1.26	0.971
5.0E−5	1.56	1.68	0.689	0.689	1.23	0.942
1.0E−4	1.52	1.65	0.674	0.674	1.20	0.919
2.0E−4	1.49	1.63	0.663	0.663	1.17	0.899
5.0E−4	1.46	1.58	0.645	0.644	1.14	0.878
0.001	1.45	1.56	0.642	0.642	1.13	0.876
0.002	1.47	1.57	0.649	0.651	1.15	0.894
0.005	1.57	1.66	0.708	0.710	1.24	0.978
0.01	1.78	1.86	0.819	0.818	1.41	1.14
0.02	2.19	2.25	1.04	1.03	1.76	1.46
0.03	2.58	2.62	1.26	1.24	2.10	1.76
0.05	3.30	3.29	1.64	1.61	2.70	2.31
0.07	3.94	3.90	1.99	1.95	3.23	2.80
0.1	4.78	4.70	2.46	2.41	3.94	3.46
0.15	5.99	5.84	3.14	3.07	4.95	4.41
0.2	7.02	6.82	3.73	3.64	5.83	5.23
0.3	8.78	8.50	4.76	4.65	7.34	6.63
0.5	11.6	11.2	6.49	6.33	9.81	8.93
0.7	14.1	13.6	8.00	7.81	11.9	10.9
0.9	16.2	15.6	9.39	9.17	13.8	12.6
1.0	17.2	16.6	10.0	9.81	14.6	13.4
1.2	18.9	18.3	11.3	11.0	16.2	14.8
1.5	21.2	20.5	12.9	12.7	18.2	16.8
2.0	24.5	23.8	15.4	15.1	21.3	19.6
3.0	30.3	29.4	19.8	19.5	26.6	24.5
4.0	35.1	34.1	23.6	23.2	30.9	28.5
5.0	39.0	38.0	26.8	26.5	34.7	32.0
6.0	42.3	41.3	29.7	29.3	37.9	35.0
7.0	45.3	44.3	32.3	31.9	40.8	37.7
8.0	48.0	46.9	34.6	34.2	43.3	40.1
9.0	50.5	49.4	36.7	36.3	45.7	42.3
10.0	52.7	51.6	38.7	38.3	47.7	44.3
12.0	56.6	55.4	42.2	41.8	51.1	47.6
14.0	59.4	58.1	45.0	44.6	53.5	50.0
15.0	60.5	59.2	46.1	45.7	54.4	51.0
16.0	61.3	60.0	47.2	46.8	55.1	51.7
18.0	62.5	61.2	48.9	48.5	56.1	52.8
20.0	63.2	61.8	50.3	49.9	56.6	53.5
21.0	63.4	62.1	50.9	50.5	56.8	53.7
30.0	63.9	62.6	54.4	54.1	56.7	54.4
50.0	63.4	62.8	58.3	58.1	55.6	54.5
75.0	63.3	63.2	61.2	61.0	56.3	55.9
100	62.8	62.9	62.8	62.7	58.3	58.5
130	62.8	62.6	64.3	64.3	61.4	62.1
150	63.4	63.0	65.6	65.6	63.7	64.5
180	64.9	64.1	68.1	68.1	67.0	68.3
200	66.3	65.3	69.9	69.9	69.3	70.8
300	75.6	73.7	80.8	80.8	81.0	83.5
400	87.3	85.0	93.4	93.5	92.8	96.0
500	99.6	97.0	106	106	104	108
600	112	108	119	119	115	119
700	122	118	129	130	125	129
800	131	126	138	139	132	138
900	138	132	146	146	139	145
1000	144	137	152	152	145	152
2000	176	164	189	191	181	193
5000	218	209	265	264	235	262
10,000	291	281	360	352	297	346

AP, antero-posterior; PA, postero-anterior; LLAT, left lateral; RLAT, right lateral; ROT, rotational; ISO, isotropic.

Table C.28. Neutrons, male: stomach wall absorbed dose per fluence, in units of pGy cm^2, for mono-energetic particles incident in various geometries.

Energy (MeV)	AP	PA	LLAT	RLAT	ROT	ISO
1.0E−9	1.18	0.551	0.560	0.166	0.607	0.452
1.0E−8	1.42	0.631	0.666	0.172	0.740	0.549
2.5E−8	1.60	0.726	0.748	0.191	0.834	0.632
1.0E−7	2.16	0.971	1.01	0.244	1.13	0.834
2.0E−7	2.47	1.12	1.18	0.281	1.30	0.941
5.0E−7	2.87	1.31	1.39	0.331	1.50	1.09
1.0E−6	3.10	1.43	1.51	0.357	1.63	1.21
2.0E−6	3.32	1.53	1.63	0.374	1.73	1.30
5.0E−6	3.52	1.62	1.75	0.396	1.85	1.39
1.0E−5	3.58	1.67	1.79	0.412	1.90	1.41
2.0E−5	3.59	1.69	1.80	0.421	1.92	1.42
5.0E−5	3.64	1.73	1.81	0.423	1.92	1.44
1.0E−4	3.67	1.74	1.82	0.421	1.95	1.46
2.0E−4	3.65	1.74	1.83	0.423	1.96	1.47
5.0E−4	3.65	1.76	1.82	0.424	1.96	1.46
0.001	3.64	1.76	1.79	0.426	1.95	1.45
0.002	3.62	1.75	1.76	0.424	1.95	1.44
0.005	3.61	1.76	1.78	0.430	1.96	1.44
0.01	3.62	1.78	1.81	0.442	1.96	1.45
0.02	3.66	1.82	1.81	0.439	1.99	1.46
0.03	3.71	1.86	1.84	0.437	2.02	1.47
0.05	3.82	1.92	1.92	0.443	2.07	1.51
0.07	3.95	1.97	1.98	0.463	2.12	1.56
0.1	4.15	2.04	2.08	0.492	2.21	1.64
0.15	4.52	2.14	2.30	0.528	2.39	1.78
0.2	4.92	2.25	2.54	0.557	2.59	1.92
0.3	5.80	2.46	3.11	0.612	3.02	2.21
0.5	7.68	2.92	4.38	0.729	3.91	2.84
0.7	9.53	3.45	5.73	0.874	4.84	3.53
0.9	11.4	4.05	7.13	1.06	5.81	4.26
1.0	12.3	4.39	7.86	1.17	6.32	4.65
1.2	14.2	5.15	9.39	1.44	7.38	5.46
1.5	17.0	6.43	11.7	1.94	9.03	6.73
2.0	21.3	8.76	15.6	2.96	11.8	8.91
3.0	28.8	13.6	22.4	5.46	16.9	13.2
4.0	34.9	18.2	28.1	8.25	21.6	17.1
5.0	39.9	22.5	32.9	11.1	25.8	20.8
6.0	44.1	26.4	37.0	14.0	29.5	24.0
7.0	47.7	30.0	40.7	16.6	32.9	27.0
8.0	50.9	33.1	43.9	19.1	35.9	29.6
9.0	53.7	36.0	46.8	21.4	38.6	32.0
10.0	56.3	38.7	49.5	23.5	41.0	34.2
12.0	60.6	43.4	54.1	27.5	45.4	38.0
14.0	64.0	47.5	57.9	31.0	49.0	41.3
15.0	65.4	49.2	59.5	32.7	50.6	42.7
16.0	66.6	50.9	61.0	34.3	52.1	44.1
18.0	68.7	53.8	63.5	37.4	54.7	46.5
20.0	70.3	56.3	65.6	40.2	56.9	48.6
21.0	71.0	57.4	66.5	41.5	57.9	49.5
30.0	75.6	65.1	72.2	51.0	64.6	56.4
50.0	80.8	75.2	78.9	64.7	73.3	66.3
75.0	85.1	84.6	85.9	76.6	81.3	75.4
100	88.3	93.0	92.1	86.7	88.4	83.3
130	91.3	102	97.8	97.7	96.3	91.8
150	93.1	108	101	104	101	97.0
180	95.8	116	104	114	108	104
200	97.7	121	107	119	112	109
300	110	145	119	146	133	131
400	125	168	136	171	153	152
500	142	191	155	194	173	172
600	159	212	173	216	191	191
700	174	230	189	235	207	208
800	186	245	203	250	222	223
900	197	257	214	263	233	236
1000	206	268	223	274	244	247
2000	253	333	271	349	309	325
5000	305	446	355	484	410	450
10,000	394	559	459	617	529	601

AP, antero-posterior; PA, postero-anterior; LLAT, left lateral; RLAT, right lateral; ROT, rotational; ISO, isotropic.

Table C.29. Neutrons, male: thyroid absorbed dose per fluence, in units of pGy cm^2, for mono-energetic particles incident in various geometries.

Energy (MeV)	AP	PA	LLAT	RLAT	ROT	ISO
1.0E−9	1.66	0.563	0.517	0.495	0.878	0.677
1.0E−8	1.98	0.661	0.568	0.557	0.985	0.749
2.5E−8	2.20	0.723	0.640	0.612	1.08	0.849
1.0E−7	2.84	0.940	0.836	0.805	1.34	1.07
2.0E−7	3.21	1.08	0.945	0.923	1.51	1.19
5.0E−7	3.62	1.26	1.08	1.08	1.73	1.35
1.0E−6	3.82	1.42	1.15	1.14	1.86	1.43
2.0E−6	3.94	1.56	1.19	1.17	1.96	1.46
5.0E−6	4.00	1.63	1.24	1.16	2.06	1.51
1.0E−5	4.02	1.65	1.25	1.15	2.11	1.55
2.0E−5	3.98	1.65	1.24	1.20	2.12	1.56
5.0E−5	3.85	1.67	1.21	1.23	2.08	1.53
1.0E−4	3.73	1.69	1.20	1.22	2.05	1.50
2.0E−4	3.66	1.72	1.21	1.20	2.02	1.47
5.0E−4	3.59	1.74	1.22	1.16	1.95	1.43
0.001	3.50	1.74	1.20	1.14	1.89	1.42
0.002	3.43	1.71	1.16	1.13	1.87	1.42
0.005	3.39	1.71	1.10	1.11	1.85	1.40
0.01	3.42	1.73	1.09	1.10	1.87	1.41
0.02	3.52	1.75	1.13	1.13	1.95	1.45
0.03	3.70	1.77	1.16	1.17	2.02	1.50
0.05	4.14	1.83	1.23	1.24	2.18	1.61
0.07	4.65	1.88	1.30	1.31	2.37	1.72
0.1	5.43	1.95	1.42	1.45	2.68	1.91
0.15	6.73	2.05	1.61	1.74	3.21	2.22
0.2	8.01	2.13	1.83	2.05	3.74	2.55
0.3	10.5	2.29	2.29	2.68	4.77	3.18
0.5	14.9	2.76	3.26	3.93	6.69	4.42
0.7	18.7	3.38	4.22	5.09	8.47	5.66
0.9	21.9	4.14	5.17	6.21	10.1	6.89
1.0	23.4	4.57	5.64	6.77	10.9	7.50
1.2	26.1	5.51	6.59	7.90	12.5	8.69
1.5	29.7	7.09	8.01	9.59	14.7	10.4
2.0	34.7	9.91	10.3	12.3	18.2	13.2
3.0	42.4	15.5	14.6	17.1	24.2	18.1
4.0	48.3	20.6	18.4	21.2	29.2	22.3
5.0	53.0	25.2	21.8	24.8	33.6	26.1
6.0	56.8	29.2	24.9	28.0	37.3	29.4
7.0	60.1	32.8	27.6	30.8	40.5	32.3
8.0	63.0	35.9	30.1	33.4	43.4	35.0
9.0	65.7	38.8	32.4	35.7	45.9	37.4
10.0	68.0	41.4	34.4	37.8	48.1	39.7
12.0	71.9	45.9	38.2	41.6	51.9	43.6
14.0	74.8	49.7	41.4	44.8	54.8	47.0
15.0	76.0	51.4	42.9	46.2	56.1	48.4
16.0	77.1	52.9	44.3	47.6	57.2	49.8
18.0	78.8	55.7	46.8	49.9	59.0	52.2
20.0	80.1	58.0	49.1	51.9	60.6	54.2
21.0	80.6	59.1	50.1	52.9	61.2	55.2
30.0	83.2	66.6	57.9	59.4	65.5	61.3
50.0	82.4	75.8	69.0	68.9	70.9	69.3
75.0	78.3	83.0	77.7	76.0	76.0	76.0
100	74.5	88.8	83.5	80.7	80.5	81.3
130	72.0	95.3	88.9	85.1	85.7	86.8
150	71.5	99.4	92.0	87.7	89.2	90.2
180	72.0	105	96.5	91.6	94.4	95.2
200	72.8	109	99.4	94.3	97.9	98.5
300	80.9	128	114	111	115	115
400	92.5	147	128	130	130	132
500	105	165	142	149	144	147
600	118	182	155	168	156	162
700	129	197	167	185	167	176
800	138	209	177	197	177	188
900	146	219	187	206	186	198
1000	152	228	195	213	193	208
2000	190	288	250	249	242	269
5000	238	379	346	317	319	374
10,000	297	457	448	441	401	523

AP, antero-posterior; PA, postero-anterior; LLAT, left lateral; RLAT, right lateral; ROT, rotational; ISO, isotropic.

Table C.30. Neutrons, male: UB (urinary bladder) wall absorbed dose per fluence, in units of pGy cm^2, for mono-energetic particles incident in various geometries.

Energy (MeV)	AP	PA	LLAT	RLAT	ROT	ISO
1.0E−9	1.21	0.655	0.226	0.205	0.613	0.453
1.0E−8	1.47	0.784	0.258	0.223	0.752	0.532
2.5E−8	1.68	0.926	0.276	0.245	0.859	0.602
1.0E−7	2.27	1.24	0.352	0.317	1.14	0.808
2.0E−7	2.63	1.40	0.407	0.365	1.27	0.938
5.0E−7	3.11	1.61	0.472	0.423	1.46	1.10
1.0E−6	3.38	1.76	0.515	0.460	1.59	1.18
2.0E−6	3.61	1.90	0.553	0.489	1.72	1.25
5.0E−6	3.84	2.02	0.579	0.519	1.83	1.32
1.0E−5	3.92	2.06	0.593	0.534	1.88	1.37
2.0E−5	3.91	2.11	0.603	0.543	1.90	1.41
5.0E−5	3.93	2.18	0.616	0.552	1.90	1.44
1.0E−4	3.93	2.22	0.612	0.554	1.93	1.43
2.0E−4	3.93	2.20	0.615	0.556	1.96	1.41
5.0E−4	3.94	2.20	0.627	0.557	1.95	1.41
0.001	3.93	2.21	0.627	0.552	1.93	1.42
0.002	3.92	2.22	0.628	0.550	1.93	1.42
0.005	3.89	2.27	0.619	0.561	1.98	1.40
0.01	3.91	2.30	0.615	0.576	2.02	1.41
0.02	3.95	2.32	0.618	0.576	2.04	1.44
0.03	4.01	2.35	0.619	0.580	2.05	1.46
0.05	4.15	2.43	0.636	0.597	2.07	1.51
0.07	4.29	2.51	0.655	0.612	2.13	1.55
0.1	4.50	2.61	0.680	0.633	2.22	1.62
0.15	4.92	2.75	0.725	0.664	2.38	1.73
0.2	5.39	2.87	0.772	0.700	2.56	1.85
0.3	6.40	3.13	0.866	0.776	2.93	2.10
0.5	8.50	3.72	1.07	0.932	3.72	2.65
0.7	10.5	4.38	1.31	1.12	4.55	3.26
0.9	12.5	5.14	1.60	1.36	5.44	3.91
1.0	13.5	5.56	1.77	1.50	5.92	4.26
1.2	15.6	6.49	2.18	1.85	6.92	4.98
1.5	18.7	8.02	2.91	2.47	8.52	6.12
2.0	23.4	10.8	4.34	3.73	11.2	8.07
3.0	31.2	16.3	7.63	6.74	16.4	12.0
4.0	37.5	21.5	11.1	9.98	21.2	15.7
5.0	42.6	26.2	14.5	13.2	25.5	19.2
6.0	46.9	30.4	17.7	16.4	29.3	22.3
7.0	50.6	34.2	20.7	19.3	32.7	25.2
8.0	53.9	37.6	23.5	21.9	35.7	27.8
9.0	56.9	40.7	25.9	24.4	38.5	30.2
10.0	59.6	43.5	28.2	26.6	41.0	32.4
12.0	64.2	48.4	32.4	30.8	45.5	36.3
14.0	67.7	52.5	36.1	34.5	49.2	39.6
15.0	69.2	54.3	37.8	36.2	50.9	41.1
16.0	70.5	55.9	39.4	37.8	52.4	42.5
18.0	72.6	58.8	42.4	40.8	55.0	45.1
20.0	74.3	61.2	45.1	43.5	57.3	47.4
21.0	75.0	62.3	46.4	44.8	58.3	48.5
30.0	79.3	69.3	55.4	53.6	65.1	56.4
50.0	83.4	78.0	67.3	65.6	74.0	68.3
75.0	86.6	86.5	78.2	76.9	82.3	79.2
100	88.9	94.4	87.7	86.8	90.0	88.6
130	90.7	103	98.2	97.9	98.5	98.5
150	92.0	108	105	105	104	105
180	94.2	114	113	114	111	113
200	95.9	118	119	119	115	119
300	108	139	143	143	135	144
400	125	161	166	166	157	165
500	143	183	189	188	179	184
600	162	204	209	210	200	202
700	179	222	227	228	218	218
800	192	236	241	243	233	232
900	203	248	253	256	245	244
1000	212	258	263	266	256	256
2000	260	317	330	335	322	338
5000	314	412	471	472	419	483
10,000	414	525	612	614	525	652

AP, antero-posterior; PA, postero-anterior; LLAT, left lateral; RLAT, right lateral; ROT, rotational; ISO, isotropic.

ANNEX D. SKELETAL FLUENCE-TO-DOSE RESPONSE FUNCTIONS: PHOTONS

(D1) The tissues of the skeleton at radiological risk, and hence assigned tissue weighting factors w_T, cannot be represented geometrically in the ICRP reference computational phantoms. The energy deposition in these tissues is influenced by their proximity to those of different densities and elemental compositions. This energy deposition can be derived during the Monte Carlo calculations of photon transport through scaling the calculated photon fluence in different skeletal regions (spongiosa or medullary cavities) by functions representing the absorbed dose to the target tissue per photon fluence (Eckerman, 1985; Eckerman et al., 2008; Johnson et al., 2011). These functions, referred to as response functions $\mathcal{R}$, are derived using models of the microscopic structure of bone geometry of different skeletal regions and the transport of the secondary ionising radiations through those geometries (Hough et al., 2011). While response function values are given in this annex for photon interactions within the skeleton, similar functions can be derived for assessing skeletal doses from neutron irradiation (see Annex E).

D.1. Response functions for assessment of bone-specific photon skeletal dose

(D2) The response function $\mathcal{R}$ for assessment of the bone-specific absorbed dose to skeletal tissues delivered by photons of energy E in bone site x is given as follows:

$$\mathcal{R}(r_T \leftarrow r_S, x, E) = \frac{D(r_T, x)}{\Phi(E, r_S, x)} \tag{D.1}$$

$$= \sum_r \frac{m(r, x)}{m(r_T, x)} \sum_i \int_o^\infty \phi(r_T \leftarrow r, T_i, x)(\mu_i/\rho)_{r,E} T_i n_r(T_i, E) dT_i \tag{D.2}$$

where x is the index for the various bone sites within the phantom (upper femora, cranium, etc.; for the long bones, regions of spongiosa and the medullary cavities are considered as different bone sites); r_T is the index for the target tissue for dose assessment (active marrow or endosteum); r_S is the index for the source tissue in bone site x in which the photon fluence is scored (spongiosa or medullary marrow); r is the index for the constituent tissues of source tissue r_S (for r_S = spongiosa, r is trabecular bone, active marrow, or inactive marrow; for medullary marrow, r is inactive marrow in the adult); E is the energy of the photon passing through and potentially interacting within skeletal tissue r_S of bone site x; $m(r, x)$ is the mass of the constituent tissue r in bone site x; $m(r_T, x)$ is the mass of the target tissue r_T in bone site x; i is the index for the photon interaction type considered (photo electric, Compton, pair production, or triplet production); T_i is the energy of the secondary electron liberated in constituent tissue r by interaction type i; $\phi(r_T \leftarrow r, T_i, x)$ is the fraction of secondary electron energy T_i liberated in constituent tissue r of bone site x that is

imparted to target tissue r_T in bone site x; $(\mu_i/\rho)_{r,E}$ is the mass attenuation coefficient for photon interaction type i in constituent tissue r at photon energy E; and $n_r(T_i, E)dT_i$ denotes the number of secondary electrons of energy between T_i and $T_i + dT_i$ liberated in constituent tissue r by photon of energy E in interaction type i.

(D3) In this report, Eq. (D.2) was evaluated as described in Johnson et al. (2011). Electron absorbed fraction data were obtained through paired-image radiation transport calculations using micro-computer-tomography images of 32 bone sites extracted from the skeleton of a 40-year-old male cadaver (Hough et al., 2011). Charged-particle equilibrium is typically established across bone sites at photon energies exceeding 200 keV, and thus in this report, values of the dose–response function above that energy are taken as their corresponding spongiosa kerma coefficients. Bone-specific dose–response functions from Eq. (D.2) are given in tabular form in Table 1, with graphical displays of the same functions given in Figs. D.1–D.3.

(D4) The absorbed dose to tissue r_T in bone site x, $D(r_T, x)$ is thus determined as the integral of the product of the bone-specific energy-dependent photon fluence $\Phi(E, r_S, x)$ and the bone-specific energy-dependent dose–response function $\mathcal{R}(r_T \leftarrow r_S, x, E)$:

$$D(r_T, x) = \int_E \Phi(E, r_S, x)\mathcal{R}(r_T \leftarrow r_S, x, E)dE \tag{D.3}$$

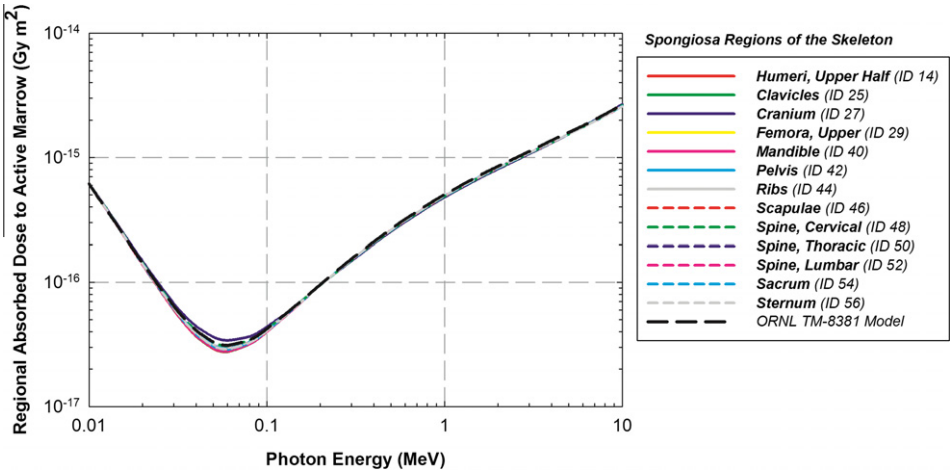

Fig. D.1. Bone-specific absorbed dose to active bone marrow per photon fluence (Gy m^2) scored within the spongiosa regions of individual bones of the ICRP reference phantoms. The ORNL-TM 8381 homogeneous skeletal model for active marrow in the lumbar vertebra is shown for comparison.

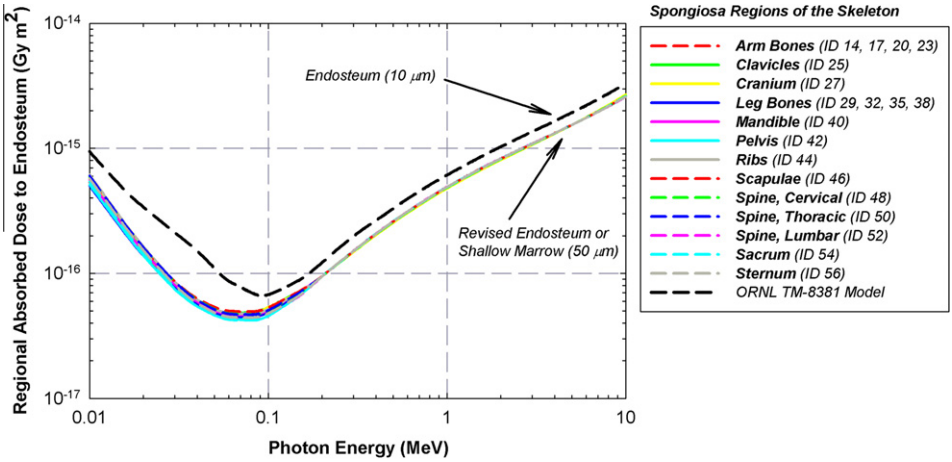

Fig. D.2. Bone-specific absorbed dose to endosteum per photon fluence (Gy m^2) scored within the spongiosa regions of individual bones of the ICRP reference phantoms. The ORNL-TM 8381 homogeneous skeletal model for endosteum within the lumbar vertebra is shown for comparison.

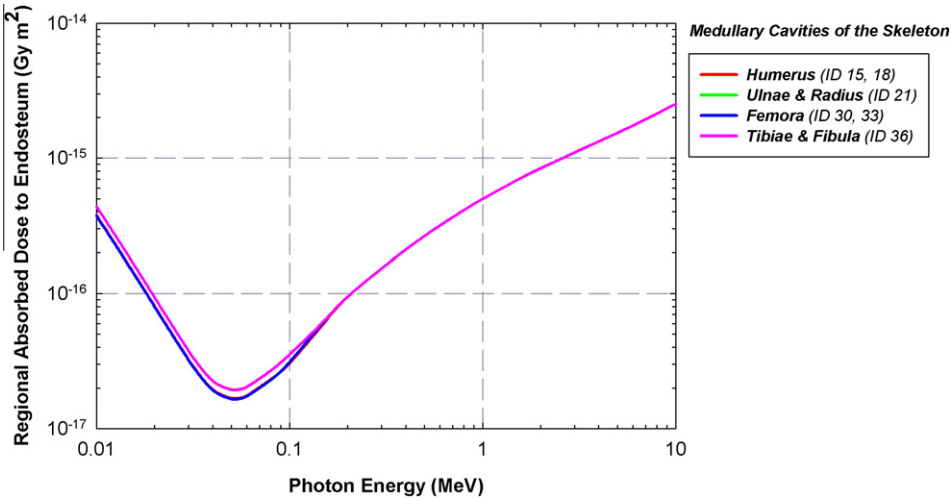

Fig. D.3. Bone-specific absorbed dose to endosteum per photon fluence (Gy m^2) scored within the medullary cavities of individual long bones of the ICRP reference phantoms.

(D5) Several estimators of photon fluence can be formulated within the Monte Carlo simulation of photon transport. As the fluence of interest is within volumes not representing voids, a 'collision density estimator' can be used as follows:

$$\Phi(E, r_S, x) = \frac{N(E, r_S, x)}{\mu(E, r_S, x)V(r_S, x)} \tag{D.4a}$$

where $V(r_S, x)$ is the volume of source tissue r_S within bone site x where the fluence is to be tallied; $N(E, r_S, x)$ is the number of photon interactions occurring within this volume; and $\mu(E, r_S, x)$ is the corresponding linear attenuation coefficient for the relevant tissue medium at photon energy E. Similarly, the fluence can be based on a 'track length estimator' as:

$$\Phi(E, r_S, x) = \frac{L(E, r_S, x)}{V(r_S, x)} \tag{D.4b}$$

where $L(E, r_S, x)$ is the total track length of the photon of energy E in the source tissue r_S within bone site x.

D.2. Scaling factors for assessment of bone-specific photon skeletal dose

(D6) An alternative to the dose–response function method is to apply energy-dependent scaling factors to spongiosa kerma (Kramer, 1979; Zankl et al., 2002; Lee et al., 2006). In this approach, the absorbed dose to active marrow and endosteum is determined by three factors:

$$D(AM, x) = \int_E K(SP, x, E) \left[\frac{\mu_{en}}{\rho}(E)\right]_{SP}^{AM} \mathcal{S}(AM, x, E) dE \tag{D.5}$$

and:

$$D(TM_{50}, x) = \int_E K(SP/MM, x, E) \left[\frac{\mu_{en}}{\rho}(E)\right]_{SP/MM}^{TM} \mathcal{S}(TM_{50}, x, E) dE \tag{D.6}$$

where $K(SP/MM, x, E)$ is the kerma to either spongiosa (SP) or medullary marrow (MM) within bone site x contributed by photons of energy E; $\left[\frac{\mu_{en}}{\rho}(E)\right]_{SP}^{AM}$ is the MEAC ratio in active marrow to that in spongiosa; $\left[\frac{\mu_{en}}{\rho}(E)\right]_{SP/MM}^{TM}$ is the MEAC ratio in total marrow to that in either spongiosa or the medullary marrow; $\mathcal{S}(AM, x, E)$ is the dose enhancement factor to active marrow and $\mathcal{S}(TM_{50}, x, E)$ is the dose enhancement factor to endosteum.

(D7) Eqs (D.5) and (D.6) can also be re-expressed in terms of ratios of kerma coefficients (kerma per fluence – lowercase k) and the dose–response function as follows:

$$D(AM, x) = \int_E K(SP, x, E) \left[\frac{k(AM, x, E)}{k(SP, x, E)}\right] \left[\frac{\mathcal{R}(AM \leftarrow SP, x, E)}{k(AM, x, E)}\right] dE \tag{D.7}$$

and:

$$D(TM_{50}, x) = \int_E K(SP/MM, x, E) \left[\frac{k(TM, x, E)}{k(SP/MM, x, E)}\right] \left[\frac{\mathcal{R}(TM_{50} \leftarrow SP, x, E)}{k(TM, x, E)}\right] dE \tag{D.8}$$

(D8) In application of the three-factor method, energy-dependent kerma is first scored within each spongiosa and medullary marrow region of the computational phantom. These values are then additionally scaled by the

corresponding MEAC ratio (active marrow to spongiosa or total marrow to either spongiosa or medullary marrow) and the dose enhancement factor (active marrow or endosteum targets). MEAC ratios should be assembled by the specific user based upon the unique elemental compositions of the skeletal tissues of the computational phantom employed, and the MEAC values specific to the cross section library used during photon radiation transport. For reference, such ratios are provided in Tables D.2 and D.3 for the ICRP computational male and female reference phantoms, respectively, based on the skeletal elemental compositions given in Annex B of ICRP *Publication 110* (ICRP, 2009), and MEAC values based on these elemental compositions as taken from the Physical Data Library of the National Institute of Standards and Technology (Hubbell and Seltzer, 2004). Values of the dose enhancement factor are given in Table D.4 for both active marrow and endosteum as a function of photon energy and skeletal site, as in the study of Johnson et al. (2011). As the composition of the medullary cavities is identical to its endosteum, the MEAC ratio and dose enhancement factor are unity for endosteum along the medullary cavities. As with the dose–response function, the energy E is the energy of the photon passing through and potentially interacting within skeletal tissues, and not the energy of the photon incident upon the external surfaces of the computational phantom.

D.3. Skeletal-averaged photon absorbed dose

(D9) Estimates of bone-specific absorbed dose to the skeletal tissues can be of interest during partial-body irradiation as during interventional fluoroscopy or computed tomography. For purposes of radiological protection and calculation of the effective dose, however, skeletal-averaged absorbed doses to active marrow and endosteum are required. Accordingly, skeletal-averaged dose is given as a mass-weighted average of the bone-site absorbed dose:

$$D_{skel}(r_T) = \sum_x \frac{m(r_T, x)}{m(r_T)} D(r_T, x) \tag{D.9}$$

where $m(r_T, x)$ is the bone-specific mass of the target tissue r_T in bone site x; $m(r_T)$ is the total mass of target tissue r_T across the entire skeleton; and $D(r_T, x)$ is the bone-specific absorbed dose given by Eq. (D.3) [or Eqs (D.5) and (D.6)]. The masses of the skeletal tissues in the ICRP adult male and adult female reference phantoms are summarised in Section 3.4 of this report.

D.4. Approximating dose to skeletal target tissues via dose to trabecular spongiosa

(D10) As shown in Eqs (D.5) and (D.6), kerma to trabecular spongiosa is only an approximate estimate of the absorbed dose to either active marrow or

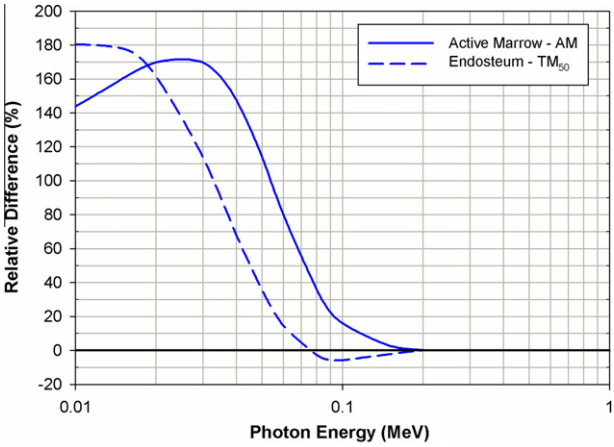

Fig. D.4. Relative difference (%) between photon kerma coefficients in spongiosa and the corresponding dose–response functions for both active marrow (AM) and endosteum (TM_{50}) targets in the reference adult skeleton.

endosteum. Two additional scaling factors should nominally be applied – the MEAC ratio and the dose enhancement factor. As shown in Table D.2 for the reference adult male, MEAC ratios are less than unity below ~200 keV, and at 30 keV can reach minimum values of between 0.26 (total marrow to spongiosa in the mandible) and 0.945 (active marrow to spongiosa in the sacrum). These reductions in spongiosa absorbed dose are then partially, but not fully, compensated by the application of the third term of Eqs (D.5) and (D.6) – the dose enhancement factor. Values of $\mathcal{S}$ for active marrow are given in Table D.4 and have maximal values at 50 keV that range from 1.00 in the proximal humerus to 1.25 in the cranium. Values of $\mathcal{S}$ for endosteum, also given in Table D.2, have maximal values at 50 keV that range from 1.68 in the sacrum to 2.33 in the hands and wrists (Johnson et al., 2011).

(D11) In Fig. D.4, the combined influences of the MEAC ratio and the dose enhancement factor are shown as relative differences between spongiosa kerma and the absorbed dose to both active marrow and endosteum. For active marrow, the relative difference from spongiosa kerma is 144% at 10 keV, 172% at 25 keV (maximal value), and ~16% at 100 keV. For endosteum, the relative difference from spongiosa kerma is 180% at 10 keV, 135% at 25 keV, and 15% at 60 keV. Spongiosa kerma is shown to underpredict endosteum absorbed dose by a few percent over the energy range 80–200 keV. Overall, the absorbed doses to active marrow and endosteum are conservatively estimated by spongiosa kerma for photons interacting within the skeleton at energies below 200 keV and below 80 keV, respectively.

D.5. References

Eckerman, K.F., 1985. Aspects of the dosimetry of radionuclides within the skeleton with particular emphasis on the active marrow. In: Schlafke-Stelson, A.T., Watson, E.E. (Eds.), Proceedings of the Fourth International Radiopharmaceutical Dosimetry Symposium. Oak Ridge Associated Universities, Oak Ridge, TN, pp. 514–534.

Eckerman, K.F., Bolch, W.E., Zankl, M., Petoussi-Henss, N., 2008. Response functions for computing absorbed dose to skeletal tissues for photon irradiation. Radiat. Prot. Dosim. 127, 187–191.

Hough, M., Johnson, P., Rajon, D., Jokisch, D., Lee, C., Bolch, W., 2011. An image-based skeletal dosimetry model for the ICRP reference adult male-internal electron sources. Phys. Med. Biol. 56, 2309–2346.

Hubbell, J., Seltzer, S., 2004. Tables of X-ray Mass Attenuation Coefficients and Mass Energy-Absorption Coefficients. Version 1.4. National Institute of Standards and Technology, Gaithersburg, MD.

ICRP, 2009. Adult reference computational phantoms. ICRP Publication 110. Ann. ICRP 39(2).

Johnson, P.B., Bahadori, A.A., Eckerman, K.F., Lee, C., Bolch, W.E., 2011. Response functions for computing absorbed dose to skeletal tissues from photon irradiation – an update. Phys. Med. Biol. 56, 2347–2365.

Kramer, R., 1979. Determination of Conversion Factors Between Tissue Dose and Relevant Radiation Quantities for External X-ray and Gamma-ray Radiation. GSF Report S-556. GSF – National Research Centre for Environment and Health, Neuherberg.

Lee, C., Lee, C., Shah, A.P., Bolch, W.E., 2006. An assessment of bone marrow and bone endosteum dosimetry methods for photon sources. Phys. Med. Biol. 51, 5391–5407.

Zankl, M., Fill, U., Petoussi-Henss, N., Regulla, D., 2002. Organ dose conversion coefficients for external photon irradiation of male and female voxel models. Phys. Med. Biol. 47, 2367–2385.

Table D.1. Bone-specific absorbed dose per photon fluence (Gy m^2) to active marrow (AM) and endosteum (TM_{50}) as a function of photon energy and skeletal region in the ICRP *Publication 110* reference phantoms.

Photon energy (MeV)	Organ ID: 14 Humeri, upper half Source: spongiosa Target tissue		Organ ID: 15 Humeri, upper half Source: medullary cavity Target tissue		Organ ID: 17 Humeri, lower half Source: spongiosa Target tissue		Organ ID: 18 Humeri, lower half Source: medullary cavity Target tissue		Organ ID: 20 Ulnae and radii Source: spongiosa Target tissue		Organ ID: 21 Ulnae and radii Source: medullary cavity Target tissue	
	AM	TM_{50}	AM	TM_{50}	AM	TM_{50}	AM	TM_{50}	AM	TM_{50}	AM	TM_{50}
0.010	6.13E−16	5.36E−16	NA	3.78E−16	NA	4.71E−16	NA	3.78E−16	NA	4.75E−16	NA	4.38E−16
0.015	2.58E−16	2.44E−16	NA	1.54E−16	NA	2.17E−16	NA	1.54E−16	NA	2.19E−16	NA	1.79E−16
0.020	1.38E−16	1.46E−16	NA	8.06E−17	NA	1.33E−16	NA	8.06E−17	NA	1.33E−16	NA	9.35E−17
0.030	5.98E−17	8.00E−17	NA	3.25E−17	NA	7.44E−17	NA	3.25E−17	NA	7.49E−17	NA	3.76E−17
0.040	3.68E−17	5.90E−17	NA	1.95E−17	NA	5.62E−17	NA	1.95E−17	NA	5.61E−17	NA	2.26E−17
0.050	2.92E−17	5.04E−17	NA	1.67E−17	NA	4.88E−17	NA	1.67E−17	NA	4.88E−17	NA	1.94E−17
0.060	2.76E−17	4.73E−17	NA	1.75E−17	NA	4.58E−17	NA	1.75E−17	NA	4.58E−17	NA	2.03E−17
0.080	3.18E−17	4.75E−17	NA	2.32E−17	NA	4.59E−17	NA	2.32E−17	NA	4.60E−17	NA	2.69E−17
0.10	3.99E−17	5.17E−17	NA	3.04E−17	NA	4.97E−17	NA	3.04E−17	NA	4.99E−17	NA	3.53E−17
0.15	6.56E−17	7.05E−17	NA	5.99E−17	NA	6.97E−17	NA	5.99E−17	NA	6.89E−17	NA	6.20E−17
0.20	9.48E−17	9.48E−17	NA	9.48E−17	NA	9.49E−17	NA	9.48E−17	NA	9.49E−17	NA	9.48E−17
0.30	1.52E−16	1.52E−16	NA	1.53E−16	NA	1.51E−16	NA	1.53E−16	NA	1.51E−16	NA	1.53E−16
0.40	2.08E−16	2.08E−16	NA	2.10E−16	NA	2.07E−16	NA	2.10E−16	NA	2.08E−16	NA	2.10E−16
0.50	2.61E−16	2.61E−16	NA	2.65E−16	NA	2.60E−16	NA	2.65E−16	NA	2.61E−16	NA	2.65E−16
0.60	3.12E−16	3.12E−16	NA	3.17E−16	NA	3.11E−16	NA	3.17E−16	NA	3.12E−16	NA	3.17E−16
0.80	4.07E−16	4.07E−16	NA	4.12E−16	NA	4.05E−16	NA	4.12E−16	NA	4.06E−16	NA	4.12E−16
1.0	4.92E−16	4.92E−16	NA	4.99E−16	NA	4.90E−16	NA	4.99E−16	NA	4.92E−16	NA	4.99E−16
1.5	6.76E−16	6.76E−16	NA	6.86E−16	NA	6.73E−16	NA	6.86E−16	NA	6.75E−16	NA	6.86E−16
2.0	8.30E−16	8.30E−16	NA	8.41E−16	NA	8.26E−16	NA	8.41E−16	NA	8.28E−16	NA	8.41E−16
3.0	1.09E−15	1.09E−15	NA	1.10E−15	NA	1.09E−15	NA	1.10E−15	NA	1.09E−15	NA	1.10E−15
4.0	1.32E−15	1.32E−15	NA	1.33E−15	NA	1.32E−15	NA	1.33E−15	NA	1.32E−15	NA	1.33E−15
5.0	1.54E−15	1.54E−15	NA	1.54E−15	NA	1.54E−15	NA	1.54E−15	NA	1.54E−15	NA	1.54E−15
6.0	1.75E−15	1.75E−15	NA	1.74E−15	NA	1.75E−15	NA	1.74E−15	NA	1.75E−15	NA	1.74E−15
8.0	2.16E−15	2.16E−15	NA	2.13E−15	NA	2.17E−15	NA	2.13E−15	NA	2.16E−15	NA	2.13E−15
10.0	2.58E−15	2.58E−15	NA	2.52E−15	NA	2.60E−15	NA	2.52E−15	NA	2.58E−15	NA	2.52E−15

Photon energy (MeV)	Organ ID: 23 Wrist and hands Source: spongiosa		Organ ID: 25 Clavicles Source: spongiosa		Organ ID: 27 Cranium Source: spongiosa		Organ ID: 29 Femora, upper half Source: spongiosa		Organ ID: 30 Femora, upper half Source: medullary cavity		Organ ID: 32 Femora, lower half Source: spongiosa	
	Target tissue		Target tissue		Target tissue		Target tissue		Target tissue		Target tissue	
	AM	TM_{50}	AM	TM_{50}	AM	TM_{50}	AM	TM_{50}	AM	TM_{50}	AM	TM_{50}
0.010	NA	5.15E−16	6.14E−16	5.81E−16	6.21E−16	5.78E−16	6.16E−16	5.03E−16	NA	3.74E−16	NA	5.30E−16
0.015	NA	2.39E−16	2.58E−16	2.62E−16	2.67E−16	2.58E−16	2.60E−16	2.31E−16	NA	1.53E−16	NA	2.44E−16
0.020	NA	1.47E−16	1.38E−16	1.55E−16	1.48E−16	1.50E−16	1.40E−16	1.39E−16	NA	7.97E−17	NA	1.48E−16
0.030	NA	8.36E−17	6.00E−17	8.32E−17	6.75E−17	7.57E−17	6.16E−17	7.68E−17	NA	3.21E−17	NA	8.23E−17
0.040	NA	6.33E−17	3.71E−17	6.03E−17	4.44E−17	5.48E−17	3.84E−17	5.65E−17	NA	1.93E−17	NA	6.15E−17
0.050	NA	5.49E−17	2.95E−17	5.14E−17	3.63E−17	4.74E−17	3.07E−17	4.84E−17	NA	1.66E−17	NA	5.35E−17
0.060	NA	5.16E−17	2.78E−17	4.80E−17	3.40E−17	4.51E−17	2.89E−17	4.51E−17	NA	1.73E−17	NA	5.06E−17
0.080	NA	5.13E−17	3.18E−17	4.87E−17	3.66E−17	4.71E−17	3.28E−17	4.51E−17	NA	2.29E−17	NA	5.11E−17
0.10	NA	5.48E−17	3.99E−17	5.37E−17	4.39E−17	5.37E−17	4.08E−17	4.87E−17	NA	3.11E−17	NA	5.56E−17
0.15	NA	7.15E−17	6.55E−17	7.21E−17	6.66E−17	7.10E−17	6.63E−17	6.80E−17	NA	6.13E−17	NA	7.26E−17
0.20	NA	9.49E−17	9.48E−17	9.48E−17	9.50E−17	9.50E−17	9.48E−17	9.48E−17	NA	9.48E−17	NA	9.49E−17
0.30	NA	1.51E−16	1.51E−16	1.51E−16	1.48E−16	1.48E−16	1.51E−16	1.51E−16	NA	1.53E−16	NA	1.51E−16
0.40	NA	2.07E−16	2.07E−16	2.07E−16	2.03E−16	2.03E−16	2.07E−16	2.07E−16	NA	2.10E−16	NA	2.07E−16
0.50	NA	2.60E−16	2.61E−16	2.61E−16	2.54E−16	2.54E−16	2.60E−16	2.60E−16	NA	2.65E−16	NA	2.61E−16
0.60	NA	3.11E−16	3.12E−16	3.12E−16	3.04E−16	3.04E−16	3.11E−16	3.11E−16	NA	3.17E−16	NA	3.11E−16
0.80	NA	4.05E−16	4.06E−16	4.06E−16	3.95E−16	3.95E−16	4.04E−16	4.04E−16	NA	4.12E−16	NA	4.05E−16
1.0	NA	4.90E−16	4.91E−16	4.91E−16	4.78E−16	4.78E−16	4.90E−16	4.90E−16	NA	4.99E−16	NA	4.90E−16
1.5	NA	6.73E−16	6.74E−16	6.74E−16	6.56E−16	6.56E−16	6.72E−16	6.72E−16	NA	6.86E−16	NA	6.73E−16
2.0	NA	8.26E−16	8.28E−16	8.28E−16	8.08E−16	8.08E−16	8.25E−16	8.25E−16	NA	8.41E−16	NA	8.27E−16
3.0	NA	1.09E−15	1.09E−15	1.09E−15	1.07E−15	1.07E−15	1.09E−15	1.09E−15	NA	1.10E−15	NA	1.09E−15
4.0	NA	1.32E−15	1.32E−15	1.32E−15	1.31E−15	1.31E−15	1.32E−15	1.32E−15	NA	1.33E−15	NA	1.32E−15
5.0	NA	1.54E−15	1.54E−15	1.54E−15	1.54E−15	1.54E−15	1.54E−15	1.54E−15	NA	1.54E−15	NA	1.54E−15
6.0	NA	1.75E−15	1.75E−15	1.75E−15	1.76E−15	1.76E−15	1.75E−15	1.75E−15	NA	1.74E−15	NA	1.75E−15
8.0	NA	2.17E−15	2.17E−15	2.17E−15	2.22E−15	2.22E−15	2.17E−15	2.17E−15	NA	2.13E−15	NA	2.17E−15
10.0	NA	2.60E−15	2.59E−15	2.59E−15	2.69E−15	2.69E−15	2.60E−15	2.60E−15	NA	2.52E−15	NA	2.59E−15

(*continued on next page*)

Table D.1. (*continued*)

Photon energy (MeV)	Organ ID: 33 Femora, lower half Source: medullary cavity Target tissue		Organ ID: 35 Tibiae, fibulae Source: spongiosa Target tissue		Organ ID: 36 Tibiae and fibulae Source: medullary cavity Target tissue		Organ ID: 38 Ankles and feet Source: spongiosa Target tissue		Organ ID: 40 Mandible Source: spongiosa Target tissue		Organ ID: 42 Pelvis Source: spongiosa Target tissue		Organ ID: 44 Ribs Source: spongiosa Target tissue	
	AM	TM_{50}	AM	TM_{50}	AM	TM_{50}	AM	TM_{50}	AM	TM_{50}	AM	TM_{50}	AM	TM_{50}
0.010	NA	3.74E−16	NA	4.57E−16	NA	4.38E−16	NA	5.11E−16	6.14E−16	5.56E−16	6.16E−16	5.13E−16	6.18E−16	6.15E−16
0.015	NA	1.53E−16	NA	2.10E−16	NA	1.79E−16	NA	2.35E−16	2.58E−16	2.54E−16	2.60E−16	2.35E−16	2.62E−16	2.77E−16
0.020	NA	7.97E−17	NA	1.27E−16	NA	9.35E−17	NA	1.42E−16	1.39E−16	1.51E−16	1.40E−16	1.39E−16	1.42E−16	1.64E−16
0.030	NA	3.21E−17	NA	7.10E−17	NA	3.76E−17	NA	7.90E−17	6.02E−17	8.16E−17	6.15E−17	7.48E−17	6.29E−17	8.61E−17
0.040	NA	1.93E−17	NA	5.30E−17	NA	2.25E−17	NA	5.96E−17	3.72E−17	5.94E−17	3.84E−17	5.45E−17	3.95E−17	6.17E−17
0.050	NA	1.66E−17	NA	4.61E−17	NA	1.94E−17	NA	5.17E−17	2.96E−17	5.06E−17	3.06E−17	4.63E−17	3.16E−17	5.19E−17
0.060	NA	1.73E−17	NA	4.34E−17	NA	2.03E−17	NA	4.87E−17	2.79E−17	4.70E−17	2.88E−17	4.30E−17	2.96E−17	4.80E−17
0.080	NA	2.29E−17	NA	4.38E−17	NA	2.69E−17	NA	4.90E−17	3.19E−17	4.68E−17	3.26E−17	4.24E−17	3.33E−17	4.77E−17
0.10	NA	3.11E−17	NA	4.83E−17	NA	3.53E−17	NA	5.32E−17	4.00E−17	5.10E−17	4.06E−17	4.58E−17	4.12E−17	5.17E−17
0.15	NA	6.13E−17	NA	6.84E−17	NA	6.30E−17	NA	7.12E−17	6.56E−17	7.17E−17	6.61E−17	6.71E−17	6.76E−17	7.12E−17
0.20	NA	9.48E−17	NA	9.49E−17	NA	9.48E−17	NA	9.49E−17	9.47E−17	9.47E−17	9.47E−17	9.47E−17	9.47E−17	9.47E−17
0.30	NA	1.53E−16	NA	1.51E−16	NA	1.53E−16	NA	1.51E−16	1.52E−16	1.52E−16	1.51E−16	1.51E−16	1.51E−16	1.51E−16
0.40	NA	2.10E−16	NA	2.08E−16	NA	2.10E−16	NA	2.07E−16	2.08E−16	2.08E−16	2.07E−16	2.07E−16	2.07E−16	2.07E−16
0.50	NA	2.65E−16	NA	2.61E−16	NA	2.65E−16	NA	2.61E−16	2.61E−16	2.61E−16	2.61E−16	2.61E−16	2.60E−16	2.60E−16
0.60	NA	3.17E−16	NA	3.12E−16	NA	3.17E−16	NA	3.11E−16	3.12E−16	3.12E−16	3.12E−16	3.12E−16	3.11E−16	3.11E−16
0.80	NA	4.12E−16	NA	4.06E−16	NA	4.12E−16	NA	4.05E−16	4.07E−16	4.07E−16	4.06E−16	4.06E−16	4.05E−16	4.05E−16
1.0	NA	4.99E−16	NA	4.92E−16	NA	4.99E−16	NA	4.90E−16	4.92E−16	4.92E−16	4.91E−16	4.91E−16	4.90E−16	4.90E−16
1.5	NA	6.86E−16	NA	6.75E−16	NA	6.86E−16	NA	6.73E−16	6.76E−16	6.76E−16	6.74E−16	6.74E−16	6.72E−16	6.72E−16
2.0	NA	8.41E−16	NA	8.29E−16	NA	8.41E−16	NA	8.27E−16	8.30E−16	8.30E−16	8.28E−16	8.28E−16	8.26E−16	8.26E−16
3.0	NA	1.10E−15	NA	1.09E−15	NA	1.10E−15	NA	1.09E−15	1.09E−15	1.09E−15	1.09E−15	1.09E−15	1.09E−15	1.09E−15
4.0	NA	1.33E−15	NA	1.32E−15	NA	1.33E−15	NA	1.32E−15	1.32E−15	1.32E−15	1.32E−15	1.32E−15	1.32E−15	1.32E−15
5.0	NA	1.54E−15	NA	1.54E−15	NA	1.54E−15	NA	1.54E−15	1.54E−15	1.54E−15	1.54E−15	1.54E−15	1.54E−15	1.54E−15
6.0	NA	1.74E−15	NA	1.75E−15	NA	1.74E−15	NA	1.75E−15	1.75E−15	1.75E−15	1.75E−15	1.75E−15	1.75E−15	1.75E−15
8.0	NA	2.13E−15	NA	2.16E−15	NA	2.13E−15	NA	2.17E−15	2.16E−15	2.16E−15	2.16E−15	2.16E−15	2.17E−15	2.17E−15
10.0	NA	2.52E−15	NA	2.58E−15	NA	2.52E−15	NA	2.59E−15	2.58E−15	2.58E−15	2.59E−15	2.59E−15	2.60E−15	2.60E−15

Table D.1. (*continued*)

Photon energy (MeV)	Organ ID: 46 Scapulae Source: spongiosa Target tissue		Organ ID: 48 Spine, cervical Source: spongiosa Target tissue		Organ ID: 50 Spine, thoracic Source: spongiosa Target tissue		Organ ID: 52 Spine, lumbar Source: spongiosa Target tissue		Organ ID: 54 Sacrum Source: spongiosa Target tissue		Organ ID: 56 Sternum Source: spongiosa Target tissue	
	AM	TM_{50}	AM	TM_{50}	AM	TM_{50}	AM	TM_{50}	AM	TM_{50}	AM	TM_{50}
0.010	6.16E−16	5.74E−16	6.19E−16	5.96E−16	6.16E−16	6.04E−16	6.17E−16	5.65E−16	6.17E−16	5.44E−16	6.16E−16	5.73E−16
0.015	2.60E−16	2.63E−16	2.64E−16	2.71E−16	2.60E−16	2.74E−16	2.61E−16	2.57E−16	2.61E−16	2.47E−16	2.60E−16	2.61E−16
0.020	1.40E−16	1.57E−16	1.44E−16	1.61E−16	1.41E−16	1.62E−16	1.41E−16	1.51E−16	1.41E−16	1.45E−16	1.41E−16	1.54E−16
0.030	6.16E−17	8.61E−17	6.43E−17	8.56E−17	6.18E−17	8.57E−17	6.20E−17	8.01E−17	6.22E−17	7.69E−17	6.18E−17	8.08E−17
0.040	3.85E−17	6.29E−17	4.09E−17	6.15E−17	3.86E−17	6.11E−17	3.88E−17	5.75E−17	3.89E−17	5.47E−17	3.86E−17	5.76E−17
0.050	3.07E−17	5.37E−17	3.28E−17	5.18E−17	3.08E−17	5.14E−17	3.10E−17	4.82E−17	3.11E−17	4.61E−17	3.08E−17	4.84E−17
0.060	2.89E−17	4.99E−17	3.08E−17	4.76E−17	2.89E−17	4.73E−17	2.91E−17	4.44E−17	2.92E−17	4.26E−17	2.89E−17	4.47E−17
0.080	3.27E−17	4.94E−17	3.42E−17	4.69E−17	3.27E−17	4.68E−17	3.28E−17	4.39E−17	3.29E−17	4.21E−17	3.27E−17	4.43E−17
0.10	4.07E−17	5.33E−17	4.18E−17	5.05E−17	4.06E−17	5.07E−17	4.07E−17	4.75E−17	4.08E−17	4.57E−17	4.06E−17	4.79E−17
0.15	6.61E−17	7.24E−17	6.68E−17	7.01E−17	6.60E−17	7.07E−17	6.61E−17	6.64E−17	6.62E−17	6.73E−17	6.59E−17	6.70E−17
0.20	9.48E−17	9.48E−17	9.47E−17	9.47E−17	9.46E−17	9.46E−17	9.46E−17	9.46E−17	9.47E−17	9.47E−17	9.46E−17	9.46E−17
0.30	1.51E−16	1.51E−16	1.50E−16	1.50E−16	1.51E−16	1.51E−16	1.51E−16	1.51E−16	1.51E−16	1.51E−16	1.51E−16	1.51E−16
0.40	2.06E−16	2.06E−16	2.06E−16	2.06E−16	2.07E−16	2.07E−16	2.07E−16	2.07E−16	2.07E−16	2.07E−16	2.07E−16	2.07E−16
0.50	2.60E−16	2.60E−16	2.59E−16	2.59E−16	2.61E−16	2.61E−16	2.60E−16	2.60E−16	2.60E−16	2.60E−16	2.61E−16	2.61E−16
0.60	3.10E−16	3.10E−16	3.09E−16	3.09E−16	3.11E−16	3.11E−16	3.11E−16	3.11E−16	3.11E−16	3.11E−16	3.12E−16	3.12E−16
0.80	4.04E−16	4.04E−16	4.02E−16	4.02E−16	4.05E−16	4.05E−16	4.05E−16	4.05E−16	4.04E−16	4.04E−16	4.06E−16	4.06E−16
1.0	4.89E−16	4.89E−16	4.87E−16	4.87E−16	4.91E−16	4.91E−16	4.91E−16	4.91E−16	4.90E−16	4.90E−16	4.92E−16	4.92E−16
1.5	6.71E−16	6.71E−16	6.68E−16	6.68E−16	6.73E−16	6.73E−16	6.73E−16	6.73E−16	6.72E−16	6.72E−16	6.74E−16	6.74E−16
2.0	8.24E−16	8.24E−16	8.21E−16	8.21E−16	8.28E−16	8.28E−16	8.27E−16	8.27E−16	8.26E−16	8.26E−16	8.29E−16	8.29E−16
3.0	1.09E−15	1.09E−15	1.08E−15	1.08E−15	1.09E−15	1.09E−15	1.09E−15	1.09E−15	1.09E−15	1.09E−15	1.09E−15	1.09E−15
4.0	1.32E−15	1.32E−15	1.32E−15	1.32E−15	1.32E−15	1.32E−15	1.32E−15	1.32E−15	1.32E−15	1.32E−15	1.32E−15	1.32E−15
5.0	1.54E−15	1.54E−15	1.54E−15	1.54E−15	1.54E−15	1.54E−15	1.54E−15	1.54E−15	1.54E−15	1.54E−15	1.54E−15	1.54E−15
6.0	1.75E−15	1.75E−15	1.76E−15	1.76E−15	1.75E−15	1.75E−15	1.75E−15	1.75E−15	1.75E−15	1.75E−15	1.75E−15	1.75E−15
8.0	2.17E−15	2.17E−15	2.18E−15	2.18E−15	2.17E−15	2.17E−15	2.17E−15	2.17E−15	2.17E−15	2.17E−15	2.16E−15	2.16E−15
10.0	2.61E−15	2.61E−15	2.62E−15	2.62E−15	2.59E−15	2.59E−15	2.60E−15	2.60E−15	2.60E−15	2.60E−15	2.59E−15	2.59E−15

NA, not applicable.

Table D.2. Ratios of mass energy absorption coefficients (MEAC, μ_{en}/ρ) for active marrow (AM) to spongiosa (SP) and for total marrow (TM) to either spongiosa or medullary marrow (MM), as a function of photon energy and skeletal site, for the ICRP reference adult male.

Photon energy (MeV)	Organ ID: 14 Humeri, upper half Source: spongiosa MEAC ratio		Organ ID: 15 Humeri, upper half Source: medullary cavity MEAC ratio		Organ ID: 17 Humeri, lower half Source: spongiosa MEAC ratio		Organ ID: 18 Humeri, lower half Source: medullary cavity MEAC ratio		Organ ID: 20 Ulnae and radii Source: spongiosa MEAC ratio		Organ ID: 21 Ulnae and radii Source: medullary cavity MEAC ratio	
	AM/Spong	TM/Spong	AM/MM	TM/MM	AM/Spong	TM/Spong	AM/MM	TM/MM	AM/Spong	TM/Spong	AM/MM	TM/MM
0.010	0.399	0.318	NA	1.0	NA	0.368	NA	1.0	NA	0.368	NA	1.0
0.015	0.372	0.293	NA	1.0	NA	0.339	NA	1.0	NA	0.339	NA	1.0
0.020	0.357	0.280	NA	1.0	NA	0.324	NA	1.0	NA	0.324	NA	1.0
0.030	0.351	0.277	NA	1.0	NA	0.322	NA	1.0	NA	0.322	NA	1.0
0.040	0.373	0.304	NA	1.0	NA	0.359	NA	1.0	NA	0.359	NA	1.0
0.050	0.426	0.364	NA	1.0	NA	0.433	NA	1.0	NA	0.433	NA	1.0
0.060	0.504	0.452	NA	1.0	NA	0.533	NA	1.0	NA	0.533	NA	1.0
0.080	0.681	0.649	NA	1.0	NA	0.729	NA	1.0	NA	0.729	NA	1.0
0.10	0.816	0.800	NA	1.0	NA	0.856	NA	1.0	NA	0.856	NA	1.0
0.15	0.958	0.958	NA	1.0	NA	0.972	NA	1.0	NA	0.972	NA	1.0
0.20	0.995	0.998	NA	1.0	NA	1.000	NA	1.0	NA	1.000	NA	1.0

Photon energy (MeV)	Organ ID: 23 Wrist and hands Source: spongiosa MEAC ratio		Organ ID: 25 Clavicles Source: spongiosa MEAC ratio		Organ ID: 27 Cranium Source: spongiosa MEAC ratio		Organ ID: 29 Femora, upper half Source: spongiosa MEAC ratio		Organ ID: 30 Femora, upper half Source: medullary cavity MEAC ratio		Organ ID: 32 Femora, lower half Source: spongiosa MEAC ratio	
	AM/Spong	TM/Spong	AM/Spong	TM/Spong	AM/Spong	TM/Spong	AM/Spong	TM/Spong	AM/MM	TM/MM	AM/Spong	TM/Spong
0.010	NA	0.368	0.472	0.370	0.463	0.370	0.522	0.399	NA	1.0	NA	0.368
0.015	NA	0.339	0.443	0.342	0.434	0.343	0.492	0.371	NA	1.0	NA	0.339
0.020	NA	0.324	0.427	0.328	0.418	0.329	0.475	0.356	NA	1.0	NA	0.324
0.030	NA	0.322	0.420	0.325	0.411	0.326	0.467	0.353	NA	1.0	NA	0.322
0.040	NA	0.359	0.443	0.355	0.435	0.355	0.491	0.385	NA	1.0	NA	0.359
0.050	NA	0.433	0.497	0.420	0.489	0.419	0.545	0.453	NA	1.0	NA	0.433
0.060	NA	0.533	0.575	0.511	0.567	0.509	0.621	0.546	NA	1.0	NA	0.533
0.080	NA	0.729	0.739	0.703	0.733	0.699	0.774	0.732	NA	1.0	NA	0.729
0.10	NA	0.856	0.855	0.837	0.851	0.834	0.876	0.856	NA	1.0	NA	0.856
0.15	NA	0.972	0.967	0.967	0.967	0.966	0.972	0.971	NA	1.0	NA	0.972
0.20	NA	1.000	0.995	0.999	0.995	0.999	0.995	0.999	NA	1.0	NA	1.000

Photon energy (MeV)	Organ ID: 33 Femora, lower half Source: medullary cavity MEAC ratio		Organ ID: 35 Tibiae, fibulae, patellae Source: spongiosa MEAC ratio		Organ ID: 36 Tibiae and fibulae Source: medullary cavity Target tissue		Organ ID: 38 Ankles and feet Source: spongiosa Target tissue		Organ ID: 40 Mandible Source: spongiosa Target tissue		Organ ID: 42 Pelvis Source: spongiosa Target tissue		Organ ID: 44 Ribs Source: spongiosa Target tissue	
	AM/MM	TM/MM	AM/Spong	TM/Spong	AM/MM	TM/MM	AM/Spong	TM/Spong	AM/Spong	TM/Spong	AM/Spong	TM/Spong	AM/Spong	TM/Spong
0.010	NA	1.0	NA	0.368	NA	1.0	NA	0.368	0.376	0.301	0.532	0.443	0.456	0.413
0.015	NA	1.0	NA	0.339	NA	1.0	NA	0.339	0.349	0.276	0.503	0.415	0.428	0.385
0.020	NA	1.0	NA	0.324	NA	1.0	NA	0.324	0.335	0.264	0.487	0.400	0.413	0.371
0.030	NA	1.0	NA	0.322	NA	1.0	NA	0.322	0.329	0.261	0.479	0.396	0.407	0.366
0.040	NA	1.0	NA	0.359	NA	1.0	NA	0.359	0.351	0.287	0.503	0.426	0.430	0.393
0.050	NA	1.0	NA	0.433	NA	1.0	NA	0.433	0.403	0.345	0.557	0.491	0.485	0.452
0.060	NA	1.0	NA	0.533	NA	1.0	NA	0.533	0.480	0.431	0.632	0.579	0.563	0.536
0.080	NA	1.0	NA	0.729	NA	1.0	NA	0.729	0.660	0.630	0.783	0.753	0.730	0.715
0.10	NA	1.0	NA	0.856	NA	1.0	NA	0.856	0.802	0.786	0.882	0.868	0.850	0.842
0.15	NA	1.0	NA	0.972	NA	1.0	NA	0.972	0.955	0.954	0.974	0.974	0.967	0.967
0.20	NA	1.0	NA	1.000	NA	1.0	NA	1.000	0.995	0.998	0.996	0.999	0.996	0.998

Photon energy (MeV)	Organ ID: 46 Scapulae Source: spongiosa Target tissue		Organ ID: 48 Spine, cervical Source: spongiosa Target tissue		Organ ID: 50 Spine, thoracic Source: spongiosa Target tissue		Organ ID: 52 Spine, lumbar Source: spongiosa Target tissue		Organ ID: 54 Sacrum Source: spongiosa Target tissue		Organ ID: 56 Sternum Source: spongiosa Target tissue	
	AM/Spong	TM/Spong	AM/Spong	TM/Spong	AM/Spong	TM/Spong	AM/Spong	TM/Spong	AM/Spong	TM/Spong	AM/Spong	TM/Spong
0.010	0.425	0.340	0.818	0.740	0.696	0.630	0.567	0.513	0.960	0.869	0.882	0.798
0.015	0.397	0.314	0.799	0.719	0.671	0.604	0.538	0.485	0.953	0.858	0.867	0.781
0.020	0.382	0.300	0.788	0.708	0.656	0.590	0.523	0.470	0.948	0.852	0.859	0.771
0.030	0.375	0.297	0.782	0.705	0.650	0.586	0.516	0.465	0.945	0.852	0.854	0.769
0.040	0.398	0.325	0.798	0.728	0.671	0.613	0.540	0.493	0.949	0.867	0.865	0.790
0.050	0.452	0.387	0.831	0.774	0.718	0.669	0.594	0.553	0.958	0.893	0.888	0.828
0.060	0.530	0.476	0.870	0.828	0.776	0.739	0.667	0.634	0.968	0.921	0.915	0.871
0.080	0.703	0.671	0.933	0.913	0.879	0.860	0.808	0.790	0.984	0.963	0.957	0.936
0.10	0.831	0.815	0.966	0.957	0.938	0.929	0.897	0.889	0.992	0.982	0.978	0.969
0.15	0.962	0.961	0.993	0.992	0.987	0.986	0.978	0.978	0.997	0.997	0.995	0.995
0.20	0.995	0.999	0.998	1.000	0.998	0.999	0.997	0.999	0.999	1.000	0.998	1.000

NA, not applicable.

Table D.3. Ratios of mass energy absorption coefficients (MEAC, μ_{en}/ρ) for active marrow (AM) to spongiosa (SP) and for total marrow (TM) to either spongiosa or medullary marrow (MM), as a function of photon energy and skeletal site, for the ICRP reference adult female.

Photon energy (MeV)	Organ ID: 14 Humeri, upper half Source: spongiosa MEAC ratio		Organ ID: 15 Humeri, upper half Source: medullary cavity MEAC ratio		Organ ID: 17 Humeri, lower half Source: spongiosa MEAC ratio		Organ ID: 18 Humeri, lower half Source: medullary cavity MEAC ratio		Organ ID: 20 Ulnae and radii Source: spongiosa MEAC ratio		Organ ID: 21 Ulnae and radii Source: medullary cavity MEAC ratio	
	AM/Spong	TM/Spong	AM/MM	TM/MM	AM/Spong	TM/Spong	AM/MM	TM/MM	AM/Spong	TM/Spong	AM/MM	TM/MM
0.010	0.414	0.325	NA	1.0	NA	0.347	NA	1.0	NA	0.347	NA	1.0
0.015	0.385	0.298	NA	1.0	NA	0.317	NA	1.0	NA	0.317	NA	1.0
0.020	0.369	0.285	NA	1.0	NA	0.302	NA	1.0	NA	0.302	NA	1.0
0.030	0.362	0.281	NA	1.0	NA	0.300	NA	1.0	NA	0.300	NA	1.0
0.040	0.384	0.309	NA	1.0	NA	0.335	NA	1.0	NA	0.335	NA	1.0
0.050	0.436	0.370	NA	1.0	NA	0.407	NA	1.0	NA	0.407	NA	1.0
0.060	0.514	0.458	NA	1.0	NA	0.506	NA	1.0	NA	0.506	NA	1.0
0.080	0.689	0.656	NA	1.0	NA	0.706	NA	1.0	NA	0.706	NA	1.0
0.10	0.821	0.804	NA	1.0	NA	0.841	NA	1.0	NA	0.841	NA	1.0
0.15	0.959	0.958	NA	1.0	NA	0.968	NA	1.0	NA	0.968	NA	1.0
0.20	0.994	0.997	NA	1.0	NA	0.999	NA	1.0	NA	0.999	NA	1.0

Photon energy (MeV)	Organ ID: 23 Wrist and hands Source: spongiosa MEAC ratio		Organ ID: 25 Clavicles Source: spongiosa MEAC ratio		Organ ID: 27 Cranium Source: spongiosa MEAC ratio		Organ ID: 29 Femora, upper half Source: spongiosa MEAC ratio		Organ ID: 30 Femora, upper half Source: medullary cavity MEAC ratio		Organ ID: 32 Femora, lower half Source: spongiosa MEAC ratio	
	AM/Spong	TM/Spong	AM/Spong	TM/Spong	AM/Spong	TM/Spong	AM/Spong	TM/Spong	AM/MM	TM/MM	AM/Spong	TM/Spong
0.010	NA	0.347	0.406	0.318	0.352	0.282	0.788	0.611	NA	1.0	NA	0.347
0.015	NA	0.317	0.377	0.292	0.326	0.258	0.760	0.581	NA	1.0	NA	0.317
0.020	NA	0.302	0.362	0.278	0.311	0.245	0.743	0.565	NA	1.0	NA	0.302
0.030	NA	0.300	0.354	0.275	0.305	0.242	0.733	0.561	NA	1.0	NA	0.300
0.040	NA	0.335	0.376	0.302	0.326	0.266	0.748	0.594	NA	1.0	NA	0.335
0.050	NA	0.407	0.429	0.362	0.375	0.322	0.785	0.659	NA	1.0	NA	0.407
0.060	NA	0.506	0.506	0.450	0.451	0.405	0.832	0.736	NA	1.0	NA	0.506
0.080	NA	0.706	0.682	0.649	0.633	0.604	0.910	0.863	NA	1.0	NA	0.706
0.10	NA	0.841	0.817	0.799	0.782	0.767	0.953	0.932	NA	1.0	NA	0.841
0.15	NA	0.968	0.957	0.957	0.948	0.948	0.988	0.987	NA	1.0	NA	0.968
0.20	NA	0.999	0.994	0.997	0.993	0.996	0.996	0.999	NA	1.0	NA	0.999

Photon energy (MeV)	Organ ID: 33 Femora, lower half Source: medullary cavity MEAC ratio		Organ ID: 35 Tibiae, fibulae, patellae Source: spongiosa MEAC ratio		Organ ID: 36 Tibiae and fibulae Source: medullary cavity Target tissue		Organ ID: 38 Ankles and feet Source: spongiosa Target tissue		Organ ID: 40 Mandible Source: spongiosa Target tissue		Organ ID: 42 Pelvis Source: spongiosa Target tissue		Organ ID: 44 Ribs Source: spongiosa Target tissue	
	AM/MM	TM/MM	AM/Spong	TM/Spong	AM/MM	TM/MM	AM/Spong	TM/Spong	AM/Spong	TM/Spong	AM/Spong	TM/Spong	AM/Spong	TM/Spong
0.010	NA	1.0	NA	0.347	NA	1.0	NA	0.347	0.409	0.328	0.556	0.463	0.620	0.561
0.015	NA	1.0	NA	0.317	NA	1.0	NA	0.317	0.380	0.301	0.524	0.433	0.591	0.532
0.020	NA	1.0	NA	0.302	NA	1.0	NA	0.302	0.365	0.287	0.507	0.417	0.575	0.517
0.030	NA	1.0	NA	0.300	NA	1.0	NA	0.300	0.358	0.283	0.499	0.413	0.567	0.511
0.040	NA	1.0	NA	0.335	NA	1.0	NA	0.335	0.380	0.310	0.522	0.443	0.590	0.539
0.050	NA	1.0	NA	0.407	NA	1.0	NA	0.407	0.432	0.371	0.576	0.507	0.642	0.598
0.060	NA	1.0	NA	0.506	NA	1.0	NA	0.506	0.510	0.458	0.649	0.594	0.710	0.676
0.080	NA	1.0	NA	0.706	NA	1.0	NA	0.706	0.685	0.654	0.795	0.765	0.837	0.819
0.10	NA	1.0	NA	0.841	NA	1.0	NA	0.841	0.819	0.803	0.889	0.874	0.914	0.906
0.15	NA	1.0	NA	0.968	NA	1.0	NA	0.968	0.958	0.957	0.975	0.975	0.981	0.981
0.20	NA	1.0	NA	0.999	NA	1.0	NA	0.999	0.994	0.997	0.996	0.998	0.997	0.999

Photon energy (MeV)	Organ ID: 46 Scapulae Source: spongiosa Target tissue		Organ ID: 48 Spine, cervical Source: spongiosa Target tissue		Organ ID: 50 Spine, thoracic Source: spongiosa Target tissue		Organ ID: 52 Spine, lumbar Source: spongiosa Target tissue		Organ ID: 54 Sacrum Source: spongiosa Target tissue		Organ ID: 56 Sternum Source: spongiosa Target tissue	
	AM/Spong	TM/Spong	AM/Spong	TM/Spong	AM/Spong	TM/Spong	AM/Spong	TM/Spong	AM/Spong	TM/Spong	AM/Spong	TM/Spong
0.010	0.508	0.406	0.504	0.456	0.649	0.587	0.441	0.399	0.800	0.724	0.679	0.614
0.015	0.476	0.377	0.474	0.427	0.621	0.559	0.412	0.371	0.778	0.701	0.651	0.587
0.020	0.459	0.362	0.457	0.411	0.605	0.544	0.397	0.356	0.766	0.688	0.636	0.572
0.030	0.451	0.357	0.450	0.406	0.597	0.538	0.390	0.351	0.759	0.684	0.629	0.566
0.040	0.474	0.388	0.474	0.433	0.620	0.566	0.413	0.377	0.776	0.708	0.650	0.594
0.050	0.528	0.453	0.528	0.493	0.670	0.624	0.467	0.435	0.811	0.756	0.698	0.651
0.060	0.604	0.543	0.605	0.576	0.735	0.699	0.545	0.518	0.854	0.813	0.759	0.723
0.080	0.762	0.727	0.763	0.746	0.853	0.834	0.715	0.700	0.924	0.904	0.868	0.850
0.10	0.868	0.852	0.870	0.862	0.923	0.915	0.839	0.832	0.961	0.953	0.932	0.923
0.15	0.970	0.969	0.971	0.971	0.983	0.983	0.964	0.964	0.991	0.991	0.985	0.985
0.20	0.995	0.998	0.996	0.998	0.997	0.999	0.995	0.997	0.998	1.000	0.997	0.999

NA, not applicable.

Table D.4. Dose enhancement factor S to active marrow (AM) and endosteum (TM_{50}) as a function of photon energy and skeletal site.

Photon energy (MeV)	Organ ID: 14 Humeri, upper half Source: spongiosa		Organ ID: 15 Humeri, upper half Source: medullary cavity		Organ ID: 17 Humeri, lower half Source: spongiosa		Organ ID: 18 Humeri, lower half Source: medullary cavity		Organ ID: 20 Ulnae and radii Source: spongiosa		Organ ID: 21 Ulnae and radii Source: medullary cavity		Organ ID: 23 Wrist and hands Source: spongiosa	
	Target tissue		Target tissue		Target tissue		Target tissue		Target tissue		Target tissue		Target tissue	
	AM	TM_{50}	AM	TM_{50}	AM	TM_{50}	AM	TM_{50}	AM	TM_{50}	AM	TM_{50}	AM	TM_{50}
0.010	1.00	1.10	NA	1.0	NA	1.07	NA	1.0	NA	1.09	NA	1.0	NA	1.17
0.015	1.00	1.21	NA	1.0	NA	1.19	NA	1.0	NA	1.20	NA	1.0	NA	1.31
0.020	1.00	1.36	NA	1.0	NA	1.37	NA	1.0	NA	1.37	NA	1.0	NA	1.51
0.030	1.00	1.70	NA	1.0	NA	1.74	NA	1.0	NA	1.75	NA	1.0	NA	1.96
0.040	1.00	1.97	NA	1.0	NA	2.03	NA	1.0	NA	2.03	NA	1.0	NA	2.29
0.050	1.00	2.02	NA	1.0	NA	2.07	NA	1.0	NA	2.07	NA	1.0	NA	2.33
0.060	1.01	1.92	NA	1.0	NA	1.93	NA	1.0	NA	1.93	NA	1.0	NA	2.17
0.080	1.01	1.58	NA	1.0	NA	1.55	NA	1.0	NA	1.55	NA	1.0	NA	1.73
0.10	1.01	1.34	NA	1.0	NA	1.29	NA	1.0	NA	1.30	NA	1.0	NA	1.43
0.15	1.01	1.08	NA	1.0	NA	1.06	NA	1.0	NA	1.05	NA	1.0	NA	1.09
0.20	1.00	1.00	NA	1.0	NA	1.00	NA	1.0	NA	1.00	NA	1.0	NA	1.00

Photon energy (MeV)	Organ ID: 25 Clavicles Source: spongiosa		Organ ID: 27 Cranium Source: spongiosa		Organ ID: 29 Femora, upper half Source: spongiosa		Organ ID: 30 Femora, upper half Source: medullary cavity		Organ ID: 32 Femora, lower half Source: spongiosa		Organ ID: 33 Femora, lower half Source: medullary cavity		Organ ID: 35 Tibiae, fibulae Source: spongiosa	
	Target tissue		Target tissue		Target tissue		Target tissue		Target tissue		Target tissue		Target tissue	
	AM	TM_{50}	AM	TM_{50}	AM	TM_{50}	AM	TM_{50}	AM	TM_{50}	AM	TM_{50}	AM	TM_{50}
0.010	1.00	1.16	1.01	1.14	1.00	1.03	NA	1.0	NA	1.20	NA	1.0	NA	1.08
0.015	1.00	1.26	1.03	1.21	1.01	1.14	NA	1.0	NA	1.34	NA	1.0	NA	1.16
0.020	1.00	1.39	1.07	1.32	1.01	1.28	NA	1.0	NA	1.52	NA	1.0	NA	1.31
0.030	1.00	1.72	1.13	1.53	1.03	1.63	NA	1.0	NA	1.93	NA	1.0	NA	1.66
0.040	1.01	1.96	1.21	1.76	1.04	1.88	NA	1.0	NA	2.23	NA	1.0	NA	1.92
0.050	1.01	2.02	1.25	1.84	1.05	1.94	NA	1.0	NA	2.27	NA	1.0	NA	1.96
0.060	1.01	1.92	1.24	1.79	1.05	1.83	NA	1.0	NA	2.13	NA	1.0	NA	1.83
0.080	1.02	1.61	1.17	1.55	1.05	1.50	NA	1.0	NA	1.72	NA	1.0	NA	1.48
0.10	1.01	1.39	1.11	1.38	1.03	1.26	NA	1.0	NA	1.45	NA	1.0	NA	1.24
0.15	1.01	1.10	1.02	1.09	1.02	1.04	NA	1.0	NA	1.11	NA	1.0	NA	1.05
0.20	1.00	1.00	1.01	1.00	1.01	1.00	NA	1.0	NA	1.00	NA	1.0	NA	1.00

Table D.4. (*continued*)

Photon energy (MeV)	Organ ID: 36 Tibiae and fibulae Source: medullary cavity		Organ ID: 38 Ankles and feet Source: spongiosa		Organ ID: 40 Mandible Source: spongiosa		Organ ID: 42 Pelvis Source: spongiosa		Organ ID: 44 Ribs Source: spongiosa		Organ ID: 46 Scapulae Source: spongiosa		Organ ID: 48 Spine, cervical Source: spongiosa	
	Target tissue		Target tissue		Target tissue		Target tissue		Target tissue		Target tissue		Target tissue	
	AM	TM_{50}	AM	TM_{50}	AM	TM_{50}	AM	TM_{50}	AM	TM_{50}	AM	TM_{50}	AM	TM_{50}
0.010	NA	1.0	NA	1.16	1.00	1.09	1.00	1.00	1.01	1.09	1.00	1.13	1.01	1.06
0.015	NA	1.0	NA	1.29	1.00	1.20	1.01	1.07	1.01	1.17	1.01	1.24	1.02	1.15
0.020	NA	1.0	NA	1.46	1.00	1.33	1.01	1.18	1.02	1.29	1.01	1.38	1.04	1.27
0.030	NA	1.0	NA	1.85	1.01	1.65	1.03	1.46	1.05	1.57	1.03	1.74	1.08	1.56
0.040	NA	1.0	NA	2.16	1.01	1.90	1.04	1.69	1.07	1.81	1.04	2.02	1.11	1.80
0.050	NA	1.0	NA	2.20	1.02	1.97	1.05	1.76	1.08	1.89	1.05	2.09	1.13	1.88
0.060	NA	1.0	NA	2.05	1.02	1.87	1.05	1.68	1.08	1.82	1.05	1.98	1.12	1.81
0.080	NA	1.0	NA	1.65	1.02	1.55	1.04	1.39	1.06	1.55	1.04	1.63	1.09	1.52
0.10	NA	1.0	NA	1.38	1.01	1.31	1.03	1.18	1.05	1.32	1.03	1.37	1.06	1.29
0.15	NA	1.0	NA	1.09	1.01	1.10	1.01	1.03	1.04	1.09	1.01	1.11	1.03	1.07
0.20	NA	1.0	NA	1.00	1.00	1.00	1.00	1.00	1.00	1.00	1.00	1.00	1.00	1.00

Photon energy (MeV)	Organ ID: 50 Spine, thoracic Source: spongiosa		Organ ID: 52 Spine, lumbar Source: spongiosa		Organ ID: 54 Sacrum Source: spongiosa		Organ ID: 56 Sternum Source: spongiosa	
	Target tissue		Target tissue		Target tissue		Target tissue	
	AM	TM_{50}	AM	TM_{50}	AM	TM_{50}	AM	TM_{50}
0.010	1.00	1.07	1.00	1.00	1.00	1.00	1.00	1.02
0.015	1.01	1.16	1.01	1.09	1.01	1.04	1.01	1.10
0.020	1.02	1.28	1.02	1.19	1.02	1.14	1.02	1.21
0.030	1.03	1.56	1.04	1.46	1.04	1.40	1.03	1.47
0.040	1.05	1.79	1.06	1.68	1.06	1.60	1.05	1.69
0.050	1.06	1.87	1.06	1.75	1.07	1.68	1.06	1.76
0.060	1.06	1.80	1.06	1.69	1.07	1.62	1.06	1.70
0.080	1.04	1.52	1.05	1.42	1.05	1.36	1.04	1.43
0.10	1.03	1.30	1.03	1.21	1.04	1.17	1.03	1.22
0.15	1.01	1.08	1.01	1.02	1.02	1.03	1.01	1.03
0.20	1.00	1.00	1.00	1.00	1.00	1.00	1.00	1.00

NA, not applicable.

ANNEX E. SKELETAL FLUENCE-TO-DOSE RESPONSE FUNCTIONS: NEUTRONS

(E1) Annex D presents the concept of a fluence-to-dose response function, which allows one to calculate the absorbed doses to active marrow and endosteum following photon irradiation of the skeleton in the ICRP reference phantoms. In this annex, corresponding dose–response functions for neutron irradiation of the skeletal tissues are presented. These functions are given over the energy range from 10^{-3} eV to 150 MeV. They explicitly consider the transport of recoil protons across both the bone trabeculae and marrow cavities of each skeletal site. In the energy range from 10^{-3} eV to 20 MeV, recoil protons from hydrogen collisions alone are considered, while protons originating from collisions with all skeletal tissue nuclei are considered at neutron energies from 20 to 150 MeV. Non-proton recoil nuclei are assumed to deposit their energy locally at the site of neutron interaction (i.e. the kerma approximation). Above 150 MeV, the absorbed dose to homogeneous spongiosa is shown to be a reasonable estimate of the absorbed dose to both active marrow (errors <1%) and endosteum (errors <5%).

E.1. Response functions for assessment of bone-specific neutron skeletal dose

(E2) The response function $\mathcal{R}$ for assessment of the bone-specific absorbed dose to skeletal tissues delivered by neutrons of energy E_n in bone site x is given as follows (Kerr and Eckerman, 1985; Bahadori et al., 2011):

$$\mathcal{R}(r_T \leftarrow r_S, x, E_n) = \frac{D(r_T, x)}{\Phi(E_n, r_s, x)} \tag{E.1}$$

$$= \sum_j \frac{\lambda}{m(r_T, x)} \frac{N_A}{A_j} \sum_r f_j(r) m(r, x) \sum_i \int_0^\infty \phi(r_T \leftarrow r, T_i, x) \sigma_{i,j}^{prod}(E_n) T_i n_{i,j}(T_i, E_n) dT_i \tag{E.2}$$

where x is the index for the various bone sites within the phantom (upper femora, cranium, etc.; for the long bones, regions of spongiosa and the medullary cavities are considered as different bone sites); r_T is the index for the target tissue for dose assessment (active marrow or endosteum); r_S is the index for the source tissue in bone site x in which the neutron fluence is scored (spongiosa or medullary marrow); r is the index for the constituent spongiosa tissues of trabecular bone, active marrow, or inactive marrow; λ is a conversion factor to obtain the proper units; N_A is Avogadro's number; A_j is the atomic mass of nuclide j; $f_j(r)$ is the percent mass abundance of nuclide j in the source region r; E_n is the energy of the neutron passing through and potentially interacting within the spongiosa of bone site x; $m(r, x)$ is the mass of the constituent tissue r in bone site x; $m(r_T, x)$ is the mass of the target tissue r_T in bone site x; i is the index for the neutron interaction type considered; T_i is the energy of the secondary charged particles liberated in constituent tissue r by neutron interaction type i; $\phi(r_T \leftarrow r, T_i, x)$ is the fraction of secondary charged-particle

energy T_i liberated in constituent tissue r of bone site x that is imparted to target tissue r_T in bone site x; $\sigma_{i,j}^{prod}(E_n)$ is the secondary charged-particle production cross section for nuclide j and secondary particle i; and $n_{i,j}(T_i, E_n)$ denotes the number of secondary charged particles of energy between T_i and $T_i + dT_i$ liberated in nuclide j by neutrons of energy E_n through interaction type i.

(E3) In this report, Eq. (E.2) was evaluated using methods given in Bahadori et al. (2011). Proton absorbed fraction data were obtained through Continuous Slowing Down Approximation (CSDA) transport methods using linear pathlength distributions acquired from micro-computer-tomography images of 32 bone sites within the skeleton of a 40-year-old male cadaver (Jokisch et al., 2011a,b). Values of the bone-specific dose–response function from Eq. (E.2) are given in tabular form in Table E.1.

(E4) The bone-specific absorbed dose to tissue r_T in bone site x, $D(r_T, x)$, is thus determined as the integral of the product of the bone-specific energy-dependent neutron fluence $\Phi(E_n, r_s, x)$ and the bone-specific energy-dependent dose–response function $\mathcal{R}(r_T \leftarrow r_s, x, E_n)$:

$$D(r_T, x) = \int_{E_n} \Phi(E_n, r_s, x)\mathcal{R}(r_T \leftarrow r_s, x, E_n)dE_n \tag{E.3}$$

(E5) Fluence estimators are given in Eqs. D.4a and D.4b of Annex D. It should be noted that energy E_n is the energy of the neutron passing through and potentially interacting within skeletal tissues, and not the energy of the neutron incident upon the external surfaces of the computational phantom.

E.2. Skeletal-averaged neutron absorbed dose

(E6) Estimates of bone-specific absorbed dose can be of interest during partial-body irradiation of the skeleton such as during criticality accidents or boron neutron-capture therapy. For the purposes of radiological protection and calculation of the effective dose, however, skeletal-averaged absorbed doses to active marrow and endosteum are required. Accordingly, skeletal-averaged dose is given as a mass-weighted average of the bone-site absorbed dose:

$$D_{skel}(r_T) = \sum_x \frac{m(r_T, x)}{m(r_T)} D(r_T, x) \tag{E.4}$$

where $m(r_T,x)$ is the mass of the target tissue r_T in bone site x; $m(r_T)$ is the total mass of target tissue r_T across the entire skeleton; and $D(r_T, x)$ is the bone-specific absorbed dose given by Eq. (E.3). The masses of the skeletal tissues in the ICRP adult male and adult female reference phantoms are summarised in Section 3.4.

E.3. Approximating dose to skeletal target tissues via dose to homogeneous spongiosa

(E7) Skeletal-averaged values of the neutron dose–response function, along with kerma coefficients to active marrow, total marrow, and spongiosa, are shown in

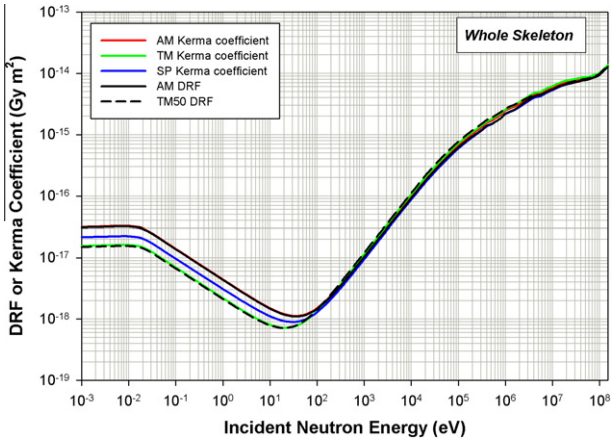

Fig. E.1. Skeletal-averaged neutron dose–response functions (DRFs) and kerma coefficients for the ICRP reference computational phantoms. AM, active marrow; TM, total marrow; TM_{50}, endosteum; SP, spongiosa.

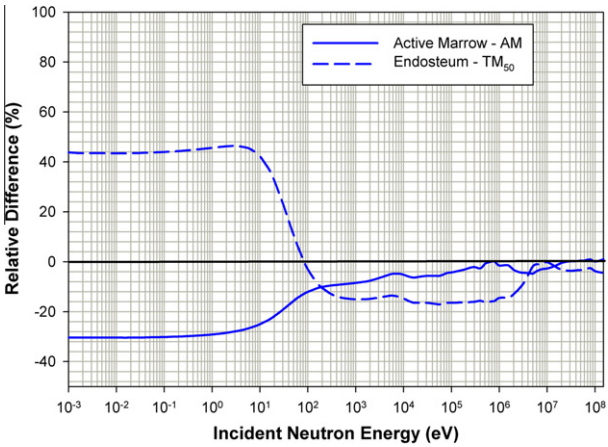

Fig. E.2. Relative difference between neutron kerma coefficients and the corresponding dose–response function for both active marrow (AM) and endosteum (TM_{50}) targets in the skeleton.

Fig. E.1. Relative differences between kerma coefficients and the dose–response functions for active marrow and endosteum are shown in Fig. E.2 as a function of neutron energy incident upon skeletal spongiosa and medullary marrow. At neutron energies below 1 eV, spongiosa kerma is shown to underestimate absorbed dose to active marrow by ~30%. This relative difference decreases with increasing neutron energy to below 20% at 30 eV, to below 10% at 300 eV, to below 5% at 60 keV, and to below 1% at 20 MeV. At neutron energies below 8 eV, the spongiosa kerma is shown to overestimate the absorbed dose to endosteum by ~45%. This relative difference decreases over the energy range of 8 eV to 1 keV, where it plateaus at about

15–20% across the energy range from 300 eV to 1 MeV. This relative difference decreases with increasing neutron energy, reaching ~3–4% above ~10 MeV.

E.4. References

Bahadori, A.A., Johnson, P.B., Jokisch, D.W., Eckerman, K.F., Bolch, W.E., 2011. Response functions for computing absorbed dose to skeletal tissues from neutron irradiation. Phys. Med. Biol. 56, 6873–6897.

Jokisch, D.W., Rajon, D.A., Bahadori, A.A., Bolch, W.E., 2011a. An image-based skeletal dosimetry model for the ICRP reference adult male – specific absorbed fractions for neutron-generated recoil protons. Phys. Med. Biol. 56, 6857–6872.

Jokisch, D.W., Rajon, D.A., Patton, P.W., Bolch, W.E., 2011b. Methods for the inclusion of shallow marrow and adipose tissue in pathlength-based skeletal dosimetry. Phys. Med. Biol. 56, 2699–2713.

Kerr, G.D., Eckerman, K.F., 1985. Neutron and photon fluence-to-dose conversion factors for active marrow of the skeleton. In: Schraube, H., Burger, G., Booz, J. (Eds.), Proceedings of the Fifth Symposium on Neutron Dosimetry. Commission of the European Communities, Luxembourg, pp. 133–145, 17–21 September 1984, Munich, Germany.

Table E.1. Bone-specific absorbed dose per neutron fluence (Gy m^2) to active marrow (AM) and endosteum (TM_{50}) as a function of neutron energy and skeletal region within the ICRP *Publication 110* computational reference phantoms.

Neutron energy (eV)	Organ ID: 14 Humeri, upper half Source: spongiosa Target tissue		Organ ID: 15 Humeri, upper half Source: medullary cavity Target tissue		Organ ID: 17 Humeri, lower half Source: spongiosa Target tissue		Organ ID: 18 Humeri, lower half Source: medullary cavity Target tissue		Organ ID: 20 Ulnae and radii Source: spongiosa Target tissue		Organ ID: 21 Ulnae and radii Source: medullary cavity Target tissue		Organ ID: 23 Wrist and hands Source: spongiosa Target tissue	
	AM	TM_{50}	AM	TM_{50}	AM	TM_{50}	AM	TM_{50}	AM	TM_{50}	AM	TM_{50}	AM	TM_{50}
1.00E−03	3.08E−17	1.25E−17	NA	6.86E−18	NA	6.33E−18	NA	6.86E−18	NA	6.33E−18	NA	6.86E−18	NA	6.33E−18
1.50E−03	3.10E−17	1.25E−17	NA	6.90E−18	NA	6.37E−18	NA	6.90E−18	NA	6.37E−18	NA	6.90E−18	NA	6.37E−18
2.00E−03	3.12E−17	1.26E−17	NA	6.94E−18	NA	6.40E−18	NA	6.94E−18	NA	6.40E−18	NA	6.94E−18	NA	6.40E−18
3.00E−03	3.15E−17	1.27E−17	NA	7.01E−18	NA	6.46E−18	NA	7.01E−18	NA	6.46E−18	NA	7.01E−18	NA	6.46E−18
4.00E−03	3.17E−17	1.28E−17	NA	7.06E−18	NA	6.51E−18	NA	7.06E−18	NA	6.51E−18	NA	7.06E−18	NA	6.51E−18
5.00E−03	3.19E−17	1.29E−17	NA	7.09E−18	NA	6.54E−18	NA	7.09E−18	NA	6.54E−18	NA	7.09E−18	NA	6.54E−18
6.00E−03	3.20E−17	1.29E−17	NA	7.12E−18	NA	6.57E−18	NA	7.12E−18	NA	6.57E−18	NA	7.12E−18	NA	6.57E−18
8.00E−03	3.20E−17	1.29E−17	NA	7.13E−18	NA	6.58E−18	NA	7.13E−18	NA	6.58E−18	NA	7.13E−18	NA	6.58E−18
1.00E−02	3.19E−17	1.29E−17	NA	7.11E−18	NA	6.55E−18	NA	7.11E−18	NA	6.55E−18	NA	7.11E−18	NA	6.55E−18
1.50E−02	3.09E−17	1.25E−17	NA	6.88E−18	NA	6.34E−18	NA	6.88E−18	NA	6.34E−18	NA	6.88E−18	NA	6.34E−18
2.00E−02	2.92E−17	1.18E−17	NA	6.50E−18	NA	5.99E−18	NA	6.50E−18	NA	5.99E−18	NA	6.50E−18	NA	5.99E−18
3.00E−02	2.50E−17	1.01E−17	NA	5.56E−18	NA	5.13E−18	NA	5.56E−18	NA	5.13E−18	NA	5.56E−18	NA	5.13E−18
4.00E−02	2.18E−17	8.79E−18	NA	4.85E−18	NA	4.47E−18	NA	4.85E−18	NA	4.47E−18	NA	4.85E−18	NA	4.47E−18
5.00E−02	1.94E−17	7.85E−18	NA	4.32E−18	NA	3.99E−18	NA	4.32E−18	NA	3.99E−18	NA	4.32E−18	NA	3.99E−18
6.00E−02	1.77E−17	7.13E−18	NA	3.93E−18	NA	3.63E−18	NA	3.93E−18	NA	3.63E−18	NA	3.93E−18	NA	3.63E−18
8.00E−02	1.53E−17	6.19E−18	NA	3.41E−18	NA	3.15E−18	NA	3.41E−18	NA	3.15E−18	NA	3.41E−18	NA	3.15E−18
1.00E−01	1.37E−17	5.53E−18	NA	3.05E−18	NA	2.81E−18	NA	3.05E−18	NA	2.81E−18	NA	3.05E−18	NA	2.81E−18
1.50E−01	1.12E−17	4.53E−18	NA	2.50E−18	NA	2.31E−18	NA	2.50E−18	NA	2.31E−18	NA	2.50E−18	NA	2.31E−18
2.00E−01	9.72E−18	3.93E−18	NA	2.16E−18	NA	2.00E−18	NA	2.16E−18	NA	2.00E−18	NA	2.16E−18	NA	2.00E−18
3.00E−01	7.91E−18	3.20E−18	NA	1.76E−18	NA	1.63E−18	NA	1.76E−18	NA	1.63E−18	NA	1.76E−18	NA	1.63E−18
4.00E−01	6.86E−18	2.78E−18	NA	1.53E−18	NA	1.41E−18	NA	1.53E−18	NA	1.41E−18	NA	1.53E−18	NA	1.41E−18
5.00E−01	6.14E−18	2.48E−18	NA	1.37E−18	NA	1.27E−18	NA	1.37E−18	NA	1.27E−18	NA	1.37E−18	NA	1.27E−18
6.00E−01	5.61E−18	2.27E−18	NA	1.25E−18	NA	1.16E−18	NA	1.25E−18	NA	1.16E−18	NA	1.25E−18	NA	1.16E−18
8.00E−01	4.87E−18	1.97E−18	NA	1.09E−18	NA	1.01E−18	NA	1.09E−18	NA	1.01E−18	NA	1.09E−18	NA	1.01E−18
1.00E+00	4.34E−18	1.76E−18	NA	9.76E−19	NA	9.02E−19	NA	9.76E−19	NA	9.02E−19	NA	9.76E−19	NA	9.02E−19
1.50E+00	3.56E−18	1.45E−18	NA	8.08E−19	NA	7.46E−19	NA	8.08E−19	NA	7.46E−19	NA	8.08E−19	NA	7.46E−19
2.00E+00	3.08E−18	1.26E−18	NA	7.07E−19	NA	6.54E−19	NA	7.07E−19	NA	6.54E−19	NA	7.07E−19	NA	6.54E−19
3.00E+00	2.53E−18	1.04E−18	NA	5.93E−19	NA	5.49E−19	NA	5.93E−19	NA	5.49E−19	NA	5.93E−19	NA	5.49E−19
4.00E+00	2.20E−18	9.21E−19	NA	5.30E−19	NA	4.93E−19	NA	5.30E−19	NA	4.94E−19	NA	5.30E−19	NA	4.93E−19
5.00E+00	1.98E−18	8.38E−19	NA	4.90E−19	NA	4.58E−19	NA	4.90E−19	NA	4.58E−19	NA	4.90E−19	NA	4.58E−19
6.00E+00	1.82E−18	7.80E−19	NA	4.64E−19	NA	4.35E−19	NA	4.64E−19	NA	4.35E−19	NA	4.64E−19	NA	4.35E−19
8.00E+00	1.60E−18	7.07E−19	NA	4.35E−19	NA	4.10E−19	NA	4.35E−19	NA	4.10E−19	NA	4.35E−19	NA	4.10E−19
1.00E+01	1.45E−18	6.62E−19	NA	4.21E−19	NA	4.00E−19	NA	4.21E−19	NA	4.00E−19	NA	4.21E−19	NA	4.00E−19
1.50E+01	1.24E−18	6.17E−19	NA	4.24E−19	NA	4.09E−19	NA	4.24E−19	NA	4.09E−19	NA	4.24E−19	NA	4.09E−19
2.00E+01	1.13E−18	6.10E−19	NA	4.50E−19	NA	4.38E−19	NA	4.50E−19	NA	4.38E−19	NA	4.50E−19	NA	4.38E−19
3.00E+01	1.03E−18	6.46E−19	NA	5.26E−19	NA	5.19E−19	NA	5.26E−19	NA	5.20E−19	NA	5.26E−19	NA	5.19E−19
4.00E+01	1.01E−18	7.13E−19	NA	6.20E−19	NA	6.17E−19	NA	6.20E−19	NA	6.18E−19	NA	6.20E−19	NA	6.17E−19
5.00E+01	1.01E−18	7.92E−19	NA	7.21E−19	NA	7.21E−19	NA	7.21E−19	NA	7.22E−19	NA	7.21E−19	NA	7.21E−19
6.00E+01	1.04E−18	8.80E−19	NA	8.26E−19	NA	8.29E−19	NA	8.26E−19	NA	8.30E−19	NA	8.26E−19	NA	8.29E−19
8.00E+01	1.13E−18	1.07E−18	NA	1.04E−18	NA	1.05E−18	NA	1.04E−18	NA	1.05E−18	NA	1.04E−18	NA	1.05E−18
1.00E+02	1.23E−18	1.26E−18	NA	1.26E−18	NA	1.28E−18	NA	1.26E−18	NA	1.28E−18	NA	1.26E−18	NA	1.28E−18

(*continued on next page*)

Table E.1. (*continued*)

Neutron energy (eV)	Organ ID: 14 Humeri, upper half Source: spongiosa Target tissue		Organ ID: 15 Humeri, upper half Source: medullary cavity Target tissue		Organ ID: 17 Humeri, lower half Source: spongiosa Target tissue		Organ ID: 18 Humeri, lower half Source: medullary cavity Target tissue		Organ ID: 20 Ulnae and radii Source: spongiosa Target tissue		Organ ID: 21 Ulnae and radii Source: medullary cavity Target tissue		Organ ID: 23 Wrist and hands Source: spongiosa Target tissue	
	AM	TM_{50}	AM	TM_{50}	AM	TM_{50}	AM	TM_{50}	AM	TM_{50}	AM	TM_{50}	AM	TM_{50}
1.50E+02	1.55E−18	1.78E−18	NA	1.83E−18	NA	1.85E−18	NA	1.83E−18	NA	1.86E−18	NA	1.83E−18	NA	1.85E−18
2.00E+02	1.91E−18	2.30E−18	NA	2.40E−18	NA	2.43E−18	NA	2.40E−18	NA	2.44E−18	NA	2.40E−18	NA	2.43E−18
3.00E+02	2.64E−18	3.36E−18	NA	3.55E−18	NA	3.60E−18	NA	3.55E−18	NA	3.61E−18	NA	3.55E−18	NA	3.60E−18
4.00E+02	3.39E−18	4.44E−18	NA	4.71E−18	NA	4.77E−18	NA	4.71E−18	NA	4.78E−18	NA	4.71E−18	NA	4.77E−18
5.00E+02	4.14E−18	5.51E−18	NA	5.87E−18	NA	5.93E−18	NA	5.87E−18	NA	5.94E−18	NA	5.87E−18	NA	5.93E−18
6.00E+02	4.90E−18	6.58E−18	NA	7.02E−18	NA	7.09E−18	NA	7.02E−18	NA	7.11E−18	NA	7.02E−18	NA	7.09E−18
8.00E+02	6.40E−18	8.73E−18	NA	9.33E−18	NA	9.40E−18	NA	9.33E−18	NA	9.42E−18	NA	9.33E−18	NA	9.40E−18

Neutron energy (eV)	Organ ID: 25 Clavicles Source: spongiosa Target tissue		Organ ID: 27 Cranium Source: spongiosa Target tissue		Organ ID: 29 Femora, upper half Source: spongiosa Target tissue		Organ ID: 30 Femora, upper half Source: medullary cavity Target tissue		Organ ID: 32 Femora, lower half Source: spongiosa Target tissue		Organ ID: 33 Femora, lower half Source: medullary cavity Target tissue		Organ ID: 35 Tibiae, fibulae, patellae Source: spongiosa Target tissue	
	AM	TM_{50}	AM	TM_{50}	AM	TM_{50}	AM	TM_{50}	AM	TM_{50}	AM	TM_{50}	AM	TM_{50}
1.00E−03	3.08E−17	1.44E−17	3.08E−17	1.56E−17	3.08E−17	1.25E−17	NA	6.86E−18	NA	6.33E−18	NA	6.86E−18	NA	6.33E−18
1.50E−03	3.10E−17	1.45E−17	3.10E−17	1.57E−17	3.10E−17	1.25E−17	NA	6.90E−18	NA	6.37E−18	NA	6.90E−18	NA	6.37E−18
2.00E−03	3.12E−17	1.46E−17	3.12E−17	1.58E−17	3.12E−17	1.26E−17	NA	6.94E−18	NA	6.40E−18	NA	6.94E−18	NA	6.40E−18
3.00E−03	3.15E−17	1.47E−17	3.15E−17	1.60E−17	3.15E−17	1.27E−17	NA	7.01E−18	NA	6.46E−18	NA	7.01E−18	NA	6.46E−18
4.00E−03	3.17E−17	1.48E−17	3.17E−17	1.61E−17	3.17E−17	1.28E−17	NA	7.06E−18	NA	6.51E−18	NA	7.06E−18	NA	6.51E−18
5.00E−03	3.19E−17	1.49E−17	3.19E−17	1.62E−17	3.19E−17	1.29E−17	NA	7.09E−18	NA	6.54E−18	NA	7.09E−18	NA	6.54E−18
6.00E−03	3.20E−17	1.50E−17	3.20E−17	1.62E−17	3.20E−17	1.29E−17	NA	7.12E−18	NA	6.57E−18	NA	7.12E−18	NA	6.57E−18
8.00E−03	3.20E−17	1.50E−17	3.20E−17	1.63E−17	3.20E−17	1.29E−17	NA	7.13E−18	NA	6.58E−18	NA	7.13E−18	NA	6.58E−18
1.00E−02	3.19E−17	1.49E−17	3.19E−17	1.62E−17	3.19E−17	1.29E−17	NA	7.11E−18	NA	6.55E−18	NA	7.11E−18	NA	6.55E−18
1.50E−02	3.09E−17	1.45E−17	3.09E−17	1.57E−17	3.09E−17	1.25E−17	NA	6.88E−18	NA	6.34E−18	NA	6.88E−18	NA	6.34E−18
2.00E−02	2.92E−17	1.37E−17	2.92E−17	1.48E−17	2.92E−17	1.18E−17	NA	6.50E−18	NA	5.99E−18	NA	6.50E−18	NA	5.99E−18
3.00E−02	2.50E−17	1.17E−17	2.50E−17	1.27E−17	2.50E−17	1.01E−17	NA	5.56E−18	NA	5.13E−18	NA	5.56E−18	NA	5.13E−18
4.00E−02	2.18E−17	1.02E−17	2.18E−17	1.10E−17	2.18E−17	8.79E−18	NA	4.85E−18	NA	4.47E−18	NA	4.85E−18	NA	4.47E−18
5.00E−02	1.94E−17	9.09E−18	1.94E−17	9.86E−18	1.94E−17	7.85E−18	NA	4.32E−18	NA	3.99E−18	NA	4.32E−18	NA	3.99E−18
6.00E−02	1.77E−17	8.26E−18	1.77E−17	8.96E−18	1.77E−17	7.13E−18	NA	3.93E−18	NA	3.63E−18	NA	3.93E−18	NA	3.63E−18
8.00E−02	1.53E−17	7.17E−18	1.53E−17	7.77E−18	1.53E−17	6.19E−18	NA	3.41E−18	NA	3.15E−18	NA	3.41E−18	NA	3.15E−18
1.00E−01	1.37E−17	6.40E−18	1.37E−17	6.94E−18	1.37E−17	5.53E−18	NA	3.05E−18	NA	2.81E−18	NA	3.05E−18	NA	2.81E−18
1.50E−01	1.12E−17	5.25E−18	1.12E−17	5.69E−18	1.12E−17	4.53E−18	NA	2.50E−18	NA	2.31E−18	NA	2.50E−18	NA	2.31E−18
2.00E−01	9.72E−18	4.55E−18	9.72E−18	4.93E−18	9.72E−18	3.93E−18	NA	2.16E−18	NA	2.00E−18	NA	2.16E−18	NA	2.00E−18
3.00E−01	7.91E−18	3.70E−18	7.91E−18	4.02E−18	7.91E−18	3.20E−18	NA	1.76E−18	NA	1.63E−18	NA	1.76E−18	NA	1.63E−18
4.00E−01	6.86E−18	3.21E−18	6.86E−18	3.48E−18	6.86E−18	2.78E−18	NA	1.53E−18	NA	1.41E−18	NA	1.53E−18	NA	1.41E−18
5.00E−01	6.14E−18	2.87E−18	6.14E−18	3.12E−18	6.14E−18	2.48E−18	NA	1.37E−18	NA	1.27E−18	NA	1.37E−18	NA	1.27E−18
6.00E−01	5.61E−18	2.63E−18	5.61E−18	2.85E−18	5.61E−18	2.27E−18	NA	1.25E−18	NA	1.16E−18	NA	1.25E−18	NA	1.16E−18
8.00E−01	4.87E−18	2.28E−18	4.87E−18	2.48E−18	4.87E−18	1.97E−18	NA	1.09E−18	NA	1.01E−18	NA	1.09E−18	NA	1.01E−18
1.00E+00	4.34E−18	2.04E−18	4.35E−18	2.21E−18	4.34E−18	1.76E−18	NA	9.76E−19	NA	9.02E−19	NA	9.76E−19	NA	9.02E−19
1.50E+00	3.56E−18	1.68E−18	3.56E−18	1.82E−18	3.56E−18	1.45E−18	NA	8.08E−19	NA	7.46E−19	NA	8.08E−19	NA	7.46E−19
2.00E+00	3.09E−18	1.46E−18	3.09E−18	1.58E−18	3.09E−18	1.26E−18	NA	7.07E−19	NA	6.54E−19	NA	7.07E−19	NA	6.54E−19
3.00E+00	2.53E−18	1.20E−18	2.53E−18	1.30E−18	2.53E−18	1.05E−18	NA	5.93E−19	NA	5.49E−19	NA	5.93E−19	NA	5.50E−19

Table E.1. (*continued*)

4.00E+00	2.21E−18	1.06E−18	2.21E−18	1.15E−18	2.21E−18	9.23E−19	NA	5.30E−19	NA	4.93E−19	NA	5.30E−19	NA	4.94E−19
5.00E+00	1.98E−18	9.62E−19	1.99E−18	1.04E−18	1.98E−18	8.41E−19	NA	4.90E−19	NA	4.57E−19	NA	4.90E−19	NA	4.58E−19
6.00E+00	1.82E−18	8.94E−19	1.83E−18	9.65E−19	1.82E−18	7.84E−19	NA	4.64E−19	NA	4.34E−19	NA	4.64E−19	NA	4.35E−19
8.00E+00	1.61E−18	8.06E−19	1.62E−18	8.68E−19	1.60E−18	7.12E−19	NA	4.35E−19	NA	4.10E−19	NA	4.35E−19	NA	4.11E−19
1.00E+01	1.46E−18	7.51E−19	1.47E−18	8.07E−19	1.46E−18	6.68E−19	NA	4.21E−19	NA	4.00E−19	NA	4.21E−19	NA	4.01E−19
1.50E+01	1.26E−18	6.91E−19	1.28E−18	7.38E−19	1.25E−18	6.26E−19	NA	4.24E−19	NA	4.09E−19	NA	4.24E−19	NA	4.10E−19
2.00E+01	1.16E−18	6.76E−19	1.18E−18	7.18E−19	1.15E−18	6.23E−19	NA	4.50E−19	NA	4.37E−19	NA	4.50E−19	NA	4.39E−19
3.00E+01	1.07E−18	7.02E−19	1.11E−18	7.40E−19	1.06E−18	6.66E−19	NA	5.26E−19	NA	5.19E−19	NA	5.26E−19	NA	5.22E−19
4.00E+01	1.05E−18	7.63E−19	1.11E−18	7.99E−19	1.04E−18	7.39E−19	NA	6.20E−19	NA	6.16E−19	NA	6.20E−19	NA	6.20E−19
5.00E+01	1.07E−18	8.40E−19	1.14E−18	8.75E−19	1.06E−18	8.25E−19	NA	7.21E−19	NA	7.20E−19	NA	7.21E−19	NA	7.25E−19
6.00E+01	1.11E−18	9.25E−19	1.19E−18	9.61E−19	1.09E−18	9.19E−19	NA	8.26E−19	NA	8.28E−19	NA	8.26E−19	NA	8.33E−19
8.00E+01	1.22E−18	1.11E−18	1.33E−18	1.15E−18	1.19E−18	1.12E−18	NA	1.04E−18	NA	1.05E−18	NA	1.04E−18	NA	1.06E−18
1.00E+02	1.35E−18	1.31E−18	1.49E−18	1.35E−18	1.31E−18	1.33E−18	NA	1.26E−18	NA	1.28E−18	NA	1.26E−18	NA	1.28E−18
1.50E+02	1.73E−18	1.82E−18	1.94E−18	1.87E−18	1.68E−18	1.87E−18	NA	1.83E−18	NA	1.85E−18	NA	1.83E−18	NA	1.86E−18
2.00E+02	2.14E−18	2.35E−18	2.41E−18	2.41E−18	2.07E−18	2.43E−18	NA	2.40E−18	NA	2.43E−18	NA	2.40E−18	NA	2.45E−18
3.00E+02	2.99E−18	3.42E−18	3.40E−18	3.50E−18	2.88E−18	3.55E−18	NA	3.55E−18	NA	3.60E−18	NA	3.55E−18	NA	3.62E−18
4.00E+02	3.86E−18	4.50E−18	4.41E−18	4.60E−18	3.71E−18	4.68E−18	NA	4.71E−18	NA	4.76E−18	NA	4.71E−18	NA	4.80E−18
5.00E+02	4.73E−18	5.58E−18	5.42E−18	5.70E−18	4.55E−18	5.81E−18	NA	5.87E−18	NA	5.92E−18	NA	5.87E−18	NA	5.96E−18
6.00E+02	5.60E−18	6.66E−18	6.44E−18	6.80E−18	5.38E−18	6.93E−18	NA	7.02E−18	NA	7.08E−18	NA	7.02E−18	NA	7.13E−18
8.00E+02	7.34E−18	8.81E−18	8.46E−18	9.00E−18	7.04E−18	9.18E−18	NA	9.33E−18	NA	9.39E−18	NA	9.33E−18	NA	9.45E−18

Neutron energy (eV)	Organ ID: 36 Tibiae and fibulae Source: medullary cavity Target tissue		Organ ID: 38 Ankles and feet Source: spongiosa Target tissue		Organ ID: 40 Mandible Source: spongiosa Target tissue		Organ ID: 42 Pelvis Source: spongiosa Target tissue		Organ ID: 44 Ribs Source: spongiosa Target tissue		Organ ID: 46 Scapulae Source: spongiosa Target tissue		Organ ID: 48 Spine, cervical Source: spongiosa Target tissue	
	AM	TM_{50}	AM	TM_{50}	AM	TM_{50}	AM	TM_{50}	AM	TM_{50}	AM	TM_{50}	AM	TM_{50}
1.00E−03	NA	6.86E−18	NA	6.33E−18	3.08E−17	1.56E−17	3.08E−17	1.81E−17	3. 08E−17	2.35E−17	3.08E−17	1.56E−17	3.08E−17	2.35E−17
1.50E−03	NA	6.90E−18	NA	6.37E−18	3.10E−17	1.57E−17	3.10E−17	1.82E−17	3. 10E−17	2.36E−17	3.10E−17	1.57E−17	3.10E−17	2.36E−17
2.00E−03	NA	6.94E−18	NA	6.40E−18	3.12E−17	1.58E−17	3.12E−17	1.83E−17	3. 12E−17	2.38E−17	3.12E−17	1.58E−17	3.12E−17	2.38E−17
3.00E−03	NA	7.01E−18	NA	6.46E−18	3.15E−17	1.60E−17	3.15E−17	1.85E−17	3. 15E−17	2.40E−17	3.15E−17	1.60E−17	3.15E−17	2.40E−17
4.00E−03	NA	7.06E−18	NA	6.51E−18	3.17E−17	1.61E−17	3.17E−17	1.86E−17	3. 17E−17	2.41E−17	3.17E−17	1.61E−17	3.17E−17	2.41E−17
5.00E−03	NA	7.09E−18	NA	6.54E−18	3.19E−17	1.62E−17	3.19E−17	1.87E−17	3. 19E−17	2.43E−17	3.19E−17	1.62E−17	3.19E−17	2.43E−17
6.00E−03	NA	7.12E−18	NA	6.57E−18	3.20E−17	1.62E−17	3.20E−17	1.88E−17	3. 20E−17	2.44E−17	3.20E−17	1.62E−17	3.20E−17	2.44E−17
8.00E−03	NA	7.13E−18	NA	6.58E−18	3.20E−17	1.63E−17	3.20E−17	1.88E−17	3. 20E−17	2.44E−17	3.20E−17	1.63E−17	3.20E−17	2.44E−17
1.00E−02	NA	7.11E−18	NA	6.55E−18	3.19E−17	1.62E−17	3.19E−17	1.87E−17	3. 19E−17	2.43E−17	3.19E−17	1.62E−17	3.19E−17	2.43E−17
1.50E−02	NA	6.88E−18	NA	6.34E−18	3.09E−17	1.57E−17	3.09E−17	1.81E−17	3. 09E−17	2.35E−17	3.09E−17	1.57E−17	3.09E−17	2.35E−17
2.00E−02	NA	6.50E−18	NA	5.99E−18	2.92E−17	1.48E−17	2.92E−17	1.71E−17	2. 92E−17	2.22E−17	2.92E−17	1.48E−17	2.92E−17	2.22E−17
3.00E−02	NA	5.56E−18	NA	5.13E−18	2.50E−17	1.27E−17	2.50E−17	1.46E−17	2. 50E−17	1.90E−17	2.50E−17	1.27E−17	2.50E−17	1.90E−17
4.00E−02	NA	4.85E−18	NA	4.47E−18	2.18E−17	1.10E−17	2.18E−17	1.28E−17	2. 18E−17	1.66E−17	2.18E−17	1.10E−17	2.18E−17	1.66E−17
5.00E−02	NA	4.32E−18	NA	3.99E−18	1.94E−17	9.85E−18	1.94E−17	1.14E−17	1. 94E−17	1.48E−17	1.94E−17	9.85E−18	1.94E−17	1.48E−17
6.00E−02	NA	3.93E−18	NA	3.63E−18	1.77E−17	8.96E−18	1.77E−17	1.04E−17	1. 77E−17	1.34E−17	1.77E−17	8.96E−18	1.77E−17	1.34E−17
8.00E−02	NA	3.41E−18	NA	3.15E−18	1.53E−17	7.77E−18	1.53E−17	8.99E−18	1. 53E−17	1.17E−17	1.53E−17	7.77E−18	1.53E−17	1.17E−17
1.00E−01	NA	3.05E−18	NA	2.81E−18	1.37E−17	6.94E−18	1.37E−17	8.03E−18	1. 37E−17	1.04E−17	1.37E−17	6.94E−18	1.37E−17	1.04E−17
1.50E−01	NA	2.50E−18	NA	2.31E−18	1.12E−17	5.69E−18	1.12E−17	6.58E−18	1. 12E−17	8.55E−18	1.12E−17	5.69E−18	1.12E−17	8.54E−18
2.00E−01	NA	2.16E−18	NA	2.00E−18	9.72E−18	4.93E−18	9.72E−18	5.70E−18	9.72E−18	7.40E−18	9.72E−18	4.93E−18	9.72E−18	7.40E−18
3.00E−01	NA	1.76E−18	NA	1.63E−18	7.91E−18	4.01E−18	7.91E−18	4.64E−18	7. 91E−18	6.03E−18	7.91E−18	4.01E−18	7.91E−18	6.03E−18
4.00E−01	NA	1.53E−18	NA	1.41E−18	6.86E−18	3.48E−18	6.86E−18	4.03E−18	6. 86E−18	5.23E−18	6.86E−18	3.48E−18	6.86E−18	5.23E−18
5.00E−01	NA	1.37E−18	NA	1.27E−18	6.14E−18	3.12E−18	6.14E−18	3.60E−18	6. 14E−18	4.68E−18	6.14E−18	3.12E−18	6.14E−18	4.68E−18
6.00E−01	NA	1.25E−18	NA	1.16E−18	5.61E−18	2.85E−18	5.61E−18	3.29E−18	5. 61E−18	4.27E−18	5.61E−18	2.85E−18	5.61E−18	4.27E−18

(*continued on next page*)

Table E.1. (*continued*)

Neutron energy (eV)	Organ ID: 36 Tibiae and fibulae Source: medullary cavity Target tissue		Organ ID: 38 Ankles and feet Source: spongiosa Target tissue		Organ ID: 40 Mandible Source: spongiosa Target tissue		Organ ID: 42 Pelvis Source: spongiosa Target tissue		Organ ID: 44 Ribs Source: spongiosa Target tissue		Organ ID: 46 Scapulae Source: spongiosa Target tissue		Organ ID: 48 Spine, cervical Source: spongiosa Target tissue	
	AM	TM_{50}	AM	TM_{50}	AM	TM_{50}	AM	TM_{50}	AM	TM_{50}	AM	TM_{50}	AM	TM_{50}
8.00E−01	NA	1.09E−18	NA	1.01E−18	4.87E−18	2.47E−18	4.87E−18	2.86E−18	4. 87E−18	3.71E−18	4.87E−18	2.47E−18	4.87E−18	3.71E−18
1.00E+00	NA	9.76E−19	NA	9.02E−19	4.34E−18	2.21E−18	4.35E−18	2.55E−18	4. 35E−18	3.31E−18	4.34E−18	2.21E−18	4.35E−18	3.31E−18
1.50E+00	NA	8.08E−19	NA	7.46E−19	3.56E−18	1.82E−18	3.56E−18	2.10E−18	3. 56E−18	2.72E−18	3.56E−18	1.82E−18	3.56E−18	2.72E−18
2.00E+00	NA	7.07E−19	NA	6.54E−19	3.09E−18	1.58E−18	3.09E−18	1.82E−18	3.09E−18	2.36E−18	3.09E−18	1.58E−18	3.09E−18	2.36E−18
3.00E+00	NA	5.93E−19	NA	5.49E−19	2.53E−18	1.30E−18	2.53E−18	1.50E−18	2. 53E−18	1.94E−18	2.53E−18	1.30E−18	2.53E−18	1.94E−18
4.00E+00	NA	5.30E−19	NA	4.93E−19	2.21E−18	1.14E−18	2.21E−18	1.32E−18	2. 21E−18	1.70E−18	2.21E−18	1.14E−18	2.21E−18	1.70E−18
5.00E+00	NA	4.90E−19	NA	4.57E−19	1.99E−18	1.04E−18	1.99E−18	1.19E−18	1. 99E−18	1.53E−18	1.99E−18	1.04E−18	1.99E−18	1.53E−18
6.00E+00	NA	4.64E−19	NA	4.34E−19	1.83E−18	9.62E−19	1.83E−18	1.10E−18	1. 83E−18	1.41E−18	1.83E−18	9.61E−19	1.83E−18	1.41E−18
8.00E+00	NA	4.35E−19	NA	4.10E−19	1.61E−18	8.65E−19	1.62E−18	9.86E−19	1. 62E−18	1.26E−18	1.62E−18	8.64E−19	1.62E−18	1.26E−18
1.00E+01	NA	4.21E−19	NA	4.00E−19	1.47E−18	8.03E−19	1.47E−18	9.10E−19	1. 48E−18	1.15E−18	1.47E−18	8.01E−19	1.48E−18	1.15E−18
1.50E+01	NA	4.24E−19	NA	4.09E−19	1.27E−18	7.32E−19	1.28E−18	8.18E−19	1. 28E−18	1.02E−18	1.27E−18	7.30E−19	1.28E−18	1.02E−18
2.00E+01	NA	4.50E−19	NA	4.37E−19	1.17E−18	7.10E−19	1.18E−18	7.84E−19	1. 19E−18	9.62E−19	1.18E−18	7.08E−19	1.19E−18	9.61E−19
3.00E+01	NA	5.26E−19	NA	5.19E−19	1.09E−18	7.28E−19	1.10E−18	7.84E−19	1. 11E−18	9.35E−19	1.10E−18	7.23E−19	1.11E−18	9.34E−19
4.00E+01	NA	6.20E−19	NA	6.16E−19	1.08E−18	7.83E−19	1.10E−18	8.29E−19	1. 11E−18	9.65E−19	1.09E−18	7.77E−19	1.11E−18	9.65E−19
5.00E+01	NA	7.21E−19	NA	7.20E−19	1.10E−18	8.55E−19	1.13E−18	8.93E−19	1. 15E−18	1.02E−18	1.12E−18	8.48E−19	1.15E−18	1.02E−18
6.00E+01	NA	8.26E−19	NA	8.28E−19	1.15E−18	9.37E−19	1.19E−18	9.69E−19	1. 20E−18	1.09E−18	1.17E−18	9.28E−19	1.20E−18	1.09E−18
8.00E+01	NA	1.04E−18	NA	1.05E−18	1.27E−18	1.12E−18	1.32E−18	1.14E−18	1. 34E−18	1.26E−18	1.30E−18	1.10E−18	1.34E−18	1.26E−18
1.00E+02	NA	1.26E−18	NA	1.28E−18	1.41E−18	1.31E−18	1.48E−18	1.32E−18	1. 50E−18	1.44E−18	1.45E−18	1.29E−18	1.50E−18	1.44E−18
1.50E+02	NA	1.83E−18	NA	1.85E−18	1.83E−18	1.81E−18	1.92E−18	1.81E−18	1. 96E−18	1.93E−18	1.88E−18	1.79E−18	1.96E−18	1.93E−18
2.00E+02	NA	2.40E−18	NA	2.43E−18	2.27E−18	2.33E−18	2.39E−18	2.31E−18	2. 45E−18	2.45E−18	2.34E−18	2.30E−18	2.45E−18	2.45E−18
3.00E+02	NA	3.55E−18	NA	3.60E−18	3.18E−18	3.38E−18	3.37E−18	3.34E−18	3. 45E−18	3.50E−18	3.29E−18	3.34E−18	3.46E−18	3.50E−18
4.00E+02	NA	4.71E−18	NA	4.76E−18	4.12E−18	4.44E−18	4.37E−18	4.38E−18	4. 48E−18	4.57E−18	4.26E−18	4.39E−18	4.49E−18	4.57E−18
5.00E+02	NA	5.87E−18	NA	5.92E−18	5.06E−18	5.51E−18	5.37E−18	5.42E−18	5. 52E−18	5.65E−18	5.23E−18	5.44E−18	5.52E−18	5.65E−18
6.00E+02	NA	7.02E−18	NA	7.08E−18	5.99E−18	6.57E−18	6.37E−18	6.46E−18	6.55E−18	6.73E−18	6.20E−18	6.48E−18	6.56E−18	6.73E−18
8.00E+02	NA	9.33E−18	NA	9.39E−18	7.87E−18	8.70E−18	8.38E−18	8.53E−18	8. 62E−18	8.88E−18	8.15E−18	8.58E−18	8.63E−18	8.88E−18

Neutron energy (eV)	Organ ID: 50 Spine, thoracic Source: spongiosa Target tissue		Organ ID: 52 Spine, lumbar Source: spongiosa Target tissue		Organ ID: 54 Sacrum Source: spongiosa Target tissue		Organ ID: 56 Sternum Source: spongiosa Target tissue	
	AM	TM_{50}	AM	TM_{50}	AM	TM_{50}	AM	TM_{50}
1.00E−03	3.08E−17	2.35E−17	3.08E−17	2.35E−17	3.08E−17	2.37E−17	3.08E−17	2.35E−17
1.50E−03	3.10E−17	2.36E−17	3.10E−17	2.36E−17	3.10E−17	2.39E−17	3.10E−17	2.36E−17
2.00E−03	3.12E−17	2.38E−17	3.12E−17	2.38E−17	3.12E−17	2.40E−17	3.12E−17	2.37E−17
3.00E−03	3.15E−17	2.40E−17	3.15E−17	2.40E−17	3.15E−17	2.42E−17	3.15E−17	2.40E−17
4.00E−03	3.17E−17	2.41E−17	3.17E−17	2.41E−17	3.17E−17	2.44E−17	3.17E−17	2.41E−17
5.00E−03	3.19E−17	2.43E−17	3.19E−17	2.43E−17	3.19E−17	2.45E−17	3.19E−17	2.43E−17
6.00E−03	3.20E−17	2.44E−17	3.20E−17	2.44E−17	3.20E−17	2.46E−17	3.20E−17	2.43E−17
8.00E−03	3.20E−17	2.44E−17	3.20E−17	2.44E−17	3.20E−17	2.47E−17	3.20E−17	2.44E−17
1.00E−02	3.19E−17	2.43E−17	3.19E−17	2.43E−17	3.19E−17	2.46E−17	3.19E−17	2.43E−17
1.50E−02	3.09E−17	2.35E−17	3.09E−17	2.35E−17	3.09E−17	2.38E−17	3.09E−17	2.35E−17
2.00E−02	2.92E−17	2.22E−17	2.92E−17	2.22E−17	2.92E−17	2.25E−17	2.92E−17	2.22E−17
3.00E−02	2.50E−17	1.90E−17	2.50E−17	1.90E−17	2.50E−17	1.92E−17	2.50E−17	1.90E−17

Table E.1. (*continued*)

4.00E−02	2.18E−17	1.66E−17	2.18E−17	1.66E−17	2.18E−17	1.68E−17	2.18E−17	1.66E−17
5.00E−02	1.94E−17	1.48E−17	1.94E−17	1.48E−17	1.94E−17	1.50E−17	1.94E−17	1.48E−17
6.00E−02	1.77E−17	1.34E−17	1.77E−17	1.34E−17	1.77E−17	1.36E−17	1.77E−17	1.34E−17
8.00E−02	1.53E−17	1.17E−17	1.53E−17	1.17E−17	1.53E−17	1.18E−17	1.53E−17	1.17E−17
1.00E−01	1.37E−17	1.04E−17	1.37E−17	1.04E−17	1.37E−17	1.05E−17	1.37E−17	1.04E−17
1.50E−01	1.12E−17	8.55E−18	1.12E−17	8.55E−18	1.12E−17	8.64E−18	1.12E−17	8.54E−18
2.00E−01	9.72E−18	7. 40E−18	9.72E−18	7.40E−18	9.72E−18	7.48E−18	9.72E−18	7.40E−18
3.00E−01	7.91E−18	6.03E−18	7.91E−18	6.03E−18	7.91E−18	6.09E−18	7.91E−18	6.02E−18
4.00E−01	6.86E−18	5.23E−18	6.86E−18	5.23E−18	6.86E−18	5.29E−18	6.86E−18	5.23E−18
5.00E−01	6.14E−18	4.68E−18	6.14E−18	4.68E−18	6.14E−18	4.73E−18	6.14E−18	4.67E−18
6.00E−01	5.61E−18	4.27E−18	5.61E−18	4.27E−18	5.61E−18	4.32E−18	5.61E−18	4.27E−18
8.00E−01	4.87E−18	3.71E−18	4.87E−18	3.71E−18	4.87E−18	3.75E−18	4.87E−18	3.71E−18
1.00E+00	4.35E−18	3.31E−18	4.35E−18	3.31E−18	4.35E−18	3.35E−18	4.35E−18	3.31E−18
1.50E+00	3.56E−18	2.72E−18	3.56E−18	2.72E−18	3.56E−18	2.75E−18	3.56E−18	2.72E−18
2.00E+00	3.09E−18	2.36E−18	3.09E−18	2.36E−18	3.09E−18	2.38E−18	3.09E−18	2.36E−18
3.00E+00	2.53E−18	1.94E−18	2.53E−18	1.94E−18	2.53E−18	1.96E−18	2.53E−18	1.94E−18
4.00E+00	2.21E−18	1.70E−18	2.21E−18	1.70E−18	2.21E−18	1.71E−18	2.21E−18	1.69E−18
5.00E+00	1.99E−18	1.53E−18	1.99E−18	1.53E−18	1.99E−18	1.55E−18	1.99E−18	1.53E−18
6.00E+00	1.83E−18	1.41E−18	1.83E−18	1.41E−18	1.83E−18	1.42E−18	1.83E−18	1.41E−18
8.00E+00	1.62E−18	1.26E−18	1.62E−18	1.26E−18	1.62E−18	1.27E−18	1.62E−18	1.25E−18
1.00E+01	1.48E−18	1.15E−18	1.48E−18	1.15E−18	1.48E−18	1.16E−18	1.48E−18	1.15E−18
1.50E+01	1.28E−18	1.02E−18	1.28E−18	1.02E−18	1.28E−18	1.02E−18	1.28E−18	1.01E−18
2.00E+01	1.19E−18	9.62E−19	1.19E−18	9.63E−19	1.19E−18	9.60E−19	1.19E−18	9.48E−19
3.00E+01	1.11E−18	9.35E−19	1.11E−18	9.37E−19	1.11E−18	9.27E−19	1.11E−18	9.14E−19
4.00E+01	1.11E−18	9.66E−19	1.11E−18	9.68E−19	1.11E−18	9.52E−19	1.11E−18	9.38E−19
5.00E+01	1.15E−18	1.02E−18	1.15E−18	1.02E−18	1.15E−18	1.00E−18	1.15E−18	9.87E−19
6.00E+01	1.20E−18	1.09E−18	1.20E−18	1.10E−18	1.20E−18	1.07E−18	1.20E−18	1.05E−18
8.00E+01	1.34E−18	1.26E−18	1.34E−18	1.26E−18	1.34E−18	1.22E−18	1.34E−18	1.20E−18
1.00E+02	1.50E−18	1.44E−18	1.50E−18	1.44E−18	1.50E−18	1.39E−18	1.50E−18	1.37E−18
1.50E+02	1.96E−18	1.93E−18	1.96E−18	1.94E−18	1.96E−18	1.86E−18	1.96E−18	1.83E−18
2.00E+02	2.45E−18	2.45E−18	2.45E−18	2.46E−18	2.45E−18	2.35E−18	2.44E−18	2.31E−18
3.00E+02	3.45E−18	3.50E−18	3.46E−18	3.52E−18	3.45E−18	3.36E−18	3.45E−18	3.30E−18
4.00E+02	4.48E−18	4.58E−18	4.48E−18	4.60E−18	4.48E−18	4.38E−18	4.48E−18	4.31E−18
5.00E+02	5.51E−18	5.65E−18	5.52E−18	5.68E−18	5.51E−18	5.41E−18	5.51E−18	5.32E−18
6.00E+02	6.55E−18	6.73E−18	6.55E−18	6.76E−18	6.55E−18	6.43E−18	6.54E−18	6.34E−18
8.00E+02	8.62E−18	8.88E−18	8.63E−18	8.92E−18	8.62E−18	8.48E−18	8.61E−18	8.36E−18

Neutron energy (eV)	Organ ID: 14 Humeri, upper half Source: spongiosa Target tissue		Organ ID: 15 Humeri, upper half Source: medullary cavity Target tissue		Organ ID: 17 Humeri, lower half Source: spongiosa Target tissue		Organ ID: 18 Humeri, lower half Source: medullary cavity Target tissue		Organ ID: 20 Ulnae and radii Source: spongiosa Target tissue		Organ ID: 21 Ulnae and radii Source: medullary cavity Target tissue		Organ ID: 23 Wrist and hands Source: spongiosa Target tissue	
	AM	TM_{50}	AM	TM_{50}	AM	TM_{50}	AM	TM_{50}	AM	TM_{50}	AM	TM_{50}	AM	TM_{50}
1.00E+03	7.89E−18	1.09E−17	NA	1.16E−17	NA	1.17E−17	NA	1.16E−17	NA	1.17E−17	NA	1.16E−17	NA	1.17E−17
1.50E+03	1.15E−17	1.62E−17	NA	1.74E−17	NA	1.73E−17	NA	1.74E−17	NA	1.74E−17	NA	1.74E−17	NA	1.73E−17
2.00E+03	1.50E−17	2.16E−17	NA	2.30E−17	NA	2.29E−17	NA	2.30E−17	NA	2.29E−17	NA	2.30E−17	NA	2.29E−17
3.00E+03	2.18E−17	3.22E−17	NA	3.43E−17	NA	3.38E−17	NA	3.43E−17	NA	3.38E−17	NA	3.43E−17	NA	3.38E−17
4.00E+03	2.81E−17	4.28E−17	NA	4.55E−17	NA	4.44E−17	NA	4.55E−17	NA	4.44E−17	NA	4.55E−17	NA	4.44E−17
5.00E+03	3.43E−17	5.33E−17	NA	5.66E−17	NA	5.49E−17	NA	5.66E−17	NA	5.49E−17	NA	5.66E−17	NA	5.49E−17
6.00E+03	4.04E−17	6.36E−17	NA	6.75E−17	NA	6.54E−17	NA	6.75E−17	NA	6.53E−17	NA	6.75E−17	NA	6.54E−17
8.00E+03	5.24E−17	8.40E−17	NA	8.87E−17	NA	8.63E−17	NA	8.87E−17	NA	8.63E−17	NA	8.87E−17	NA	8.63E−17

(*continued on next page*)

Table E.1. (*continued*)

Neutron energy (eV)	Organ ID: 14 Humeri, upper half Source: spongiosa Target tissue		Organ ID: 15 Humeri, upper half Source: medullary cavity Target tissue		Organ ID: 17 Humeri, lower half Source: spongiosa Target tissue		Organ ID: 18 Humeri, lower half Source: medullary cavity Target tissue		Organ ID: 20 Ulnae and radii Source: spongiosa Target tissue		Organ ID: 21 Ulnae and radii Source: medullary cavity Target tissue		Organ ID: 23 Wrist and hands Source: spongiosa Target tissue	
	AM	TM_{50}	AM	TM_{50}	AM	TM_{50}	AM	TM_{50}	AM	TM_{50}	AM	TM_{50}	AM	TM_{50}
1.00E+04	6.44E−17	1.04E−16	NA	1.09E−16	NA	1.08E−16	NA	1.09E−16	NA	1.07E−16	NA	1.09E−16	NA	1.08E−16
1.50E+04	9.41E−17	1.54E−16	NA	1.59E−16	NA	1.60E−16	NA	1.59E−16	NA	1.60E−16	NA	1.59E−16	NA	1.60E−16
2.00E+04	1.21E−16	2.00E−16	NA	2.07E−16	NA	2.08E−16	NA	2.07E−16	NA	2.08E−16	NA	2.07E−16	NA	2.08E−16
3.00E+04	1.71E−16	2.85E−16	NA	2.95E−16	NA	2.96E−16	NA	2.95E−16	NA	2.96E−16	NA	2.95E−16	NA	2.96E−16
4.00E+04	2.16E−16	3.63E−16	NA	3.74E−16	NA	3.76E−16	NA	3.74E−16	NA	3.76E−16	NA	3.74E−16	NA	3.76E−16
5.00E+04	2.57E−16	4.35E−16	NA	4.45E−16	NA	4.49E−16	NA	4.45E−16	NA	4.49E−16	NA	4.45E−16	NA	4.49E−16
6.00E+04	2.95E−16	5.01E−16	NA	5.12E−16	NA	5.17E−16	NA	5.12E−16	NA	5.17E−16	NA	5.12E−16	NA	5.17E−16
8.00E+04	3.60E−16	6.17E−16	NA	6.36E−16	NA	6.36E−16	NA	6.36E−16	NA	6.37E−16	NA	6.36E−16	NA	6.36E−16
1.00E+05	4.17E−16	7.16E−16	NA	7.41E−16	NA	7.42E−16	NA	7.41E−16	NA	7.42E−16	NA	7.41E−16	NA	7.42E−16
1.50E+05	5.35E−16	9.23E−16	NA	9.60E−16	NA	9.58E−16	NA	9.60E−16	NA	9.58E−16	NA	9.60E−16	NA	9.58E−16
2.00E+05	6.30E−16	1.10E−15	NA	1.14E−15	NA	1.13E−15	NA	1.14E−15	NA	1.13E−15	NA	1.14E−15	NA	1.13E−15
3.00E+05	7.90E−16	1.38E−15	NA	1.42E−15	NA	1.41E−15	NA	1.42E−15	NA	1.41E−15	NA	1.42E−15	NA	1.41E−15
4.00E+05	9.72E−16	1.64E−15	NA	1.67E−15	NA	1.67E−15	NA	1.67E−15	NA	1.67E−15	NA	1.67E−15	NA	1.67E−15
5.00E+05	1.02E−15	1.79E−15	NA	1.83E−15	NA	1.82E−15	NA	1.83E−15	NA	1.83E−15	NA	1.83E−15	NA	1.82E−15
6.00E+05	1.11E−15	1.95E−15	NA	2.00E−15	NA	1.99E−15	NA	2.00E−15	NA	1.99E−15	NA	2.00E−15	NA	1.99E−15
8.00E+05	1.32E−15	2.23E−15	NA	2.31E−15	NA	2.28E−15	NA	2.31E−15	NA	2.28E−15	NA	2.31E−15	NA	2.28E−15
1.00E+06	1.67E−15	2.58E−15	NA	2.63E−15	NA	2.60E−15	NA	2.63E−15	NA	2.60E−15	NA	2.63E−15	NA	2.60E−15
1.50E+06	2.04E−15	2.96E−15	NA	3.09E−15	NA	3.02E−15	NA	3.09E−15	NA	3.01E−15	NA	3.09E−15	NA	3.02E−15
2.00E+06	2.52E−15	3.31E−15	NA	3.52E−15	NA	3.37E−15	NA	3.52E−15	NA	3.36E−15	NA	3.52E−15	NA	3.37E−15
3.00E+06	3.32E−15	3.88E−15	NA	4.30E−15	NA	3.98E−15	NA	4.30E−15	NA	3.95E−15	NA	4.30E−15	NA	3.98E−15
4.00E+06	3.93E−15	4.24E−15	NA	4.87E−15	NA	4.36E−15	NA	4.87E−15	NA	4.30E−15	NA	4.87E−15	NA	4.36E−15
5.00E+06	4.15E−15	4.26E−15	NA	5.00E−15	NA	4.35E−15	NA	5.00E−15	NA	4.28E−15	NA	5.00E−15	NA	4.35E−15
6.00E+06	4.38E−15	4.48E−15	NA	5.30E−15	NA	4.58E−15	NA	5.30E−15	NA	4.49E−15	NA	5.30E−15	NA	4.58E−15
8.00E+06	5.00E−15	5.08E−15	NA	5.96E−15	NA	5.18E−15	NA	5.96E−15	NA	5.07E−15	NA	5.96E−15	NA	5.18E−15
1.00E+07	5.43E−15	5.46E−15	NA	6.33E−15	NA	5.51E−15	NA	6.33E−15	NA	5.41E−15	NA	6.33E−15	NA	5.51E−15
1.50E+07	6.26E−15	6.44E−15	NA	7.30E−15	NA	6.52E−15	NA	7.30E−15	NA	6.40E−15	NA	7.30E−15	NA	6.52E−15
2.00E+07	6.62E−15	7.02E−15	NA	7.80E−15	NA	7.11E−15	NA	7.80E−15	NA	6.97E−15	NA	7.80E−15	NA	7.10E−15
3.00E+07	7.09E−15	7.57E−15	NA	8.29E−15	NA	7.69E−15	NA	8.29E−15	NA	7.55E−15	NA	8.29E−15	NA	7.69E−15
4.00E+07	7.52E−15	7.94E−15	NA	8.63E−15	NA	8.09E−15	NA	8.63E−15	NA	7.95E−15	NA	8.63E−15	NA	8.09E−15
5.00E+07	7.76E−15	8.15E−15	NA	8.78E−15	NA	8.31E−15	NA	8.78E−15	NA	8.15E−15	NA	8.78E−15	NA	8.31E−15
6.00E+07	8.02E−15	8.38E−15	NA	8.95E−15	NA	8.53E−15	NA	8.95E−15	NA	8.35E−15	NA	8.95E−15	NA	8.53E−15
8.00E+07	8.68E−15	9.05E−15	NA	9.62E−15	NA	9.23E−15	NA	9.62E−15	NA	9.01E−15	NA	9.62E−15	NA	9.23E−15
1.00E+08	9.40E−15	9.91E−15	NA	1.03E−14	NA	1.01E−14	NA	1.03E−14	NA	9.85E−15	NA	1.03E−14	NA	1.01E−14
1.50E+08	1.26E−14	1.35E−14	NA	1.40E−14	NA	1.39E−14	NA	1.40E−14	NA	1.35E−14	NA	1.40E−14	NA	1.39E−14

Neutron energy (eV)	Organ ID: 25 Clavicles Source: spongiosa Target tissue		Organ ID: 27 Cranium Source: spongiosa Target tissue		Organ ID: 29 Femora, upper half Source: spongiosa Target tissue		Organ ID: 30 Femora, upper half Source: medullary cavity Target tissue		Organ ID: 32 Femora, lower half Source: spongiosa Target tissue		Organ ID: 33 Femora, lower half Source: medullary cavity Target tissue		Organ ID: 35 Tibiae, fibulae, patellae Source: spongiosa Target tissue	
	AM	TM_{50}	AM	TM_{50}	AM	TM_{50}	AM	TM_{50}	AM	TM_{50}	AM	TM_{50}	AM	TM_{50}
1.00E+03	9.05E−18	1.09E−17	1.05E−17	1.12E−17	8.69E−18	1.14E−17	NA	1.16E−17	NA	1.17E−17	NA	1.16E−17	NA	1.17E−17
1.50E+03	1.32E−17	1.62E−17	1.55E−17	1.66E−17	1.27E−17	1.69E−17	NA	1.74E−17	NA	1.73E−17	NA	1.74E−17	NA	1.74E−17

Table E.1. (*continued*)

2.00E+03	1.73E−17	2.15E−17	2.03E−17	2.20E−17	1.66E−17	2.24E−17	NA	2.30E−17	NA	2.29E−17	NA	2.30E−17	NA	2.30E−17
3.00E+03	2.50E−17	3.18E−17	2.99E−17	3.25E−17	2.40E−17	3.31E−17	NA	3.43E−17	NA	3.37E−17	NA	3.43E−17	NA	3.38E−17
4.00E+03	3.23E−17	4.19E−17	3.91E−17	4.29E−17	3.11E−17	4.36E−17	NA	4.55E−17	NA	4.43E−17	NA	4.55E−17	NA	4.44E−17
5.00E+03	3.94E−17	5.19E−17	4.82E−17	5.31E−17	3.79E−17	5.40E−17	NA	5.66E−17	NA	5.48E−17	NA	5.66E−17	NA	5.48E−17
6.00E+03	4.64E−17	6.18E−17	5.72E−17	6.33E−17	4.46E−17	6.42E−17	NA	6.75E−17	NA	6.52E−17	NA	6.75E−17	NA	6.52E−17
8.00E+03	6.01E−17	8.17E−17	7.50E−17	8.35E−17	5.78E−17	8.46E−17	NA	8.87E−17	NA	8.61E−17	NA	8.87E−17	NA	8.61E−17
1.00E+04	7.37E−17	1.02E−16	9.26E−17	1.04E−16	7.10E−17	1.05E−16	NA	1.09E−16	NA	1.07E−16	NA	1.09E−16	NA	1.07E−16
1.50E+04	1.07E−16	1.51E−16	1.36E−16	1.53E−16	1.03E−16	1.55E−16	NA	1.59E−16	NA	1.59E−16	NA	1.59E−16	NA	1.59E−16
2.00E+04	1.38E−16	1.97E−16	1.76E−16	1.99E−16	1.33E−16	2.01E−16	NA	2.07E−16	NA	2.08E−16	NA	2.07E−16	NA	2.08E−16
3.00E+04	1.94E−16	2.81E−16	2.48E−16	2.84E−16	1.86E−16	2.87E−16	NA	2.95E−16	NA	2.96E−16	NA	2.95E−16	NA	2.96E−16
4.00E+04	2.44E−16	3.58E−16	3.13E−16	3.60E−16	2.34E−16	3.65E−16	NA	3.74E−16	NA	3.76E−16	NA	3.74E−16	NA	3.76E−16
5.00E+04	2.90E−16	4.29E−16	3.72E−16	4.31E−16	2.78E−16	4.37E−16	NA	4.45E−16	NA	4.49E−16	NA	4.45E−16	NA	4.49E−16
6.00E+04	3.32E−16	4.94E−16	4.26E−16	4.95E−16	3.18E−16	5.03E−16	NA	5.12E−16	NA	5.16E−16	NA	5.12E−16	NA	5.16E−16
8.00E+04	4.05E−16	6.09E−16	5.21E−16	6.11E−16	3.88E−16	6.20E−16	NA	6.36E−16	NA	6.36E−16	NA	6.36E−16	NA	6.36E−16
1.00E+05	4.69E−16	7.10E−16	6.03E−16	7.12E−16	4.50E−16	7.23E−16	NA	7.41E−16	NA	7.41E−16	NA	7.41E−16	NA	7.40E−16
1.50E+05	5.99E−16	9.21E−16	7.69E−16	9.19E−16	5.75E−16	9.35E−16	NA	9.60E−16	NA	9.57E−16	NA	9.60E−16	NA	9.56E−16
2.00E+05	7.02E−16	1.09E−15	8.98E−16	1.08E−15	6.75E−16	1.11E−15	NA	1.14E−15	NA	1.13E−15	NA	1.14E−15	NA	1.13E−15
3.00E+05	8.71E−16	1.38E−15	1.10E−15	1.35E−15	8.40E−16	1.39E−15	NA	1.42E−15	NA	1.41E−15	NA	1.42E−15	NA	1.41E−15
4.00E+05	1.06E−15	1.64E−15	1.31E−15	1.60E−15	1.03E−15	1.64E−15	NA	1.67E−15	NA	1.66E−15	NA	1.67E−15	NA	1.66E−15
5.00E+05	1.11E−15	1.78E−15	1.38E−15	1.73E−15	1.08E−15	1.79E−15	NA	1.83E−15	NA	1.82E−15	NA	1.83E−15	NA	1.82E−15
6.00E+05	1.21E−15	1.95E−15	1.49E−15	1.89E−15	1.18E−15	1.95E−15	NA	2.00E−15	NA	1.99E−15	NA	2.00E−15	NA	1.99E−15
8.00E+05	1.42E−15	2.25E−15	1.71E−15	2.17E−15	1.38E−15	2.23E−15	NA	2.31E−15	NA	2.28E−15	NA	2.31E−15	NA	2.28E−15
1.00E+06	1.76E−15	2.58E−15	2.03E−15	2.50E−15	1.71E−15	2.55E−15	NA	2.63E−15	NA	2.59E−15	NA	2.63E−15	NA	2.60E−15
1.50E+06	2.13E−15	2.96E−15	2.35E−15	2.85E−15	2.08E−15	2.93E−15	NA	3.09E−15	NA	3.01E−15	NA	3.09E−15	NA	3.02E−15
2.00E+06	2.60E−15	3.30E−15	2.75E−15	3.17E−15	2.54E−15	3.29E−15	NA	3.52E−15	NA	3.37E−15	NA	3.52E−15	NA	3.37E−15
3.00E+06	3.39E−15	3.83E−15	3.42E−15	3.70E−15	3.30E−15	3.87E−15	NA	4.30E−15	NA	3.98E−15	NA	4.30E−15	NA	3.98E−15
4.00E+06	3.99E−15	4.16E−15	3.92E−15	4.02E−15	3.89E−15	4.26E−15	NA	4.87E−15	NA	4.36E−15	NA	4.87E−15	NA	4.36E−15
5.00E+06	4.23E−15	4.11E−15	4.05E−15	3.96E−15	4.10E−15	4.28E−15	NA	5.00E−15	NA	4.36E−15	NA	5.00E−15	NA	4.36E−15
6.00E+06	4.46E−15	4.25E−15	4.18E−15	4.06E−15	4.31E−15	4.49E−15	NA	5.30E−15	NA	4.58E−15	NA	5.30E−15	NA	4.59E−15
8.00E+06	5.04E−15	4.76E−15	4.61E−15	4.48E−15	4.91E−15	5.06E−15	NA	5.96E−15	NA	5.18E−15	NA	5.96E−15	NA	5.20E−15
1.00E+07	5.45E−15	5.09E−15	4.90E−15	4.72E−15	5.35E−15	5.41E−15	NA	6.33E−15	NA	5.52E−15	NA	6.33E−15	NA	5.56E−15
1.50E+07	6.19E−15	5.98E−15	5.53E−15	5.48E−15	6.16E−15	6.37E−15	NA	7.30E−15	NA	6.53E−15	NA	7.30E−15	NA	6.58E−15
2.00E+07	6.52E−15	6.49E−15	5.94E−15	6.06E−15	6.58E−15	6.93E−15	NA	7.80E−15	NA	7.12E−15	NA	7.80E−15	NA	7.17E−15
3.00E+07	6.91E−15	7.04E−15	6.48E−15	6.70E−15	7.11E−15	7.50E−15	NA	8.29E−15	NA	7.72E−15	NA	8.29E−15	NA	7.75E−15
4.00E+07	7.24E−15	7.43E−15	6.96E−15	7.19E−15	7.54E−15	7.91E−15	NA	8.63E−15	NA	8.11E−15	NA	8.63E−15	NA	8.15E−15
5.00E+07	7.39E−15	7.63E−15	7.26E−15	7.51E−15	7.77E−15	8.15E−15	NA	8.78E−15	NA	8.33E−15	NA	8.78E−15	NA	8.36E−15
6.00E+07	7.59E−15	7.85E−15	7.60E−15	7.86E−15	8.03E−15	8.40E−15	NA	8.95E−15	NA	8.55E−15	NA	8.95E−15	NA	8.57E−15
8.00E+07	8.19E−15	8.45E−15	8.36E−15	8.63E−15	8.72E−15	9.09E−15	NA	9.62E−15	NA	9.24E−15	NA	9.62E−15	NA	9.25E−15
1.00E+08	8.96E−15	9.25E−15	9.36E−15	9.71E−15	9.52E−15	9.98E−15	NA	1.03E−14	NA	1.01E−14	NA	1.03E−14	NA	1.01E−14
1.50E+08	1.20E−14	1.26E−14	1.30E−14	1.37E−14	1.28E−14	1.37E−14	NA	1.40E−14	NA	1.39E−14	NA	1.40E−14	NA	1.39E−14

Neutron energy (eV)	Organ ID: 36 Tibiae and fibulae Source: medullary cavity Target tissue		Organ ID: 38 Ankles and feet Source: spongiosa Target tissue		Organ ID: 40 Mandible Source: spongiosa Target tissue		Organ ID: 42 Pelvis Source: spongiosa Target tissue		Organ ID: 44 Ribs Source: spongiosa Target tissue		Organ ID: 46 Scapulae Source: spongiosa Target tissue		Organ ID: 48 Spine, cervical Source: spongiosa Target tissue	
	AM	TM_{50}	AM	TM_{50}	AM	TM_{50}	AM	TM_{50}	AM	TM_{50}	AM	TM_{50}	AM	TM_{50}
1.00E+03	NA	1.16E−17	NA	1.17E−17	9.72E−18	1.08E−17	1.04E−17	1.06E−17	1. 07E−17	1.10E−17	1.01E−17	1.07E−17	1.07E−17	1.10E−17
1.50E+03	NA	1.74E−17	NA	1.73E−17	1.43E−17	1.61E−17	1.53E−17	1.57E−17	1. 58E−17	1.63E−17	1.48E−17	1.58E−17	1.58E−17	1.63E−17
2.00E+03	NA	2.30E−17	NA	2.29E−17	1.88E−17	2.13E−17	2.02E−17	2.08E−17	2. 09E−17	2.16E−17	1.95E−17	2.10E−17	2.09E−17	2.16E−17
3.00E+03	NA	3.43E−17	NA	3.37E−17	2.74E−17	3.16E−17	2.96E−17	3.08E−17	3. 08E−17	3.19E−17	2.85E−17	3.11E−17	3.09E−17	3.19E−17

(*continued on next page*)

Table E.1. (*continued*)

Neutron energy (eV)	Organ ID: 36 Tibiae and fibulae Source: medullary cavity Target tissue		Organ ID: 38 Ankles and feet Source: spongiosa Target tissue		Organ ID: 40 Mandible Source: spongiosa Target tissue		Organ ID: 42 Pelvis Source: spongiosa Target tissue		Organ ID: 44 Ribs Source: spongiosa Target tissue		Organ ID: 46 Scapulae Source: spongiosa Target tissue		Organ ID: 48 Spine, cervical Source: spongiosa Target tissue	
	AM	TM_{50}	AM	TM_{50}	AM	TM_{50}	AM	TM_{50}	AM	TM_{50}	AM	TM_{50}	AM	TM_{50}
4.00E+03	NA	4.55E−17	NA	4.43E−17	3.57E−17	4.17E−17	3.88E−17	4.06E−17	4. 06E−17	4.21E−17	3.73E−17	4.11E−17	4.07E−17	4.21E−17
5.00E+03	NA	5.66E−17	NA	5.48E−17	4.38E−17	5.18E−17	4.79E−17	5.03E−17	5. 03E−17	5.21E−17	4.58E−17	5.10E−17	5.03E−17	5.21E−17
6.00E+03	NA	6.75E−17	NA	6.52E−17	5.18E−17	6.17E−17	5.69E−17	5.99E−17	5. 98E−17	6.21E−17	5.43E−17	6.08E−17	5.99E−17	6.21E−17
8.00E+03	NA	8.87E−17	NA	8.61E−17	6.78E−17	8.16E−17	7.46E−17	7.93E−17	7. 88E−17	8.19E−17	7.10E−17	8.05E−17	7.90E−17	8.19E−17
1.00E+04	NA	1.09E−16	NA	1.07E−16	8.36E−17	1.01E−16	9.23E−17	9.87E−17	9. 78E−17	1.02E−16	8.76E−17	1.00E−16	9.81E−17	1.02E−16
1.50E+04	NA	1.59E−16	NA	1.59E−16	1.23E−16	1.51E−16	1.36E−16	1.47E−16	1. 45E−16	1.51E−16	1.29E−16	1.49E−16	1.45E−16	1.50E−16
2.00E+04	NA	2.07E−16	NA	2.08E−16	1.58E−16	1.96E−16	1.76E−16	1.91E−16	1. 88E−16	1.96E−16	1.66E−16	1.94E−16	1.88E−16	1.95E−16
3.00E+04	NA	2.95E−16	NA	2.96E−16	2.24E−16	2.80E−16	2.49E−16	2.73E−16	2. 67E−16	2.79E−16	2.34E−16	2.77E−16	2.68E−16	2.78E−16
4.00E+04	NA	3.74E−16	NA	3.76E−16	2.82E−16	3.56E−16	3.15E−16	3.47E−16	3. 39E−16	3.54E−16	2.96E−16	3.52E−16	3.40E−16	3.53E−16
5.00E+04	NA	4.45E−16	NA	4.49E−16	3.36E−16	4.26E−16	3.76E−16	4.14E−16	4. 05E−16	4.23E−16	3.52E−16	4.20E−16	4.06E−16	4.22E−16
6.00E+04	NA	5.12E−16	NA	5.16E−16	3.84E−16	4.90E−16	4.31E−16	4.77E−16	4. 65E−16	4.87E−16	4.03E−16	4.84E−16	4.67E−16	4.85E−16
8.00E+04	NA	6.36E−16	NA	6.36E−16	4.71E−16	6.05E−16	5.29E−16	5.89E−16	5. 73E−16	5.99E−16	4.94E−16	5.97E−16	5.75E−16	5.98E−16
1.00E+05	NA	7.41E−16	NA	7.41E−16	5.46E−16	7.05E−16	6.15E−16	6.88E−16	6. 67E−16	6.98E−16	5.73E−16	6.97E−16	6.69E−16	6.97E−16
1.50E+05	NA	9.60E−16	NA	9.57E−16	6.98E−16	9.14E−16	7.89E−16	8.93E−16	8. 61E−16	9.01E−16	7.32E−16	9.05E−16	8.64E−16	9.02E−16
2.00E+05	NA	1.14E−15	NA	1.13E−15	8.19E−16	1.08E−15	9.27E−16	1.06E−15	1. 02E−15	1.07E−15	8.58E−16	1.07E−15	1.02E−15	1.07E−15
3.00E+05	NA	1.42E−15	NA	1.41E−15	1.01E−15	1.36E−15	1.15E−15	1.32E−15	1. 27E−15	1.33E−15	1.06E−15	1.34E−15	1.27E−15	1.33E−15
4.00E+05	NA	1.67E−15	NA	1.66E−15	1.22E−15	1.62E−15	1.37E−15	1.58E−15	1. 52E−15	1.59E−15	1.27E−15	1.60E−15	1.52E−15	1.59E−15
5.00E+05	NA	1.83E−15	NA	1.82E−15	1.29E−15	1.76E−15	1.45E−15	1.72E−15	1. 62E−15	1.71E−15	1.34E−15	1.74E−15	1.62E−15	1.71E−15
6.00E+05	NA	2.00E−15	NA	1.99E−15	1.40E−15	1.92E−15	1.57E−15	1.88E−15	1. 76E−15	1.86E−15	1.45E−15	1.90E−15	1.77E−15	1.86E−15
8.00E+05	NA	2.31E−15	NA	2.28E−15	1.62E−15	2.21E−15	1.81E−15	2.17E−15	2. 02E−15	2.14E−15	1.67E−15	2.18E−15	2.02E−15	2.13E−15
1.00E+06	NA	2.63E−15	NA	2.59E−15	1.96E−15	2.55E−15	2.14E−15	2.51E−15	2. 37E−15	2.48E−15	2.00E−15	2.53E−15	2.38E−15	2.48E−15
1.50E+06	NA	3.09E−15	NA	3.01E−15	2.31E−15	2.94E−15	2.47E−15	2.90E−15	2. 69E−15	2.81E−15	2.34E−15	2.92E−15	2.70E−15	2.80E−15
2.00E+06	NA	3.52E−15	NA	3.37E−15	2.74E−15	3.29E−15	2.88E−15	3.26E−15	3. 08E−15	3.14E−15	2.76E−15	3.28E−15	3.07E−15	3.13E−15
3.00E+06	NA	4.30E−15	NA	3.98E−15	3.49E−15	3.85E−15	3.60E−15	3.84E−15	3. 75E−15	3.66E−15	3.48E−15	3.86E−15	3.73E−15	3.66E−15
4.00E+06	NA	4.87E−15	NA	4.36E−15	4.06E−15	4.23E−15	4.16E−15	4.23E−15	4. 28E−15	4.03E−15	4.04E−15	4.26E−15	4.24E−15	4.04E−15
5.00E+06	NA	5.00E−15	NA	4.36E−15	4.28E−15	4.25E−15	4.36E−15	4.29E−15	4. 44E−15	4.08E−15	4.23E−15	4.28E−15	4.39E−15	4.09E−15
6.00E+06	NA	5.30E−15	NA	4.58E−15	4.49E−15	4.44E−15	4.56E−15	4.49E−15	4. 61E−15	4.25E−15	4.44E−15	4.46E−15	4.55E−15	4.25E−15
8.00E+06	NA	5.96E−15	NA	5.18E−15	5.09E−15	5.01E−15	5.15E−15	5.09E−15	5. 14E−15	4.82E−15	5.02E−15	5.01E−15	5.05E−15	4.80E−15
1.00E+07	NA	6.33E−15	NA	5.52E−15	5.49E−15	5.39E−15	5.56E−15	5.47E−15	5. 50E−15	5.22E−15	5.41E−15	5.38E−15	5.39E−15	5.19E−15
1.50E+07	NA	7.30E−15	NA	6.53E−15	6.31E−15	6.34E−15	6.37E−15	6.41E−15	6. 24E−15	6.12E−15	6.19E−15	6.26E−15	6.11E−15	6.06E−15
2.00E+07	NA	7.80E−15	NA	7.12E−15	6.70E−15	6.86E−15	6.77E−15	6.93E−15	6. 62E−15	6.62E−15	6.57E−15	6.77E−15	6.51E−15	6.57E−15
3.00E+07	NA	8.29E−15	NA	7.72E−15	7.15E−15	7.40E−15	7.23E−15	7.46E−15	7. 07E−15	7.15E−15	7.03E−15	7.32E−15	6.98E−15	7.11E−15
4.00E+07	NA	8.63E−15	NA	8.11E−15	7.54E−15	7.80E−15	7.63E−15	7.86E−15	7. 46E−15	7.56E−15	7.43E−15	7.72E−15	7.40E−15	7.53E−15
5.00E+07	NA	8.78E−15	NA	8.33E−15	7.73E−15	8.01E−15	7.84E−15	8.08E−15	7. 67E−15	7.78E−15	7.63E−15	7.94E−15	7.63E−15	7.77E−15
6.00E+07	NA	8.95E−15	NA	8.55E−15	7.96E−15	8.23E−15	8.09E−15	8.33E−15	7. 93E−15	8.04E−15	7.89E−15	8.18E−15	7.91E−15	8.05E−15
8.00E+07	NA	9.62E−15	NA	9.24E−15	8.60E−15	8.89E−15	8.75E−15	8.99E−15	8. 56E−15	8.69E−15	8.56E−15	8.85E−15	8.58E−15	8.72E−15
1.00E+08	NA	1.03E−14	NA	1.01E−14	9.36E−15	9.72E−15	9.55E−15	9.83E−15	9. 38E−15	9.55E−15	9.36E−15	9.73E−15	9.44E−15	9.63E−15
1.50E+08	NA	1.40E−14	NA	1.39E−14	1.25E−14	1.32E−14	1.28E−14	1.34E−14	1. 26E−14	1.30E−14	1.26E−14	1.33E−14	1.28E−14	1.31E−14

Table E.1. (*continued*)

Neutron energy (eV)	Organ ID: 50 Spine, thoracic Source: spongiosa Target tissue		Organ ID: 52 Spine, lumbar Source: spongiosa Target tissue		Organ ID: 54 Sacrum Source: spongiosa Target tissue		Organ ID: 56 Sternum Source: spongiosa Target tissue	
	AM	TM_{50}	AM	TM_{50}	AM	TM_{50}	AM	TM_{50}
1.00E+03	1.07E−17	1.10E−17	1.07E−17	1.11E−17	1.07E−17	1.05E−17	1.07E−17	1.04E−17
1.50E+03	1.58E−17	1.63E−17	1.58E−17	1.64E−17	1.58E−17	1.56E−17	1.58E−17	1.54E−17
2.00E+03	2.09E−17	2.16E−17	2.09E−17	2.16E−17	2.09E−17	2.05E−17	2.08E−17	2.04E−17
3.00E+03	3.08E−17	3.20E−17	3.08E−17	3.19E−17	3.08E−17	3.03E−17	3.08E−17	3.02E−17
4.00E+03	4.06E−17	4.21E−17	4.06E−17	4.20E−17	4.06E−17	3.98E−17	4.05E−17	3.98E−17
5.00E+03	5.02E−17	5.22E−17	5.03E−17	5.19E−17	5.02E−17	4.93E−17	5.01E−17	4.94E−17
6.00E+03	5.98E−17	6.22E−17	5.99E−17	6.18E−17	5.98E−17	5.87E−17	5.96E−17	5.89E−17
8.00E+03	7.88E−17	8.19E−17	7.89E−17	8.16E−17	7.88E−17	7.75E−17	7.86E−17	7.77E−17
1.00E+04	9.77E−17	1.02E−16	9.79E−17	1.01E−16	9.78E−17	9.66E−17	9.75E−17	9.66E−17
1.50E+04	1.45E−16	1.50E−16	1.45E−16	1.50E−16	1.45E−16	1.44E−16	1.44E−16	1.43E−16
2.00E+04	1.88E−16	1.95E−16	1.88E−16	1.96E−16	1.88E−16	1.87E−16	1.87E−16	1.86E−16
3.00E+04	2.67E−16	2.77E−16	2.67E−16	2.78E−16	2.67E−16	2.68E−16	2.66E−16	2.65E−16
4.00E+04	3.39E−16	3.52E−16	3.39E−16	3.53E−16	3.39E−16	3.40E−16	3.38E−16	3.37E−16
5.00E+04	4.04E−16	4.20E−16	4.05E−16	4.21E−16	4.05E−16	4.06E−16	4.03E−16	4.03E−16
6.00E+04	4.65E−16	4.84E−16	4.66E−16	4.83E−16	4.65E−16	4.68E−16	4.63E−16	4.64E−16
8.00E+04	5.72E−16	5.97E−16	5.74E−16	5.96E−16	5.73E−16	5.78E−16	5.70E−16	5.73E−16
1.00E+05	6.67E−16	6.96E−16	6.68E−16	6.96E−16	6.68E−16	6.75E−16	6.64E−16	6.69E−16
1.50E+05	8.61E−16	9.02E−16	8.63E−16	9.03E−16	8.62E−16	8.79E−16	8.57E−16	8.69E−16
2.00E+05	1.02E−15	1.07E−15	1.02E−15	1.07E−15	1.02E−15	1.04E−15	1.01E−15	1.03E−15
3.00E+05	1.27E−15	1.33E−15	1.27E−15	1.33E−15	1.27E−15	1.31E−15	1.26E−15	1.29E−15
4.00E+05	1.52E−15	1.59E−15	1.52E−15	1.59E−15	1.52E−15	1.57E−15	1.51E−15	1.55E−15
5.00E+05	1.62E−15	1.71E−15	1.62E−15	1.70E−15	1.62E−15	1.69E−15	1.61E−15	1.68E−15
6.00E+05	1.76E−15	1.86E−15	1.76E−15	1.85E−15	1.76E−15	1.85E−15	1.75E−15	1.83E−15
8.00E+05	2.02E−15	2.14E−15	2.02E−15	2.12E−15	2.02E−15	2.13E−15	2.01E−15	2.11E−15
1.00E+06	2.38E−15	2.48E−15	2.38E−15	2.47E−15	2.38E−15	2.47E−15	2.36E−15	2.48E−15
1.50E+06	2.70E−15	2.82E−15	2.70E−15	2.80E−15	2.70E−15	2.82E−15	2.69E−15	2.85E−15
2.00E+06	3.09E−15	3.15E−15	3.08E−15	3.11E−15	3.09E−15	3.18E−15	3.08E−15	3.22E−15
3.00E+06	3.77E−15	3.69E−15	3.74E−15	3.62E−15	3.77E−15	3.76E−15	3.77E−15	3.79E−15
4.00E+06	4.31E−15	4.09E−15	4.25E−15	3.99E−15	4.31E−15	4.15E−15	4.32E−15	4.20E−15
5.00E+06	4.49E−15	4.17E−15	4.40E−15	4.03E−15	4.49E−15	4.23E−15	4.51E−15	4.30E−15
6.00E+06	4.68E−15	4.35E−15	4.57E−15	4.19E−15	4.67E−15	4.39E−15	4.71E−15	4.49E−15
8.00E+06	5.24E−15	4.96E−15	5.08E−15	4.75E−15	5.22E−15	4.94E−15	5.28E−15	5.09E−15
1.00E+07	5.63E−15	5.38E−15	5.43E−15	5.15E−15	5.60E−15	5.32E−15	5.68E−15	5.49E−15
1.50E+07	6.40E−15	6.30E−15	6.17E−15	6.03E−15	6.35E−15	6.29E−15	6.47E−15	6.40E−15
2.00E+07	6.79E−15	6.81E−15	6.55E−15	6.51E−15	6.74E−15	6.80E−15	6.87E−15	6.89E−15
3.00E+07	7.25E−15	7.35E−15	6.99E−15	7.03E−15	7.21E−15	7.31E−15	7.33E−15	7.42E−15
4.00E+07	7.64E−15	7.76E−15	7.37E−15	7.41E−15	7.60E−15	7.72E−15	7.72E−15	7.82E−15
5.00E+07	7.85E−15	7.98E−15	7.57E−15	7.61E−15	7.82E−15	7.95E−15	7.93E−15	8.04E−15
6.00E+07	8.11E−15	8.24E−15	7.82E−15	7.85E−15	8.09E−15	8.22E−15	8.20E−15	8.30E−15
8.00E+07	8.76E−15	8.89E−15	8.44E−15	8.48E−15	8.75E−15	8.88E−15	8.85E−15	8.96E−15
1.00E+08	9.58E−15	9.75E−15	9.24E−15	9.30E−15	9.59E−15	9.77E−15	9.67E−15	9.82E−15
1.50E+08	1.29E−14	1.32E−14	1.24E−14	1.26E−14	1.29E−14	1.33E−14	1.30E−14	1.33E−14

NA, not applicable.

ANNEX F. SPECIAL CONSIDERATIONS FOR ASSESSING ABSORBED DOSE IN THE LENS OF THE EYE

(F1) ICRP *Publication 103* (ICRP, 2007) states that recent studies have suggested that the lens of the eye may be more radiosensitive than previously considered. A detailed reappraisal of the radiosensitivity of the lens of the eye (ICRP, 2012) has led to the assumption that the 2007 Recommendations (ICRP, 2007) may underestimate risk. New data from animal models and exposed human populations suggest that lens opacities occur at doses far lower than those generally assumed to be cataractogenic. These observations are thus consistent with either (1) the presence of a small absorbed dose threshold, or (2) the lack of a dose threshold altogether. The threshold dose for radiation-induced cataracts is now considered to be around 0.5 Gy for both acute and fractionated exposures, in line with various recent epidemiological studies. Consequently, a reduction of the occupational annual equivalent dose limit for the lens of the eye from 150 mSv to 20 mSv, averaged over defined periods of 5 years, with no dose in a single year exceeding 50 mSv, has been recommended (ICRP, 2012).

(F2) The annual dose limit for the lens of the eye is given in terms of the equivalent dose, H_T, and by definition this value is based on the mean absorbed dose, $D_{T,R}$, averaged over the volume of the lens. Although ICRP Committee 1 will continue to evaluate the location of the stem cells associated with cataract induction, the dosimetric assessments of this annex support the continued use of the mean absorbed dose for the lens of the eye.

(F3) However, it is well known that there are strong differences in sensitivity to ionising radiation exposure with respect to cataract induction among the tissues of the lens of the eye (Charles and Brown, 1975). Even as early as 1955, ICRP stated in its first general recommendations (ICRP, 1955): 'When the spatial distribution of radiation in the organ is very non-uniform, an average of the physical dose is not necessarily indicative of the potential damage to the organ in its relation to the normal physiological functions of the body as a whole. Therefore, in such cases it is necessary to consider a local volume within the organ in which the dose is highest. This may be called the significant volume... For the lens of the eye the significant volume is that in which the cell nuclei are located.' This motivated several groups to look deeper into the issue of the dose to a sensitive cell population within the lens, especially for radiations with low penetrability that have steep dose gradients inside the lens of the eye, such as electrons (Behrens et al., 2009, 2010; Behrens and Dietze, 2010, 2011a; Nogueira et al., 2011) and low-energy photons (Behrens and Dietze, 2011b). Recently, the issue of lens dosimetry for neutrons has been under investigation (Manger et al., 2011).

(F4) Since the reference computational phantoms – with voxel sizes of $2.137 \times 2.137 \times 8\ \mathrm{mm}^3$ (male) and $1.775 \times 1.775 \times 4.84\ \mathrm{mm}^3$ (female), respectively – represent the lens of the eye at a relatively low level of resolution, the Task Group decided to adopt stylised models of the eye and lens for electrons, photons, and neutrons for estimating the dose conversion coefficients for irradiations resulting in a steep dose gradient (see next paragraph). The eye model of Behrens et al. (2009),

based upon recommended data given in Charles and Brown (1975), was adopted for photon, electron, and neutron radiations. For electron irradiation, the bare eye model was assumed to be exposed (Fig. F.1); for photon and neutron irradiation calculations (Behrens and Dietze, 2011b; Manger et al., 2011), the eye model was incorporated into the head of a mathematical model averaged from Adam and Eva (Kramer et al., 1982) (Fig. F.2) and the UF-ORNL mathematical phantom (Han et al., 2006), respectively.

(F5) Dose conversion coefficients for the more refined lens geometries of the stylised phantom were calculated for the following irradiation conditions: photons from 5 keV to 10 MeV in antero-posterior (AP), postero-anterior (PA), lateral (LAT), and rotational (ROT) geometries; electrons from 100 keV to 12 MeV in AP geometry, and neutrons from 0.001 eV to 10 MeV in AP, LAT, and ROT geometries.

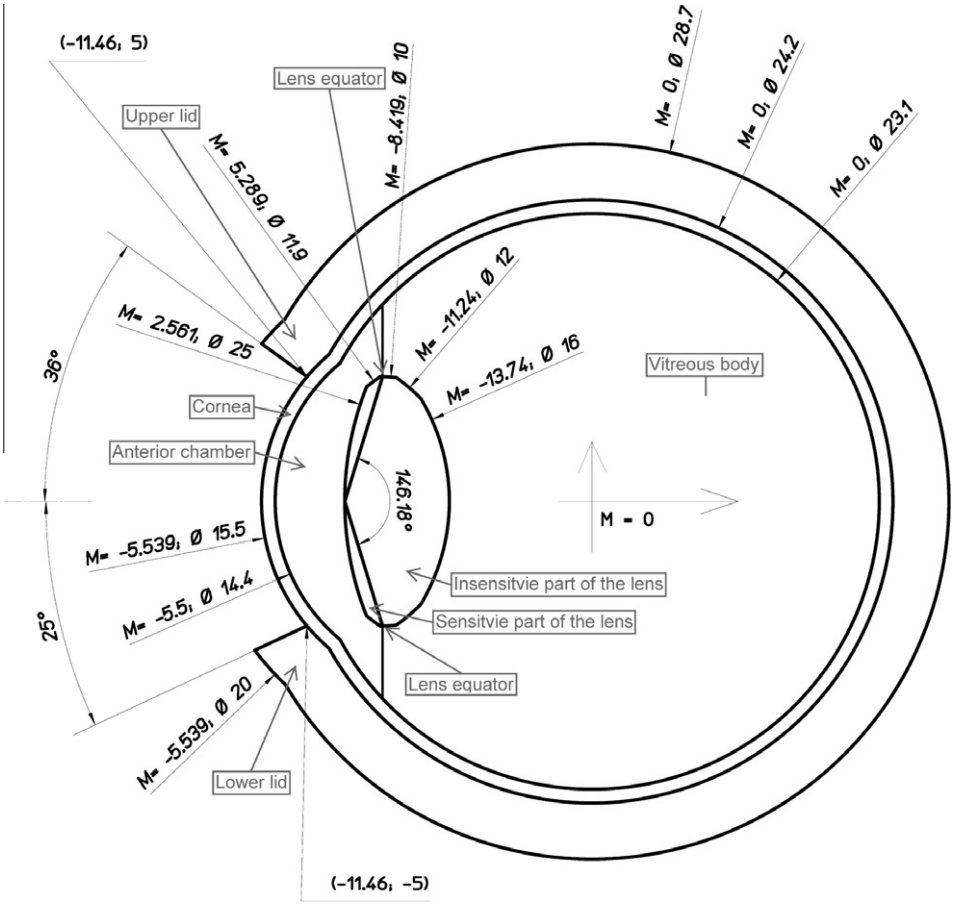

Fig. F.1. The detailed stylised eye model adapted by Behrens et al. (2009), as simulated in the Monte Carlo calculations. All dimensions are given in mm. *M* denotes the *x*-position of the centres of the spheres and Ø denotes the corresponding diameters.

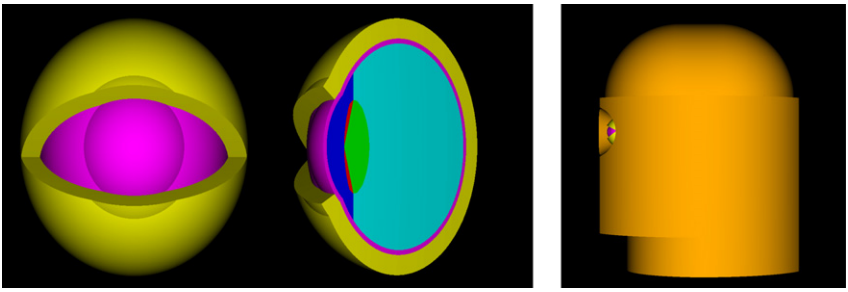

Fig. F.2. Three-dimensional views of the eye as simulated in the Monte Carlo calculations (left). Side view of the eye model implemented in a stylised head phantom (right) (Behrens and Dietze, 2011b).

(F6) Reference data sets for the lens of the eye were defined as follows: (1) for photons of energies from 10 keV to 2 MeV and for AP, LAT, and ROT geometries; (2) for electrons of energies from 100 keV to 10 MeV and for AP geometry; and (3) for neutrons of energies from 0.001 eV to 4 MeV and for AP, LAT, and ROT geometries. The dose conversion coefficients for the lens of the eye were evaluated from the calculations using the stylised eye model phantoms shown in Figs. F.1 and F.2. For all other energies and irradiation geometries, as well as other irradiation types (i.e. positrons, protons, muons, pions, helium ions), the reference conversion coefficients were evaluated as the average of the conversion coefficients of the lens of the eye within the male and female reference computational phantoms. The reference data were evaluated as the average of both eyes with the exception of the electron data, for which the simulations were performed for a single bare eye. The conversion coefficients for the LAT geometry are the arithmetic means of the conversion coefficients for left and right LAT geometries.

F.1. Photons

(F7) Behrens and Dietze (2011b) simulated irradiation of the eye in a stylised head phantom [average size of the head of the stylised Adam and Eva phantoms (Kramer et al., 1982)] by broad parallel beams of mono-energetic photons incident in AP, PA, LAT, and ROT geometries. Fig. F.2 shows the detailed stylised model. The calculations were performed with the Monte Carlo code EGSnrc. In addition to the mean absorbed dose in the lens of the eye, mean absorbed doses in a sensitive region of the lens were also considered in this study. The data of Behrens and Dietze are shown in Fig. F.3 together with the lens dose as calculated with the reference computational phantoms for AP, LAT, and ROT geometries. All conversion coefficients were evaluated as the arithmetic mean values of the coefficients for the left and right eye.

(F8) It can be seen from Fig. F.3 that, with the exception of photon energies below approximately 20 keV for AP geometry and 50 keV for the other geometries, there is good agreement between the lens doses evaluated by Behrens and Dietze using the stylised model and those calculated with the reference computational phantoms up to approximately 2 MeV. Above 2 MeV, the data for the stylised model have a

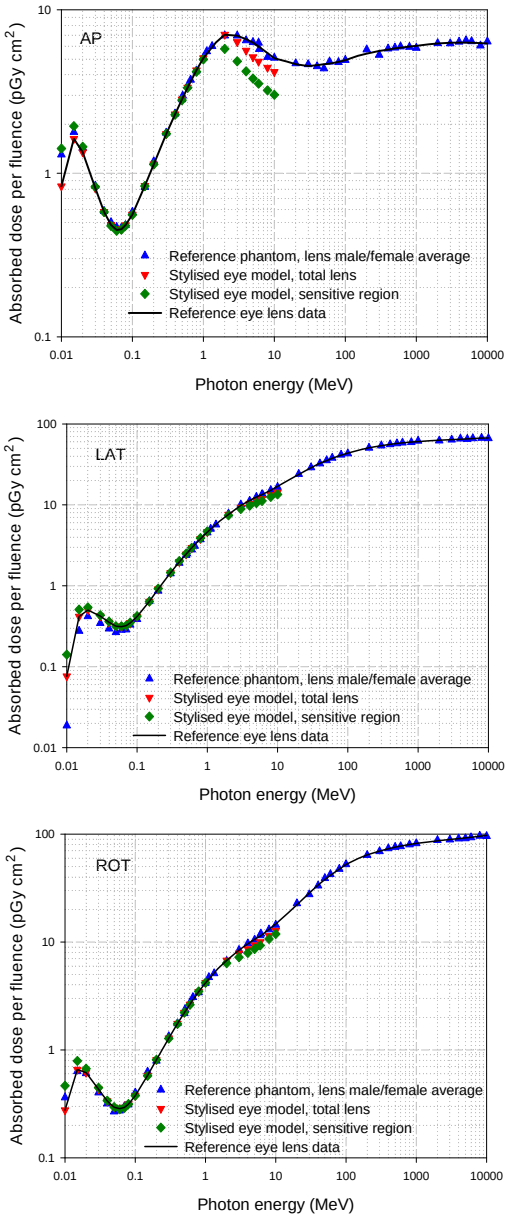

Fig. F.3. Absorbed doses for the lens of the eye per fluence (pGy cm^2) for antero-posterior (AP), lateral (LAT), and rotational (ROT) irradiation as calculated with the male and female reference computational phantoms and with the stylised eye model (Behrens and Dietze, 2011b). The data for the sensitive region are also shown. All conversion coefficients are mean values of both eyes. The solid curve shows the reference data.

tendency to be lower than those for the reference computational phantoms. It can be further seen from Fig. F.3 that the absorbed doses in the sensitive region of the lens are reasonably represented by the reference values for photon energies up to 1 MeV.

(F9) In order to follow a conservative approach, the data from the stylised model were used for the reference conversion coefficients for AP, PA, LAT, and ROT geometries for energies up to 2 MeV. For all other situations, the reference lens conversion coefficients were evaluated as the average of the lens dose conversion coefficients of the male and female reference computational phantoms. The reference conversion coefficients for the absorbed doses for the lens of the eye were smoothed and are shown in Table F.1.

F.2. Electrons

(F10) Fig. F.4 shows the lens dose conversion coefficients as calculated by Behrens et al. (2009, 2010) with the stylised eye model, together with the lens dose conversion coefficients as calculated with the reference computational phantoms for AP geometry. It can be seen that, below 1 MeV, the lens doses for the detailed stylised eye model are significantly lower than those for the lower resolution lens representation of the reference computational phantoms. This is because there is one lens voxel in each eye of the male reference phantom that is in direct contact with the vacuum, which is not equivalent to the real geometry. However, there is good agreement between these values for energies between 1 and 10 MeV.

(F11) Among the irradiation geometries considered for this report, the only significant lens doses for electron energies below 1 MeV are caused by electrons incident in

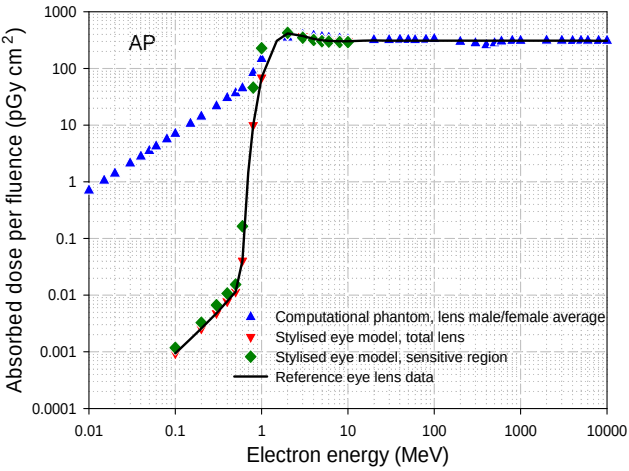

Fig. F.4. Absorbed dose for the lens of the eye per electron fluence (pGy cm^2) for antero-posterior (AP) irradiation, as calculated with the male and female reference computational phantoms and the stylised eye model (Behrens et al., 2010). The data for the sensitive region are also shown. All conversion coefficients are mean values of both eyes. The solid curve shows the reference data.

AP geometry. Therefore, the data for AP geometry can be considered as a conservative estimate of the doses for the other geometries below 1 MeV electron energy. For ISO irradiation and energies above 1 MeV, and for PA irradiation and all energies, no significant differences between the reference computational phantoms and the detailed eye model are expected.

(F12) As a consequence of the abovementioned considerations, the reference conversion coefficients presented in this report for AP irradiation have been taken from the calculations of the stylised model (Behrens et al., 2010) for energies from 100 keV to 10 MeV. For ISO geometry and electrons with energies lower than 1 MeV, the same conversion coefficients as for AP geometry were used. For all other situations, the reference data were evaluated as average values obtained from the reference computational phantoms. The reference conversion coefficients for the absorbed doses for the lens of the eye have been smoothed and are given in Table F.2.

F.3. Neutrons

(F13) Manger et al. (2011) simulated irradiation of the eye model of Behrens and Dietze (2011b), implemented in the head of the adult UF-ORNL phantom (Han et al., 2006), for broad parallel beams of mono-energetic neutrons incident in AP, LAT, and ROT geometries. The calculations were performed with the Monte Carlo code MCNPX Version 2.6.0 (Pelowitz, 2008) for energies from 0.001 eV to 10 MeV. In addition to the mean absorbed dose in the lens of the eye, absorbed doses in a sensitive region of the lens were also considered in this study. The simulated eye geometry is shown in Figs. F.1 and F.2. The doses per fluence for the total lens and the sensitive region are shown in Fig. F.5 for AP, LAT, and ROT geometries. Manger et al. concluded that the dose to the sensitive region was similar to that of the total lens over all neutron energies and exposure geometries, with the greatest difference being 13% at the lowest incoming neutron energy. Regardless of orientation, no significant difference was found in the absorbed dose in the sensitive region of the lens and the total lens. This was expected because there is no significant difference in fluence between the sensitive region and the total lens.

(F14) Fig. F.5 also displays the lens dose conversion coefficients, as calculated using the reference phantoms. It is shown that up to approximately 20 MeV, there is very good agreement between the lens absorbed doses evaluated using the stylised model and those calculated with the reference computational phantoms. It can be further seen that the absorbed doses in the sensitive region of the lens are reasonably represented by the reference values for most neutron energies. Due to the good agreement for AP and ROT neutron incidence, it was concluded that for all other irradiation geometries, the conversion coefficients calculated using the reference computational phantoms can be assumed to reasonably represent the conversion coefficients that would be obtained for a more detailed model of the whole lens and the sensitive region.

(F15) Therefore, the reference conversion coefficients presented in this report have been taken from Manger et al. (2011) for AP, LAT, and ROT neutron incidence and energies up to 4 MeV. All other reference lens conversion coefficients have been

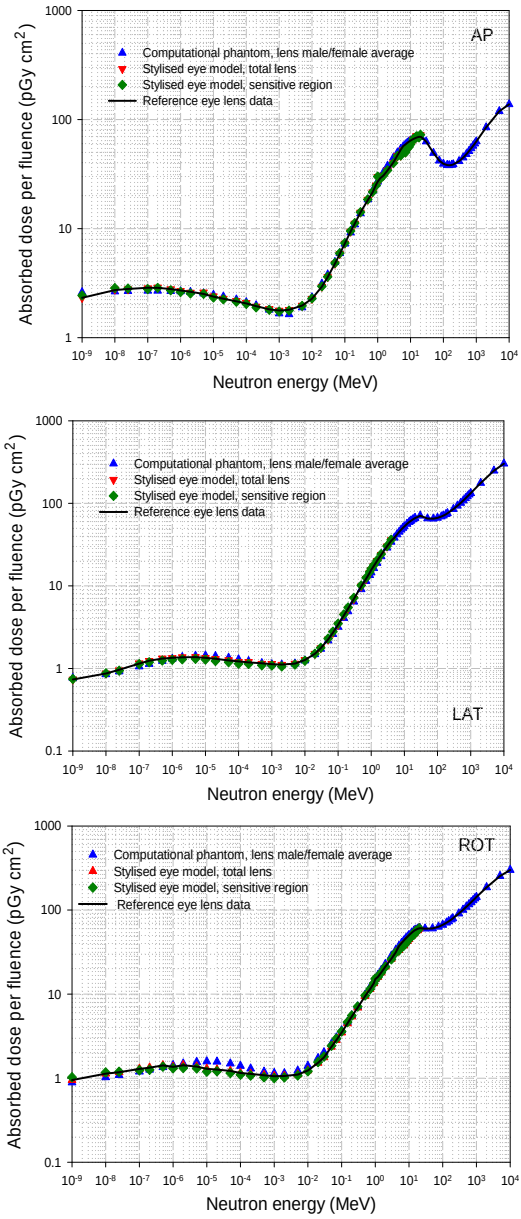

Fig. F.5. Absorbed doses for the lens of the eye per neutron fluence (pGy cm^2) for antero-posterior (AP), lateral (LAT), and rotational (ROT) geometries, as calculated with the male and female reference computational phantoms and the stylised eye model (Manger et al., 2011). The data for the sensitive region are also shown. All conversion coefficients are mean values of both eyes. The solid curve shows the reference data.

evaluated as the average male and female values calculated with the reference computational phantoms. The reference conversion coefficients for the absorbed doses for the lens of the eye have been smoothed and are given in Table F.3.

F.4. References

Behrens, R., Dietze, G., 2010. Monitoring the eye lens: which dose quantity is adequate? Phys. Med. Biol. 55, 4047–4062.

Behrens, R., Dietze, G., 2011a. Corrigendum. Monitoring the eye lens: which dose quantity is adequate? Phys. Med. Biol. 56, 511.

Behrens, R., Dietze, G., 2011b. Dose conversion coefficients for photon exposure of the human eye lens. Phys. Med. Biol. 56, 415–437.

Behrens, R., Dietze, G., Zankl, M., 2009. Dose conversion coefficients for electron exposure of the human eye lens. Phys. Med. Biol. 54, 4069–4087.

Behrens, R., Dietze, G., Zankl, M., 2010. Corrigendum. Dose conversion coefficients for electron exposure of the human eye lens. Phys. Med. Biol. 55, 3937–3945.

Charles, M.W., Brown, N., 1975. Dimensions of the human eye relevant to radiation protection (dosimetry). Phys. Med. Biol. 20, 202–218.

Han, E.Y., Bolch, W.E., Eckerman, K.F., 2006. Revisions to the ORNL series of adult and pediatric computational phantoms for use with the MIRD schema. Health Phys. 90, 337–356.

ICRP, 1955. Recommendations of the International Commission on Radiological Protection. Br. J. Radiol. 28 (Suppl. 6), 1–92.

ICRP, 2007. The 2007 Recommendations of the International Commission on Radiological Protection. ICRP Publication 103. Ann. ICRP 37(2–4).

ICRP, 2012. ICRP statement on tissue reactions and early and late effects of radiation in normal tissues and organs: threshold doses for tissue reactions in a radiation protection context. ICRP Publication 118. Ann. ICRP 41(1–3).

Kramer, R., Zankl, M., Williams, G., et al., 1982. The Calculation of Dose from External Photon Exposures Using Reference Human Phantoms and Monte Carlo Methods. Part I: the Male (Adam) and Female (Eva) Adult Mathematical Phantoms. GSF Report S-885. GSF – National Research Centre for Environment and Health, Neuherberg.

Manger, R.P., Bellamy, M.B., Eckerman, K.F., 2011. Dose conversion coefficients for neutron exposure to the lens of the human eye. Radiat. Prot. Dosim. doi:10.1093/rpd/ncr202.

Nogueira, P., Zankl, M., Schlattl, H., et al., 2011. Dose conversion coefficients for monoenergetic electrons incident on a realistic human eye model with different lens cell populations. Phys. Med. Biol. 56(21), 6919–6934.

Pelowitz, D.B.E., 2008. MCNPX User's Manual, Version 2.6.0. LA-CP-07-1473. Los Alamos National Laboratory, Los Alamos, NM.

Table F.1. Absorbed dose for the lens of the eye per fluence, in units of pGy cm^2, for mono-energetic photons incident in various geometries.

Energy (MeV)	AP	PA	LAT	ROT	ISO
0.01	0.833	–	0.0762	0.277	0.247
0.015	1.62	–	0.417	0.657	0.393
0.02	1.35	–	0.501	0.616	0.409
0.03	0.812	0.0048	0.422	0.432	0.342
0.04	0.581	0.0201	0.353	0.336	0.282
0.05	0.483	0.0328	0.317	0.294	0.248
0.06	0.450	0.0417	0.312	0.285	0.244
0.07	0.455	0.0504	0.322	0.293	0.251
0.08	0.482	0.0590	0.347	0.314	0.265
0.10	0.559	0.0780	0.416	0.376	0.313
0.15	0.838	0.142	0.642	0.580	0.484
0.2	1.13	0.225	0.912	0.810	0.686
0.3	1.74	0.427	1.45	1.28	1.13
0.4	2.30	0.659	1.97	1.75	1.59
0.5	2.83	0.907	2.46	2.21	2.04
0.6	3.34	1.17	2.94	2.65	2.46
0.8	4.26	1.71	3.81	3.46	3.23
1.0	5.06	2.23	4.62	4.18	3.93
1.5	6.30	3.49	6.30	5.65	5.27
2.0	7.04	4.63	7.61	6.75	6.34
3.0	6.93	6.89	9.85	8.41	8.06
4.0	6.60	9.07	11.3	9.63	9.62
5.0	6.29	10.8	12.5	10.6	10.7
6.0	5.96	12.4	13.4	11.3	11.8
8.0	5.44	15.6	15.2	13.1	13.9
10.0	5.05	18.8	17.0	14.7	15.8
15.0	4.82	26.9	20.7	18.6	20.4
20.0	4.64	35.8	23.8	22.2	23.4
30.0	4.52	53.5	28.8	28.4	29.7
40.0	4.58	69.6	32.7	33.7	34.6
50.0	4.64	83.5	35.3	37.9	40.0
60.0	4.68	95.7	37.6	41.5	43.4
80.0	4.80	118	41.1	47.4	51.3
100	4.92	135	43.7	52.4	57.9
150	5.22	162	48.0	59.6	65.6
200	5.39	180	50.8	64.3	71.7
300	5.60	199	53.9	69.7	81.3
400	5.70	214	56.1	73.1	87.5
500	5.80	224	57.4	75.7	91.7
600	5.86	232	58.5	77.6	95.9
800	5.96	243	59.9	80.1	104
1000	6.01	251	60.6	82.0	108
1500	6.15	264	62.0	84.6	115
2000	6.22	273	63.0	86.7	122
3000	6.28	285	64.0	89.2	129
4000	6.29	293	64.8	90.9	137
5000	6.29	299	65.4	92.2	143
6000	6.28	304	66.1	93.4	146
8000	6.25	313	67.0	95.6	148
10,000	6.22	320	67.1	97.5	149

AP, antero-posterior; PA, postero-anterior; LLAT, left lateral; RLAT, right lateral; ROT, rotational; ISO, isotropic.

Table F.2. Absorbed dose for the lens of the eye per fluence, in units of pGy cm^2, for mono-energetic electrons incident in various geometries.

Energy (MeV)	AP	PA	ISO
0.01	–	–	–
0.015	–	–	–
0.02	–	–	–
0.03	–	–	–
0.04	–	–	–
0.05	–	–	–
0.06	–	–	–
0.08	–	–	–
0.10	9.4E−4	–	9.4E−4
0.15	0.0017	–	0.0017
0.2	0.0026	–	0.0026
0.3	0.0048	7.3E−7	0.0048
0.4	0.0078	1.2E−5	0.0078
0.5	0.0115	7.3E−5	0.0115
0.6	0.0406	2.6E−4	0.0406
0.7	1.46	6.4E−4	1.46
0.8	9.97	0.0013	9.97
1.0	69.1	0.0026	22.6
1.5	307	0.0070	47.3
2.0	414	0.0141	71.0
3.0	373	0.0312	99.7
4.0	332	0.0592	115
5.0	314	0.114	123
6.0	306	0.171	128
8.0	302	0.375	142
10.0	301	0.675	160
15.0	309	1.98	184
20.0	311	4.07	208
30.0	309	19.0	240
40.0	309	78.3	262
50.0	309	170	277
60.0	309	246	290
80.0	309	300	304
100	309	329	316
150	309	372	330
200	309	401	336
300	309	440	349
400	308	458	365
500	308	472	374
600	308	483	381
800	308	506	395
1000	308	524	405
1500	308	559	422
2000	309	586	434
3000	308	626	454
4000	308	657	470
5000	308	682	477
6000	308	704	483
8000	307	740	492
10,000	307	762	498

AP, antero-posterior; PA, postero-anterior; ISO, isotropic.

Table F.3. Absorbed dose for the lens of the eye per fluence, in units of pGy cm^2, for mono-energetic neutrons incident in various geometries.

Energy (MeV)	AP	PA	LAT	ROT	ISO
1.0E−9	2.32	0.283	0.735	0.949	0.786
1.0E−8	2.73	0.329	0.868	1.12	0.848
2.5E−8	2.80	0.327	0.963	1.20	0.855
1.0E−7	2.87	0.322	1.14	1.28	0.863
2.0E−7	2.86	0.331	1.24	1.34	0.871
5.0E−7	2.79	0.356	1.32	1.39	0.890
1.0E−6	2.71	0.378	1.35	1.40	0.915
2.0E−6	2.63	0.395	1.37	1.40	0.949
5.0E−6	2.52	0.406	1.37	1.37	1.00
1.0E−5	2.38	0.406	1.34	1.32	1.04
2.0E−5	2.28	0.419	1.31	1.27	1.07
5.0E−5	2.16	0.452	1.25	1.22	1.09
1.0E−4	2.06	0.472	1.22	1.15	1.09
2.0E−4	1.95	0.483	1.18	1.13	1.08
5.0E−4	1.82	0.483	1.16	1.08	1.05
0.001	1.77	0.479	1.13	1.05	1.02
0.002	1.80	0.477	1.11	1.06	1.01
0.005	1.97	0.465	1.14	1.10	1.04
0.01	2.28	0.446	1.27	1.23	1.13
0.02	2.93	0.424	1.51	1.52	1.35
0.03	3.59	0.417	1.76	1.77	1.55
0.05	4.77	0.420	2.24	2.36	1.94
0.07	5.86	0.417	2.71	2.84	2.29
0.10	7.29	0.415	3.38	3.49	2.78
0.15	9.38	0.423	4.38	4.49	3.52
0.2	11.1	0.440	5.30	5.41	4.20
0.3	14.1	0.493	6.95	6.91	5.45
0.5	18.3	0.644	9.86	9.47	7.64
0.7	21.5	0.837	12.2	11.5	9.58
0.9	25.4	1.07	14.4	13.4	11.3
1.0	27.0	1.19	15.6	14.5	12.2
1.2	29.0	1.47	17.5	16.2	13.8
1.5	30.6	1.94	20.1	18.2	15.9
2.0	34.2	2.86	23.9	21.0	19.2
3.0	40.5	5.02	30.1	26.5	24.7
4.0	47.0	7.41	35.2	31.8	29.2
5.0	52.8	9.88	38.4	36.6	33.1
6.0	57.2	12.3	42.0	40.5	36.4
7.0	59.2	14.7	45.2	43.4	39.4
8.0	61.2	17.0	47.9	46.0	42.0
9.0	62.8	19.2	50.4	48.2	44.3
10.0	64.2	21.3	52.6	50.3	46.4
12.0	66.2	25.2	56.3	53.8	50.1
14.0	67.7	28.7	59.3	56.5	53.2
15.0	68.2	30.4	60.6	57.5	54.5
16.0	68.7	32.0	61.8	58.5	55.8
18.0	69.3	35.0	63.8	59.8	58.0
20.0	69.4	37.8	65.5	60.7	59.9
21.0	69.1	39.1	66.3	60.9	60.8
30.0	62.8	49.5	70.7	60.2	66.9

Table F.3. (*continued*)

Energy (MeV)	AP	PA	LAT	ROT	ISO
50.0	49.3	65.7	65.6	60.5	74.5
75.0	42.0	79.1	65.2	63.3	79.4
100	39.3	88.7	66.6	66.7	82.3
130	38.2	97.6	69.1	70.7	84.8
150	38.1	103	71.0	73.4	86.0
180	38.3	109	73.8	77.2	87.5
200	38.7	113	75.7	79.6	88.4
300	41.5	130	85.0	90.8	91.6
400	44.7	145	93.4	101	94.1
500	48.1	159	101	109	96.2
600	51.3	172	108	117	98.1
700	54.4	184	115	124	99.9
800	57.3	195	121	131	102
900	60.2	206	127	137	103
1000	62.9	217	133	143	105
2000	84.7	299	177	186	119
5000	119	431	249	254	157
10,000	138	552	302	300	215

AP, antero-posterior; PA, postero-anterior; LLAT, left lateral; RLAT, right lateral; ROT, rotational; ISO, isotropic.

ANNEX G. SPECIAL CONSIDERATIONS FOR ASSESSING THE LOCAL SKIN-EQUIVALENT DOSE

(G1) In ICRP *Publication 103* (ICRP, 2007), the Commission retained the effective dose limits and equivalent dose limits for skin, hands/feet, and eye given in ICRP *Publication 60* (ICRP, 1991), and discussed the limits on equivalent dose applicable for preventing the occurrence of tissue reactions (deterministic effects). It was noted that further considerations might be indicated as additional information evolved, particularly with respect to the eye, and the reader is referred to Annex F of the present report for additional considerations in assessing the dose to the lens of the eye.

(G2) In radiation protection, the mean value of the absorbed dose averaged over the specified organ or tissue is correlated with the detriment due to stochastic effects. The averaging of absorbed doses in organs and tissues, and the summing of weighted mean doses in different organs and tissues comprise the basis for the radiation protection quantity 'effective dose'. The extent to which the mean value is representative of the absorbed dose in all regions of the organ or tissue depends, for external irradiation, on the homogeneity of the exposure and on the range of the incident radiation. In cases of extreme partial-body exposure, tissue damage can occur even if the tissue-equivalent dose or effective dose is below the dose limit. A special limit on local skin dose is specified to take account of this situation in the case of exposure by weakly penetrating radiations (e.g. electrons).

(G3) The basal cells of the epidermis, the skin tissue at radiogenic risk, cannot be represented in the voxel geometry of the reference phantoms – voxel sizes of $2.137 \times 2.137 \times 8$ mm^3 and $1.775 \times 1.775 \times 4.84$ mm^3 in the male and female phantoms, respectively (ICRP, 2009). Due to undulations in the basal cell layer and the finite thickness of its cells, a range from 50 to 100 μm (or 5–10 mg/cm^2) is considered appropriate for specifying the depth of the sensitive layer of most parts of the skin that, in practice, are not protected by clothing and are therefore exposed directly to incident radiation. For practical dose assessment, the Commission recommends the use of a depth of 70 μm as a reasonable mean depth of this cell layer (ICRP, 1991, 2007). The Commission notes that in the case of stochastic effects, the equivalent dose can be averaged over the whole area of the skin, and the annual effective dose limit of 20 mSv provides sufficient protection (ICRP, 1991, 2007). Thus, the skin conversion coefficients (dose per fluence) derived in calculations with the voxel phantoms, and given in the CD of this report, are appropriate for assessing the effective dose and, with its annual limit of 20 mSv, are sufficient to limit the occurrence of skin stochastic effects. However, these coefficients do not provide a basis for assessing the equivalent dose specified for localised skin exposure that is related to tissue reactions (deterministic effects). The equivalent dose is to be averaged over any 1 cm^2 area of exposed skin, regardless of the area exposed, at the nominal depth of 70 μm. The annual limit applicable to this dose quantity is 500 mSv (ICRP, 1991, 2007).

(G4) In this annex, data on localised skin dose per fluence values are given as derived by Monte Carlo calculations simulating the transport of a normally incident, parallel beam of electrons and alpha particles on a tissue-equivalent slab. For that

Table G.1. Local skin absorbed dose per fluence (D/Φ), in pGy cm^2, for mono-energetic electrons normally incident on skin.

Energy (MeV)	D/Φ	Energy (MeV)	D/Φ
0.01	1.22E−03	0.40	4.41E+02
0.015	2.80E−03	0.50	3.82E+02
0.02	4.73E−03	0.60	3.43E+02
0.03	8.85E−03	0.80	3.15E+02
0.04	1.47E−02	1.0	3.04E+02
0.05	2.10E−02	1.5	2.84E+02
0.06	1.37E+01	2.0	2.80E+02
0.07	2.15E+02	3.0	2.64E+02
0.08	6.62E+02	4.0	2.59E+02
0.09	1.08E+03	5.0	2.59E+02
0.10	1.40E+03	6.0	2.59E+02
0.15	1.21E+03	8.0	2.67E+02
0.20	8.41E+02	10.0	2.62E+02
0.30	5.38E+02		

purpose, the Monte Carlo code MCNPX Version 2.6.0 (Pelowitz, 2008) was employed to simulate a circular beam of 7 cm diameter centred on the face of a tissue-equivalent cube ($10 \times 10 \times 10$ cm^3). The absorbed dose was averaged over the volume of a centred cylinder of 1 cm^2 area and 50 μm height located 50 μm below the skin surface (i.e. averaged over the 50–100 μm depth). The normal incidence of the particles ensures that the conversion coefficients bound those for any given angular distribution. The conversion coefficients are shown in Tables G.1 and G.2, and graphically in Figs. G.1 and G.2.

(G5) As noted above, the skin dose conversion coefficients given in the CD accompanying this report have been averaged over all skin voxels of the male and female computational phantoms, and the resultant quantity is used in deriving the effective dose conversion coefficient. The voxel thickness in both phantoms (2.14 mm and 1.78 mm in the male and female, respectively) is far larger than the thickness of the basal cell layer, taken here to be between 50 and 100 μm of the skin surface. The local skin dose conversion coefficients tabulated in this annex differ from skin

Table G.2. Local skin absorbed dose per fluence (D/Φ), in μGy cm^2, for mono-energetic alpha particles normally incident on skin.

Energy (MeV)	D/Φ
6.5	0.00111
6.8	0.0256
7.0	0.0420
7.5	0.0752
8.0	0.103
8.5	0.128
9.0	0.150
9.5	0.140
10.0	0.180

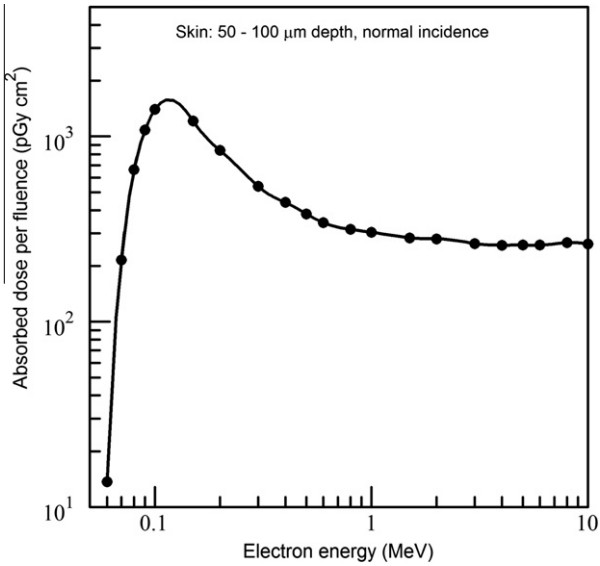

Fig. G.1. Local skin absorbed dose per fluence for mono-energetic electrons normally incident on the skin.

dose conversion coefficients calculated with the reference phantoms in that: (1) the outer keratinized skin layer (50 μm) is considered, and (2) the coefficient is averaged over the mass of the irradiated basal cells. For incident electrons and helium ions

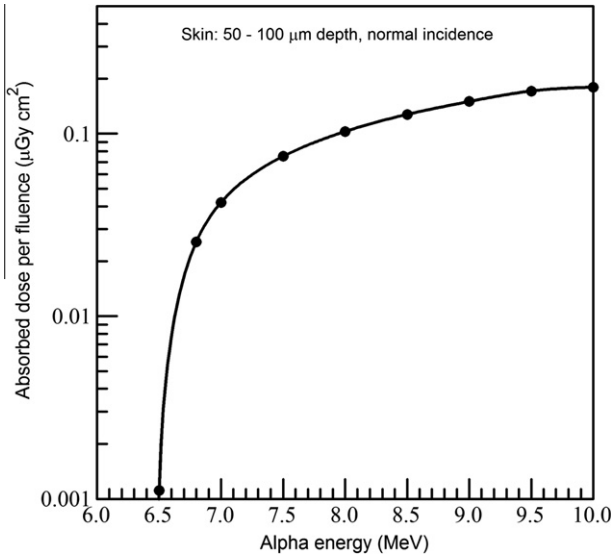

Fig. G.2. Local skin absorbed dose per fluence for mono-energetic alpha particles normally incident on the skin.

(alpha particles) of insufficient energy to penetrate to the basal cell layer, the local skin dose conversion coefficient is zero and thus numerically less than the skin dose conversion coefficients derived by averaging the energy deposition in all the skin voxels of the computational phantoms. At sufficient energies for the incident particles to reach and penetrate the basal layer, the local skin dose conversion coefficient exceeds the skin dose conversion coefficients calculated with the reference phantoms and given in the CD, as the latter are averaged over all skin voxels in the computational phantom regardless of whether or not they have been irradiated under the specified exposure geometry. At these energies, the local coefficient exceeds the body-averaged coefficients for all exposure geometries.

G.1. References

ICRP, 1991. 1990 Recommendations of the International Commission on Radiological Protection. ICRP Publication 60. Ann. ICRP 21(1–3).

ICRP, 2007. The 2007 Recommendations of the International Commission on Radiological Protection. ICRP Publication 103. Ann. ICRP 37(2–4).

ICRP, 2009. Adult reference computational phantoms. ICRP Publication 110. Ann. ICRP 39(2).

Pelowitz, D.B. (Ed.), 2008. MCNPX User's Manual, Version 2.6.0. LA-CP-07-1473. Los Alamos National Laboratory, Los Alamos, NM.

ANNEX H. EFFECTIVE DOSE FOR SUPERIOR HEMISPHERE SEMI-ISOTROPIC IRRADIATION FOR AIRCRAFT CREW DOSIMETRY

(H1) The present report provides organ absorbed dose conversion coefficients and effective dose conversion coefficients calculated with the ICRP/ICRU adult reference phantoms (ICRP, 2009), as implemented in various Monte Carlo radiation transport codes. Antero-posterior (AP), postero-anterior (PA), left lateral (LLAT), right lateral (RLAT), rotational (ROT), and isotropic (ISO) whole-body idealised geometries were considered, which are recommended to simulate the field of most occupationally exposed people (for description of the geometries, see Section 3.2).

(H2) The ICRP has recommended (ICRP, 1991, 2007) that exposures of aircraft crew to cosmic radiation in the operation of commercial jet aircraft should be considered as occupational exposure. In 2010, a joint ICRU/ICRP report was published entitled 'Reference Data for the Validation of Doses from Cosmic Radiation Exposures of Aircraft Crew' (ICRU, 2010). The annual dose assessment for aircraft crew is based, among other findings, on radiation transport calculations of effective dose rates. The relationships between ambient dose equivalent and effective dose allow the calculation of effective dose from values of ambient dose equivalent.

(H3) The major component of particle fluence rate and effective dose for aircraft crew originating from galactic cosmic radiation fields at cruising aircraft altitudes is downward directed (Ferrari and Pelliccioni, 2003; Battistoni et al., 2004, 2005; Sato and Niita, 2006; Sato et al., 2008, 2011). The magnitude of the effect of this biasing depends partly on the degree of structural shielding by the aircraft. This is particularly true for neutrons (Ferrari et al., 2004), but the differences between superior hemisphere semi-isotropic (SS-ISO), ISO, and simulated aircraft crew irradiation conditions are not large (Sato et al., 2011).

(H4) For fields in aircraft at cruising altitudes, the uncertainties in using conversion coefficients from ambient dose equivalent to estimate the effective dose for ISO or SS-ISO geometry are small compared to other uncertainties in the measurements and calculations. In ICRU Report 84 (ICRU, 2010), conversion coefficients from ambient dose equivalents to effective dose for SS-ISO irradiation have been selected for the assessment of aircraft crew exposures.

(H5) The conversion coefficients were determined using the following Monte Carlo codes: photons, electrons, positrons (EGS4); neutrons, protons (PHITS); negative and positive muons (FLUKA); and negative and positive pions (FLUKA and PHITS). For more information on the codes, see Section 3.3. The statistical uncertainties were similar to those observed for the standard irradiation geometries (AP, PA, etc). The relative statistical uncertainties were less than 5% for photons, electrons/positrons, neutrons, and protons, and less than 0.5% for muons and pions, as described in Sections 4.1–4.6.

(H6) The conversion coefficients from fluence to effective dose for SS-ISO irradiation are given in the attached CD. These conversion coefficients were used together with the conversion coefficients for particle fluence to ambient dose equivalent

(Pelliccioni, 2000) to establish the atmospheric particle fluence rates and reference conditions (Ferrari et al., 2001), and the relationship between effective dose and ambient dose equivalent (ICRU, 2010).

(H7) It should be noted that ISO is defined by a radiation field in which the particle fluence per solid angle is independent of direction. Conversion coefficients for ISO [cc(ISO)] are then related to those for SS-ISO [cc(SS-ISO)] and IS-ISO [cc(IS-ISO)] by:

$$\mathrm{cc(ISO)} = (\mathrm{cc(SS\text{-}ISO)} + \mathrm{cc(IS\text{-}ISO)})/2 \tag{H.1}$$

The upward-directed component conversion coefficients [i.e. inferior hemisphere semi-isotropic cc(IS-ISO)], may be derived from the above equation.

H.1. References

Battistoni, G., Ferrari, A., Pelliccioni, M., et al., 2004. Monte Carlo calculation of the angular distribution of cosmic rays at flight altitudes. Radiat. Prot. Dosim. 112, 331–343.

Battistoni, G., Ferrari, A., Pelliccioni, M., et al., 2005. Evaluation of the doses to aircrew members taking into consideration the aircraft structures. In: Smart, D.F., Worgul, B.V. (Eds.), Space Life Sciences: Aircraft and Space Radiation Environment. Elsevier Science Ltd, Oxford, pp. 1645–1652.

Ferrari, A., Pelliccioni, M., 2003. On the conversion coefficients for cosmic ray dosimetry. Radiat. Prot. Dosim. 104, 211–220.

Ferrari, A., Pelliccioni, M., Rancati, T., 2001. Calculation of the radiation environment caused by galactic cosmic rays for determining air crew exposure. Radiat. Prot. Dosim. 93, 101–114.

Ferrari, A., Pelliccioni, M., Villari, R., 2004. Evaluation of the influence of aircraft shielding on the aircrew exposure through an aircraft mathematical model. Radiat. Prot. Dosim. 108, 91–105.

ICRP, 1991. 1990 Recommendations of the International Commission on Radiological Protection. ICRP Publication 60. Ann. ICRP 21(1–3)..

ICRP, 2007. The 2007 Recommendations of the International Commission on Radiological Protection. ICRP Publication 103. Ann. ICRP 37(2–4)..

ICRP, 2009. Adult reference computational phantoms. ICRP Publication 110. Ann. ICRP 39(2)..

ICRU, 2010. Reference Data for the Validation of Doses from Cosmic Radiation Exposures of Aircraft Crew. ICRU Report 84. International Commission on Radiation Units and Measurements, Bethesda, MD..

Pelliccioni, M., 2000. Overview of fluence-to-effective dose and fluence-to-ambient dose equivalent conversion coefficients for high energy radiation calculated using the FLUKA code. Radiat. Prot. Dosim. 88, 279–297.

Sato, T., Niita, K., 2006. Analytical functions to predict cosmic-ray neutron spectra in the atmosphere. Radiat. Res. 166, 544–555.

Sato, T., Yasuda, H., Niita, K., et al., 2008. Development of PARMA: PHITS-based analytical radiation model in the atmosphere. Radiat. Res. 170, 244–259.

Sato, T., Endo, A., Zankl, M., et al., 2011. Fluence-to-dose conversion coefficients for aircrew dosimetry based on the new ICRP recommendations. Prog. Nucl. Sci. Technol. 1, 134–137.

ANNEX I. METHODS USED FOR EVALUATION OF REFERENCE DATA

(I1) The reference data for dose conversion coefficients presented in this publication were evaluated by averaging and smoothing dose conversion coefficients calculated with various Monte Carlo radiation transport codes by several groups listed in Table 4.1. This annex describes procedures for evaluation of the reference data with an example of the evaluation procedures for dose conversion coefficients of the adrenals for neutron irradiation in the male reference phantom.

(I2) Fig. I.1 shows absorbed dose conversion coefficients calculated by four Monte Carlo codes (PHITS, FLUKA, MCNPX-2.6, and GEANT4) for the male adrenals. Consistency of all data was examined carefully, and origins of data deviations were analysed. If the deviation resulted from inappropriate transport and interaction models employed in the Monte Carlo codes, the data were omitted from the evaluation of the reference data.

(I3) Averaged values at the energy points specified by the DOCAL Task Group were obtained from all accepted raw data given in Fig. I.1 Next, data fitting was applied using various smoothing functions to obtain a smooth curve of the absorbed dose conversion coefficients as a function of neutron energy, as shown in Fig. I.2. Smoothing functions used for data fitting included cubic spline smoothing, least-square B-spline smoothing, and non-uniform rational B-spline smoothing (de Boor, 1978). Absorbed dose conversion coefficients at the specified energy points were evaluated using the resulting smoothed data curve.

(I4) The evaluated values were compared with the raw data to confirm their validity (Fig. I.3), and defined as the reference data set.

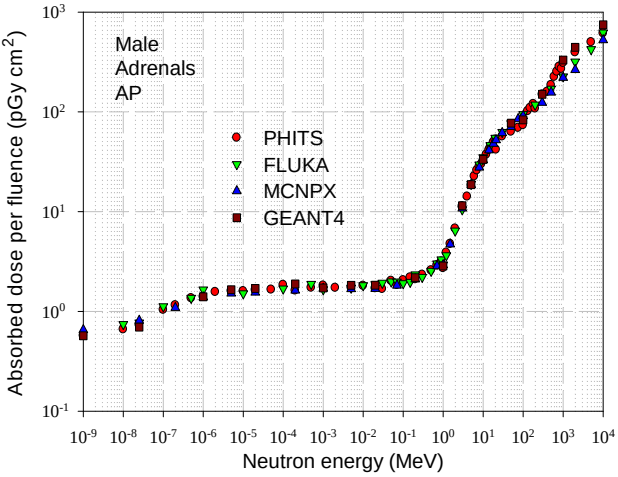

Fig. I.1. Raw (original) data calculated using Monte Carlo codes.

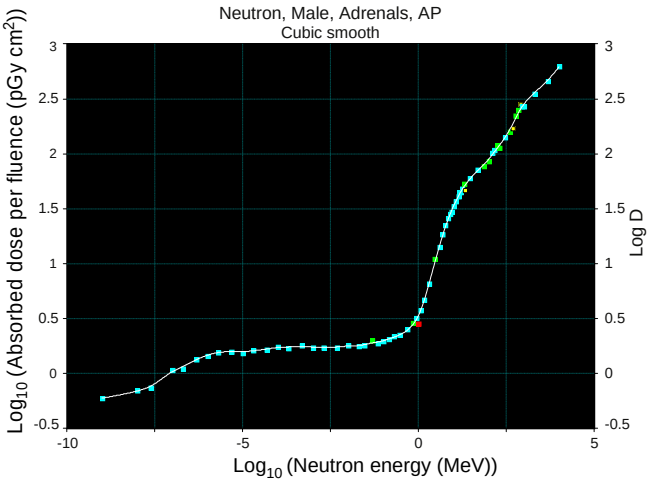

Fig. I.2. Averaged values and their fitting curve obtained using cubic spline smoothing. The x- and y-axes are converted to log–log scales.

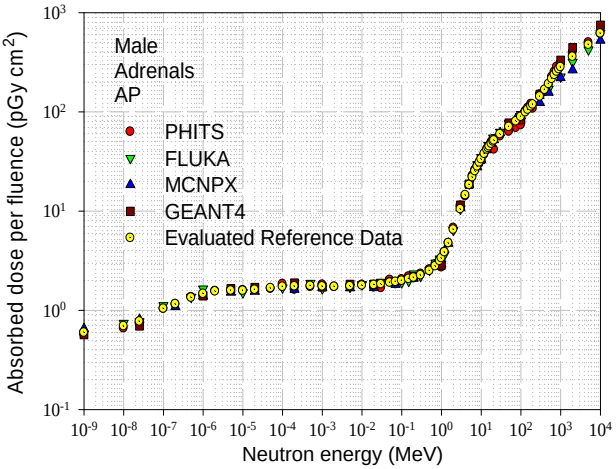

Fig. I.3. Comparison of evaluated reference data and the raw data calculated by Monte Carlo codes.

I.1. Reference

de Boor, C., 1978. A Practical Guide to Splines. Springer Verlag, New York.

ANNEX J. CD USER GUIDE

(J1) The CD-ROM attached to this report presents reference conversion coefficients for effective doses and organ absorbed doses for various types of external exposures, calculated following the 2007 Recommendations (ICRP, 2007) and the ICRP/ICRU reference phantoms (ICRP, 2009) representing Reference Male and Reference Female (ICRP, 2002, 2007).

(J2) The CD-ROM is organised in 13 main folders, and the contents of all folders are in ASCII format. The folder 'Skeletal fluence to dose response functions' also provides data in Microsoft Excel format.

(J3) The table entries of the folders (except 'Skeletal fluence to dose response functions') are reference values of effective and organ dose conversion coefficients, and were derived from dose conversion coefficients calculated using the ICRP/ICRU reference phantoms and various Monte Carlo radiation transport codes (see Sections 3.1 and 3.3) following the application of averaging and smoothing techniques (see Annex I).

(J4) The folder 'Effective' lists reference values of the effective dose conversion coefficients for photons, electrons, positrons, neutrons, negative and positive muons, negative and positive pions, and helium ions.

- Conversion coefficients are given for the following whole-body idealised geometries: antero-posterior (AP), postero-anterior (PA), left lateral (LLAT), right lateral (RLAT), rotational (ROT), and isotropic (ISO) (for description of the geometries, see Section 3.2).
- The fluence to effective dose conversion coefficients were derived from the organ dose conversion coefficients, the radiation weighting factor w_R and the tissue weighting factor w_T, following the procedure described in ICRP *Publication 103* (ICRP, 2007).
- The effective doses are normalised to incident particle fluence, and are given in units of pSv cm^2. For photons of energies up to 10 MeV, the conversion coefficients are also tabulated as the effective dose per air kerma free-in-air, K_a, in units of Sv/Gy.

(J5) The folders 'Photons', 'Electrons', 'Positrons', 'Neutrons', 'Protons', 'Negative pions', 'Positive pions', 'Negative muons', Positive muons', and 'Helium ions' list reference values of the organ absorbed dose conversion coefficients for the respective particles and the specific irradiation geometries considered, for the following organs:

- Active (red) marrow, colon, lungs, stomach, breast, ovaries, testes, urinary bladder wall, oesophagus, liver, thyroid, bone surface, brain, salivary glands, skin, remainder tissues, adrenals, extrathoracic (ET) region, gall bladder, heart, kidneys, lymphatic nodes, muscle, oral mucosa, pancreas, prostate, small intestine, spleen, thymus, uterus/cervix, and eye lens. For list of target organs and their respective acronyms, see Table 4.2.

- Conversion coefficients are given for the following whole-body idealised geometries: AP, PA, LLAT, RLAT, ROT, and ISO (for description of the geometries, see Section 3.2).
- Data are given separately for the male and female phantoms.
- The organ absorbed doses are normalised to particle fluence, and are given in units of pGy cm^2.

(J6) The folder 'Effective_SS_ISOandISO' lists the conversion coefficients from fluence to effective dose for superior hemisphere semi-isotropic irradiation and ISO geometry for photons, electrons, positrons, neutrons, protons, negative and positive pions, and negative and positive muons.

- The effective doses are normalised to incident particle fluence, and are given in units of pSv cm^2.

(J7) The folder 'Skeletal fluence to dose response functions' contains two Excel spreadsheets – one for photons (Annex D – Photon DRF) and one for neutrons (Annex E – Neutron DRF). In addition, five ASCII files are given corresponding to the following tables in Annexes D and E:

- Table D.1. Regional DRF: Bone-specific absorbed dose per photon fluence (Gy m^2) to active marrow (AM) and endosteum (TM_{50}) as a function of photon energy and skeletal region in the ICRP *Publication 110* reference phantoms.
- Table D.2. – MEAC Ratios Male: Ratios of mass energy absorption coefficients for active marrow (AM) to spongiosa (SP) and for total marrow (TM) to either spongiosa or medullary marrow (MM), as a function of photon energy and skeletal site, for the ICRP reference adult male.
- Table D.3. – MEAC Ratios Female: Ratios of mass energy absorption coefficients for active marrow (AM) to spongiosa (SP) and for total marrow (TM) to either spongiosa or medullary marrow (MM), as a function of photon energy and skeletal site, for the ICRP reference adult female.
- Table D.4. – DEF: Dose enhancement factor S to active marrow (AM) and endosteum (TM_{50}) as a function of photon energy and skeletal site.
- Table E.1. – Neutron DRF: Bone-specific absorbed dose per neutron fluence (Gy m^2) to active marrow (AM) and endosteum (TM_{50}) as a function of neutron energy and skeletal region within the ICRP 110 computational reference phantoms.

(J8) The additional Excel spreadsheet (Tables 3.1 and 3.2) and two corresponding ASCII files (Tables 3.1 and 3.2) include the following information:

- Elemental compositions of active marrow, inactive marrow, and the bone trabeculae for the ICRP reference adult male and female computational phantoms.
- Skeletal tissue masses in the ICRP reference male and female computational phantoms.

(J9) Finally, the CD ROM contains Excel-based window software which allows comfortable access in tabular and graphical form to the reference organ dose and effective dose conversion coefficients listed in the folders described above.

J.1. References

ICRP, 2002. Basic anatomical and physiological data for use in radiological protection: reference values. ICRP Publication 89. Ann. ICRP 32(3/4).

ICRP, 2007. The 2007 Recommendations of the International Commission on Radiological Protection. ICRP Publication 103. Ann. ICRP 37(2–4).

ICRP, 2009. Adult reference computational phantoms. ICRP Publication 110. Ann. ICRP 39(2).